

PHOTOCATALYTIC DEHYDROGENATION  
OF LIQUID ALCOHOLS BY  
PLATINIZED ANATASE AND  
OTHER CATALYSTS

by

FALAH H. HUSSEIN, B.Sc., M.Sc.

Thesis submitted to the University  
of Nottingham for the Degree  
of Doctor of Philosophy,

November, 1984.

To my late father,  
whose encouragement  
led me to study science.

### ACKNOWLEDGEMENTS

The author wishes to express his sincere gratitude to Dr. R. Rudham, under whose supervision this work was carried out, and for his continued advice and encouragement.

Thanks are due to the technical staff of the Chemistry Department of the University of Nottingham for their invaluable assistance, especially Mr. John Heard. I would like to thank my friends and colleagues at Nottingham University for making my time so enjoyable. I would like also to thank Mrs. L. Watson for her care and patience in typing this thesis.

Finally, my grateful and sincere thanks are due to the Salah-Al-Deen University/Ministry of Higher Education and Scientific Research of the Republic of IRAQ, for the studentship which enabled the work for this thesis to be undertaken.

## ABSTRACT

The work described in this thesis was undertaken at the University of Nottingham between October 1981 and November 1984, under the supervision of Dr. R. Rudham. Except where indicated by reference, it is the original work of the author and has not been submitted for any other degree.

The photocatalytic dehydrogenation of liquid alcohols (methanol, ethanol, propan-1-ol and propan-2-ol) by suspensions of platinum and other metals supported on anatase have been investigated by following carbonyl compound formation under a nitrogen atmosphere. Measurements were made over the temperature range 278-303 K using filtered 366 nm U.V. radiation. Reaction on photodeposited catalysts was consistently associated with an activation energy of  $20 \pm 1 \text{ kJ mol}^{-1}$ , although the activity fell in the sequence:

$$\text{Pt/TiO}_2 > \text{Pd/TiO}_2 > \text{Rh/TiO}_2 > \text{Au/TiO}_2 = 0,$$

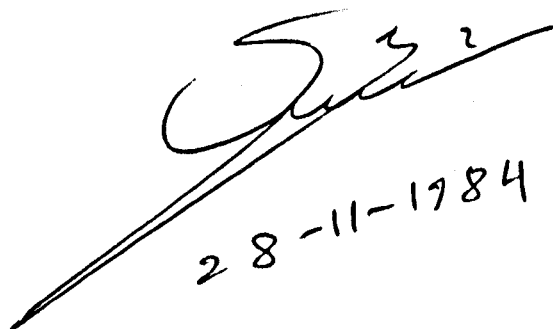
for catalysts with a metal content of 0.5 wt%. The activation energy is identical to that for photoreaction on the anatase support in the presence of oxygen and is believed to be associated with the transport of photo-electrons through the anatase to either metal particles or adsorbed oxygen.

Activities and activation energies for carbonyl compound formation from the photocatalytic dehydrogenation of the individual alcohols were effectively identical on the same catalyst, indicating that the photocatalytic dehydrogenation reaction is not governed by the physical or chemical properties of the reactant alcohol.

With platinized anatase prepared by hydrogen reduction there was an appreciable dark reaction, which was absent with catalysts prepared by

photodeposition. It is believed that reduction in hydrogen at elevated temperature renders the anatase support non-stoichiometric, a process favoured by spillover of hydrogen atoms from the platinum particles. The low activation energy for photocatalysis on hydrogen reduced catalyst is considered to be associated with the non-stoichiometric nature of the anatase, which presumably provides an energetically favourable mechanism for photoelectron transport to the metal particles and negates the photoelectron traps responsible for an activation energy of  $20 \pm 1 \text{ kJ mol}^{-1}$  on the non-reduced catalysts.

A radical mechanism for photocatalytic dehydrogenation is proposed. This mechanism predicts a limiting quantum yield of one half, which is in good agreement with the value obtained from experiments at different light intensities.



28-11-1984

## CONTENTS

### Page

### Chapter One - Introduction

1.1	General introduction ... ..	1
1.2	Crystal morphology of $\text{TiO}_2$ and metallized $\text{TiO}_2$ ... ..	2
1.3	The electronic properties of $\text{TiO}_2$ and metallized $\text{TiO}_2$ ..	4
1.4	Deposition of metals on $\text{TiO}_2$ ... ..	10
1.5	Adsorption on $\text{TiO}_2$ and metallized $\text{TiO}_2$ . ... ..	13
1.5.1	Water . ... ..	13
1.5.2	Oxygen ... ..	16
1.5.3	Hydrogen ... ..	26
1.5.4	Carbon monoxide and Carbon dioxide ... ..	31
1.5.5	Alcohols ... ..	34
1.5.6	Other species ... ..	37
1.6	Photocatalysis on $\text{TiO}_2$ and metallized $\text{TiO}_2$ ... ..	39
1.6.1	Photocatalytic oxidation of alcohols ... ..	39
1.6.2	Water ... ..	53
1.6.3	Other species ... ..	57
1.7	The present work ... ..	63

### Chapter Two - Experimental

2.1	Apparatus ... ..	64
2.2	Chemicals . ... ..	66
2.3	Catalyst preparations ... ..	67
	a) Method A ... ..	67
	b) Method B ... ..	67
	c) Method C ... ..	68
2.4	Reaction procedure ... ..	69
2.4.1	Reaction pretreatment ... ..	69

	<u>Page</u>
2.4.2 Monitoring reaction ... ..	69
2.4.3 Analysis of reaction products ... ..	69
a) Gas-liquid chromatographic analysis ... ..	69
b) Spectrophotometric analysis ... ..	71
2.5 Measurements of light intensity and quantum yields ...	73

### Chapter Three - Results

3.1 Photocatalytic oxidation of propan-2-ol on $\text{TiO}_2$ ... ..	75
3.1.1 Preliminary experiments ... ..	75
3.1.2 Temperature dependence of reaction rate for the photo- catalytic oxidation of propan-2-ol ... ..	77
3.1.3 Light intensity dependence of reaction rate for the photocatalytic oxidation of propan-2-ol ... ..	78 78
3.1.4 Temperature dependence of reaction rate at different light intensities for the photocatalytic oxidation of propan-2-ol ... ..	81
a) Full light intensity ... ..	81
b) 20.2% relative light intensity ... ..	83
c) 4.4% relative light intensity ... ..	84
3.2 Dehydrogenation of alcohols on platinized anatase ( $\text{Pt}(0.5)/\text{TiO}_2$ ) prepared by hydrogen reduction (Method A)	86
3.2.1 The dark reaction ... ..	86
a) The dark reaction of propan-2-ol ... ..	86
b) The dark reaction with other alcohols at 293 K ...	88
3.2.2 The photocatalytic reactions ... ..	89
a) Temperature dependence for photocatalytic dehydro- genation of propan-2-ol ... ..	89
b) Photocatalytic dehydrogenation of propan-2-ol and other alcohols at 293 K ... ..	91

	<u>Page</u>
3.2.3 Photocatalytic dehydrogenation of alcohols on oxygen treated catalysts . . . . .	92
a) Temperature dependence for photocatalytic dehydrogenation of propan-2-ol on the catalyst treated at 573 K for 3 h. . . . .	92
b) Photocatalytic dehydrogenation of alcohols on the catalyst treated at 753 K for 16 h. . . . .	93
i) Temperature dependence for photocatalytic dehydrogenation of propan-2-ol . . . . .	93
ii) Photocatalytic dehydrogenation of other alcohols at 293 K . . . . .	95
3.3 Photocatalytic dehydrogenation of propan-2-ol on platinized anatase Pt(0.5)/TiO <sub>2</sub> prepared by photodeposition (method B)	97
3.3.1 Temperature dependence for the photocatalytic dehydrogenation of propan-2-ol . . . . .	97
3.3.2 Light intensity dependence for the photocatalytic dehydrogenation of propan-2-ol . . . . .	98
3.4 Photocatalytic dehydrogenation of alcohols on platinized anatase prepared by photodeposition (Method C) . . . . .	100
3.4.1 Photocatalytic dehydrogenation of propan-2-ol on different masses of catalysts . . . . .	100
a) Pt(0.5)/TiO <sub>2</sub> . . . . .	100
b) Pt(2.0)/TiO <sub>2</sub> . . . . .	101
3.4.2 Temperature dependence for the photocatalytic dehydrogenation of propan-2-ol on Pt(x)/TiO <sub>2</sub> . . . . .	103
a) Pt(0.25)/TiO <sub>2</sub> . . . . .	103
b) Pt(0.5)/TiO <sub>2</sub> . . . . .	104
c) Pt(2.0)/TiO <sub>2</sub> . . . . .	106

3.4.3	The effect of platinum content on reaction rate for the photocatalytic dehydrogenation of propan-2-ol ...	107
3.4.4	Light intensity dependence for the photocatalytic dehydrogenation of propan-2-ol ... ..	108
	a) Pt(0.25)/TiO <sub>2</sub> ... ..	108
	b) Pt(0.5)/TiO <sub>2</sub> ... ..	109
3.4.5	Temperature dependence for the photocatalytic dehydrogenation of propan-2-ol at different light intensities on Pt(0.5)/TiO <sub>2</sub> ... ..	112
	a) Full light intensity ... ..	112
	b) 20.2% relative light intensity ... ..	113
	c) 4.4% relative light intensity ... ..	115
3.4.6	Photocatalytic dehydrogenation of other alcohols at 278 K and 293 K on Pt(0.5)/TiO <sub>2</sub> ... ..	116
3.4.7	Temperature dependence for the photocatalytic dehydrogenation of other alcohols on Pt(0.5)/TiO <sub>2</sub> ... ..	118
	a) Methanol ... ..	118
	b) Ethanol ... ..	120
	c) Propan-1-ol ... ..	121
3.4.8	Dehydrogenation of propan-2-ol on Pt(0.5)/TiO <sub>2</sub> , hydrogen reduced at 753 K ... ..	122
	a) The dark reaction ... ..	122
	b) The photocatalytic reaction ... ..	123
3.4.9	Photocatalytic dehydrogenation of propan-2-ol on Pt(0.5)/TiO <sub>2</sub> pretreated with propan-2-ol vapour at 373 K	125
3.4.10	Photocatalytic dehydrogenation of propan-2-ol in a high purity helium atmosphere ... ..	126
3.5	Photocatalytic dehydrogenation of propan-2-ol on metallized anatase (other than Pt) ... ..	128

	<u>Page</u>
3.5.1 Temperature dependence for the photocatalytic dehydro- of propan-2-ol on Pd(0.5)/TiO <sub>2</sub> prepared by method B ...	128
3.5.2 Temperature dependence for photocatalytic dehydro- genation of propan-2-ol on Pd(0.5)/TiO <sub>2</sub> prepared by method C ... ..	129
3.5.3 Temperature dependence for the photocatalytic dehydro- genation of propan-2-ol on Rh(0.5)/TiO <sub>2</sub> prepared by method C ... ..	130
3.5.4 Photocatalytic dehydrogenation of propan-2-ol on Au(0.5)/ TiO <sub>2</sub> prepared by method C ... ..	131
3.5.5 Comparison between the activity of metallized anatase prepared by photodeposition (method B and C) for the photocatalytic dehydrogenation of propan-2-ol at 293 K	132

#### Chapter Four - Discussion

4.1 The photocatalytic oxidation of propan-2-ol on P-25 anatase ... ..	134
4.1.1 Introductory discussion ... ..	134
4.1.2 Preliminary experiments ... ..	135
4.1.3 Temperature dependence for propanone formation ... ..	137
4.1.4 Light intensity dependence for the photocatalytic oxidation of propan-2-ol ... ..	139
4.1.5 The mechanism for photocatalytic oxidation of propan-2-ol	144
4.2 Photocatalytic dehydrogenation of alcohols on metallized anatase ... ..	146
4.2.1 Introductory discussion ... ..	146
4.2.2 Catalyst mass effects ... ..	147
4.2.3 The effect of platinum content ... ..	149

	<u>Page</u>
4.2.4     The dark reaction on hydrogen reduced Pt(0.5)/TiO <sub>2</sub> ...	151
4.2.5     The temperature dependence of the photocatalytic dehydrogenation of propan-2-ol     ... ..	155
4.2.6     Temperature dependence for the photocatalytic dehydro- generation of other alcohols     ... ..	159
4.2.7     Light intensity dependence of the photocatalytic dehydro- generation of propan-2-ol     ... ..	162
4.2.8     The mechanism for photocatalytic dehydrogenation of alcohols on metallized anatase     ... ..	166
References     ... ..	169

## Chapter One

### INTRODUCTION

#### 1.1 General Introduction

Following the use of titanium dioxide in the first reported study of a photocatalytic reaction<sup>1</sup>, most investigations continued to use pure n-type semiconducting oxides as the photocatalyst. However, recent years have seen the development of metals deposited on semiconducting oxides as particularly active photocatalysts.

Photocatalysis on both pure and metallized semiconducting oxides relies on the absorption of photons with energy equal to, or greater than, the band gap of the oxide so that electrons are promoted from the valence band to the conduction band. If the photoelectrons and photoholes produced by this process migrate to the surface they may interact with adsorbed species in the elementary steps which collectively constitute photocatalysis. In addition to participating in conventional surface reaction steps, the supported metal assists in the separation of photoelectrons and photoholes which may otherwise recombine within the semiconductor particles<sup>2</sup>.

Amongst possible supported metals a partial coverage of platinum gives the highest photocatalytic activity; this is attributed to the particular ability of this metal to dissociate molecular hydrogen or recombine hydrogen atoms<sup>3,4</sup>. Suspensions of platinized titanium dioxide (Pt/TiO<sub>2</sub>) in liquid phase reactants have been observed to photocatalyse: the dissociation of water<sup>5,6</sup>, the decarboxylation of carboxylic acids<sup>7-9</sup>, the oxidation of hydrocarbons<sup>10</sup>, the radical polymerization of methyl methacrylate<sup>11</sup>, the dehydrogenation of alcohols<sup>12-14</sup> and the synthesis of amino acids from CH<sub>4</sub>, H<sub>2</sub>O and NH<sub>3</sub><sup>15</sup>. These reactions proceed at temperatures close to room temperature, but with widely different efficiencies.

## 1.2 Crystal morphology of $\text{TiO}_2$ and Metallized $\text{TiO}_2$

There are three polymorphic forms of  $\text{TiO}_2$ <sup>16</sup> namely, anatase (tetragonal), rutile (tetragonal) and the rare mineral brookite (orthorhombic), but only anatase and rutile are considered in catalytic work. The rutile form is more stable than anatase, which transforms irreversibly and exothermally to rutile in the temperature range of 880-1000 K<sup>17,18</sup>. Yoganarasimhan and Rao<sup>17</sup> reported that smaller particle size and larger surface area favour the transition.

The crystal structures of anatase and rutile are similar, and in each form Ti ions occupy body centred lattice sites with oxygen ions ( $\text{O}^{2-}$ ) in six fold coordination about them. Thus the oxygen ions are arranged in the form of a somewhat distorted octahedron. The difference in structure arises from the way in which the octahedra are linked together. In anatase each octahedron shares four of its edges with other octahedra, while in rutile each octahedron shares two of its edges with other octahedra, four corners are each shared with one octahedron and two corners are each shared with two octahedra<sup>19</sup>. The Ti-O bonds in anatase are nearly equal ( $1.91-1.95 \text{ \AA}$ ) to one another and to those of rutile, however, there are two short oxygen to oxygen separations ( $2.43 \text{ \AA}$ ) in anatase and one in rutile<sup>20</sup>. The O-O distance for the shared edges of the octahedra are shorter than the unshared edges<sup>21</sup>.

A structural comparison of bulk and finely divided anatase has recently been made using X-ray absorption fine structure (EXAFS)<sup>22</sup>. It was found that the interatomic distances within the octahedra for material in which 30% of the octahedra lay on the surface were identical with those for crystalline material. It follows that the true surface of anatase is not substantially different from models drawn from bulk crystallographic planes.

Bobyrenko et al.,<sup>23</sup> calculated the electronic components of the energy of conversion of anatase to rutile from the ultraviolet absorption spectra and concluded that rutile is more ionic than anatase.

Nonstoichiometry in  $\text{TiO}_2$ , which is responsible for many of the chemical and physical properties of the solid, is exhibited when it is in a reduced form  $\text{TiO}_{(2-n)}$ <sup>24,25</sup>; the structure is regarded as imperfect, with missing oxygen ions up to 0.034 ions per unit cell<sup>24</sup>. To compensate for the loss of negative charges, an equivalent amount of  $\text{Ti}^{4+}$  should be in a  $\text{Ti}^{3+}$  state<sup>25</sup>.

The structure of platinum on thin films of  $\text{TiO}_2$  has been investigated<sup>26</sup> using transmission electron microscopy (TEM) after reducing the sample at 825 K. The high resolution showed that the metal particles were predominantly hexagonal in outline and uniformly very thin, indicating a "pill-box" morphology. However, after oxidation in  $\text{H}_2\text{O}$  or  $\text{O}_2$ <sup>27</sup>, an appreciable increase in the size of Pt particles was observed, which remained hexagonal although no longer present as a thin "pill-box" structure.

The bulk of this chapter is concerned mainly with the properties of anatase and metallized anatase, since these catalysts are used throughout the present work. Comprehensive reviews by Grant<sup>28</sup> and Parfitt<sup>29</sup> give details of the rutile structure and its electrical properties.

### 1.3 The electronic properties of $\text{TiO}_2$ and Metallized $\text{TiO}_2$

The band theory of solids is a good model to describe both semi-conductivity and photoconductivity in solids. Semiconductors can be defined as a class of materials in which the electronic conductivity lies between that of insulators and good metallic conductors.

At  $0^\circ \text{K}$ , an intrinsic semiconductor or insulating oxide is characterised by a filled valence band and an empty conduction band. Electrons can be promoted from the valence band to the conduction band at temperatures above  $0^\circ \text{K}$ . Insulators have a large energy gap between the valence and conduction bands, whilst in an intrinsic semiconductor the band gap is smaller and thermally excited electrons can be promoted to the conduction band. This gives rise to electrical conductivity by both electrons and positive holes. However, introduction of donor levels below the conduction band or acceptor levels above the valence band increases the concentration of thermally generated current carriers giving rise to extrinsic semiconduction. Where such conduction is predominantly by electrons in the conduction band it is termed n-type semiconductivity, whilst predominant conduction by positive holes in the valence band is termed p-type semiconductivity<sup>30</sup>.

Pure stoichiometric  $\text{TiO}_2$  would be an intrinsic semiconductor with a band gap of  $\sim 3 \text{ eV}$  between the valence band and the conduction band. Earle<sup>31</sup> found that  $\text{TiO}_2$  is an electronic semiconductor in which the current carriers are free electrons. The electron donor level in  $\text{TiO}_2$  is produced by non-stoichiometry, which is created either by oxygen vacancies or by tri- and tetra-valent interstitial titanium ions, or by both, and consequently  $\text{TiO}_2$  is an n-type extrinsic semiconductor.

Both anatase and rutile crystals absorb strongly in the ultra-violet region; anatase absorbing light of wavelength  $< 400 \text{ nm}$  and rutile absorbing light of wavelength  $< 420 \text{ nm}$ . Companion and Wyatt<sup>32</sup>

reported that the reflectance spectra of rutile and anatase show absorptions beginning at 3.0 eV and 3.23 eV respectively. When  $\text{TiO}_2$  is illuminated with light of wavelength  $< 400$  nm, electrons will be promoted to the conduction band leaving positive holes in the valence band;



If the electrons and holes are used in a reaction, a steady state will be reached when the removal of electrons and holes equals the rate of generation by illumination. Recombination and trapping processes are the de-excitation processes which are responsible for the creation of the steady state if no reaction occurs.

There are three important mechanisms of recombination, namely, direct recombination, recombination at recombination centres and surface recombination. In direct recombination an electron from the conduction band drops directly into an unoccupied state in the valence band. With recombination centres an electron is captured first, which then electrostatically attracts and combines with a positive hole, thus leaving the centre free to trap another electron. The recombination centres are located at lattice sites within the bulk of the crystal. In the surface recombination the electrons and holes must diffuse to the surface before they recombine at sites on the crystal surface. Recombination<sup>33</sup> between photoexcited electrons and holes is followed by dissipation of the excess energy of the excited carriers. The dissipation can occur by:

- (i) Photon emission when the energy of each emitted photon equals the energy difference between the two carriers before recombination,
- (ii) Phonon emission where the total energy equals the excess energy to be dissipated, (iii) three body collisions where the excess energy is given up to a third carrier in what is called an "Auger" recombination.

Numerous techniques have been employed to investigate the properties of trap level in  $\text{TiO}_2$  and other materials. Addiss et al.,<sup>34</sup> used thermally stimulated current (TSC) and thermoluminescence (TL) with rutile crystals and detected the existence of a series of shallow electron traps ( $<1$  eV) below the bottom of the conduction band. The eight levels were characteristic of all the samples examined, being independent of the source of the crystal, orientation and extent of reduction. Gray<sup>35</sup> used TSC to establish the existence of six or more electronic levels in ultra pure anatase, and three or more additional levels in anatase doped with niobium. Ghosh et al.,<sup>36</sup> used measurements of photoconductivity, photoluminescence excitation spectra, electroreflectance spectra and optical and thermal bleaching of traps in addition to TSC and TL, to further investigate these traps. They were able to detect at least eight shallow-traps levels ( $<1$  eV) in rutile and discussed the assignment of one of these levels to oxygen vacancies. The properties of room temperature (310 K) electron traps in rutile were studied<sup>37</sup> by combining TSC and TL techniques with photoconductivity measurements and suggested that the trap may consist of two overlapping traps.

Breckenridge and Hosler<sup>38</sup> measured the electrical resistivity and Hall coefficient of rutile in the form of ceramic compacts and single crystals over the temperature range 83-775 K. Two types of donor centres were detected and it was suggested that these centres may be oxygen ion vacancies associated with one or two electrons trapped as  $\text{Ti}^{3+}$  ions. These two trap levels were detected by other workers<sup>39,40</sup> using transit time techniques to measure the photoconductivity of rutile single crystals over the temperature range 40-300 K.

Hillhouse and Woods<sup>41</sup> studied TSC in plasma grown rutile crystals and demonstrated the presence of at least six discrete electron trapping levels. They found that crystals from different sources consistently

contained three trapping levels with ionization energies of 0.13, 0.24 and 0.37 eV, and that the density of these traps increased when the crystals were chemically reduced. The same workers<sup>42</sup> subsequently determined values of trap depth, detrapping frequency, recombination rate constant, retrapping ratio and ratio of thermally disconnected to thermally connected traps. They used TSC and TL techniques in this study which confirmed the existence of the six discrete electron trapping levels.

The effects of adsorbed gases on trap levels have been observed with ultrapure and niobium doped anatase<sup>43</sup>, and the following levels have been identified: 0.05 eV and 0.12-0.13 eV, common to  $\text{TiO}_2$  pure and Nb doped; 0.24-0.28 eV, unique to Nb doped specimens; 0.34-0.36 eV, common to all samples and reflecting oxygen treatment; 0.41-0.42 eV, common to all samples but relatively insensitive to oxygen; 0.46-0.47 eV, apparently most affected by loosely held oxygen. Another six deeper lying levels were also reported to be present, but were not satisfactorily resolved or identified.

The effect of the adsorption of gases on photocurrents has been studied by many workers<sup>44-46</sup>. Addis and Wakim<sup>44</sup> investigated the effect of adsorbed oxygen on the photocurrent in  $\text{TiO}_2$  and considered the decrease in conduction to be due to the trapping of an electron from the conduction band by the oxygen molecules. The adsorbed gas thus acted as a recombination centre, which was confirmed by the observation that the photo-desorption of oxygen increased the current due to the return electrons to the conduction band.

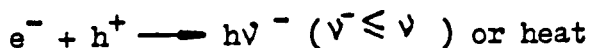
The wavelength dependence of the time to achieve a steady photocurrent in single crystal  $\text{TiO}_2$  was studied by Wakim<sup>47</sup>. He observed that the photocurrent growth time increased more slowly with shorter wavelengths, due to decreased penetration leading to increased surface

recombination. Peaks in TSC, produced in 404 nm irradiated  $\text{TiO}_2$ , were higher than those produced by 390 nm radiation. An explanation for this was that a larger number of traps were filled by the more deeply penetrating 404 nm radiation.

Metallized  $\text{TiO}_2$  shows great potential as a photocatalyst<sup>48</sup>, but there is little work published on the characterisation of its physical properties. When these systems are illuminated, photoelectrons generated in the  $\text{TiO}_2$  are considered to pass to the metal particles deposited on the semiconductor, whilst photoholes are trapped at the  $\text{TiO}_2$  surface by adsorbed reactant species<sup>49</sup>.

Kao et al.,<sup>50</sup> used ultraviolet photoelectron spectroscopy (UPS), Auger electron spectroscopy (AES), low energy electron diffraction (LEED) and X-ray photoelectron spectroscopy (XPS) to study the electronic properties and the surface structure of rutile and the  $\text{Ni/TiO}_2$  interface. They concluded that the amount of charge transfer between  $\text{Ni}$  and  $\text{TiO}_2$  surface depended on how the  $\text{TiO}_2$  surface was treated before  $\text{Ni}$  deposition, which explained why methanation activity depended on the nature of the support. They found that the amount of electron transfer to  $\text{Ni}$  decreased with decreasing  $\text{O/Ti}$  ratio (obtained by different annealing temperatures) on the  $\text{TiO}_2$  surface. The authors<sup>50</sup> concluded that electron transfer proceeded via  $\text{Ni-O}^{2-}$  interaction, so that the oxygen vacancies produced with increasing  $\text{O/Ti}$  ratio initiated electron transfer to the nickel.

Disdier et al.,<sup>51</sup> measured the photoconductivity of a series of  $\text{Pt/TiO}_2$  powders containing from 0.05 to 10 wt%  $\text{Pt}$ , and found that the presence of  $\text{Pt}$  above 1 wt% caused a decrease in the equilibrium photoconductance under vacuum. They attributed this to electron transfer from the titania to the platinum which they considered to be an advantage in photocatalytic reactions, since it can be envisaged as a decrease in electron-hole recombination:



Hope and Bard<sup>52</sup> used current-voltage measurements, as a function of surface preparation, to study the nature of the electrical contact between Pt and reduced single-crystal  $\text{TiO}_2$ . They found that direct current (dc)-voltage (I-V) curves demonstrated significant variations with surface preparation and the curve shape depended upon the degree of reduction of the  $\text{TiO}_2$ , the direction of the potential scan and sample history. They also noticed a strong alteration of the electrical properties of the contact when the sample was thermally treated, where extended annealing produced low-resistance ohmic-junctions. Surface atomic Pt/Ti ratios were calculated<sup>53</sup> from the XPS peak areas and found to decrease from 0.11 to 0.07 upon reduction at 773 K. It was concluded that changes in surface morphology and surface contamination could account for the observed Pt/Ti variation. However, electrical conductivity measurements<sup>53</sup> showed that the reduced Pt/ $\text{TiO}_2$  had a lower specific electrical conductivity than the non-reduced sample and the decrease was attributed to electrons being retained at the surface of Pt particles, or species attached to the Pt, thereby decreasing the conduction electron density.

Chung and Weissbard<sup>54</sup> studied the composition, structure and electronic properties of the strontium titanate ( $\text{SrTiO}_3$ ) surface and the platinum-strontium titanate interface using AES, LEED, UPS and electron energy loss spectroscopy (EELS). They concluded from these measurements that, there was some degree of ordering when Pt was deposited on the  $\text{SrTiO}_3$  surface and the platinum deposition resulted in the removal of surface  $\text{Ti}^{3+}$  by loss of electrons to Pt.

#### 1.4 Deposition of Metals on TiO<sub>2</sub>

Several methods have been used to load metals on TiO<sub>2</sub> supports. These, included photodeposition<sup>2,3,55-59</sup>, impregnation<sup>4,13,14,60-66</sup> and ion-exchange<sup>6,67</sup> methods.

Photodeposition methods, in general, involve the ultra-violet irradiation of a semiconductor powder suspended in a solution containing the metal salt and an electron donor such as ethanoic acid<sup>55</sup> or ethanal<sup>56</sup>. This method was first used in 1978 by Kraeutler and Bard<sup>55</sup>, who described it as a general method of catalyst preparation. Highly dispersed small clusters of the metal (Pt) on the lightly doped support surface (TiO<sub>2</sub>) were obtained due to the low temperature conditions ( $328 \pm 3$  K) which minimised surface diffusion of metal atoms. The dark deposit was shown by electron spectroscopy for chemical analysis (ESCA) to be Pt<sup>0</sup> with two signals at 75.4 and 71.85 eV. However, Koudelka *et al.*,<sup>68</sup> used ESCA and cyclic voltammetry to investigate the nature of the platinum photodeposited on an anatase film supported by metallic titanium from acetate buffered H<sub>2</sub>PtCl<sub>6</sub>. Incomplete reduction to Pt<sup>0</sup> was observed, but with aqueous K<sub>2</sub>PtCl<sub>6</sub> complete reduction to Pt<sup>0</sup> was readily achieved. Bickley<sup>48</sup> considered that the efficiency of this method was mainly due to the irreversibility of oxidative decarboxylation of acetate.

Dunn and Bard<sup>59</sup> studied the pH dependence of Pt deposition rate on TiO<sub>2</sub> and found the highest rate over the pH range 5-6. They also reported that photodeposition could occur in the absence of ethanoic acid where H<sub>2</sub>O plays the role of the electron donor and is oxidized with a lower efficiency.

In the procedure used by Gratzel *et al.*,<sup>56,57</sup> and Mills<sup>69</sup>, metal ions are reduced by conduction band electrons of TiO<sub>2</sub>, while holes

created under illumination are used to oxidise methanal, and methanol.

In the impregnation technique, the  $\text{TiO}_2$  is impregnated with an aqueous solution of metal salt such as Rh, Pt, Ni, Ir, Ru or Pd chloride or alternatively Ni or Rh nitrate<sup>62-66</sup>, and dried before reduction in flowing hydrogen at the desired temperature. However, Dybowski *et al.*,<sup>60,61</sup> impregnated the  $\text{TiO}_2$  with Rh from a solution of  $\text{Rh}(\text{NO}_3)_3$  containing small amount of ammonium hydroxide. The addition of  $\text{NH}_4\text{OH}$  keeps the pH of the solution high, to prevent modification of the support during treatment and to form a rhodium-ammonia complex. High dispersion of the metal on the support resulted from this technique<sup>60</sup>.

Ion-exchanged Pt/ $\text{TiO}_2$  catalyst were prepared<sup>6</sup> by dropwise addition of hexachloroplatinic acid ( $\text{H}_2\text{PtCl}_6$ ) to a stirred aqueous suspension of  $\text{TiO}_2$ . The solution was stirred until equilibrium was established, then the slurry was dried before reduction in a hydrogen stream. It was found<sup>6</sup> that ion-exchange with  $\text{Pt}(\text{NH}_3)_4(\text{OH})_2$  yielded a catalyst with a more even distribution of platinum particles than impregnation and ion exchange with  $\text{H}_2\text{PtCl}_6$ . Takeuchi and Katzer<sup>67</sup> found that Rh/ $\text{TiO}_2$  prepared by ion-exchange from  $\text{Rh}(\text{NO}_3)_3$  solution had an extremely high degree of Rh dispersion. The combined ion-exchange and impregnation techniques<sup>70</sup> was found to lead to a rather well-dispersed metal phase on the  $\text{TiO}_2$  support.

Pichat *et al.*,<sup>14</sup> found that the optimum photocatalytic activity for alcohol dehydrogenation was achieved at low Pt contents in the range 0.1-1.0 wt%. Mills and Porter<sup>5</sup> reported that the rate of water reduction using a platinized anatase photocatalyst was a function of Pt content, possessing a maximum activity at ca 0.5 wt%. They concluded that a Pt content greater than 0.5 wt% was not only unnecessary but was also detrimental towards the rate of hydrogen production. Other workers<sup>6</sup> found a maximum activity for photocatalytic hydrogen generation

from water cleavage at 0.5 wt% when  $\text{TiO}_2$  was impregnated with  $\text{H}_2\text{PtCl}_6$  from alcoholic solution. The mean dimension of the  $\text{Pt}^0$  crystallites formed on the  $\text{TiO}_2$  by this method remained at  $\sim 34 \text{ \AA}$  up to a Pt content of 2 wt%.

## 1.5 Adsorption on $\text{TiO}_2$ and Metallized $\text{TiO}_2$

A heterogeneous photocatalytic reaction can be defined as a reaction in which at least one of the following processes:

- (i) adsorption of reactants,
- (ii) reaction of adsorbed species,
- (iii) desorption of products,

is isothermally enhanced by the absorption of light by the catalyst. Therefore it is pertinent to discuss adsorption phenomena when considering photocatalysis.

### 1.5.1 Water

The adsorption of water and the nature of the hydroxyl groups on  $\text{TiO}_2$  surfaces has been studied extensively using different experimental techniques; infrared spectroscopy (IR) and temperature programmed desorption (TPD) being those most frequently used.

Yates<sup>71</sup> investigated the surface properties of anatase and rutile by the IR technique. He detected residual molecular water after evacuation at 423 K, whilst after evacuation at 623 K, only OH groups were detected on the surface. Two forms of adsorbed molecular water were subsequently detected on the rutile surface<sup>72,73</sup>. The first was hydrogen bonded to surface hydroxyl ions and was desorbed by evacuation at room temperature, whilst the second was coordinated to surface cations and was desorbed by evacuation at 473 K<sup>73</sup>.

Jones and Hockey<sup>74</sup> reported two types of surface sites on rutile for the adsorption of molecular water, they also found two types of hydroxyl groups on rutile outgassed at room temperature. An extensive IR study of  $\text{TiO}_2$  was made by Griffiths and Rochester<sup>75</sup> who detected and assigned a large number of bands. They suggested that there were two types of hydroxyl group, isolated hydroxyls on single  $\text{Ti}^{4+}$  ions and OH

groups acting as bridges between two adjacent  $\text{Ti}^{4+}$  ions. These groups were ionic and oriented perpendicular to the surface. The authors agreed that molecular water was adsorbed in both hydrogen bonded and coordinated forms. IR studies of the adsorption of various compounds on rutile at both the solid/liquid and solid/vapour interfaces<sup>76-79</sup> have indicated the presence of subsurface hydroxyl groups which result from the transfer of a proton from bridging OH groups to adjacent subsurface oxide ions.

Munuera and co-workers<sup>80</sup> concluded that the amount of hydroxyl plus molecular water on 100% hydroxylated anatase surface was approximately equivalent to a monolayer of hydroxyl groups. They concluded that about half of the monolayer was molecular water which desorbed at temperature  $< 473$  K, while the rest was composed of OH groups. In pure anatase half of the surface OH groups, determined by deuterium exchange, were fairly strongly acidic<sup>81</sup>.

Morterra et al.,<sup>82</sup> used IR spectroscopy to investigate the dehydration of anatase surfaces over the range 298-673 K, they found that the desorption of 8 water molecules led to the formation of one coordinatively unsaturated  $\text{Ti}^{4+}$  in the surface.

Recently Tanaka and White<sup>83</sup> studied the adsorption of water on reduced and oxidised anatase using IR spectroscopy. They found that both the extent of adsorption and the thermal stability of adsorbed molecular water was greater on the oxidised surface than on the reduced surface. However, the relative amount of OH formed upon exposure to water was greater on the reduced surface. The authors suggested that reduction of anatase leads to the formation of surface  $\text{Ti}^{3+}$  ions and that these sites were active for the dissociation of water resulting in enhanced OH formation.

The IR spectrum of surface OH groups and of coordinated water

together with the effects of reduction and rehydration processes, have been studied for anatase from titanium tetrachloride<sup>84</sup> and titanyl sulphate<sup>85</sup> precursors. The authors discussed the role of the impurities in the reduction process.

A decrease in work function and an increase in electrical conductivity of  $\text{TiO}_2$  on water adsorption<sup>86</sup> was explained in terms of a partial donation of the lone pair of electrons on the oxygen of the water into the reactant d-orbitals of surface  $\text{Ti}^{4+}$  ions.

Bickley and Jayanty<sup>87</sup> studied the effect of physisorbed oxygen on the desorption of water observed by TPD, and more details of this work will be explained in section (1.5.2).

The dehydration of  $\text{Pt/TiO}_2$  at 773 K was studied by Huizinga and Prins<sup>70</sup>. Electron spin resonance (ESR) indicated that the dehydration of the support took place in the neighbourhood of the metal particles, and as a result a reduced form of  $\text{TiO}_2$ ,  $\text{Ti}_4\text{O}_7$  was produced. The formation of  $\text{Ti}_4\text{O}_7$  had previously been reported<sup>26</sup>, when supported metal catalysts were reduced at high temperatures and was believed to arise from strong metal support interaction (SMSI).

### 1.5.2 Oxygen

The chemisorption of oxygen is associated with transfer of thermal electrons from the conduction band of the n-type semiconducting  $\text{TiO}_2$  to the oxygen molecule. The space charge which arises at the oxide surface as a result of the electron transfer influences both further chemisorption and photosorption of oxygen. Since the concentration of electrons in the conduction band is limited, the equilibrium coverage of chemisorbed oxygen is low (  $\sim 1\%$  of a monolayer) as might be expected for depletive chemisorption.

The predominant form of oxygen adsorbed on  $\text{TiO}_2$  is the  $\text{O}_2^-$  ion according to ESR measurements on slightly reduced oxide samples<sup>88-92</sup>. Davydov et al.,<sup>93</sup> reported an increase in the ESR signal from  $\text{O}_2^-$  ions when oxygen was adsorbed on progressively more reduced anatase surfaces. Mikheikin and co-workers<sup>91</sup> observed an ESR signal which was later shown to be due to  $\text{O}_2^-$  ions<sup>94</sup>. Two types of  $\text{O}_2^-$  resulting from oxygen adsorption at 87 K were detected<sup>95</sup>. Iwamoto et al.,<sup>96</sup> observed three types of ion radical  $\text{O}_2^-$  in the presence of oxygen molecules or during dissociative adsorption on partially reduced anatase. The authors thought these three types arose from their association with different  $\text{Ti}^{4+}$  surface sites. Other forms of adsorbed oxygen have been reported, including  $\text{O}^-$ <sup>92,97</sup>, uncharged atomic oxygen<sup>93</sup> and  $\text{O}_4^-$  complexes<sup>90</sup>.

Photoadsorption of oxygen on  $\text{TiO}_2$  occurs in a similar manner to chemisorption. It is only observed during irradiation with incident light that is absorbed by the oxide, and is dependent upon the ability of photoelectrons to reach the surface for electron transfer to proceed. The electrons can reach the surface to interact with an acceptor molecule only when they are separated from the photoholes and recombination is prevented. The space charge layer at the surfaces due to the chemisorption of oxygen creates an electric field which aids separation

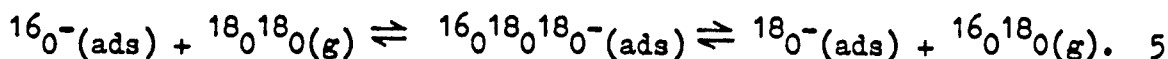
of the electrons and holes.

An early study by Kennedy et al.,<sup>98</sup> reports an irreversible uptake of oxygen on thin films of  $\text{TiO}_2$  when illuminated with 365 nm radiation. They considered the adsorption to be dissociative with the formation of  $\text{O}^-$  surface species:-



The rate of oxygen uptake was proportional to the light intensity and was determined by square root pressure relationship. McLintock and Ritchie<sup>99</sup> observed a similar result and also noted a decrease in photoconductivity with adsorption. The authors considered that  $\text{O}_2^-$  species were the reactive intermediates involved in the photooxidation of various hydrocarbons.

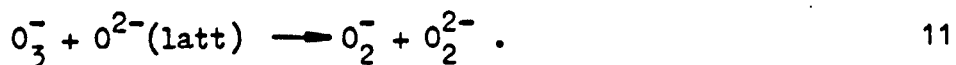
Several workers<sup>46, 100-103</sup> identified the existence of the  $\text{O}^-$  ion in photoadsorption experiments. Tanaka<sup>100</sup> studied the photocatalytic equilibrium of oxygen isotopes on  $\text{TiO}_2$ . The reaction was extremely rapid and the  $\text{O}_3^-$  species was suggested as possible intermediate species. Nikisha et al.,<sup>101</sup> also considered the  $\text{O}_3^-$  species to be the active intermediate in the oxygen isotope exchange reaction:-



Meriaudeau and Vedrine<sup>104</sup> reported the existence of the  $\text{O}_3^{3-}$  species at 77 K and suggested that it was produced from the reaction of  $\text{O}^{2-}$  ions with adsorbed oxygen and photoelectrons:

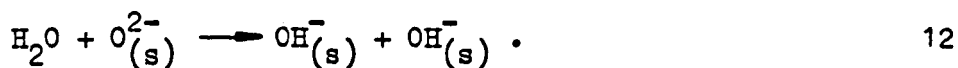


From ESR measurements the existence of  $O_2^-$ ,  $O_3^-$  and  $O_3^{3-}$  on anatase was reported by Gonzalez-Elipe and co-workers<sup>105</sup>. They concluded that  $O_3^-$  was produced from the reaction of adsorbed molecular oxygen with photoholes (trapped at surface  $O^{2-}$  in the form of reactive  $O^-$ ), and thus photoholes could initiate reactions, such as:

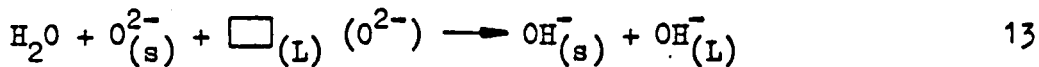


Bickley and Stone<sup>106</sup> showed that the photoadsorption of oxygen on  $TiO_2$  obeyed a parabolic law (i.e. uptake varying with the square root of time) suggesting that a surface diffusion process was the rate controlling step. The authors found anatase less active than rutile, possibly due to the stronger absorbance of rutile for light near the visible range. Rutile doped with 0.3 mol.%  $Nb_2O_5$  had a similar activity to that of pure rutile suggesting that niobium existed either as  $Nb^{4+}$  ions or as  $Nb^{5+}$  with strongly associated electrons. They also observed that the activity decreased when the  $TiO_2$  had been previously outgassed at high temperatures (1073 K), and the activity could be destroyed completely by prolonged outgassing. However, since the activity could be partially restored by exposing the  $TiO_2$  to water vapour, the authors<sup>106</sup> concluded that adsorbed water was involved in the photoadsorption process. Surface hydroxyl groups resulting from the dissociative chemisorption of water were responsible for the photoactivity. Three mechanisms for the dissociative chemisorption of water were presented:

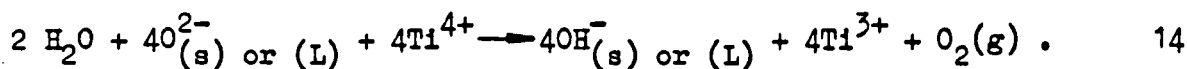
1 - Dissociative chemisorption at a surface  $Ti^{4+} O^{2-}$  pair leading to surface hydroxyl ions  $OH_{(s)}^-$ ,



2 - Dissociative chemisorption of water accompanied by annihilation of pre-existing subsurface anion vacancies  $\square_{(\text{L})}$  ( $\text{O}^{2-}$ ) producing surface  $\text{OH}_{(\text{s})}^-$  and bulk  $\text{OH}_{(\text{L})}^-$  ,



3 - High temperature dissociative chemisorption involving surface or lattice oxide ions ( $\text{O}_{(\text{s})}^{2-}$  or  $(\text{L})$ ) with simultaneous release of oxygen gas:



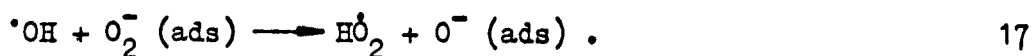
The chemisorption of oxygen in the dark was suggested<sup>106</sup> to create a space charge normal to the surface which favours the movement of photoholes to the surface, and the hydroxyl groups formed by the previous mechanisms act as traps for photoholes,



Consequently photoelectrons were then free to participate in the adsorption of oxygen,



When the illumination ceased, no desorption of oxygen occurred, suggesting that the trapped hole was stable. A reaction between the  $\cdot\text{OH}$  radical and adsorbed  $\text{O}_2^-$  , arriving by surface diffusion, was considered possible:



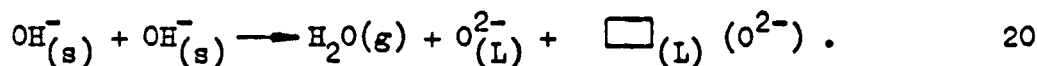
It was then suggested that in the dark the perhydroxyl radical,  $\text{HO}_2^\cdot$  , captured an electron forming the perhydroxyl ion  $\text{HO}_2^-$  :



The perhydroxyl ion was considered to be a more efficient hole trap than the hydroxyl ion and hence the activity increased when the sample was exposed to a second period of illumination.



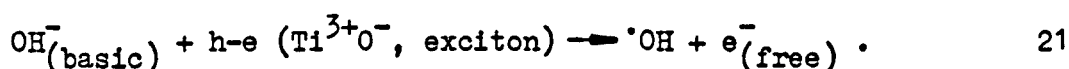
By carefully controlling the conditions of outgassing, Bickley and Jayanty<sup>87</sup> have shown that the activity of rutile for oxygen photoadsorption disappeared concomitantly with the disappearance of a peak at 573 K in the TPD spectrum of water on  $\text{TiO}_2$  which arose from the condensation of hydroxyl groups:



Hence a direct relationship between surface  $\text{OH}^-$  groups and oxygen photoadsorption was established and the modification of the water desorption spectrum by oxygen photoadsorption supported this mechanism. The authors observed that molecular water did not play an important role in the photoadsorption process and proposed a mechanism similar to that of Bickley and Stone<sup>106</sup>.

In a study of the photoadsorption of oxygen on fully hydroxylated anatase surface, Munuera et al.,<sup>80</sup> observed a fast uptake of oxygen ( $P_{\text{O}_2} = 1.5 \text{ Pa}$ ) in the early stages of illumination, followed by a slow photodesorption of oxygen. At higher pressures ( $P_{\text{O}_2} \sim 100 \text{ Pa}$ ), no photodesorption was observed and this was thought to be due to the masking of the desorption by increased photoadsorption. Photodesorbed water was also detected. The photoadsorption of oxygen was found to decrease with increasing outgassing temperature, and was eliminated by outgassing at temperatures  $> 573 \text{ K}$ . After low temperature outgassing, photoadsorption obeyed first order kinetics, but after outgassing at higher temperatures, which resulted in low hydroxyl coverages, the process

became diffusion controlled. The authors<sup>80</sup> noted that molecular water and the most acidic OH groups, which are removed at lower temperatures (IR bands at 3680 and 3620  $\text{cm}^{-1}$ ), did not greatly influence the photoactivity of the sample. However, the removal of the most basic OH groups (IR band at 3730  $\text{cm}^{-1}$ ) at temperatures  $> 573 \text{ K}$  resulted in the decay of photoactivity. Thus the interaction of excitons with basic  $\text{OH}^-$  groups was considered as an important step in photoadsorption:



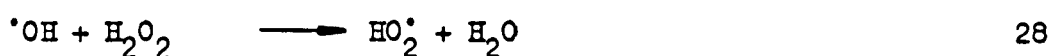
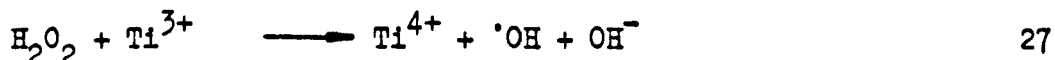
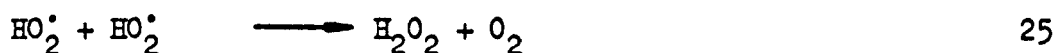
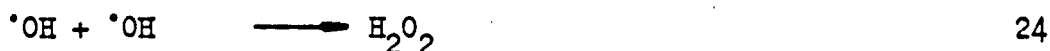
It was postulated that the excitons ( $\text{Ti}^{3+}\text{O}^-$  pairs), generated in the subsurface atomic layers by irradiation, diffused to the surface through easy pathways to reach a small number of "porthole sites" at the surface, where they immediately diffused to react with nearby basic  $\text{OH}^-$  groups. However, when the  $\text{TiO}_2$  surface was highly hydroxylated, photohole capture was fast and a steady state was rapidly established upon illumination, consequently free electrons were generated at a constant rate and were either trapped by gaseous oxygen or recombined with photoholes. Under these conditions the photoadsorption followed pseudo first-order kinetics with respect to oxygen pressure. As the reaction progressed, or as the outgassing temperature was raised, the number of  $\text{OH}^-$  groups in the neighbourhood of the "porthole sites" decreased and the excitons had to diffuse further to react with  $\text{OH}^-$  groups. After extended illumination the process became diffusion controlled (viz Bickley and Stone<sup>106</sup> who considered the control to be due to  $\text{O}_2^-$  diffusion). The authors<sup>80</sup> further speculated that the "porthole sites" were highly acidic  $\text{Ti}^{4+}$  ions, polarising their neighbouring  $\text{O}^{2-}$  lattice ions and the transfer of one electron give  $\text{Ti}^{3+}\text{O}^-$  pair (exciton).

In further studies Munuera and co-workers<sup>105, 107</sup> studied the radical intermediates formed by photoadsorption of oxygen on an anatase

surface, and discussed the role of hydrogen peroxide in the photo-desorption of oxygen. They concluded that on hydroxylated and dehydroxylated surfaces the reaction of excitons with the basic hydroxyl groups was the initiating step. The authors<sup>107</sup> proposed two reaction schemes to account the difference between hydroxylated and dehydroxylated surfaces for photoadsorption and photodesorption of oxygen.

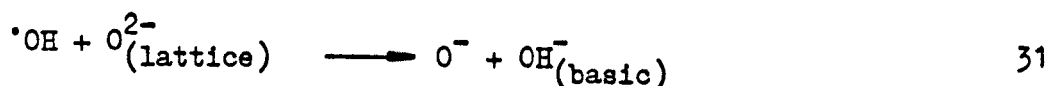
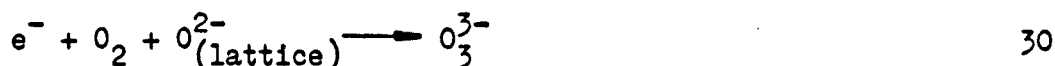
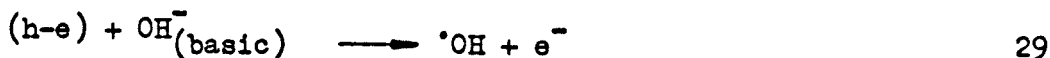
### Scheme 1

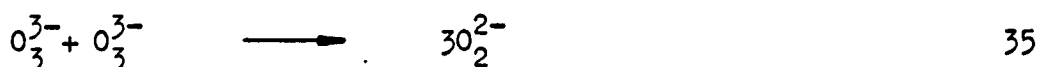
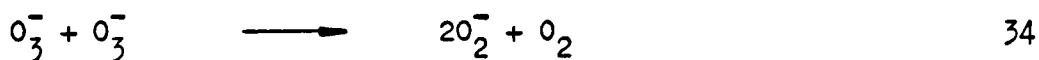
#### Hydroxylated Surfaces



### Scheme 2

#### Dehydroxylated Surfaces





The authors<sup>107</sup> considered that the difference in step 23 and 30 differentiated between the surfaces.

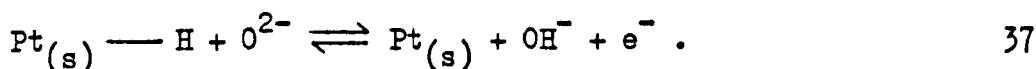
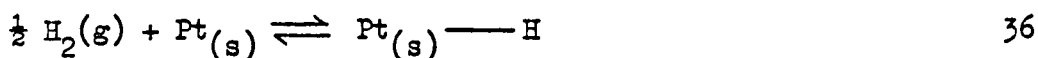
Munuera et al.,<sup>108</sup> studied the photoadsorption of oxygen on the dehydroxylated surface of anatase, and found that the photoadsorption was enhanced by chlorination. ESR spectra (at 77 K) showed progressive loss of  $O_3^-$ ,  $O_2^-$  and  $O_3^{3-}$  with chlorination, and the formation of a new signal due to  $ClO\cdot$  radicals. The authors reported that oxygen photoadsorption resulted in the oxidation of  $Cl^-$  to  $ClO^-$ . Photoadsorption and photodesorption of oxygen on oxide surfaces has been extensively reviewed by Bickley<sup>109</sup>.

Oxygen chemisorption on titania-supported metals was first investigated by Smith et al.,<sup>110</sup> who studied  $Ni/TiO_2$  with Ni contents between 1.5 and 12.3 wt%. They observed that oxygen adsorption increased with increasing the percentage reduction of nickel salt to nickel metal, and that adsorption was much higher on supported metal catalyst than on pure  $TiO_2$ . The authors<sup>110</sup> assumed that lower oxygen adsorption on pure  $TiO_2$  was because the nickel catalyses reduction to nonstoichiometric oxide, which adsorbs more oxygen than  $TiO_2$ . An ESR signal characteristic of  $O_2^-$  was observed<sup>65</sup>, when oxygen was adsorbed at 293 K on  $Pt(4.8)/TiO_2$  and  $Ir(2.7)/TiO_2$  following sample reduction at 473 K.

$Pt(0.5)/TiO_2$  and  $Pt(5.0)/TiO_2$  have been studied by Herrmann and Pichat<sup>111</sup> in an in situ investigation of electrical conductivity in hydrogen, oxygen and hydrogen-oxygen titration at 295 K following hydrogen reduction at either 473 K or 773 K. The authors followed two hypotheses to explain their results:

1 - In hydrogen reduction, the hydrogen atoms chemisorbed on the

platinum migrate to the  $O^{2-}$  sites on the  $TiO_2$  by "spillover" and an electron is released for each group formed:



2 - The conductivity of the reduced catalysts decreased under vacuum at 295 K due to an "electron pumping" effect of the platinum, which appears more substantial at low temperature (295 K). This arises from the exothermicity of the following equation ( $\Delta H < 0$ ), which corresponds to the electron affinity of the deposited platinum:

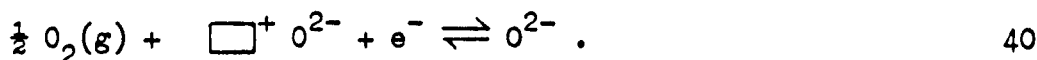


( $ePt^-$  represents an electron trapped by Pt).

The authors<sup>111</sup> found that oxygen adsorption decreased the electrical conductivity in the case of both low and high temperature treated samples. They attributed this to the generation  $Pt_{(s)} - O$  species on the metal, stoichiometrically represented by;



and to the filling of the anion vacancies of the oxide ( $\square^+ O^{2-}$ ),

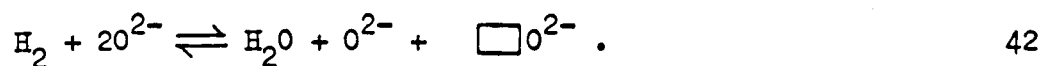


Here  $\square^+ O^{2-}$  is an ionized vacancy with one trapped electron (effectively a positive entity), which results from the ionization of the first electron of two in an anion vacancy ( $\square O^{2-}$ ),



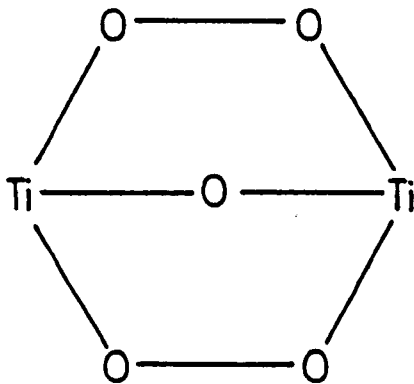
The anion vacancies were considered to arise from the formation of hydroxyl groups and the subsequent dehydration of the surface during

reduction; represented overall by:



The photo-uptake of oxygen by Rh/TiO<sub>2</sub> dispersions was studied by Yesodharan and Gratzel<sup>112</sup>, by degassing the reaction system in argon and subsequently injecting 1 cm<sup>3</sup> of oxygen. They observed that irradiation for 6 h removed 75% of the injected oxygen. Since there was a lack of oxygen production during the photodecomposition of water on metal loaded TiO<sub>2</sub> particles, the authors assumed that this was due to the photosorption of oxygen by the TiO<sub>2</sub> particles. The nature of the "stored" oxygen was tentatively identified as  $\mu$ -peroxo-bridged Ti-species (figure 1.1).

Figure 1.1



### 1.5.3 Hydrogen

Hydrogen behaves as an electron donor, so that electron transfer from hydrogen into the vacant levels of the  $\text{TiO}_2$  conduction band might be expected. However, experimental studies show that hydrogen chemisorption on pure  $\text{TiO}_2$  is extremely small<sup>61</sup>. It follows that such electron transfer must be energetically unfavourable.

Apple et al.,<sup>60</sup> have used NMR, ESR and TPD to study the adsorption of hydrogen on  $\text{TiO}_2$  and metallized  $\text{TiO}_2$ . They observed that the adsorption of hydrogen by pure  $\text{TiO}_2$  was extremely small relative to that on Rh (3.8)/ $\text{TiO}_2$ . The authors detected two forms of hydrogen on Rh (3.8)/ $\text{TiO}_2$ , one irreversibly bound to the metal and the other reversibly bound to the oxide support.

Since neither type of adsorbed hydrogen was observed on pure  $\text{TiO}_2$ , the metal is necessary to activate the hydrogen and lead to the formation of both reversibly and irreversibly bound hydrogen. No hydrogen adsorption was detected on either reduced or unreduced  $\text{TiO}_2$ <sup>61,113</sup> which agrees with the observation that  $\text{TiO}_2$  was inactive in hydrogen-deuterium equilibration<sup>53</sup>.

ESR observations by Huizinga and Prins<sup>70</sup> also demonstrated that the reduction of  $\text{TiO}_2$  by hydrogen was catalyzed by platinum ( $\text{Pt}(2.0)/\text{TiO}_2$ ) and apparently hydrogen chemisorbs dissociatively on the metal, after which the hydrogen atoms diffuse to the support and reduce  $\text{Ti}^{4+}$  to  $\text{Ti}^{3+}$ :



Tauster et al.,<sup>114</sup> found that the reduction of noble metal salts supported on  $\text{TiO}_2$  at 473 K produced well dispersed metal, which exhibited a high capacity for hydrogen adsorption. However, the reduction at 773 K

decreased the hydrogen chemisorption to near zero. Electron microscopy and X-ray diffraction showed that the loss of hydrogen adsorption capacity was not due to sintering or agglomeration of the metal particles on the surface of  $\text{TiO}_2$ . The authors<sup>114</sup> considered that SMSI was responsible for the loss of activity.

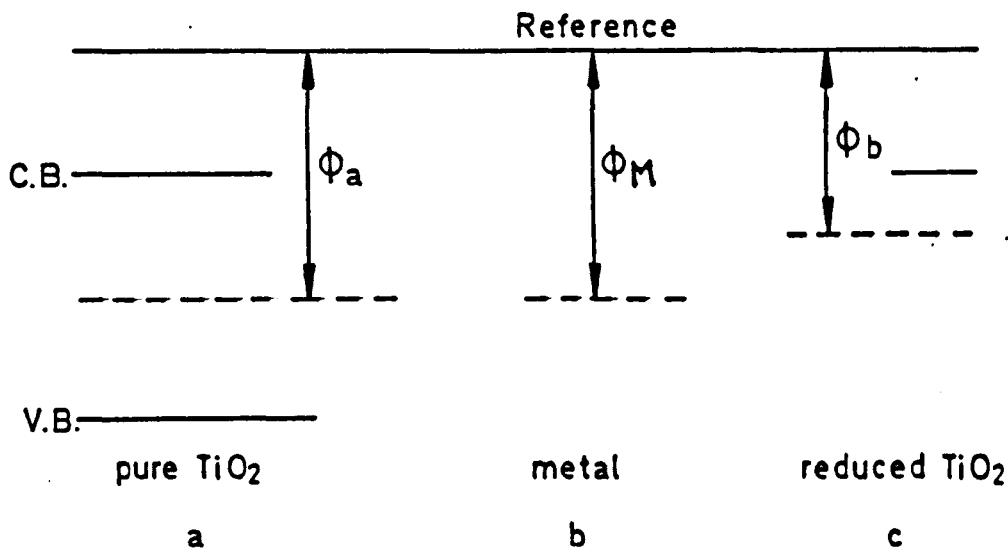
Many workers<sup>63,115-120</sup> have reported the generation of SMSI arising from the reduction of supported metal catalysts at high temperatures, and numerous attempts have been made to explain the phenomenon.

Tauster et al.,<sup>121</sup> considered that electrons are transferred from reduced cations in the transition metal oxide support to the metal particles. This electron transfer was held responsible for the profound changes in the catalytic and chemisorption properties and the morphology of the metal particles. The first convincing evidence for the transfer of electrons between metal particles and their support was produced by Schwab<sup>122</sup> and by Solymosi<sup>123</sup>. The driving force for this electron transfer is the difference in energy between the two Fermi levels, which can be altered by changing the semiconducting character of the support.

Horsley<sup>124</sup> made molecular orbital calculations of the interaction between platinum atoms in anion vacancies and  $\text{Ti}^{3+}$  cations, and concluded the existence of metal-metal bonding with donation from titanium  $\text{Ti}^{3+}$  cations to platinum atoms. Katzer et al.,<sup>125</sup> also observed charge transfer between Rh and  $\text{TiO}_2$  in  $\text{Rh}(0.95)/\text{TiO}_2$  reduced at 473 K. However, Meriaudeau and co-workers<sup>65</sup> obtained data which disagreed with electron transfer being the source of SMSI. Reduction of  $\text{TiO}_2$  supported metal at 473 K and 773 K produced  $\text{Ti}^{3+}$  cations, while only reduction at 773 K produced SMSI. ESR spectroscopy of Y zeolite in which  $\text{Ti}^{3+}$  and  $\text{Rh}^0$  were located within the supercages retained the  $\text{Ti}^{3+}$  signal. It follows that close proximity of the  $\text{Ti}^{3+}$  and  $\text{Rh}^0$  is not alone responsible for

SMSI, hence the authors<sup>65</sup> suggested a mechanism for SMSI involving the collective property of electrons in reduced  $\text{TiO}_2$ . The Fermi levels of pure  $\text{TiO}_2$ , metal (Pt) and strongly reduced  $\text{TiO}_2$  are represented in a, b and c of figure 1.2.

Figure 1.2



The Fermi level of the metal is located near the Fermi level of pure  $\text{TiO}_2$  (work functions ( $\phi$ ) are 5.6 and 5.5 eV respectively). The reduction of  $\text{TiO}_2$  at high temperature produces a high concentration of surface defects ( $\text{Ti}^{3+}$  ions and oxygen vacancies), and consequently the work function ( $\phi_b$ ) decreases to 4.6 eV. Hence the Fermi level of reduced  $\text{TiO}_2$  becomes higher than that of the metal, and when the metal particles are in contact with reduced  $\text{TiO}_2$ , there is a flow of electrons from the reduced  $\text{TiO}_2$  to the metal and as a result a negative charge develops on the metal particles. This interpretation of Meriaudeau *et al.*,<sup>65</sup> agrees with recent work by Chen and White<sup>126</sup> on the cause of SMSI. These authors<sup>126</sup> concluded from ESR spectra for  $\text{Pt}(2.0)/\text{TiO}_2$ , with and without

potassium nitrate, that surface  $\text{Ti}^{3+}$  are not required for suppression of hydrogen chemisorption, and they attributed the loss of hydrogen chemisorption capacity to electron transfer from K to Pt. However, Spencer<sup>127</sup> concluded that the loss of hydrogen chemisorption capacity on  $\text{Pt/TiO}_2$  catalyst by potassium compounds arises from  $\text{TiO}_2$  redistribution promoted by  $\text{K}_2\text{TiO}_3$  and not from electron donation from K to Pt. SMSI has recently been reviewed by Bond and Burch<sup>128</sup>.

The second type of metal-support interaction involves the spillover of adsorbed species from the metal to the support. Hydrogen spillover requires dissociative adsorption of the gas on the metal, followed by the migration of hydrogen atoms on the surface of the oxide. The first direct experimental evidence for hydrogen spillover was obtained by Khoobiar<sup>129</sup>, and several other of the important manifestations of hydrogen spillover were reviewed in 1973 by Sermon and Bond<sup>130</sup>. In another study Sermon and Bond<sup>131</sup> reported the major factors affecting the rate and the extent of hydrogen spillover which included, the nature of the hydrogen donor, the nature and concentration of initiating sites, the presence and efficiency of any promoters, the nature and concentration of acceptor sites, the physical state of the sample and the degree of contact between phases and the effects of temperature. They observed that "primary" spillover in systems where initiating and accepting phases were in physical contact was faster than "secondary" spillover in systems where these phases were not in contact. Hydrogen spillover on  $\text{Rh(3.8)/TiO}_2$  can be inhibited by the preadsorption or coadsorption of carbon monoxide<sup>132</sup>. It was proposed that hydrogen spillover was inhibited by the presence of bidentate carbonyl species at points where dissociative adsorption of hydrogen produces the spillover species. An increase in hydrogen uptake was interpreted in terms of the formation of surface structures associated with the carbon monoxide.

The way in which hydrogen spillover on Pt(5.0)/TiO<sub>2</sub>, Rh(5.0)/TiO<sub>2</sub> and Ni(5.0)/TiO<sub>2</sub> is influenced by the nature and content of the metal, the extent of dehydroxylation, SMSI and U.V. illumination has been studied by Herrmann and Pichat<sup>133</sup>. Electrical conductivity increased when hydrogen spillover occurred, but was unaffected by U.V. illumination. Beck and White<sup>134</sup> found that isotopic mixing was incomplete in the molecular hydrogen desorbed from Pt(0.6)/TiO<sub>2</sub> following sequential dosing with H<sub>2</sub> and D<sub>2</sub>. This was taken as evidence for spillover from the Pt on to the oxide. A recent review of hydrogen spillover has been given by Bond<sup>135</sup>.

#### 1.5.4 Carbon monoxide and Carbon dioxide

In an IR study, Yates<sup>71</sup> observed that CO was very weakly chemisorbed in the same configuration on both anatase and rutile, and that the adsorbed gas could be removed by evacuation at room temperature. However, CO<sub>2</sub> is strongly chemisorbed on both anatase and rutile and was believed to be present as CO<sub>2</sub><sup>-</sup> and CO<sub>3</sub><sup>-</sup> species<sup>71</sup>. Morterra et al.,<sup>82</sup> investigated the adsorption of CO and CO<sub>2</sub> on anatase, and concluded that CO adsorption took place at the most acidic Lewis centres, while CO<sub>2</sub> adsorption occurred in the form of a carbonate-like species. However, the authors reported that some CO<sub>2</sub> molecules can also adsorb and maintain their linear shape on Lewis-acidic sites. Hence CO<sub>2</sub> was considered to be a probe molecule for small concentrations of acidic centres due to the high extinction coefficient of the linear mode.

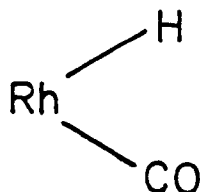
Tanaka and White<sup>83</sup> studied the adsorption of CO and CO<sub>2</sub> on oxidized and reduced anatase. They observed that exposure to CO at room temperature gave rise to some surface reduction and two different modes of adsorbed CO were detected. They also noted that surface hydroxyl groups behaved as OH<sup>-</sup> ions which reacted with coordinated CO<sub>2</sub> to form bicarbonate species.

In another study Tanaka and White<sup>136</sup> reported two types of linear CO species which were assigned to adsorption on Pt terrace (closed-packed) and Pt step (open) sites on Pt(2.0)/TiO<sub>2</sub>. When SMSI was present, Pt(2.0)/TiO<sub>2</sub> adsorbed small amounts of CO, but with oxidised Pt(2.0)/TiO<sub>2</sub> several kinds of adsorbed CO formed and their intensities were time dependent reflecting oxygen removal by reaction with CO to form CO<sub>2</sub>, particularly at step sites<sup>136</sup>.

Solymosi et al.,<sup>137</sup> believed that SMSI in Rh(1.0)/TiO<sub>2</sub> affected the adsorption of CO on the Rh metal by influencing the bonding and reactivity of the chemisorbed species. The partial electron transfer

from  $\text{TiO}_2$  to Rh would increase the electron donation from Rh into an antibonding  $\pi$ -orbital of the CO, thereby strengthening the Rh-C bond and weakening the C-O bond. The authors also demonstrated that dissociation of CO was promoted by hydrogen through the formation of the Rh-carbonyl-hydride species (figure 1.3), where electron transfer from the H to the CO through Rh, increases the Rh-C bond strength and weakens the C-O bond on the surface.

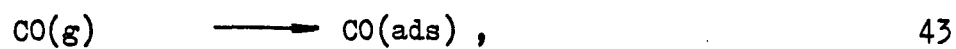
Figure 1.3



Although many workers<sup>114,115,121,138</sup> found that CO adsorption was depressed when metallized  $\text{TiO}_2$  was reduced at high temperatures, Vannice and Sudhakar<sup>139</sup> observed that the catalytic activity for CO hydrogenation was unaffected. They considered that their results argued against morphological changes and alternation of the Fermi level by electron transfer as explanations of this behaviour, but supported a model of special active sites at the Pt- $\text{TiO}_2$  interface.

Sato and Kunimatsu<sup>140</sup> observed that the amount of adsorbed CO on oxidised Pt(1.0)/ $\text{TiO}_2$  increased during the photocatalytic water-gas shift reaction. From a recent study<sup>141</sup> it was concluded that CO adsorbed both molecularly and as carboxylate species, but that molecular CO was readily desorbed by evacuation and was thus not observed. U.V.

illumination was found to have a little effect on the adsorption of CO as carboxylate. The formation of carboxylate species was reported<sup>141</sup> to occur according to:



### 1.5.5 Alcohols

The adsorption of alcohols on the catalyst surface is an important step in their photocatalytic oxidation and is related to the state of hydroxylation of the surface. The adsorption of different alcohols on  $\text{TiO}_2$  surfaces have been studied by many workers.

Munuera and Stone<sup>72</sup> studied the adsorption of propan-2-ol and propanone on a 50% hydroxylated rutile surface at 273 K. Their results showed that the adsorption was non-dissociative and they considered two types of adsorption sites, either OH-O pairs (figure 1.4a), or vacant ligand positions on isolated titanium ions (figure 1.4b).

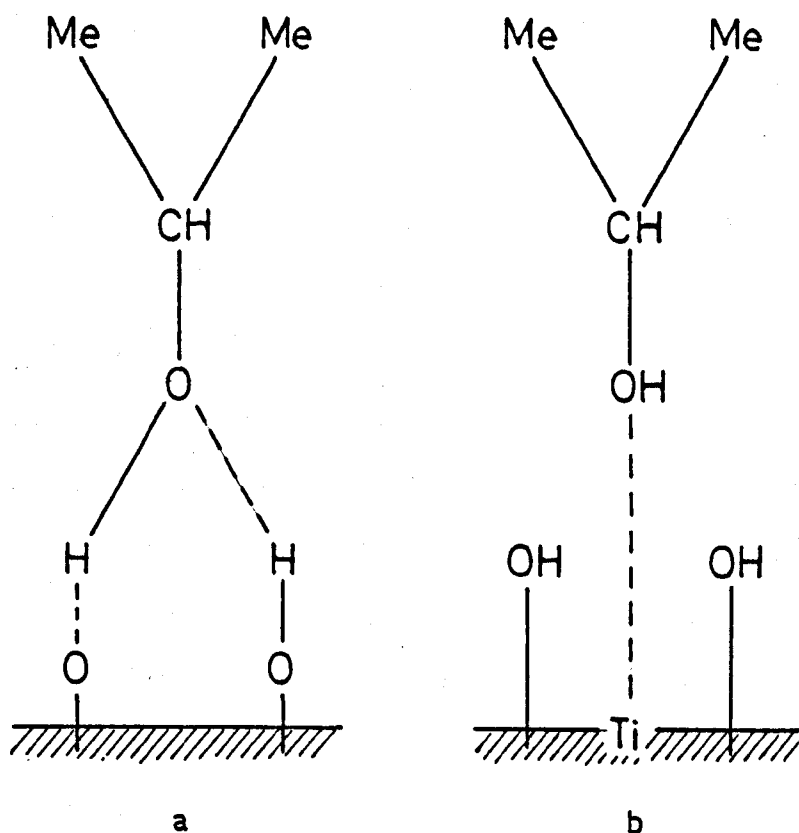


Figure 1.4

There was no evidence for the formation of alcoholate species on the surface and water did not displace propan-2-ol. The authors<sup>72</sup> have also shown that propan-2-ol interacts more strongly with the surface than propanone, so that propanone formed by photocatalytic oxidation of propan-2-ol would readily be displaced.

Bickley and Jayanty<sup>87</sup> detected two forms of adsorbed propan-2-ol on a rutile surface. They reported that the more weakly held form was adsorbed undissociatively and underwent thermal dehydrogenation to propanone, whilst the more strongly held species was adsorbed dissociatively and dehydrated to propene at higher temperatures.

The adsorption of a number of alcohols on the surface of anatase was studied<sup>142</sup>, using infrared spectroscopy (IR). The authors considered the possibility of the formation of two type's of surface alkoxide, one associated with surface oxygen ions and the other associated with the surface Ti sites.

Adsorption of alcohols on a hydroxylated anatase surface occurs on the most exposed  $\text{Ti}^{4+}$  ions filling their coordination spheres<sup>143</sup>. Carrizosa et al.,<sup>144</sup> used IR spectroscopy and TPD to study methanol adsorption, and found that about  $2\text{MeOH nm}^{-2}$  became "tightly adsorbed" on anatase which agrees with the calculated concentration of low coordination  $\text{Ti}^{4+}$  ions on the anatase surface ( $1.9 \text{ Ti}^{4+} \text{ nm}^{-2}$ ). Carrizosa and Munuera<sup>145</sup> using TPD showed that a monomolecular mechanism was responsible for the decomposition of adsorbed alcohols to olefines. They also discussed the role of this mechanism in the catalytic dehydrogenation of alcohols.

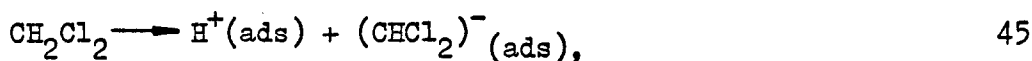
Methanol has been reported<sup>146</sup> to adsorb on  $\text{TiO}_2$  in two forms. The fraction of reversibly adsorbed methanol was about 43-61% and the oxidation of methanol to methanal was related to the presence of strongly bound oxygen and the weakly adsorbed alcohol.

Primet et al.,<sup>147</sup> recorded the IR spectra of phenol adsorbed on both anatase and rutile surfaces. They concluded that the phenol was fixed on the surface hydroxyl groups by hydrogen bonds, whilst the appearance of phenate species ( $1448\text{ cm}^{-1}$  band) was due to the dissociative adsorption of phenol on the Ti-O-Ti bridges, created during dehydroxylation. No investigations of alcohol adsorption on metallized  $\text{TiO}_2$  are known to have been made.

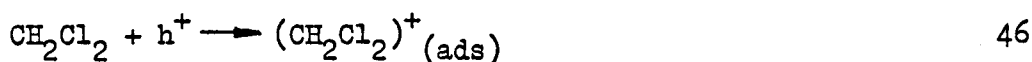
### 1.5.6 Other species

Other species for which adsorption on  $\text{TiO}_2$  or metallized  $\text{TiO}_2$  has been observed include dichloromethane, nitrogen, nitrogen oxides, ethene propene and methane.

Hsiao et al.,<sup>148</sup> suggested a dissociative form of adsorption for dichloromethane on  $\text{TiO}_2$ :



or adsorbed as an ion by reaction with a positive hole at the surface:

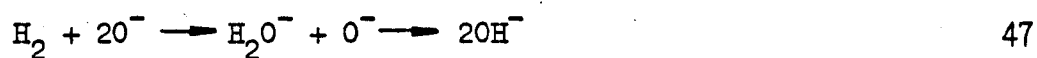


Burch and Flambard<sup>149</sup> showed that reduced titania adsorbs a large amount of nitrogen, which was most probably bound to  $\text{Ti}^{3+}$  sites adjacent to surface oxygen vacancies since adsorption was not observed on unreduced titania. The authors also concluded that the enhancement of nitrogen adsorption observed on  $\text{Ni}(1.0)/\text{TiO}_2$  and  $\text{Ni}(2.0)/\text{TiO}_2$  was due to a higher concentration of adsorption sites on the titania rather than on the nickel.

Ritchie et al.,<sup>98</sup> and McLintock and Ritchie<sup>99</sup> studied the photoadsorption of nitric oxide, ethene and propene on  $\text{TiO}_2$ . The authors found the extent of nitric oxide photoadsorption to be comparable with oxygen uptake, and observed a decomposition of nitric oxide to  $\text{N}_2\text{O}$  gas and adsorbed  $\text{N}_2\text{O}_3$  after photosorption. Ethene was irreversibly photosorbed to an extent similar to oxygen, although the ethene uptake was slower. Propene was photosorbed only if oxygen was present. The interaction of ethene with the surface was suggested to occur at undefined positive hole type sites. These, and oxygen species (probably  $\text{O}_2^-$ ) were held responsible for propene photoadsorption.

The photosorption of hydrogen and methane on a strongly oxidised

TiO<sub>2</sub> surface was studied by Solonitsyn et al.,<sup>150</sup>. They found that the quantum yield for methane was about twice that for hydrogen, and concluded that this was due to hydrogen occupying two activated centres whilst methane occupied only one. The photosorption was considered to take place at O<sup>-</sup> centres produced from interaction of O<sup>2-</sup> with photoholes:



## 1.6 Photocatalysis on $\text{TiO}_2$ and metallized $\text{TiO}_2$

The numerous gas- and liquid-phase reactions photocatalysed by  $\text{TiO}_2$  and metallized  $\text{TiO}_2$  have been reviewed<sup>48,109,151-153</sup>. There is general agreement that adsorption is necessary since the surface species act as traps for both photoelectrons and photoholes, which otherwise recombine. In the present section the photocatalytic reactions of alcohols and other reactants are discussed, where the term photocatalysis implies that radiation must be absorbed by the catalyst for reaction to occur.

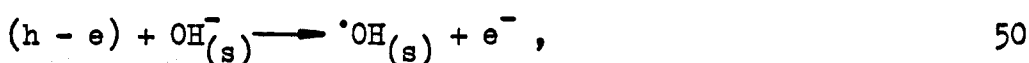
### 1.6.1 Photocatalytic oxidation of alcohols

The photocatalytic oxidation of alcohols on  $\text{TiO}_2$  and metallized  $\text{TiO}_2$  (especially platinized  $\text{TiO}_2$ ) has been studied by several workers, both gas phase and liquid phase being used.

Fillimonov<sup>154-156</sup> studied the photocatalytic oxidation of propan-2-ol vapour on  $\text{TiO}_2$ . The products were propanone and water when a propan-2-ol/oxygen mixture was in contact with irradiated anatase. A mechanism was proposed<sup>156</sup>, in which the oxidation of propan-2-ol was accomplished by the oxygen of  $\text{TiO}_2$ , and the oxygen vacancies so formed were filled by gaseous oxygen dissociating on the surface of the oxide. The presence of tightly adsorbed carboxylate species on the surface was detected and these could not be removed even after evacuation at 625 K. Limited propanone formation was also reported when no oxygen was present and it was accompanied by a darkening of the oxide, indicating the consumption of lattice oxygen.

Bickley et al.,<sup>157</sup> investigated the photocatalytic oxidation of propan-2-ol vapour over  $\text{TiO}_2$  at 300 K irradiated with a light of wavelength  $>300$  nm. The authors observed that the rate of oxygen consumption increased on increasing the amount of preadsorbed propan-2-ol

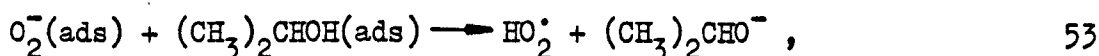
and that the parabolic law for oxygen photoadsorption passed over to a linear law, indicating that the propan-2-ol very rapidly consumed photoadsorbed oxygen, eliminating the surface diffusion step that was previously postulated<sup>106</sup>. They<sup>157</sup> concluded that surface hydroxyl groups acted as intermediates in the photocatalytic oxidation of propan-2-ol, by comparing the activity of the samples outgassed at 600 K and 1073 K which had an equal coverage of propan-2-ol. The photo-uptake of oxygen on  $\text{TiO}_2$  depended on the amount of hydroxyls on it's surface, where they acted as trapping centres for photoholes:



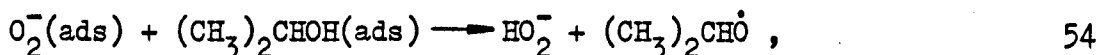
while the adsorbed oxygen molecules acted as traps for photoelectrons;



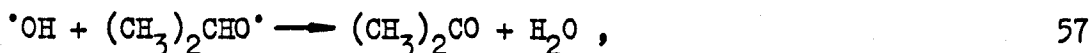
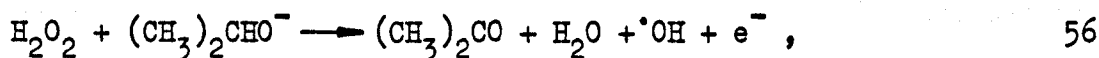
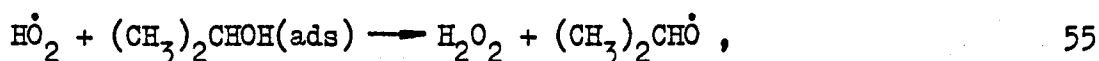
The  $\text{O}_2^-$  produced then attacked neighbouring adsorbed propan-2-ol. The reaction could occur by proton transfer;



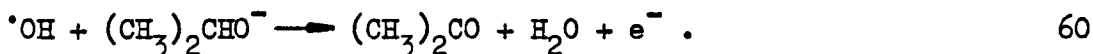
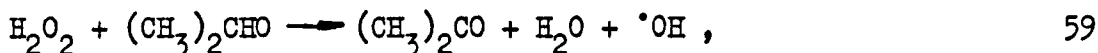
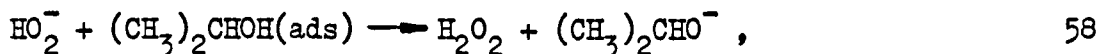
or by Hydrogen atom transfer;



leading to two possible reaction schemes. Either;



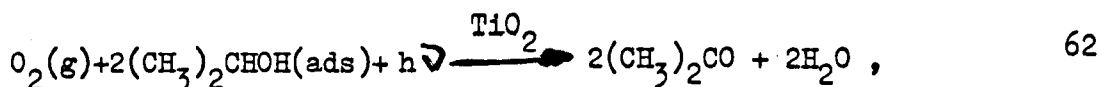
or;



The electrons produced in equation 56 and 60 returned back to the catalyst and regenerated surface hydroxyl ions;



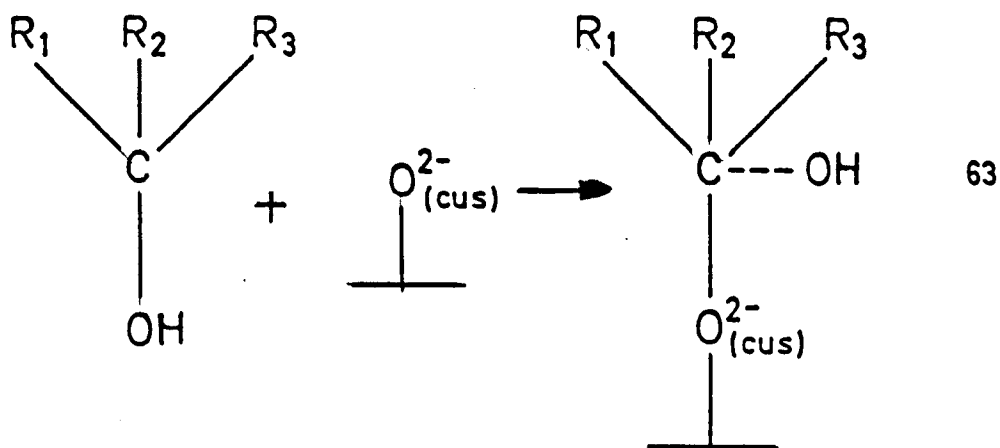
The overall reaction was;



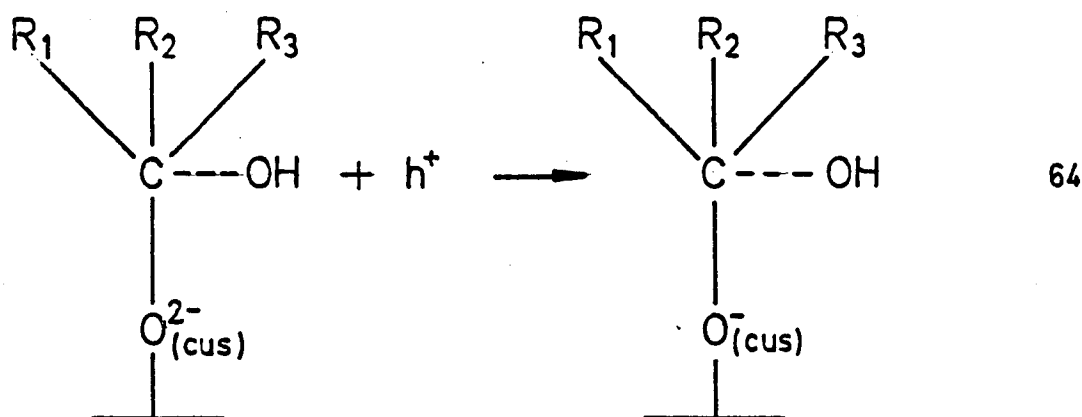
with an estimated quantum efficiency in the order of unity. This study<sup>157</sup> also included a discussion of the adsorption of propan-2-ol, water and propanone on the surface of  $\text{TiO}_2$  and how one component affected the adsorption of the others. It was also found that propanone was only fractionally oxidised even when an excess of propanone was added. The products of such oxidation were tightly bound to the surface and were found to be  $\text{CO}_2$ , CO and methanal.

Two adsorbed forms of propan-2-ol on  $\text{TiO}_2$  surfaces were detected by Bickley and Jayanty<sup>87</sup> in their TPD study of both oxygen photoadsorption and propan-2-ol photooxidation. Upon illumination in the presence of oxygen, propanone was produced from the photooxidation of preadsorbed propan-2-ol and after six hours only traces of unreacted propan-2-ol were detected and propanone was thermally desorbed from the stronger of the two adsorption states, indicating that dissociated propan-2-ol underwent photooxidation. The subsequent photooxidation of propanone produced methanoic acid and ultimately the products of prolonged photooxidation were carbon dioxide and water.

The photooxidation of propan-2-ol, butan-2-ol and 2-methyl-propan-2-ol were studied by Cunningham *et al.*,<sup>158</sup> and were found to undergo selective photooxidation over preoxidised and prereduced rutile surface when exposed to UV illumination in the presence of gaseous oxygen. The authors used  $^{18}\text{O}_2$  labelled gas and  $^{18}\text{O}$  labelled 2-methyl-propan-2-ol in this study. Photooxidation of propan-2-ol, butan-2-ol and 2-methyl-propan-2-ol over preoxidised  $\text{TiO}_2$  in the presence of oxygen produced propanone, butan-2-one and propanone respectively. No labelled oxygen ( $^{18}\text{O}$ ) was incorporated into any of these products when  $^{18}\text{O}_2$  gas was used, indicating that the lattice oxygen was involved in the reactions. The authors<sup>158</sup> considered that coordinatively unsaturated oxide ions ( $\text{O}_{(\text{cus})}^{2-}$ ) provided the adsorption sites for the alcohols;



The photoholes produced on illumination were then trapped by these species;



However, over prerduced rutile surfaces photooxidation was much slower and the propanone contained the same percentage of  $^{18}O$  as the parent alcohol, indicating the smaller number of  $O^{2-}_{(cus)}$  sites on the reduced surfaces. A mechanism was not reported for the production of propanone from 2-methyl-propan-2-ol on reduced oxide surface but  $[(CH_3)_3COH]^+$  cations were invoked as intermediates in the photoinitiated formation of 2-methyl-propene.

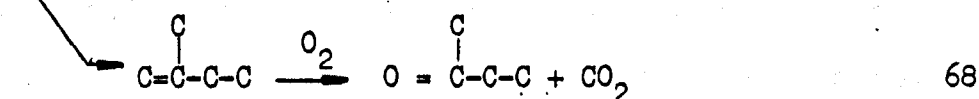
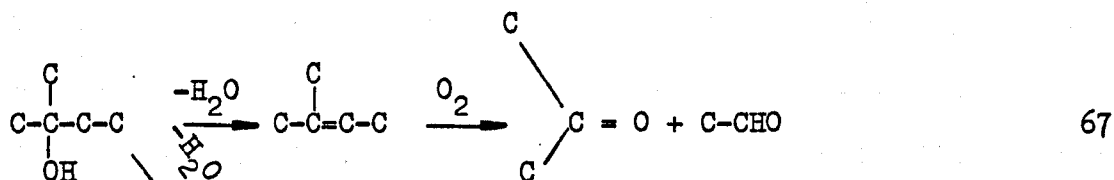
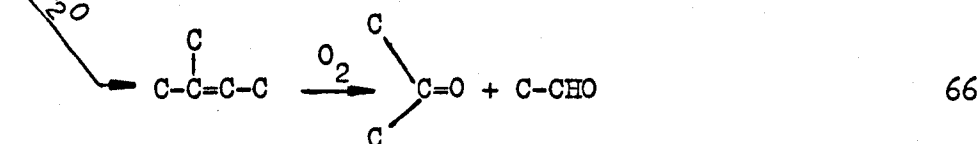
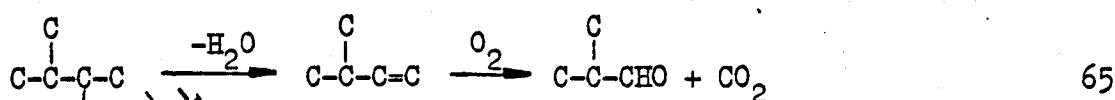
The kinetics of photooxidation of propan-2-ol and butan-2-ol on  $TiO_2$  and  $ZnO$  using a dynamic flow technique with gas-chromatographic analysis were reported in detail by Cunningham and Hodnett<sup>159</sup>. The decay in the rate of formation of propanone was attributed, in part, to poisoning by  $CO_2$ . The rate of propanone production from the photo-oxidation of propan-2-ol was found to vary with the square root of light intensity, indicating that electron-hole recombination was predominant, and this was supported by the observation that the quantum yield increased

with decreasing light intensity. Cunningham *et al.*,<sup>160</sup> studied the activity for conversion of the vapours of secondary alcohols (propan-2-ol and butan-2-ol) into products corresponding formally to elimination of hydrogen, water or ( $C_\alpha - C_\beta$ ) bond fission from the parent alcohol. These phenomena were compared for oxides of the 3d transition metal under thermal and photoactivation. The authors<sup>160</sup> only observed photoenhancement of hydrogen elimination and ( $C_\alpha - C_\beta$ ) fission products at significant levels over  $TiO_2$  and  $ZnO$  in the presence of gaseous oxygen, whereas the oxides featuring cations with partially filled 3d levels were found to be inactive. They attributed this to the  $O^-$  centre, which was only photogenerated on diamagnetic  $TiO_2$  and  $ZnO$ .

The photooxidation of primary, secondary and tertiary methylbutanol vapours was investigated over  $TiO_2$  in the presence of oxygen at 268 K<sup>161</sup>. The photooxidation followed the sequence;

Secondary > tertiary > primary.

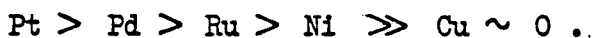
The secondary and tertiary alcohols were photooxidised via alkenes (formed by dehydration) and subsequently oxidised to aldehydes and ketones;



The primary alcohol was not dehydrated and the various aldehydes and ketones formed resulted from direct oxidation. The photooxidation of 2-methyl-2-butanol to propanone has been discussed by Childs and Ollis<sup>162</sup>, and the kinetics of the reaction were described by assuming that the rate determining step was a two site dehydration of the alcohol. The oxygen dependency suggested that the oxygen participation was dissociative.

Pichat *et al.*,<sup>163</sup> studied the photocatalytic oxidation of butan-1-ol over  $\text{TiO}_2$  and other semiconductor oxides in the presence of NO. The predominant product was butanal. The authors concluded that NO acted as an atomic oxygen source in the adsorbed phase, which corroborates the importance of dissociated oxygen species in the photocatalytic oxidations with gaseous oxygen.

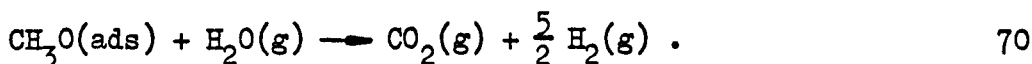
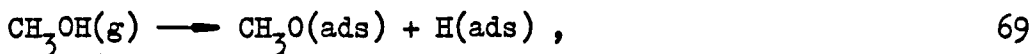
Ichou, Formenti and Teichner<sup>164</sup> investigated the photocatalytic dehydrogenation of propan-2-ol on metallized  $\text{TiO}_2$  (Pt, Pd, Ru, Ni, Cu) in the presence of nitrogen. They observed that the reaction did not occur in the dark, whilst pure  $\text{TiO}_2$  under illumination was inactive in this reactions. Pt deposited on other supports like silica and alumina was inactive and platinum was not specific for this reaction, since Pd, Ru or Ni deposited on  $\text{TiO}_2$  were also active. The photocatalytic activity of metal deposited on  $\text{TiO}_2$  yielded the sequence;



The activity decreased with Pt loading, whilst the metallic surface per gram of Pt remained effectively constant. It was observed<sup>164</sup> that in the pure  $\text{TiO}_2/\text{N}_2$  system, propanone was formed under illumination at the beginning of the reaction, but no hydrogen was released to the gas phase. This behaviour resulted from the participation of surface oxygen of the  $\text{TiO}_2$ , but ceased since the surface could not be reduced indefinitely<sup>152</sup>. The authors<sup>164</sup> also studied the influence of the surface area

of  $\text{TiO}_2$  and water vapour on the photocatalytic activity. The influence of increasing water vapour was found to be beneficial to photocatalytic activity up to 1346.5 Pa, but above that the steady state activity dropped although it remained higher than that for dry reactant. The decrease in activity was attributed to the competitive adsorption of water and alcohol, which finally negated the initial beneficial influence of water.

The photocatalytic production of hydrogen from gaseous methanol and water over  $\text{Pt}(2.0)/\text{TiO}_2$  catalyst has been studied by Kawai *et al.*,<sup>165</sup>. They revealed that  $\text{CO}_2$  and  $\text{H}_2$  were produced by reaction between adsorbed  $\text{CH}_3\text{O}$  and  $\text{H}_2\text{O}$ ;



However, in the absence of water it was suggested that methanal is formed and the reaction in equation 71 was dominant:

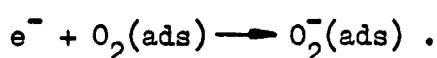
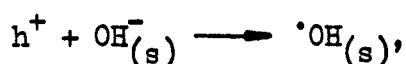


Pichat *et al.*,<sup>13</sup> also studied the photocatalytic dehydrogenation of gaseous methanol over reduced  $\text{Pt}(4.85)/\text{TiO}_2$ , and observed that hydrogen production decreased on removing the illumination, and the addition of gaseous water had the effect of diminishing the rate of hydrogen production, indicating that methanol was displaced from the surface by water. They obtained mass spectra showing that methanal was the main product, however,  $\text{CO}_2$ ,  $\text{HCOOH}$  and  $\text{CH}_4$  were detected after extended illumination.

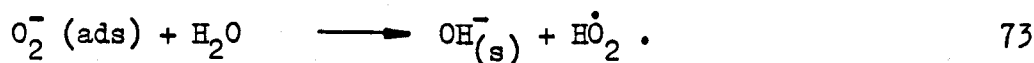
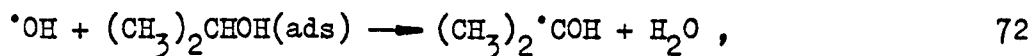
Liquid phase photooxidation of propan-2-ol on  $\text{TiO}_2$ <sup>166-171</sup> and metallized  $\text{TiO}_2$ <sup>13,49,172,173</sup> has been investigated by a number of workers. Irick<sup>166</sup> illuminated  $\text{TiO}_2$  suspended in propan-2-ol with U.V.

radiation in the presence of oxygen. Propanone, desorbed into the liquid phase, was produced at a constant rate and was detected by gas chromatography. Quantum yield measurements for propanone production over various pigments indicated that anatase was more active than rutile. Addition of hydrogen peroxide to the reaction mixture increased the activity approximately three fold, whereas the addition of water decreased the activity. When the suspensions were illuminated in the absence of oxygen, some propanone was formed and the catalyst turned a blue colour signifying the reduction of  $Ti^{4+}$  to  $Ti^{3+}$  as lattice oxygen was consumed.

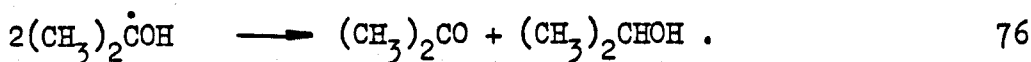
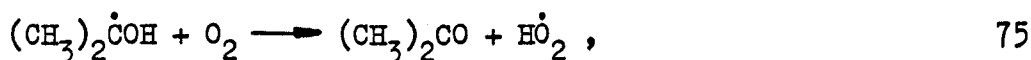
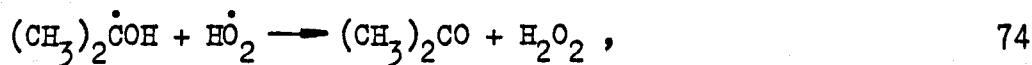
Cundall, Rudham and Salim<sup>167</sup> studied the photocatalytic oxidation of liquid propan-2-ol, using illuminated suspensions of rutile and anatase and passed either  $O_2$ , air,  $N_2O$  or  $N_2$  into the upper part of the reaction vessel. In the presence of  $N_2$  or  $N_2O$  the reaction was not sustained. The rate of propanone formation was found to vary with catalyst mass and oxygen partial pressure, and an activation energy of  $18 \text{ kJ mol}^{-1}$  was obtained over the temperature range of 297-317 K with radiation of wavelength  $> 300 \text{ nm}$ . The rate of propanone formation was directly proportional to the intensity of the incident light and a similar quantum yield was obtained for both 404 nm and 365 nm radiation. The addition of water produced a maximum in the observed reaction rate at a 0.3-0.4 mole fraction of propan-2-ol in water. The authors<sup>167</sup> agreed with Bickley et al.,<sup>157</sup> that  $O_2^-$  and  $\cdot OH$  species were formed;



However, they considered that the  $\cdot OH_{(s)}$  rather than  $O_2^-(\text{ads})$  reacted with molecularly adsorbed propan-2-ol;



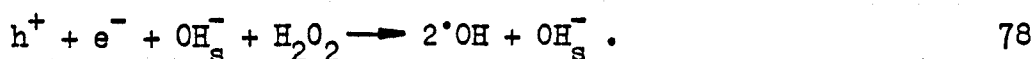
The water produced in equation 72 regenerated  $\text{OH}^-_{(\text{s})}$  in equation 73, so the energy of an absorbed quantum had been utilised in producing  $(\text{CH}_3)_2\cdot\text{COH}$  and  $\text{HO}_2\cdot$ . The effect of adding water to the reaction mixture was to inhibit the reaction in equation 72, but favour equation 73 and it was assumed that these opposing effects were responsible for the observed maximum activity in propan-2-ol/water mixtures. Formation of propanone from  $(\text{CH}_3)_2\cdot\text{COH}$  was then considered to occur by at least one of three possible reactions;



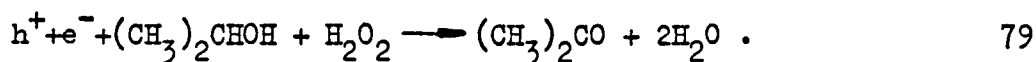
If reactions 75 and 76 occurred, then  $\text{H}_2\text{O}_2$  was formed by the interaction of  $\text{HO}_2\cdot$  radicals;



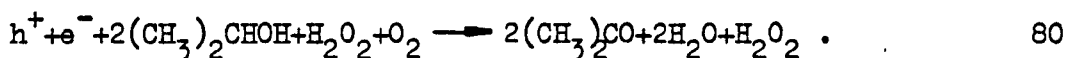
The role of  $\text{H}_2\text{O}_2$  was investigated by adding small amounts of  $\text{H}_2\text{O}_2$  to the reaction mixture. In an atmosphere of nitrogen when normally no detectable propanone was produced the addition of  $\text{H}_2\text{O}_2$  produced propanone in a 1:1 stoichiometric ratio. The decomposition of  $\text{H}_2\text{O}_2$  was represented by;



The  $\cdot\text{OH}$  radical reacted as in equation 72 to form  $(\text{CH}_3)_2\cdot\text{COH}$  and subsequently propanone, the overall reaction was;



Addition of  $H_2O_2$  in the presence of oxygen gave a fast initial rate followed by a constant rate similar to reaction without  $H_2O_2$ . A 2:1 stoichiometry between the propanone produced and the  $H_2O_2$  added was found as a result of extrapolating the linear portions of the plots to zero time. The fast initial rate of propanone formation was considered to be due to preferential transfer of electrons to  $H_2O_2$ . The overall reaction was;



It was thought unlikely, however, that the amount of  $H_2O_2$  formed continued to be equivalent to that decomposed.

In a further study Cundall et al.,<sup>168</sup> found a linear relationship between reaction rate and light intensity on pure rutile and determined the reactivity of a variety of  $TiO_2$  based pigments. Egerton and King<sup>169</sup> also studied the effect of light intensity on the reaction rate of this system. The photooxidation rate was found to be proportional to the square root of light intensity, an observation that was explained on the basis of high recombination rates of holes and electrons. At low light intensities ( $< 5 \times 10^{15}$  quanta.s<sup>-1</sup>) a linear relation was observed since recombination would be minimal.

Rudham and co-workers<sup>170</sup> investigated the photocatalytic oxidation of liquid propan-2-ol on pure and doped  $TiO_2$ , using 366 nm radiation. The presence of  $TiO_2$ , UV radiation and oxygen proved to be essential for sustained reaction to occur. A square root light intensity dependence was observed and the authors agreed with the explanation given by Egerton and King<sup>169</sup> invoking electron-hole recombination. The activation energy for propanone production on pure rutile over the temperature range of 277-313 K was 27 kJ mol.<sup>-1</sup> and was independent of

reaction conditions. However, on pure anatase and five doped rutiles and coated anatase and rutile pigments, the activation energy for propanone production was found to range from 31 to 91 kJ mol.<sup>-1</sup>, and these energies were considered to reflect the solid state properties of TiO<sub>2</sub> rather than the chemistry of propan-2-ol oxidation. In a further study the authors<sup>171</sup> investigated the photooxidation of liquid alcohols which included propan-2-ol. The single activation energy of 27 kJ mol.<sup>-1</sup> obtained for the photooxidation of different alcohols was considered to be the energy required to promote photoelectrons from traps into the conduction band. The photooxidation of binary alcohol mixtures was also investigated in this study, and the total rate of carbonyl compound formed and overall activation energy were found to be independent of mixture composition.

Buss et al.,<sup>174</sup> photooxidised methanol, ethanol and butan-1-ol on anatase to the corresponding aldehydes under a nitrogen atmosphere. Only a small fraction of the alcohol was oxidised and the anatase turned grey, indicating the presence of Ti<sup>3+</sup> ions. The authors suggested <sup>•</sup>OH radicals formed by hole trapping were the reactive species in the photocatalytic reaction. Butan-1-ol also photooxidised in nitrogen atmosphere on anatase and the formation of Ti<sup>3+</sup> ions and butanal were observed<sup>175</sup>.

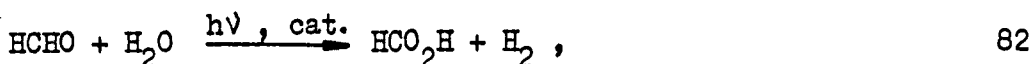
The photocatalytic activities for liquid propan-2-ol dehydrogenation on metallized TiO<sub>2</sub> under argon were found<sup>172</sup> to fall in the sequence; Pt(1.0)/TiO<sub>2</sub> > Rh(1.0)/TiO<sub>2</sub> > Pd(1.0)/TiO<sub>2</sub> > Ru(1.0)/TiO<sub>2</sub> > Ir(1.0)/TiO<sub>2</sub> > TiO<sub>2</sub>. Catalyst oxidation at elevated temperatures in a stream of air enhanced the activity of the catalysts, but did not alter the sequence.

Pichat et al.,<sup>13</sup> investigated the photocatalytic dehydrogenation of liquid aliphatic alcohols on Pt(4.85)/TiO<sub>2</sub> by following hydrogen

evolution, but showed an equivalent production of carbonyl compound in the liquid phase. The authors found that the rate of hydrogen evolution depended upon the alcohol and fell in the sequence: methanol > ethanol > propan-1-ol  $\approx$  propan-2-ol  $\approx$  butan-1-ol. Subsequently it was shown<sup>14</sup> that the optimum photocatalytic activity was achieved at considerably lower Pt contents in the range of 0.1-1.0 wt%. It was suggested that the reaction of photoholes with alcohol intermediates adsorbed on the  $\text{TiO}_2$  was rate determining at  $T \geq 313$ , whilst desorption of  $\text{H}_2$  from the Pt was rate determining at  $T < 263$  K.

Pattenden *et al.*,<sup>176</sup> studied the photocatalytic dehydrogenation of aliphatic and aromatic alcohols in benzene solution on platinized anatase and suggested that this method provides a clean and convenient procedure for the formation of aldehydes and ketones on a preparative scale.

Kawai and Sakata<sup>177</sup> showed that the irradiation of  $\text{TiO}_2$  powders mixed with either Pt, Pd,  $\text{RuO}_2$  or a Rh complex, or a mixture of these, led to the efficient production of hydrogen from a liquid methanol/water mixture at room temperature. Relatively high quantum yields were obtained on the metal loaded  $\text{TiO}_2$ , whereas a slow reaction was observed on  $\text{TiO}_2$ , indicating that electrons and holes could not be separated efficiently in  $\text{TiO}_2$  alone. The formation of  $\text{HCHO}$  and  $\text{HCO}_2\text{H}$  was confirmed by mass spectrometric analysis. It was suggested that photoholes, generated by the light, would oxidise methanol to  $\text{HCHO}$  and  $\text{HCO}_2\text{H}$  and thence to  $\text{CO}_2$ , while photoelectrons, in the conduction band of  $\text{TiO}_2$ , would simultaneously reduce protons in solution to form gaseous  $\text{H}_2$ ;



The same authors<sup>178</sup> also studied the photocatalytic production of hydrogen from ethanol and water on metallized  $\text{TiO}_2$  (Pt, Pd, Rh or Ni). The production of hydrogen, methane and methanal was observed and a mechanism for the photocatalytic reaction was discussed. However, in the case of macroscopic platinized  $\text{TiO}_2$  anodes<sup>179</sup>, the oxidation of ethanol to ethanal and ethanoic acid was reported to be predominantly a catalytic rather than photocatalytic effect, since it could be accomplished in the dark with a bias voltage of approximately 0.5-1 volt.

Recently the photocatalytic production of hydrogen from aliphatic alcohols on metallized  $\text{TiO}_2$  using UV, or visible light with a photo-activator, was studied by Borgarello and Pelizzetti<sup>173</sup>. They found that the evolution of hydrogen followed the order, methanol > ethylene glycol > ethanol > propan-1-ol > propan-2-ol > butan-1-ol > butan-2-ol > 2-methyl-propan-2-ol, under U.V. illumination.

### 1.6.2 Water

In recent years, the photodecomposition of water over semiconducting materials has received considerable attention due to the possibility of utilising such systems in the conversion of sunlight to stored energy. Such energy storage may play an important role in meeting the future energy needs of the world.

A number of reviews have been published that describe in considerable detail the UV and visible light induced cleavage of water into hydrogen and oxygen, and the photochemical aspects of solar energy conversion<sup>48,180-184</sup>.

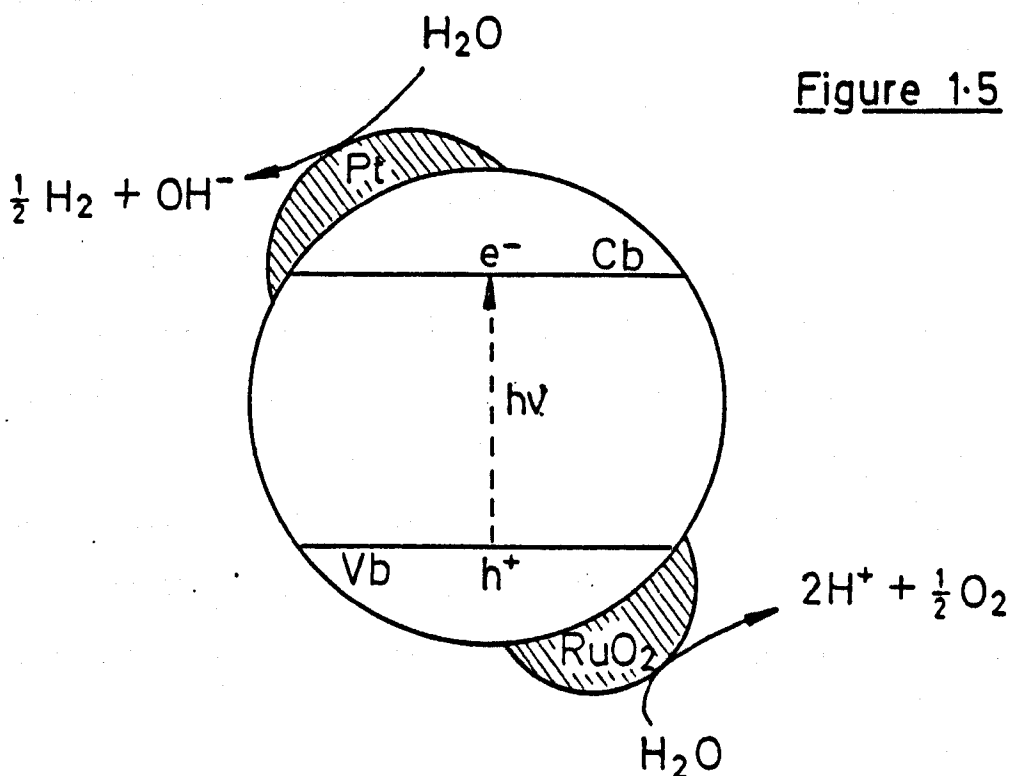
Korsunovskii<sup>185</sup> studied the photooxidation of water and measured the conductivity of  $\text{TiO}_2$  and other oxides when exposed to oxygen and water vapour. It was suggested that water was photooxidised to  $\cdot\text{OH}$  and  $\text{HO}_2\cdot$  radicals and  $\text{H}_2\text{O}_2$ . The  $\cdot\text{OH}$  and  $\text{HO}_2\cdot$  radicals were also detected by employing spin trapping and ESR techniques<sup>186</sup>. The  $\cdot\text{OH}$  radical was thought to arise from the oxidation of water and the  $\text{HO}_2\cdot$  radical from the reduction step. Kawai and Sakata<sup>187</sup> also thought that  $\cdot\text{OH}$  radicals were one of the important intermediate species for water splitting even in the gas phase experiments.

Fujishima and Honda<sup>188</sup> suggested that photoelectrochemical (PEC) cells based on single crystal n-type semiconductor ( $\text{TiO}_2$ ) might be used for the photodecomposition of water to hydrogen and oxygen. The design of semiconductor PEC systems for solar energy conversion has been discussed by Bard<sup>189</sup>.

Nikandrov et al.,<sup>190</sup> investigated hydrogen photoproduction from aqueous suspensions of  $\text{TiO}_2$  in the presence of organic electron donors. Hydrogen was evolved in the presence of tris (oxymethyl) aminomethane, triethanolamine, ethanol, glycerol, glucose and ethylenediamine tetraacetic acid (EDTA), whereas no hydrogen was observed when cysteine,

dithiotreitol, methylamine and urea were used.

Recently more attention has been given to  $\text{TiO}_2$  catalysts loaded with deposited metals to increase the activity for the photodecomposition of water to hydrogen. A particle of platinized  $\text{TiO}_2$  can be envisaged as a short circuited PEC cell<sup>153</sup>, where reaction occurs by electron and hole transfer at two different sites on the particle. The wavelength response could be extended by inclusion of a dye, which can act as a sensitiser, and hence effectively reduces the  $\text{TiO}_2$  band gap. This principle has been used by Gratzel and co-workers<sup>56,57,112,191-194</sup>, who have developed systems capable of catalysing water decomposition using visible light. It was found that water decomposition could be accomplished by UV illumination of colloidal  $\text{TiO}_2$  particles loaded with ultrafine deposits of platinum and ruthenium dioxide<sup>56</sup>. The quantum yield for hydrogen production was 0.2-0.4, whilst oxygen was produced in stoichiometric proportion.  $\text{RuO}_2$  was thought to play an important role in facilitating the transfer of photoholes from the valence band of the semiconductor to species in solution (figure 1.5).

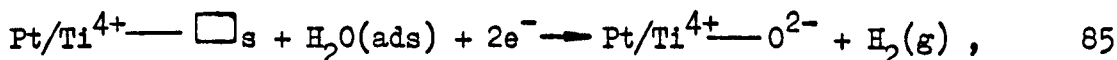
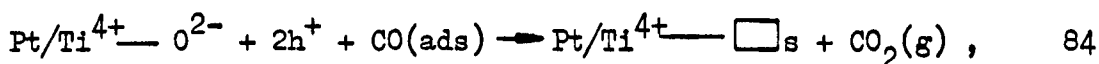


The decomposition of water with visible light was achieved when  $[\text{Ru}(\text{bpy})_3^{2+}]$  ions were used as sensitiser, and the addition of methyl viologen ( $\text{MV}^{2+}$ ) as an electron relay significantly increased the yield of hydrogen<sup>56,57</sup>.

Laser photolysis and conductance techniques<sup>191,192</sup> demonstrated that the hole transfer from  $[\text{Ru}(\text{bpy})_3^{3+}]$  to the catalyst occurred with proton release from water and that only surface adsorbed species could intervene as electron and hole scavengers.

Cunningham and Tobin<sup>195</sup> studied the splitting of water under non-equilibrium conditions using Ru-TiO<sub>2</sub> catalyst. The quantum efficiency of flash initiated hydrogen pulse formation was  $<10^{-3}$ , indicating that effective back reaction processes, such as electron-hole recombination, were predominant.

Sustained production of hydrogen was observed on platinized TiO<sub>2</sub> in the presence of water vapours and carbon monoxide (water-gas shift reaction) under UV illumination<sup>196-199</sup>. Tsai et al.,<sup>197</sup> proposed the following mechanism for the reaction;



where  $\square_{\text{s}}$  signifies an oxygen vacancy on the surface and  $\text{Pt/Ti}^{4+}\text{---O}^{2-}$  represents peripheral sites on the Pt/TiO<sub>2</sub>.

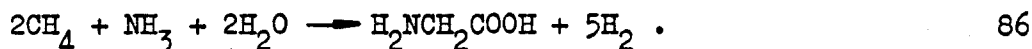
The photocatalytic reaction of gas phase water with active carbon over platinized TiO<sub>2</sub> has been investigated by Sato and White<sup>200-202</sup>. The products were H<sub>2</sub>, and a small amount of O<sub>2</sub>. The rate of producing hydrogen declined as the reaction proceeded, due to the accumulation of hydrogen and the loss of good contact between the catalyst and carbon, leading to a back reaction between hydrogen and oxygen to form water.

Hydroxyl radicals were cited in the mechanism proposed for this reaction<sup>202</sup>.

### 1.6.3 Other Reactions

Numerous papers have been published on other photocatalytic reactions which proceed on  $\text{TiO}_2$  and metallized  $\text{TiO}_2$ . Since these reactions are not central to the present research, the space necessary to give the topic consideration in depth is not justified. In keeping with this, only the current point of view concerning these reactions will be considered.

Bard and co-workers<sup>15,203</sup> studied the photosynthetic production of amino acids from an illuminated mixture of  $\text{CH}_4$ ,  $\text{NH}_3$  and  $\text{H}_2\text{O}$  over platinized anatase. It was suggested that the oxidation leading to amino acids depended on  $\cdot\text{OH}$  radical formation, whilst reduction leading to hydrogen atoms, and ultimately gaseous hydrogen occurred at platinum sites. The overall reaction was described as photosynthetic involving a net storage of energy.

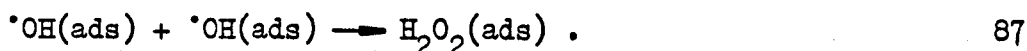


The photocatalytic conversion of primary amines to secondary amines on  $\text{Pt}(5.0)/\text{TiO}_2$  has been reported by Kagiya *et al.*,<sup>3</sup>. The reaction did not occur in the absence of catalyst or with  $\text{TiO}_2$  alone. Fox and Chen<sup>204</sup> studied the photocatalytic formylation of primary and secondary amines on irradiated platinized  $\text{TiO}_2$ , and showed the necessity of both UV radiation and oxygen.

The photooxidation of adsorbed gaseous ammonia on  $\text{TiO}_2$  films has been studied<sup>205</sup>, and it was found that three molecules of ammonia reacted with two molecules of oxygen. The main product was water, and small amounts of nitrous oxide and nitrite were found. A mechanism invoking surface intermediates such as  $\text{HONO}$  and  $(\text{NH}_3\text{NH}_2)_2$  was proposed. The oxidation of ammonia at room temperature on irradiated anatase has been investigated<sup>206</sup>, nitrogen and nitrous oxide were reported to be the

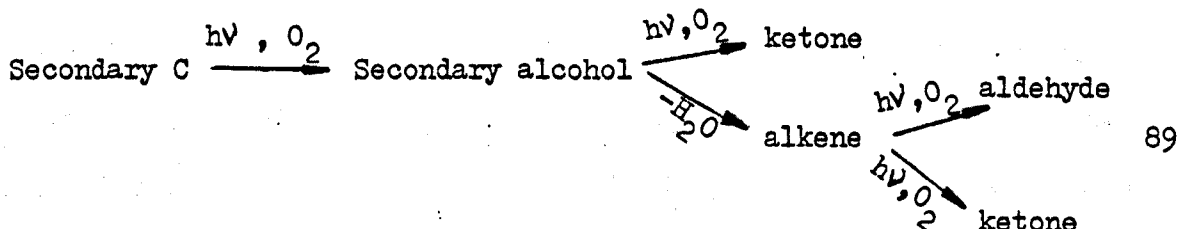
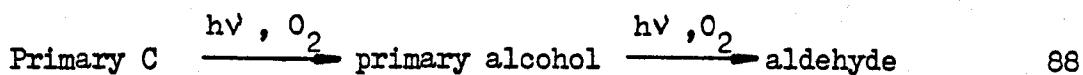
products and the rate of their formation was proportional to the light intensity and depended on the partial pressure of oxygen.

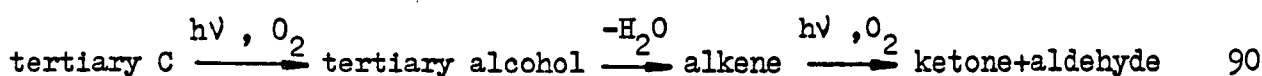
Bickley and Vishwanathan<sup>207</sup> illuminated a rutile surface containing preadsorbed water in air and oxygen, and compared the TPD results with those from surfaces containing preadsorbed hydrogen peroxide. They concluded that hydrogen peroxide must be formed on  $\text{TiO}_2$  containing preadsorbed water during illumination, probably by direct interaction of two  $\cdot\text{OH}$  radicals formed by photohole capture;



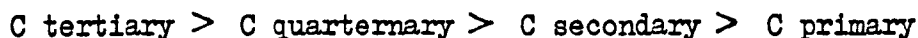
In the presence of nitrogen, NO was desorbed from these surfaces and the authors suggested that NO arose from the reaction of adsorbed nitrogen with an adsorbed oxygen species, such as  $O(ads)$  or  $O^-(ads)$ , which were formed from either the thermal or photochemical decomposition of  $H_2O_2$ .

The photooxidation of alkanes on anatase has been studied by Teichner et al.,<sup>208-210</sup>. Both straight and branched chain alkanes (except methane, which appeared to be inactive) underwent photooxidation at room temperature to ketones and aldehydes. A proposed mechanism<sup>209</sup> implied the formation of an alcoholic intermediate which underwent either further direct photooxidation to form aldehyde or ketone, or thermal dehydration to form an alkene, followed by the photooxidation of the alkene to an aldehyde or ketone;





The reactivities of the different carbon atoms followed the sequence;



The carbon atom with the highest electron density and least steric hindrance being preferentially attacked by oxygen. The photooxidation of hydrocarbons in oxygen-containing solutions on platinized  $TiO_2$  has been studied<sup>211,212</sup>. The main product was  $CO_2$  with minor quantities of alcohols, and a mechanism for the reaction based on the photogeneration of  $\cdot OH$  radicals was proposed<sup>211</sup>.

Pichat et al.,<sup>213</sup> in isotope exchange experiments using  $^{18}O_2/^{16}O_2$  confirmed that interaction between oxygen and photogenerated electron-hole pairs was the key process in the photooxidation of alkanes on anatase. The photooxidation of unsaturated hydrocarbons has also been studied<sup>99,214,215</sup>. It was considered<sup>99</sup> that  $O_2^-$  ions were the reactive species in the photooxidation of ethene and propene to methanal, carbon monoxide and water.

The photodecomposition of glucose by platinized  $TiO_2$  and platinized  $TiO_2: RuO_2$ <sup>217</sup> was studied, and the main product was reported to be hydrogen and carbon-dioxide when conducted under an inert atmosphere and carbon-dioxide alone under an  $O_2$  atmosphere<sup>216</sup>. A mechanism for the reaction was presented<sup>217</sup> in which hydroxyl radicals were invoked.

Herrmann et al.,<sup>218</sup> investigated the photocatalytic oxidation of oxalic acid in aqueous suspensions of  $TiO_2$  illuminated with UV radiation. The effects of oxygen, oxalic acid concentration, pH and temperature provided evidence for the photocatalytic character of the oxidation. A mechanism involving attack of adsorbed  $HC_2O_4^-$  ions by an atomic oxygen species, activated by photoholes, was tentatively suggested.

Bard and co-workers studied the photodecomposition of carboxylic acids on  $\text{TiO}_2$ <sup>8,219</sup> and on platinized  $\text{TiO}_2$ <sup>7-9,219-221</sup> in the presence of oxygen. It was found that  $\text{TiO}_2$  powders were more efficient when they were doped and/or partially covered with Pt<sup>8</sup>. The main products of the photodecomposition of ethanoic acid on platinized  $\text{TiO}_2$  powder were methane and carbon-dioxide, with small amounts of hydrogen and ethane. In the absence of molecular oxygen<sup>8</sup>, the rate of evolution of  $\text{CO}_2$  has reduced and the major product was methane;

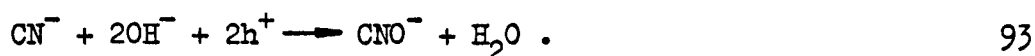


Other saturated carboxylic acids (propionic acid, butyric acid, valeric acid, pivalic acid and adamantane-1-carboxylic acid) were also photocatalytically decarboxylated to the corresponding alkanes<sup>8</sup>. The reaction product was predominantly  $\text{CO}_2$ , from the photodecomposition of benzoic acid in oxygenated solution on platinized  $\text{TiO}_2$ <sup>221</sup>, with intermediate production of salicylic acid and phenol. A mechanism for the reaction based on photogeneration of  $\cdot\text{OH}$  radicals and adsorption of intermediates on the catalyst surface was proposed.

In a recent study<sup>222</sup>, aqueous suspensions of anatase containing benzoic acid or sodium benzoate were illuminated with near U.V. light under different experimental conditions. In the presence of oxygen o-, m- and p-hydroxy benzoic acid were formed in the same isomeric distribution found for  $\cdot\text{OH}$  radical attack on benzoic acid, whereas in the absence of oxygen the yield of hydroxy compound was low. The authors proposed a mechanism for the reaction in which the  $\cdot\text{OH}$  radical attacked the aromatic ring and subsequent oxidation of the hydroxy adduct with oxygen gave the corresponding phenol.

Zakharenko et al.,<sup>223</sup> studied the photocatalytic oxidation of carbon-monoxide on rutile at 293 K, and found that the reaction proceeded at a steady rate for several hours with an activation energy of 30 kJ mol<sup>-1</sup>. Interaction of O<sup>-</sup> and CO was considered to be responsible for the photocatalytic reaction. Volodin, Cherkashin and Zakharenko<sup>224-226</sup> also studied the photocatalytic CO oxidation on anatase at 87 K using ESR, both O<sup>-</sup> and [O<sub>3</sub><sup>-</sup>] were considered to be intermediates and CO<sub>2</sub><sup>-</sup> and CO<sub>3</sub><sup>-</sup> were detected. CO<sub>2</sub> was evolved when the surface was heated to 420 K.

Frank and Bard<sup>227</sup> studied the photooxidation of cyanide ions to cyanate ions in aqueous solution, in the presence of oxygen and various TiO<sub>2</sub> pigments. Anatase was reported to be more active than rutile, with undoped anatase being the most active with a quantum yield of 0.06. The oxidising species were thought to be photoholes;



Yoneyama et al.,<sup>228</sup> found that platinization of TiO<sub>2</sub> increased the reaction rate of the photocatalytic oxidation of cyanide ions.

The photooxidation of sulphite ions to sulphate ions has been shown to have a quantum yield of 0.16<sup>229</sup>. Direct photooxidation of sulphur to sulphate ions in the presence of oxygen occurs on anatase, but not on rutile<sup>230</sup>. The rate was higher in alkaline solution than in neutral and acidic solutions.

The photocatalytic reduction of various oxidising agents in H<sub>2</sub>SO<sub>4</sub> solution on rutile have been reported by Miyake et al.,<sup>231</sup>. MnO<sub>4</sub><sup>-</sup> was reduced to MnO<sub>2</sub>, Cr<sub>2</sub>O<sub>7</sub><sup>2-</sup> to Cr<sup>3+</sup> and Fe<sup>3+</sup> to Fe<sup>2+</sup>.

Herrmann and Pichat<sup>232</sup> investigated the oxidation of halide ions in UV irradiated suspensions of anatase in the presence of oxygen. Iodide was oxidised to iodine in neutral and acidic solutions and to hypoiodite in basic solutions. Bromide behaved in a similar way to

iodide although the reaction rates were considerably lower, whereas chloride was not oxidised even after prolonged irradiation. Reichman and Byvik<sup>233</sup> studied the photooxidation of halide ions on platinized  $\text{TiO}_2$ . Chlorine, bromine and iodine were reported to be produced in oxygen saturated aqueous solutions of the respective halide ion. The authors reported that the reaction rate was significantly higher on platinized  $\text{TiO}_2$  than on pure  $\text{TiO}_2$ , indicating the efficient separation of photogenerated electron-hole pairs in platinized  $\text{TiO}_2$ . The reduction of oxygen was considered to occur at platinum sites and the oxidation of the halide on the  $\text{TiO}_2$  surface.

### 1.7 The Present Work

The present thesis reports an investigation of photocatalytic dehydrogenation of liquid alcohols on metallized anatase. The technique used has the merit of precise temperature control so that reaction rates can be reproducibly measured and activation energies can be determined with considerable precision. Metallized anatase catalysts prepared with Pt, Pd, Rh or Au supported on high area oxide, are used in kinetic studies with methanol, ethanol, propan-1-ol and propan-2-ol. The research is particularly directed towards the following questions:

- 1 - Does photodeposition or impregnation followed by hydrogen reduction produce the most active catalyst?
- 2 - What metal forms the most active catalyst?
- 3 - Do alcohols differ in reactivity and mechanism?
- 4 - Do dark reactions contribute to photocatalytic reaction?
- 5 - What parallels exist between photocatalytic oxidation on pure anatase in the presence of oxygen and photocatalytic dehydrogenation on metallized anatase in the presence of inert gas?

## Chapter Two

### EXPERIMENTAL

#### 2.1 Apparatus

A diagram of the apparatus is shown in figure 2.1. The ultraviolet light source was a Thorn ME/D 250 W medium pressure mercury lamp fitted with a Pyrex window, which was housed in a chimney to convect heat away. Light from the lamp was collected by a silica lens ( $f = 5$  cm) and passed through a heat filter, consisting of cylindrical Pyrex vessel (10 cm in length and 5 cm in diameter) containing 2 M ethanoic acid. A second silica lens then focussed the light on the reaction vessel. The 366 nm wavelength radiation which used throughout this work was isolated by using a soda glass filter to cut out wavelengths  $< 340$  nm, and a Chance OX1 filter to cut out wavelengths  $> 400$  nm.

The reaction vessel was a Pyrex cylinder (2.5 cm diameter and 8.0 cm length) fitted with a side arm and rubber septum for withdrawal of samples by syringe. The vessel had glass connections to enable a flow of gas to be passed over the reaction mixture. A Crouzet 82-330 motor driven stirrer, operating at 600 r.p.m., was used to keep the catalysts in suspension.

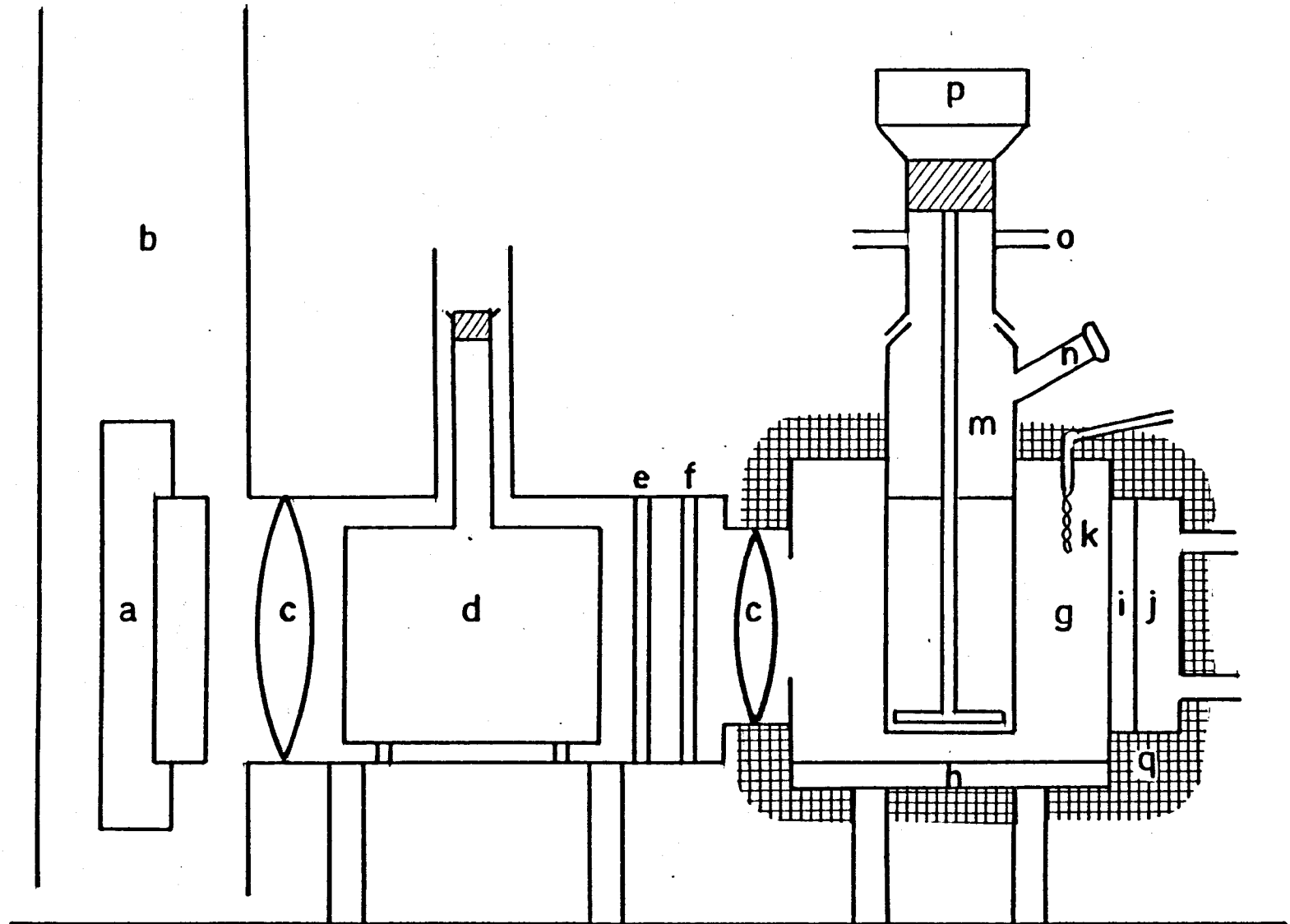
Temperature control was maintained by mounting the reaction vessel in a closely fitting aluminium block, whose temperature was controlled by a frigister and associated electronic control unit. A continuous flow of water through a water jacket in contact with the frigister facilitated the necessary heat exchange. The temperature of the aluminium block was monitored using a chromel-alumel thermocouple which was found to be in agreement with a similar thermocouple placed in the reaction mixture. Reaction temperatures were maintained to  $\pm 0.02$  K over the range 278-313 K.

The whole apparatus was installed in a black wooden box which prevented the escape of harmful ultraviolet light and minimised temperature fluctuations caused by draughts.

Figure 2-1

Key

- a U.V. lamp
- b chimney
- c lens
- d heat filter
- e soda glass filter
- f OX1 filter
- g aluminium block
- h insulated table
- i frigister
- j water jacket
- k thermocouple
- l reaction vessel
- m stirrer
- n side arm
- o attachment for ambient atmosphere control
- p synchronous motor
- q lagging



Apparatus

2.2 Chemicals

propan-2-ol	}	Analytical reagent supplied by
propan-1-ol		B.D.H. Chemicals Ltd.
ethanol	}	Analytical reagent supplied by
methanol		J. Burrough Ltd.,
propanone		Analytical reagent supplied by Mayard Baker
n-hexane	}	Analytical reagent supplied by
diethyl ether		B.D.H. Chemicals Ltd.
2,4-dinitrophenyl hydrazine		Reagent grade supplied by Aldrich Ltd.
uranyl sulphate	}	Analytical reagent supplied by
ethanoic acid		B.D.H. Chemicals Ltd.
potassium hydroxide		
chloroplatinic acid	}	Supplied by Engelhard
palladium chloride		
chloropentammine rhodium chloride	}	Supplied by Johnson-Matthey
gold wire		
oxalic acid		Research reagent grade supplied by Harrington Bros. Ltd.
methanal solution	}	Laboratory reagent grade supplied
potassium permanganate		by East Anglia Chemicals.
air, H <sub>2</sub> , N <sub>2</sub> , He and O <sub>2</sub>		Cylinders supplied by Air products.

### 2.3 Catalyst preparations

TiO<sub>2</sub> P-25 anatase possessing a surface area of  $50 \pm 15 \text{ m}^2 \text{ g}^{-1}$  was supplied by Degussa.

Three methods were used to prepare metallised anatase; following preparation all catalysts were stored in glass weighing bottles. Catalysts were designated M(x)/TiO<sub>2</sub>, where M is the metal supported at a concentration of x weight percentage.

#### a) Method A

Pt(0.5)/TiO<sub>2</sub> was prepared by hydrogen reduction following Pichat *et al.*,<sup>13</sup>. The required amount of 1% H<sub>2</sub>PtCl<sub>6</sub> solution (1 gm of H<sub>2</sub>PtCl<sub>6</sub> dissolved in 100 cm<sup>3</sup> of 0.1 M HCl) was added to an aqueous suspension of TiO<sub>2</sub> (50 cm<sup>3</sup> H<sub>2</sub>O/gm of TiO<sub>2</sub>). The impregnated slurry was evacuated at 353 K in a rotary evaporator, followed by oven drying for 2 h at 373 K. The resulting powder was transferred to a Pyrex tube, flushed with a 0.67 cm<sup>3</sup>s.<sup>-1</sup> flow of N<sub>2</sub> whilst raising the temperature to 573 K. It was then reduced in a 0.5 cm<sup>3</sup>s.<sup>-1</sup> flow of H<sub>2</sub> at 753 K for 16 h. The product was cooled to room temperature in a 0.67 cm<sup>3</sup>s.<sup>-1</sup> flow of N<sub>2</sub> before exposing to air. Further treatment of this catalyst for some experiments was achieved by heating in flowing O<sub>2</sub> for 3 h at 573 K or 16 h at 753 K.

#### b) Method B

Pt(0.5)/TiO<sub>2</sub> and Pd(0.5)/TiO<sub>2</sub> were prepared by the photodeposition method of Kraeutler and Bard<sup>55</sup>. The photocatalytic reactor acted as the preparation vessel, and unfiltered radiation was used to achieve the highest possible U.V. intensity. A known mass of TiO<sub>2</sub> was suspended in 10 cm<sup>3</sup> of 0.1 M HCl to which the required amount of H<sub>2</sub>PtCl<sub>6</sub> or H<sub>2</sub>PdCl<sub>4</sub> had been added. (H<sub>2</sub>PdCl<sub>4</sub> was prepared by dissolving PdCl<sub>2</sub> in 5 cm<sup>3</sup> of 0.1 M HCl). The suspension was neutralised with sodium

carbonate solution, and the pH adjusted to  $\sim 4$  by adding ethanoic acid. The suspension was flushed with  $0.5 \text{ cm}^3 \text{ s}^{-1}$  flow of  $\text{N}_2$  to remove  $\text{O}_2$  and  $\text{CO}_2$  while the reaction vessel temperature was raised to 328 K. These conditions were maintained over a 3.5 h irradiation period. The product was thoroughly washed with distilled water and centrifuged several times until a test with aqueous silver nitrate showed that chlorine ions were no longer present. It was finally dried at 393 K for 16 h.

c) Method C

$\text{Pt}(0.25)/\text{TiO}_2$ ,  $\text{Pt}(0.5)/\text{TiO}_2$ ,  $\text{Pt}(2.0)/\text{TiO}_2$ ,  $\text{Pd}(0.5)/\text{TiO}_2$ ,  $\text{Rh}(0.5)/\text{TiO}_2$  and  $\text{Au}(0.5)/\text{TiO}_2$  were prepared by a photodeposition method analogous to that reported by Gratzel *et al.*,<sup>56,57</sup>. A known mass of  $\text{TiO}_2$  was suspended in  $20 \text{ cm}^3$  of 40% methanal and  $5 \text{ cm}^3$  of methanol, the required amount of  $\text{H}_2\text{PtCl}_6$ ,  $\text{H}_2\text{PdCl}_4$ ,  $(\text{Rh}(\text{NH}_3)_5\text{Cl})\text{Cl}_2$  or  $\text{HAuCl}_4$  was added, and the reaction vessel thoroughly purged with a  $0.5 \text{ cm}^3 \text{ s}^{-1}$  flow of  $\text{N}_2$ , ( $\text{HAuCl}_4$  was prepared by dissolving gold wire in Aqua Regia, evaporated to dryness and dissolving in  $5 \text{ cm}^3$  of 0.1 M  $\text{HCl}$ ). The temperature was then raised to 318 K and maintained at that temperature over an irradiation period sufficient for 100% deposition of the metal ( $\sim 4$  h for Pt, 3 h for Pd and  $\sim 7$  h for Rh or Au). Unfiltered radiation was used as in method B. The product was thoroughly washed with methanol, evacuated at room temperature initially using a water pump followed by a rotary pump to remove remaining methanal and methanol. Finally it was dried in oven at 373 K for 4 h.

Spectroscopic measurements showed that photodeposition of the metal was complete within the total time irradiation period used in both method B and C for catalyst preparation.

## 2.4 Reaction procedure

### 2.4.1 Reaction pretreatment

The U.V. lamp was allowed to warm up for 1.5 h to ensure a stable light intensity before commencing a reaction. Liquid alcohol was added to the required amount of catalyst in the reaction vessel and a suspension obtained by use of the stirrer; the volume of alcohol was 20 cm<sup>3</sup> in all experiments. An inert atmosphere was achieved by flushing the vessel containing the reaction mixture for 30 minutes with a 0.33 cm<sup>3</sup> s.<sup>-1</sup> flow of pure N<sub>2</sub> or He at atmospheric pressure, the flow was maintained during subsequent photoreaction with the metallized anatase. With the anatase used as the support, experiments were made with both pure N<sub>2</sub> or with pure O<sub>2</sub> using the above procedure. The gas inlet tube to the reaction vessel was made of copper to minimise diffusion of O<sub>2</sub> or H<sub>2</sub>O into the gas stream. The reaction was then started by raising the shutter to the U.V. lamp.

### 2.4.2 Monitoring reaction

Periodically, 0.25 cm<sup>3</sup> samples of the reaction mixture were withdrawn using a syringe with a long pliable needle. These were centrifuged to separate the solid catalyst and the supernatant liquid analysed for reaction products.

### 2.4.3 Analysis of reaction products

Various methods of analysis were used depending upon the reactant/product pair.

#### a) Gas-liquid chromatographic analysis

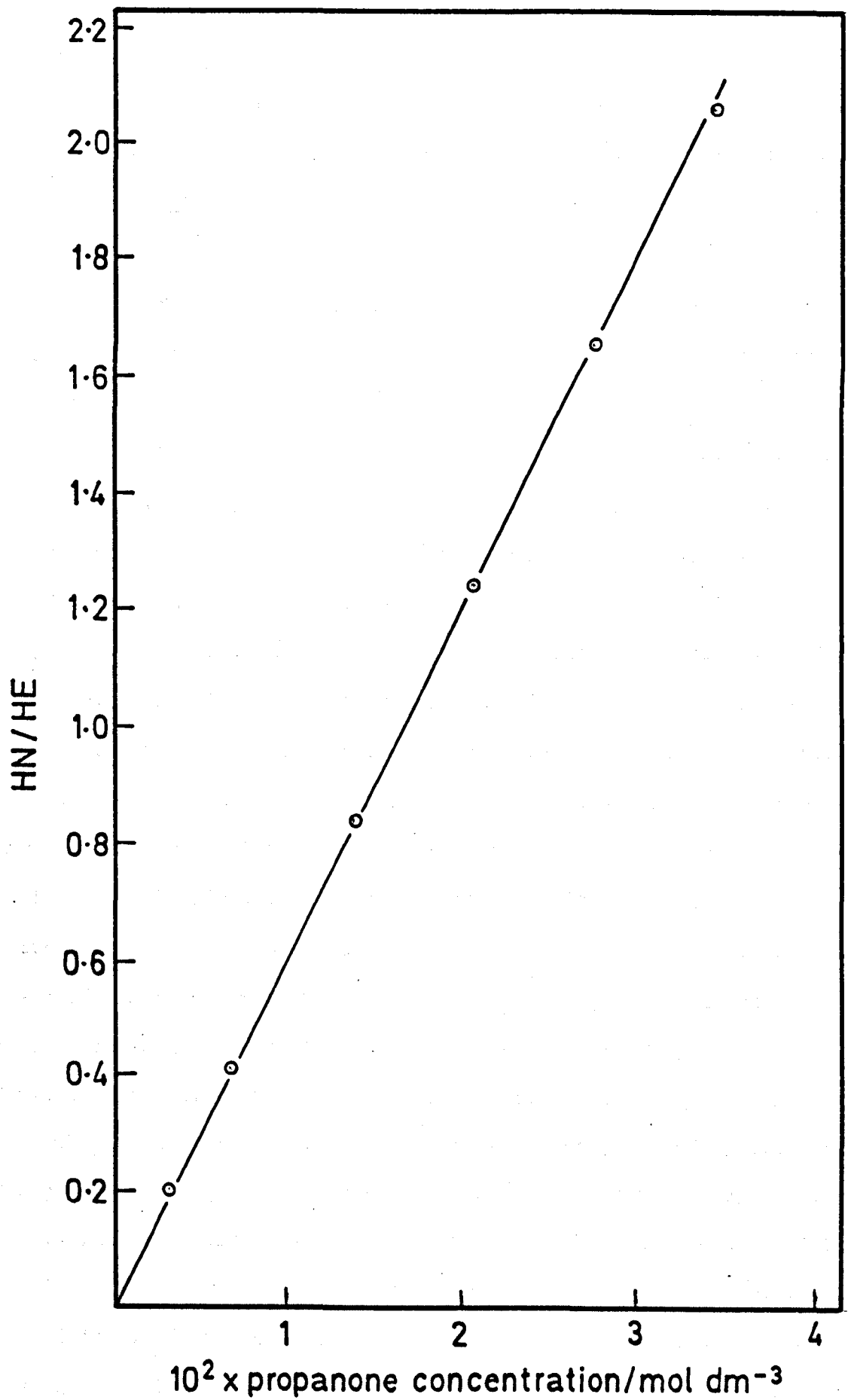
This method was suitable for analysis of the propan-2-ol/propanone system, and was developed by earlier workers<sup>234-236</sup>. Equal volumes

(0.1 cm<sup>3</sup>) of reaction mixture and a standard diethyl ether solution (10  $\mu$ l diethyl ether in 20 cm<sup>3</sup> propan-2-ol) were mixed and a sample of 0.5  $\mu$ l analysed by gas-liquid chromatography. The propanone concentration present in the reaction mixture was determined from the ratio of peak heights for propanone and diethyl ether (HN/HE) by comparison with a calibration graph (figure 2.2) which had been obtained using standard propanone solutions. In the calibration graph, the ratio of the height of the propanone (HN) divided by the height of the diethyl ether peak (HE) plotted against propanone concentration/mol. dm<sup>-3</sup> gave a linear relationship. A Pye 104 flame ionisation gas-liquid chromatograph, fitted with a 3.2 m column of 10% polyethene glycol 400/chromosorb W, was used for analysis and gave a good separation of diethyl ether, propanone and propan-2-ol. The column was maintained at 343 K using a 0.92 cm<sup>3</sup> s<sup>-1</sup> flow N<sub>2</sub> carrier gas. Both the injection port and detector were maintained at 398 K and the flame was sustained by flows of air (6.2 cm<sup>3</sup> s<sup>-1</sup>) and hydrogen (0.85 cm<sup>3</sup> s<sup>-1</sup>). Typical calibration values are given in table 2.1.

TABLE 2.1

$10^2 \times$ propanone concentration/ mol. dm <sup>-3</sup>	HN/HE
0	0
0.34	0.211
0.68	0.420
1.36	0.841
2.04	1.250
2.72	1.660
3.40	2.060

Figure 2.2



Calibration curve for propanone

b) Spectrophotometric analysis

This method was used to determine the concentration of aldehydes produced from the photocatalytic oxidation of methanol, ethanol and propan-1-ol. It is also valid for measuring propanone concentration. The method was adapted from that used by other workers<sup>237-239</sup>, and is based on the formation of 2,4-dinitrophenyl hydrazone, followed by the addition of alcoholic potassium hydroxide to produce a wine colour which could then be spectrophotometrically measured.

Samples of reaction mixture ( $0.1 \text{ cm}^3$ ) in a mixed hexane/ethanol solvent (3:7,  $5 \text{ cm}^3$ ) were reacted with 2,4-dinitrophenyl hydrazine reagent ( $2 \text{ cm}^3$ ) for 30 minutes at 328 K to produce the 2,4-dinitrophenyl hydrozone of the aldehyde. This solution was then cooled to room temperature and diluted to  $25 \text{ cm}^3$  with alcoholic potassium hydroxide solution. The solution was thoroughly mixed and the absorbance at 480 nm measured, after appropriate dilution, on a Perkin-Elmer 552 ultraviolet/visible spectrophotometer using a 1 cm glass cell. The absorbance was directly proportional to the amount of reaction product, whose concentration was determined from a calibration plot (figure 2.3). The calibration plot was obtained by using standard propanone solutions in place of the reaction mixture. The calibration plot consisted of absorbance against concentration of carbonyl compound ( $\text{mol} \cdot \text{dm}^{-3}$ ). Typical calibration values are given in table 2.2.

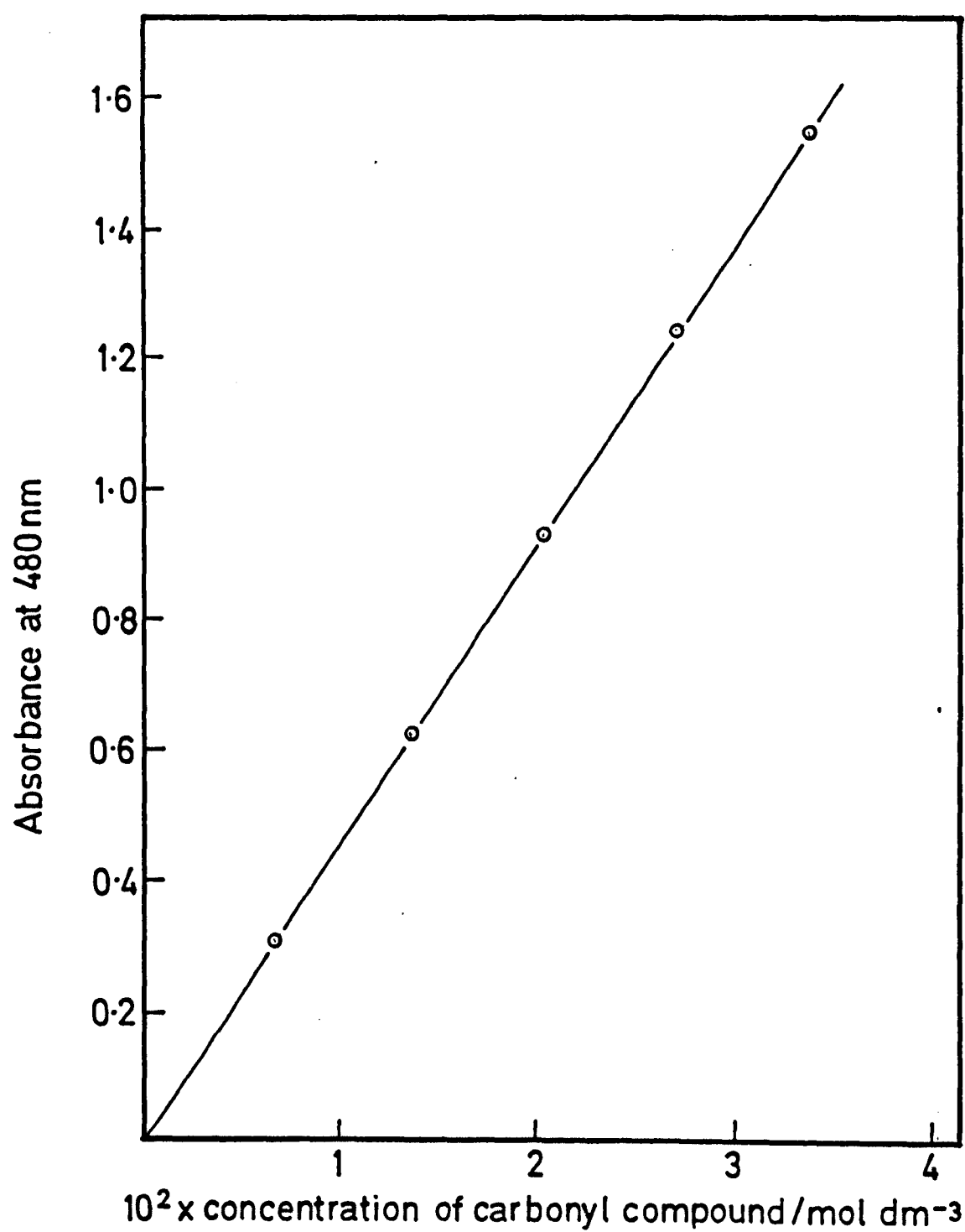
The 2,4-dinitrophenyl hydrazine reagent was prepared by dissolving 0.2 g in ethanol ( $50 \text{ cm}^3$ ) and adding  $2 \text{ cm}^3$  of concentrated hydrochloric acid. The alcoholic potassium hydroxide was prepared by adding 11.8 g to distilled water ( $50 \text{ cm}^3$ ) and diluting to  $200 \text{ cm}^3$  with ethanol.

Both G.L.C. and spectrophotometric analysis were used to monitor the photocatalytic oxidation of propan-2-ol under identical conditions, and both gave the same result.

TABLE 2.2

$10^2 \times$ concentration of carbonyl/ mol. dm. <sup>-3</sup>	Absorbance at 480 nm
0	0
0.68	0.31
1.36	0.62
2.04	0.93
2.72	1.25
3.40	1.55

Figure 2-3



Calibration curve for carbonyl products

## 2.5 Measurements of light intensity and quantum yields

Uranyl oxalate actinometry<sup>240-242</sup>, was used to determine the number of quanta entering the reaction vessel and hence quantum yields for the photocatalytic dehydrogenation reactions. A stirred actinometer solutions ( $25 \text{ cm}^3$ ) containing uranyl sulphate (0.01 M) and oxalic acid (0.05 M) was placed in the reaction vessel and irradiated for a known period of time under a flowing oxygen atmosphere at 298 K. Portions ( $10 \text{ cm}^3$ ) of irradiated and unirradiated actinometer solutions were titrated with standard potassium permanganate solution following the addition of  $3 \text{ cm}^3$  of 10 M sulphuric acid. The absorbance of the actinometer solution was measured on a Perkin-Elmer 552 ultraviolet/visible spectrophotometer at 366 nm.

The light intensity was regularly checked and new lamps were fitted whenever required. The 366 nm light intensities entering the reaction vessel are given in table 2.3.

TABLE 2.3

lamp number	light intensity/ einstein $\text{s}^{-1}$
1	$2.4 \times 10^{-7}$
2	$4.0 \times 10^{-7}$
3	$3.0 \times 10^{-7}$
4	$3.2 \times 10^{-7}$
5	$2.7 \times 10^{-7}$
6	$2.5 \times 10^{-7}$

The light intensities of the lamps and quantum yields were calculated in the following manner:-

$$I_a = \frac{\text{amount of } \text{C}_2\text{O}_4^{2-} \text{ consumed}}{\phi_0 t (1 - 10^{-0.48})}$$

94

where:-

$I_a$  = light absorbed by actinometer solution at a particular time (t).

$\phi_0$  = quantum yield for oxalate loss at 366 nm and 298 K, and equal 0.49 (from the data provided by Calvert and Pitts<sup>242</sup>).

0.48 = absorbance of the uranyl oxalate solution for 366 nm radiation, which was 0.48.

Concentration of  $\text{KMnO}_4$  solution =  $9.68 \times 10^{-3}$  M

Difference in titre reading for  $10 \text{ cm}^3$  sample after 100 minutes of illumination with lamp 4 =  $10.4 \text{ cm}^3$

then:

Amount of oxalate consumed in 100 minutes =

$$\frac{10.4 \times 9.68 \times 10^{-3} \times 5 \times 5}{1000 \times 2 \times 2} = 6.29 \times 10^{-4} \text{ moles}$$

$$I_a = \frac{6.29 \times 10^{-4}}{0.49 \times 100 \times 60 \times (1 - 10^{-0.48})} = 3.2 \times 10^{-7} \text{ einsteins s}^{-1}$$

The quantum yield  $\phi$  is given by =  $\frac{n}{I_a}$

where:

$n$  = number of moles of product formed per second.

The rate of propanone formation from the photooxidation of  $20 \text{ cm}^3$  of propan-2-ol on  $\text{Pt}(0.5)/\text{TiO}_2$  (prepared by method C) using lamp 4 at 293 K =  $4.53 \times 10^{-6} \text{ mol.dm}^{-3} \text{ s}^{-1}$

$$\therefore n = \frac{4.53 \times 10^{-6} \times 20}{1000} = 9.06 \times 10^{-8} \text{ mol.s}^{-1}$$

$$\phi = \frac{9.06 \times 10^{-8}}{3.2 \times 10^{-7}} = 0.28$$

CHAPTER THREERESULTS3.1 Photocatalytic oxidation of propan-2-ol on TiO<sub>2</sub>3.1.1 Preliminary experiments

These experiments were made to determine the conditions necessary for photocatalytic activity of the support prior to deposition of metal. The photo-oxidation of propan-2-ol at 293 K using different masses of anatase was studied with an oxygen pressure of one atmosphere ( $1.01 \times 10^5$  Pa) and 366 nm radiation from lamp 1.

The results are given in table 3.1 and plotted as  $10^2 \times$  propanone concentration/mol. dm.<sup>-3</sup> against time/min in figure 3.1. Reaction rates, expressed in mol. dm.<sup>-3</sup> s.<sup>-1</sup>, are calculated from the slopes of such linear reaction progress plots. Figure 3.2 shows that a catalyst mass of 150 mg is sufficient to achieve the maximum reaction rate.

TABLE 3.1

time/ min.	$10^2 \times$ propanone concentration/mol.dm. <sup>-3</sup>							
	mass/mg 7.1	13.9	23.7	35.7	57.2	101.4	200.0	349.9
0	0	0	0	0	0	0	0	0
15	0.196	0.255	-	-	0.267	-	-	0.281
20	-	-	0.314	0.350	-	0.375	0.369	-
30	0.377	0.467	-	-	0.550	-	-	0.561
40	-	-	0.669	0.701	-	0.744	0.746	-
45	0.534	0.705	-	-	0.824	-	-	0.842
60	0.785	0.926	0.989	1.055	1.115	1.146	1.130	-
70	-	-	-	-	-	-	-	1.309
75	0.958	1.148	-	-	1.382	-	-	-

Contd. over

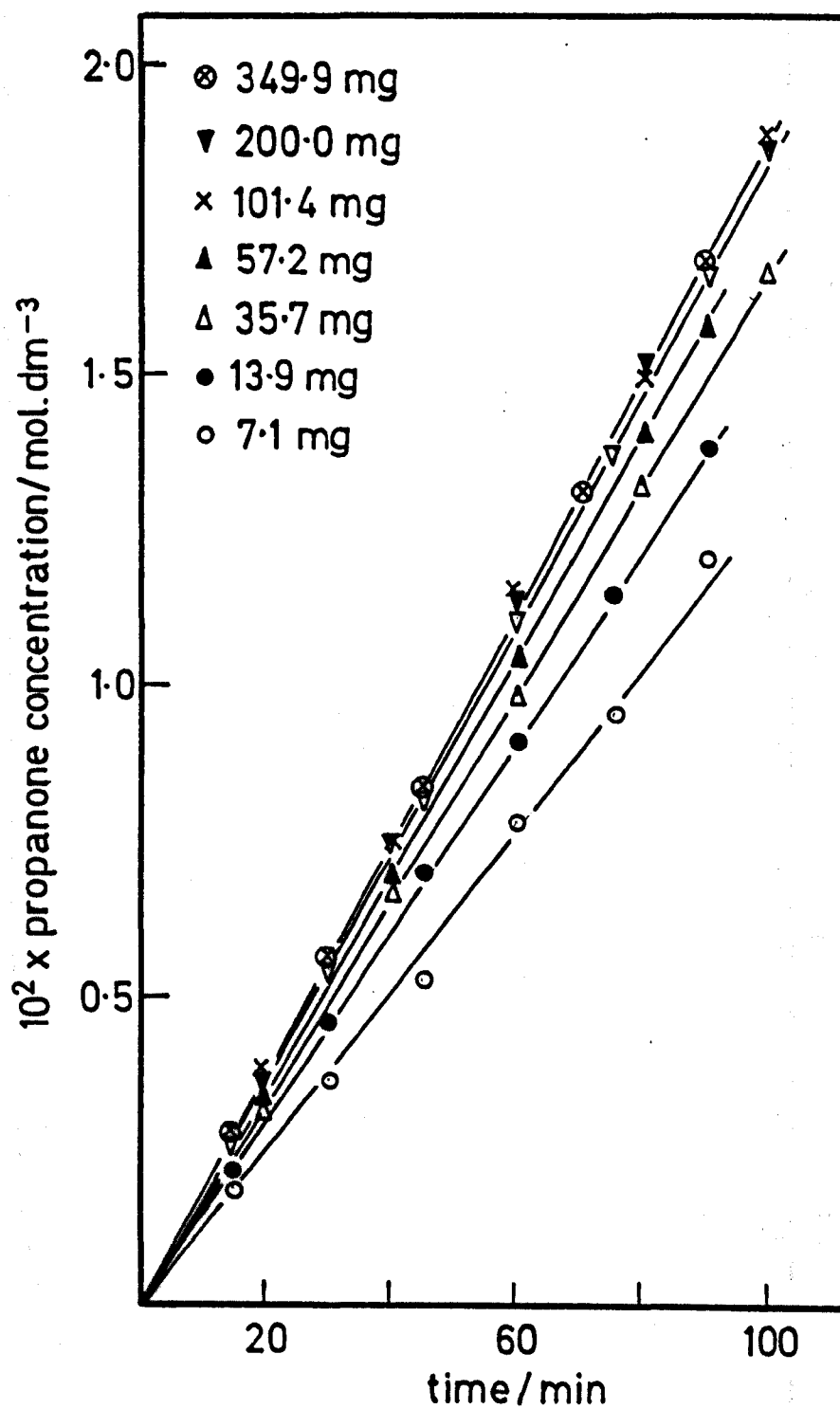
80	-	-	1.323	1.411	-	1.500	1.507	-
90	1.209	1.382	-	1.597	1.66	-	-	1.683
100	-	-	1.658	-	-	1.884	1.868	-
$10^6 \times \text{rate}/$ $\text{mol.dm}^{-3}\text{s}^{-1}$	2.17	2.55	2.77	2.95	3.07	3.12	3.11	3.12

The reaction of propan-2-ol at 293 K on anatase (150 mg) was followed in the presence of U.V. radiation from lamp 2 and oxygen, in the presence of U.V. radiation and nitrogen, in the presence of oxygen without U.V. radiation and in the presence of nitrogen without U.V. light. The following results are found:

- 1) The only reaction product detected was propanone.
- 2) In the presence of oxygen and U.V., the propanone concentration increased linearly with irradiation time.
- 3) In the presence of nitrogen and U.V. radiation, propanone production was extremely slow and ceased entirely after 1 h. irradiation. Furthermore, the observation that anatase became grey-blue in colour suggests the loss of lattice oxygen.
- 4) There was no dark reaction in the presence of either oxygen or nitrogen.

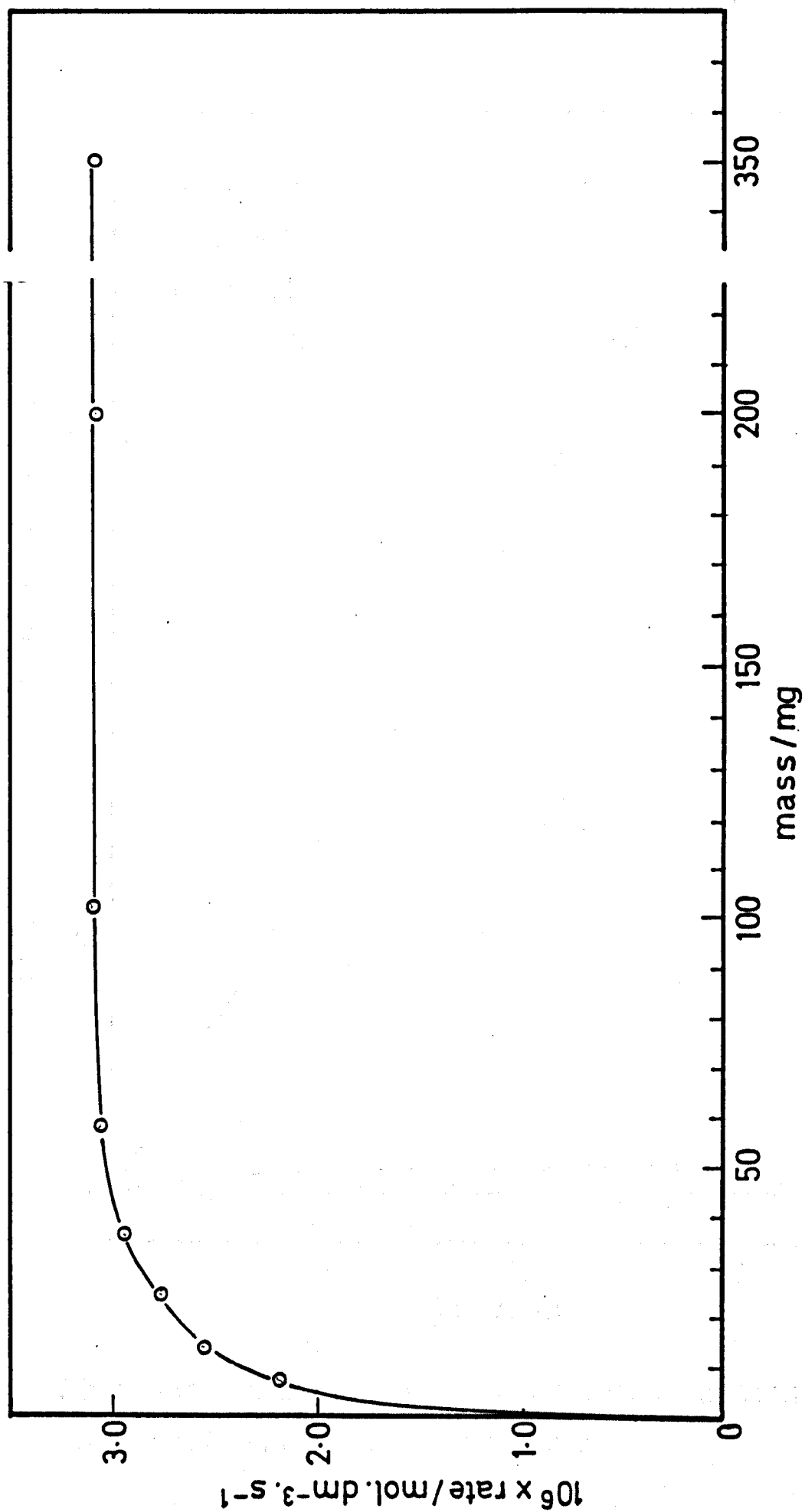
These results are shown in table 3.2 and plotted in figure 3.3 as  $10^2 \times \text{propanone concentration/mol.dm}^{-3}$  against time/min.

Figure 3.1



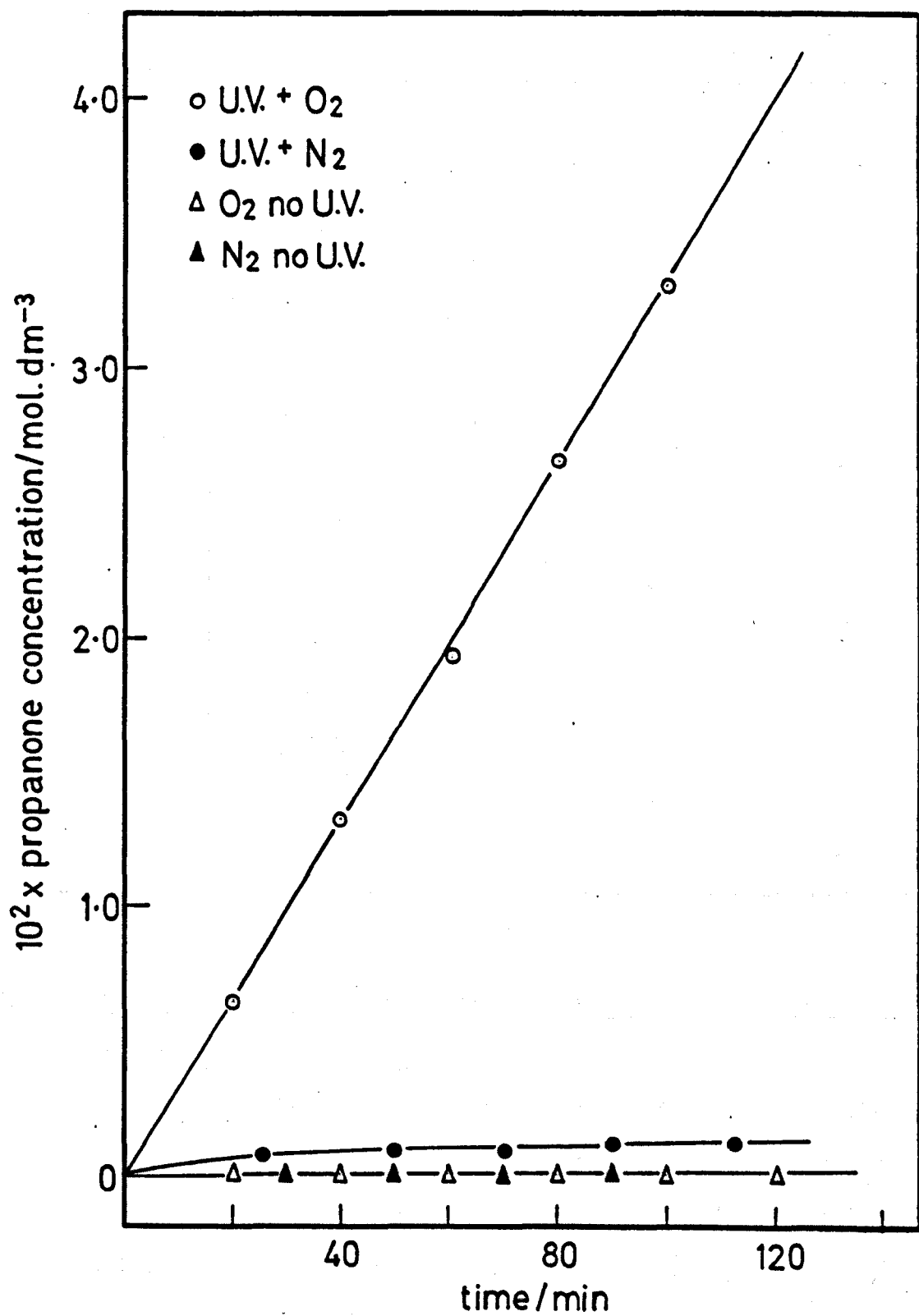
Photocatalytic oxidation of propan-2-ol on different masses of anatase at 293K

Figure 3.2



Photocatalytic oxidation of propan-2-ol on different masses of anatase at 293 K

Figure 3.3



Photocatalytic oxidation of propan-2-ol on anatase  
under different reaction conditions

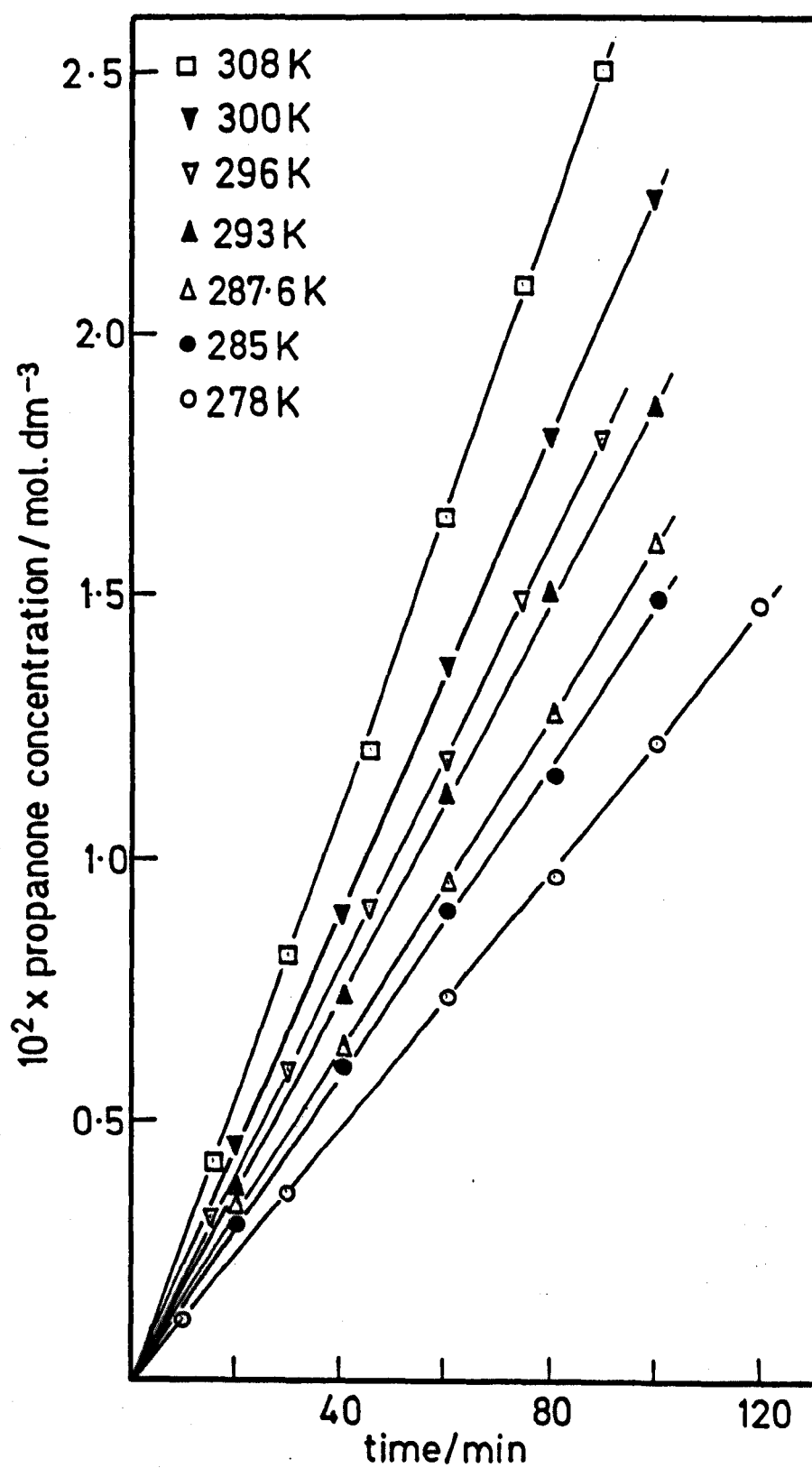
TABLE 3.2

time/min.	$10^2 \times \text{propanone concentration/mol.dm}^{-3}$			
	U.V. + O <sub>2</sub>	U.V. + N <sub>2</sub>	O <sub>2</sub> , no U.V.	N <sub>2</sub> , no U.V.
0	0	0	0	0
20	0.665	-	0	-
25	-	0.079	-	-
30	-	-	-	0
40	1.320	-	0	-
50	-	0.092	-	0
60	1.943	-	0	-
70	-	0.107	-	0
80	2.661	-	0	-
90	-	0.118	-	0
100	3.312	-	0	-
112	-	0.126	-	-
120	-	-	0	-

### 3.1.2 Temperature dependence of reaction rate for the photocatalytic oxidation of propan-2-ol

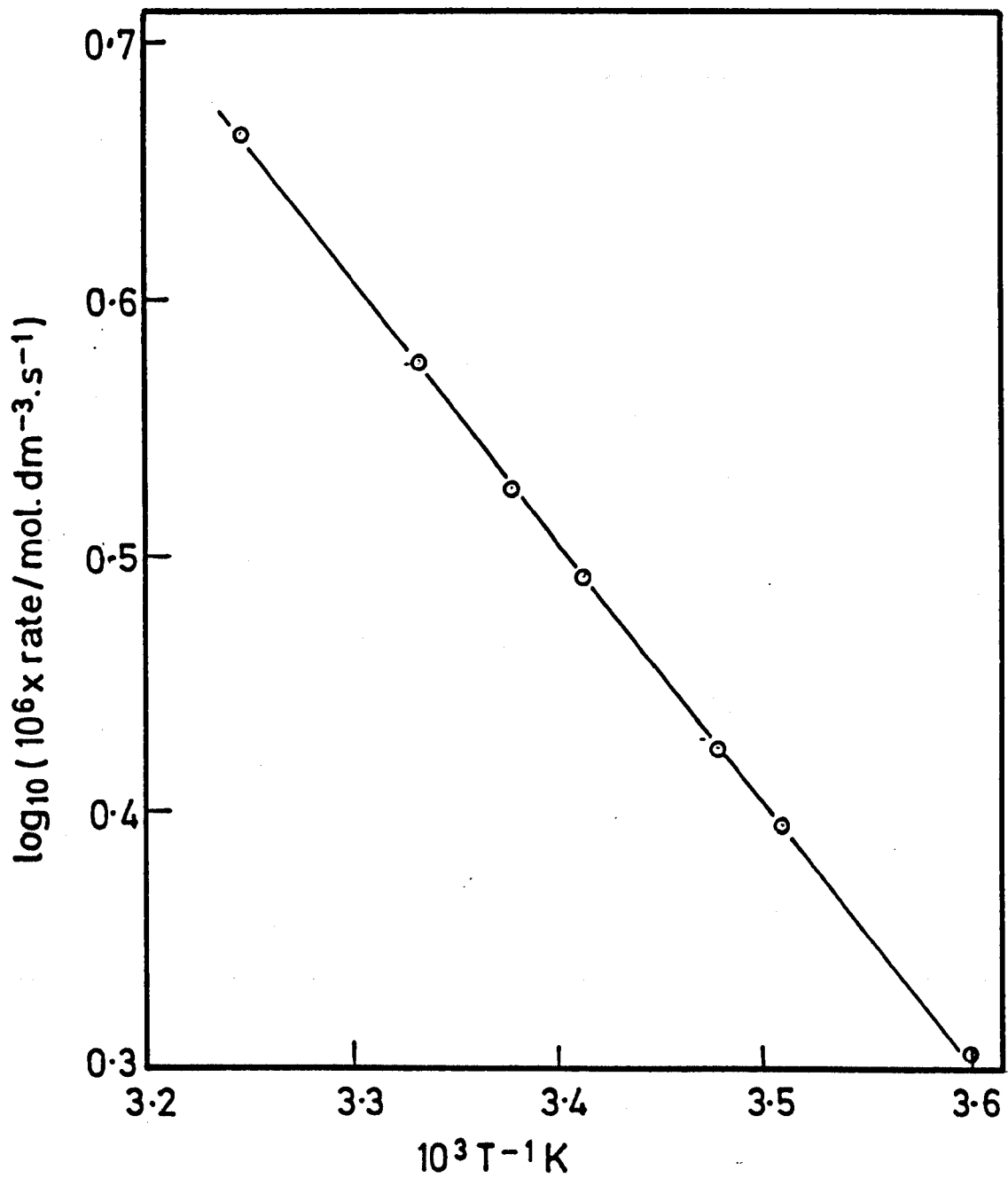
Reaction was followed at seven temperatures in the range 278-308 K using 366 nm radiation from lamp 1, 150 mg of anatase and an oxygen pressure of one atmosphere. The results are shown in table 3.3 and plotted in figure 3.4 as  $10^2 \times \text{propanone concentration/mol.dm}^{-3}$  against time/min. The activation energy of  $20 \pm 1 \text{ kJ mol}^{-1}$  for propanone formation was calculated from figure 3.5 where  $\log(10^6 \times \text{rate of reaction/mol.dm}^{-3}\text{s}^{-1})$  is plotted against  $10^3 T^{-1} \text{ K}$ .

Figure 3.4



Photocatalytic oxidation of propan-2-ol on  
anatase at different temperatures

Figure 3.5



Temperature dependence for the photocatalytic oxidation  
of propan-2-ol on anatase

TABLE 3.3

time/min.	$10^2 \times \text{propanone concentration/mol.dm}^{-3}$						
	T/K						
	278	285	287.6	293	296	300	308
0	0	0	0	0	0	0	0
10	0.114	-	-	-	-	-	-
15	-	-	-	-	0.314	-	0.420
20	-	0.298	0.338	0.369	-	0.463	-
30	0.361	-	-	-	0.597	-	0.809
40	-	0.605	0.645	0.746	-	0.895	-
45	-	-	-	-	0.903	-	1.210
60	0.732	0.895	0.958	1.130	1.193	1.374	1.648
75	-	-	-	-	1.484	-	2.101
80	0.968	1.162	1.280	1.507	-	1.802	-
90	-	-	-	-	1.798	-	2.500
100	1.215	1.492	1.601	1.868	-	2.264	-
120	1.478	-	-	-	-	-	-
$10^6 \times \text{rate/}$ $\text{mol.dm}^{-3}\text{s}^{-1}$	2.02	2.48	2.67	3.11	3.36	3.76	4.63

### 3.1.3 Light intensity dependence of reaction rate for the photocatalytic oxidation of propan-2-ol

These experiments were made at 293 K using 366 nm radiation from lamp 4 and lamp 6, 150 mg of anatase and an oxygen pressure of one atmosphere. Neutral density filters were inserted to obtain different light intensities. The results are shown in table 3.4 and plotted in

figure 3.6 as  $10^2 \times \text{propanone concentration/mol.dm}^{-3}$  against time/min. and in figure 3.7 as  $10^6 \times \text{reaction rate/mol.dm}^{-3}\text{s}^{-1}$  against  $10^4 \times \text{square root of light intensity/}(\text{einstein s}^{-1})^{\frac{1}{2}}$  for the results obtained using lamp 4. The results shown in table 3.5 and plotted in figure 3.8 as  $10^2 \times \text{propanone concentration/mol.dm}^{-3}$  against time/min., and in figure 3.9 as  $10^6 \times \text{reaction rate/mol.dm}^{-3}\text{s}^{-1}$  against  $10^4 \times \text{square root of light intensity/}(\text{einstein s}^{-1})^{\frac{1}{2}}$  for the results obtained using lamp 6.

A square root light intensity dependence was observed for light intensities  $> 0.65 \times 10^{-7} \text{ einstein s}^{-1}$  and independent of the lamp used.

TABLE 3.4

time/min.	$10^2 \times \text{propanone concentration/mol.dm}^{-3}$							
	$10^7 \times I/\text{einstein s}^{-1}$							
	3.20	2.74	2.08	1.67	1.16	0.82	0.65	0.14
0	0	0	0	0	0	0	0	0
20	0.520	0.450	0.370	0.345	0.303	0.239	0.219	-
40	1.006	-	0.772	0.700	0.608	0.518	0.441	-
41	-	0.939	-	-	-	-	-	-
50	-	-	-	-	-	-	-	0.150
60	1.509	1.360	1.201	1.030	0.932	0.731	0.659	-
80	2.021	1.820	1.621	1.421	1.221	0.982	0.850	-
100	2.500	2.300	2.011	1.782	-	1.230	1.099	-
122	-	-	-	-	-	-	-	0.390
180	-	-	-	-	-	-	-	0.568
240	-	-	-	-	-	-	-	0.730

Contd. over

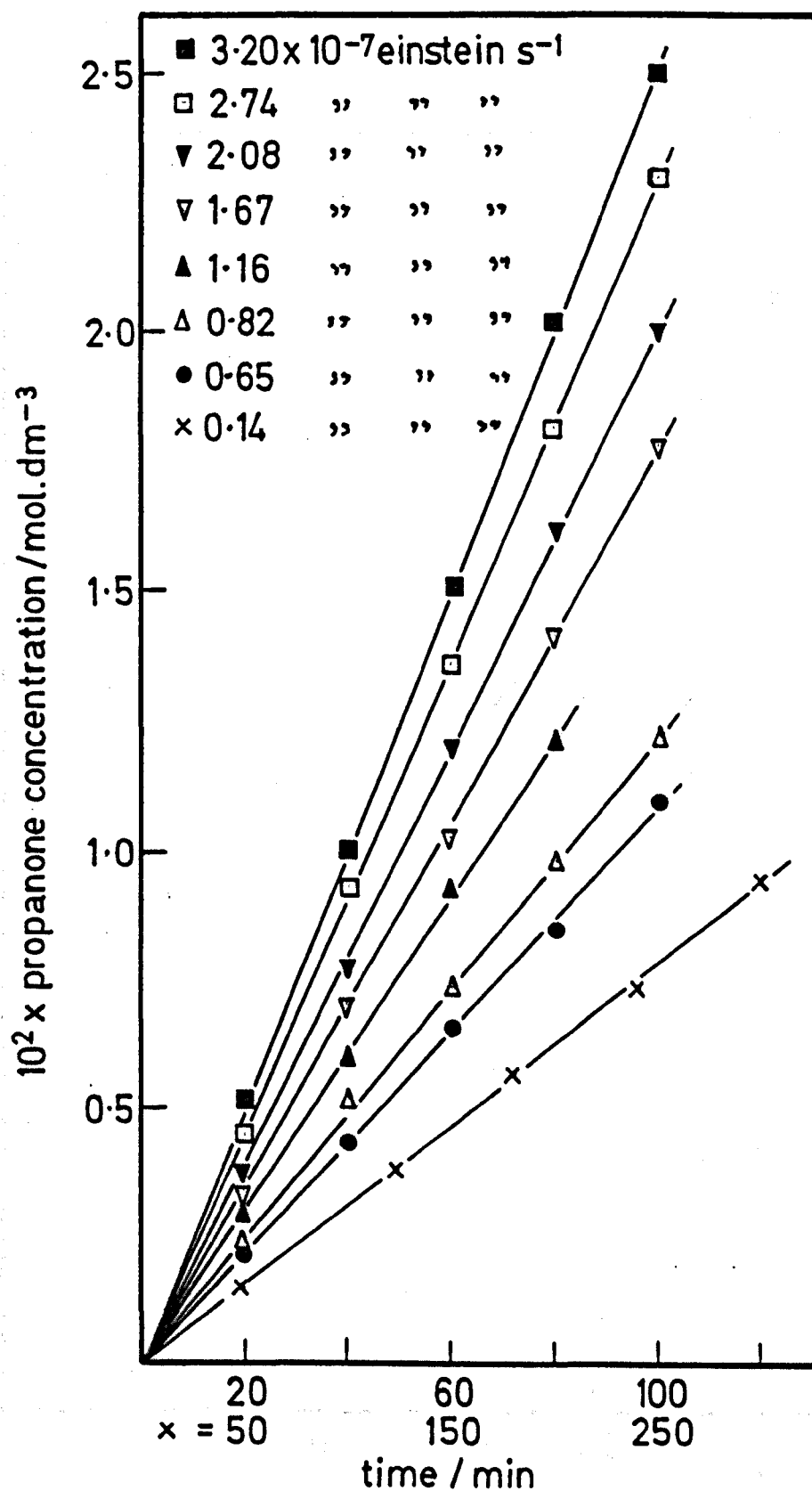
300	-	-	-	-	-	-	-	0.941
$10^6 \times \text{rate}/$ $\text{mol.dm}^{-3}\text{s}^{-1}$	4.17	3.82	3.35	2.97	2.53	2.05	1.82	0.53

TABLE 3.5

time/min.	$10^2 \times \text{propanone concentration}/\text{mol.dm}^{-3}$								
	$10^7 \times I/\text{einstein s}^{-1}$								
	2.5	2.06	1.54	1.24	0.94	0.81	0.60	0.48	0.27
0	0	0	0	0	0	0	0	0	0
10	-	-	0.181	-	-	-	-	-	-
15	-	-	-	0.239	-	-	-	-	-
20	0.481	-	0.379	-	-	-	-	-	-
25	-	0.519	-	-	-	-	-	-	-
30	-	-	-	0.489	0.438	-	-	-	-
35	-	-	-	-	-	-	0.403	-	-
40	1.802	-	0.739	-	-	0.561	-	0.381	0.219
45	-	-	-	0.702	-	-	-	-	-
50	-	1.082	-	-	-	-	-	-	-
55	-	-	-	-	0.799	-	-	-	-
60	1.380	-	-	1.003	0.900	0.802	-	0.597	-
70	-	-	1.300	-	-	-	0.819	-	-
75	-	1.602	-	1.221	-	-	-	-	-
80	1.800	-	-	-	-	1.123	-	0.722	0.479

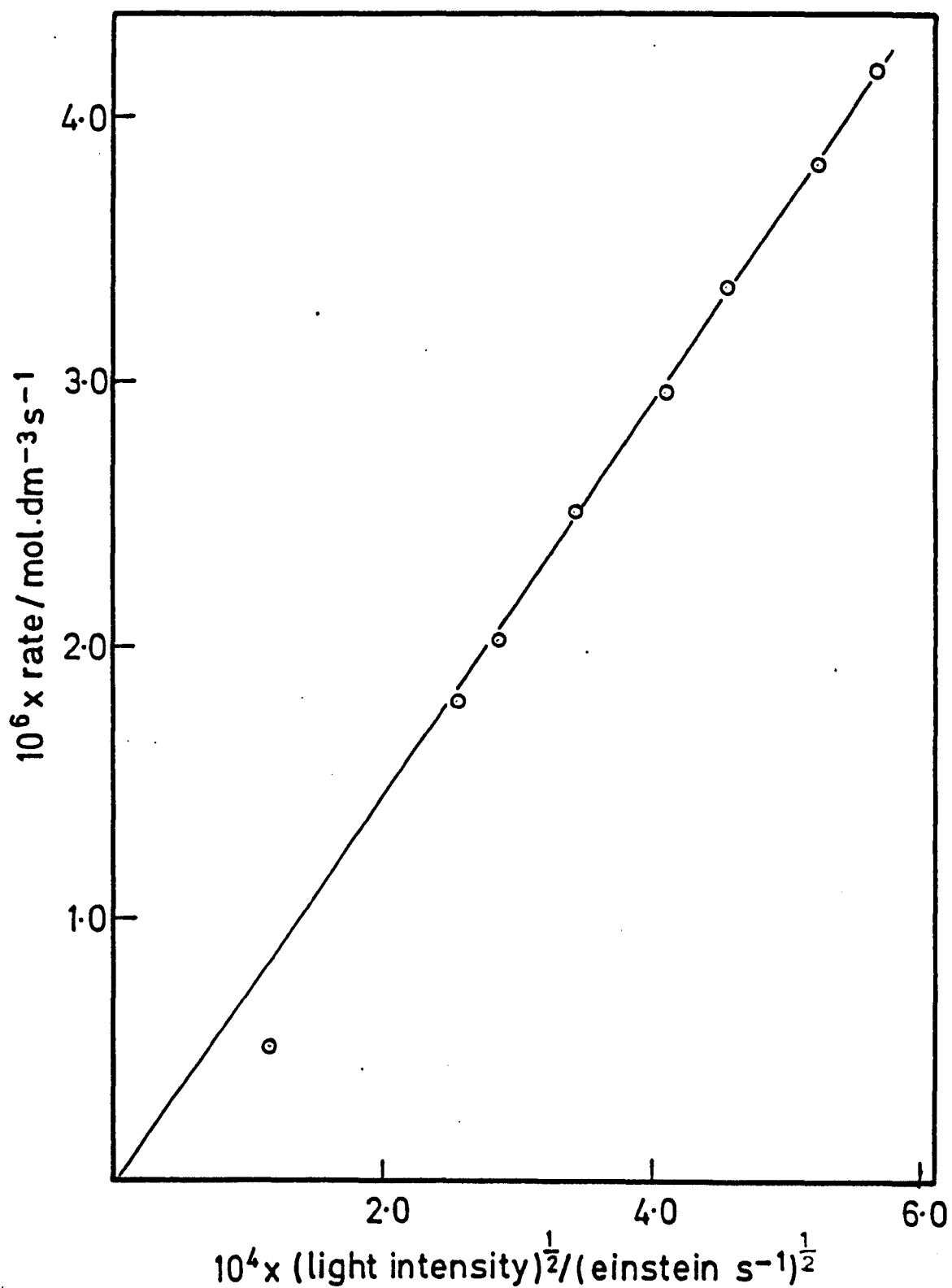
Contd. over

Figure 3.6



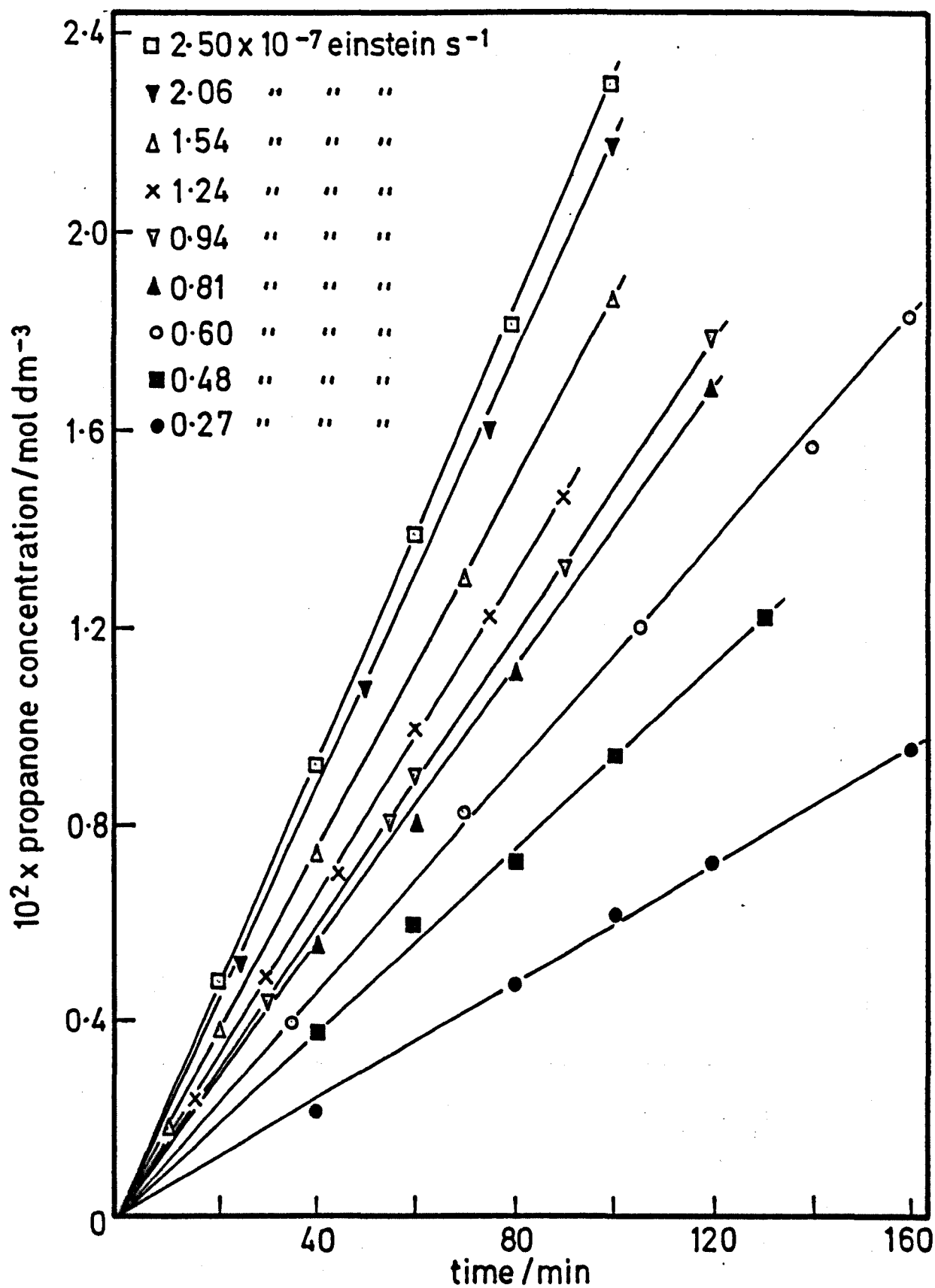
Photocatalytic oxidation of propan-2-ol on anatase  
at different light intensities

Figure 3.7



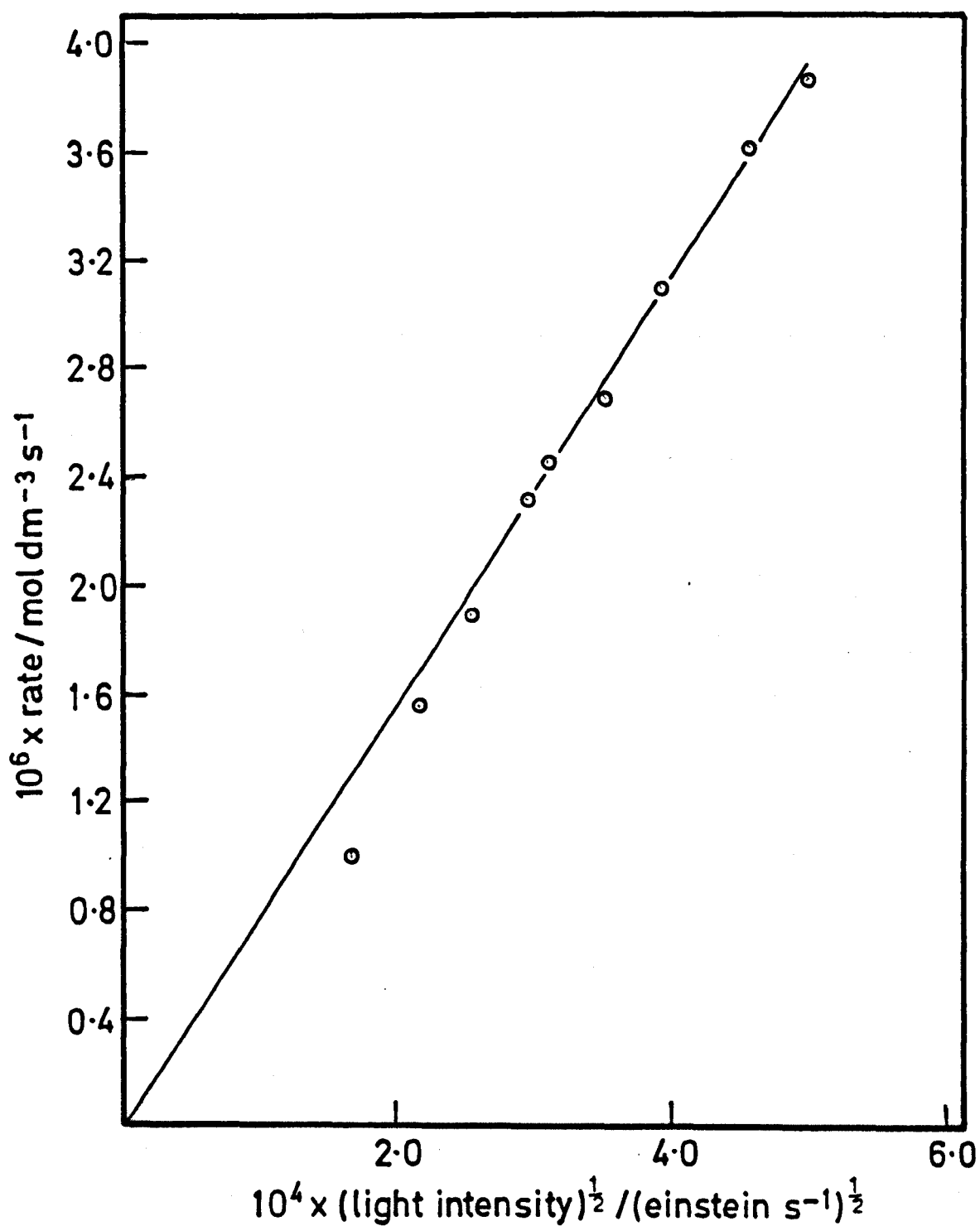
Light intensity dependence for the photocatalytic oxidation of propan-2-ol on anatase at 293K

Figure 3.8



Photocatalytic oxidation of propan-2-ol on anatase at different light intensities

Figure 3-9



Light intensity dependence for the photocatalytic oxidation  
of propan-2-ol on anatase at 293K

90	-	-	-	1.459	1.320	-	-	-	-
100	2.290	2.172	1.865	-	-	-	-	0.940	0.622
105	-	-	-	-	-	-	1.198	-	-
120	-	-	-	-	1.783	1.681	-	-	0.720
130	-	-	-	-	-	-	-	1.219	-
140	-	-	-	-	-	-	1.560	-	-
160	-	-	-	-	-	-	1.820	-	0.959
$10^6 \times \text{rate}/$ $\text{mol.dm}^{-3}\text{s}^{-1}$	3.82	3.62	3.11	2.70	2.46	2.32	1.90	1.57	1.00

#### 3.1.4 Temperature dependence of reaction rate at different light intensities for the photocatalytic oxidation of propan-2-ol

The temperature dependence of reaction rate at full intensity and the light intensity dependence at constant temperature (293 K) have been investigated in 3.1.2 and 3.1.3. To determine possible effects of light intensity on the activation energy for propanone formation, the reaction rate was determined as a function of temperature at three incident light intensities. Neutral density filters were used to produce the different light intensities from lamp 4. Catalyst masses of 150 mg and an oxygen pressure of one atmosphere were used throughout the experiments.

##### a) Full light intensity ( $3.20 \times 10^{-7}$ einstein $\text{s}^{-1}$ )

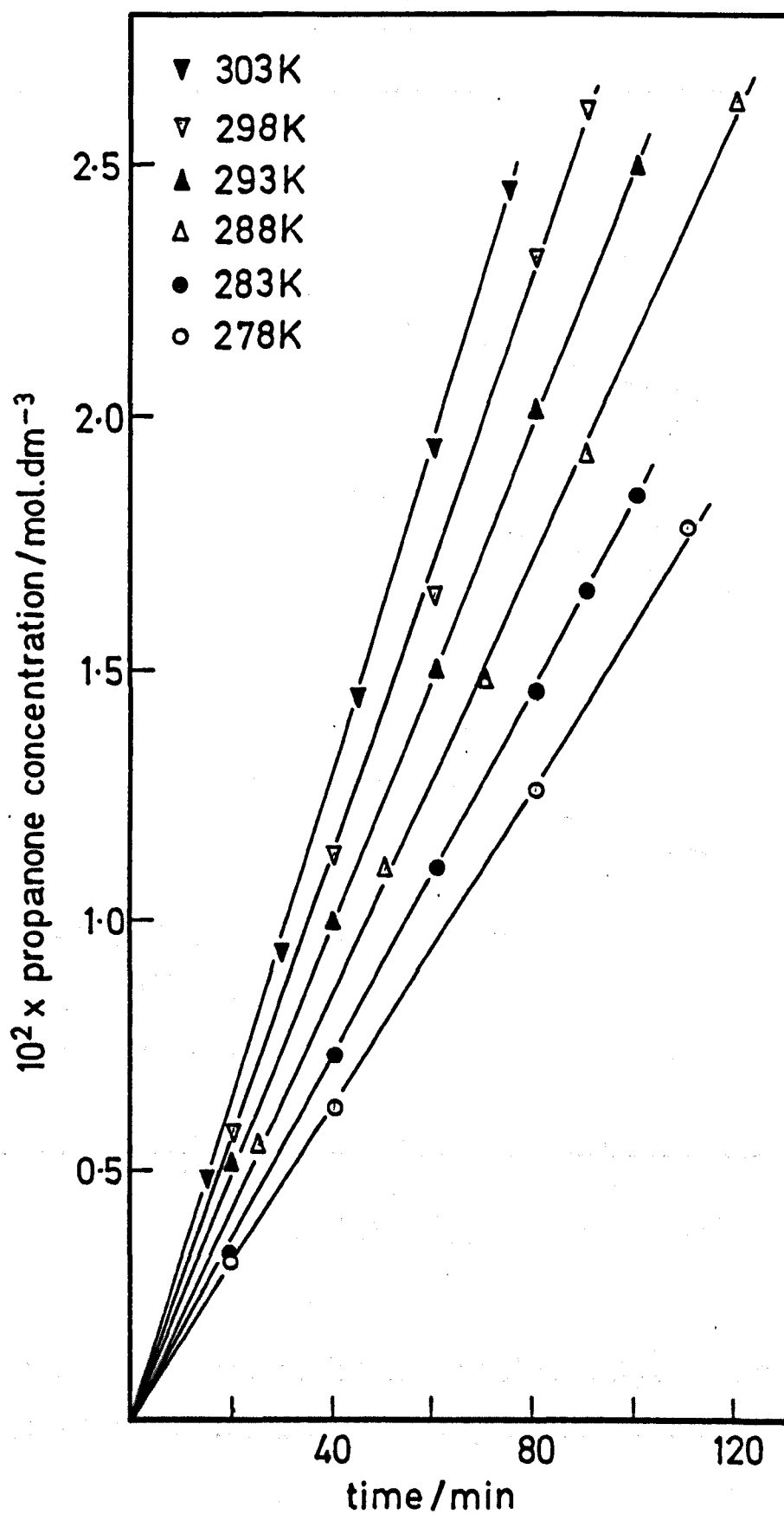
These experiments were carried out with unreduced light intensity over the temperature range 278-303 K. The results are given in table 3.6 and plotted in figure 3.10 as  $10^2 \times \text{propanone concentration}/\text{mol.dm}^{-3}$  against time/min., and in figure 3.11 as  $\log(10^6 \times \text{rate of reaction}/$

mol.dm.<sup>-3</sup>s.<sup>-1</sup>) against 10<sup>3</sup>T<sup>-1</sup>K. These results give an activation energy of 20 ± 1 kJmol.<sup>-1</sup> for propanone formation which is the same value as that obtained using full light intensity of lamp 1.

TABLE 3.6

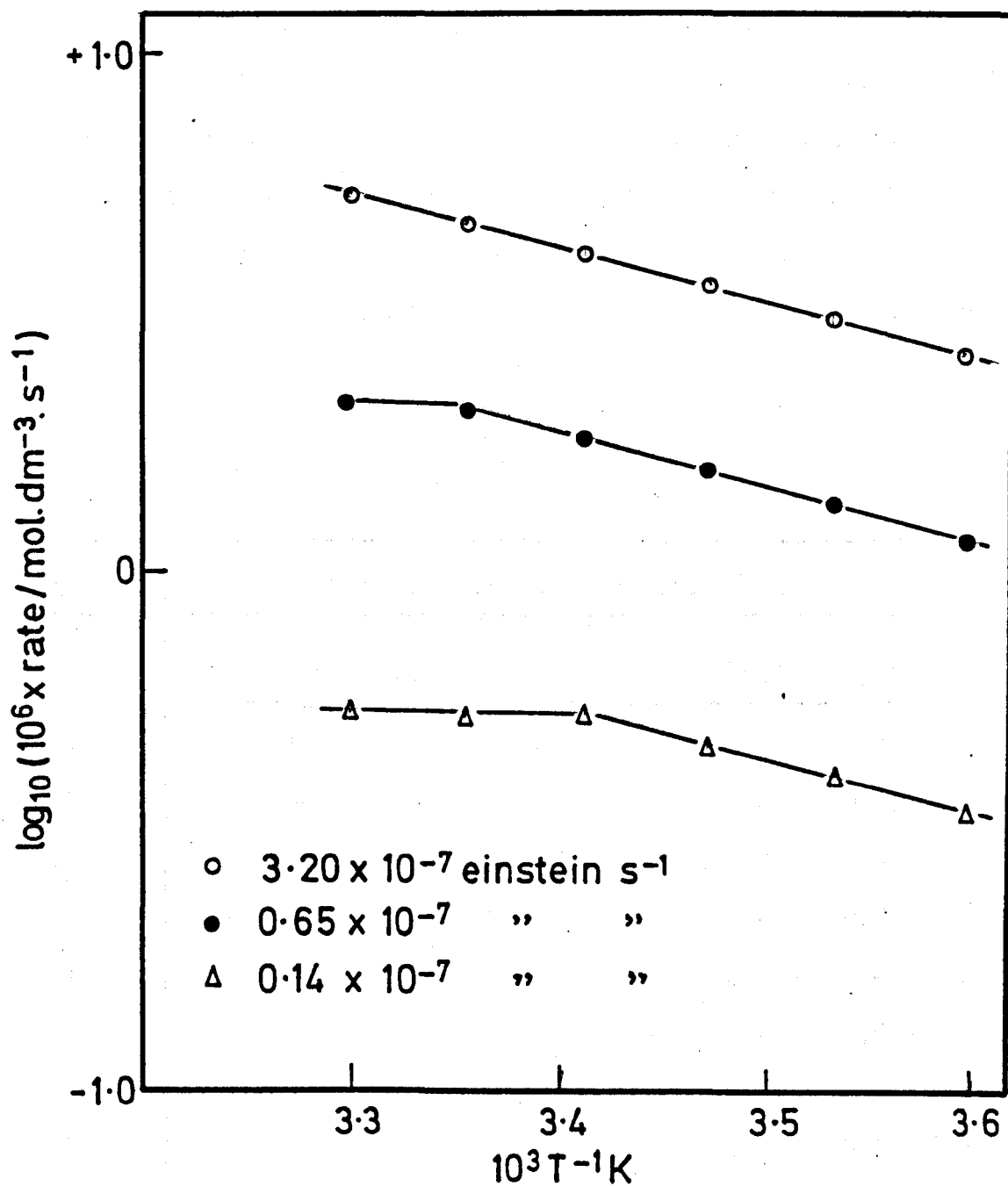
time/min.	$10^2 \times \text{propanone concentration/mol.dm}^{-3}$					
	T/K					
	278	283	288	293	298	303
0	0	0	0	0	0	0
15	-	-	-	-	-	0.491
20	0.300	0.357	-	0.520	0.581	-
25	-	-	0.560	-	-	-
30	-	-	-	-	-	0.949
40	0.635	0.742	-	1.006	1.134	-
45	-	-	-	-	-	1.449
50	-	-	1.110	-	-	-
60	-	1.110	-	1.509	1.652	1.940
70	-	-	1.485	-	-	-
75	-	-	-	-	-	2.451
80	1.268	1.462	-	2.021	2.321	-
90	-	1.658	1.931	-	2.612	-
100	-	1.850	-	2.500	-	-
110	1.786	-	-	-	-	-
120	-	-	2.630	-	-	-
$10^6 \times \text{rate/}$ $\text{mol.dm}^{-3}\text{s}^{-1}$						
	2.67	3.08	3.63	4.17	4.82	5.46

Figure 3.10



Photocatalytic oxidation of propan-2-ol on anatase at different temperatures, with a light intensity of  $3.20 \times 10^{-7}$  einstein  $\text{s}^{-1}$

Figure 3.11



Temperature dependence for the photocatalytic oxidation of propan-2-ol using different light intensities

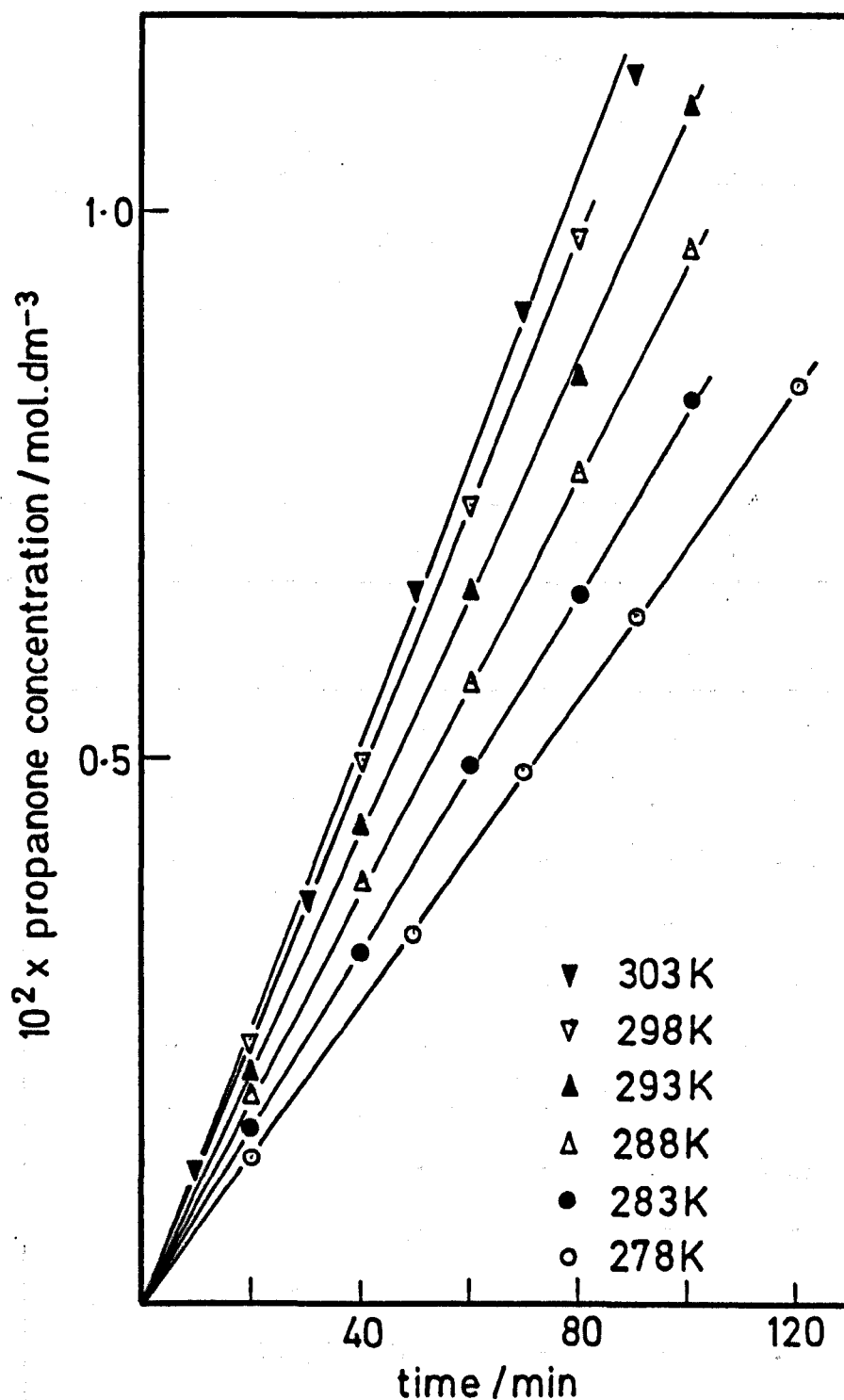
b) 20.2% relative light intensity ( $0.65 \times 10^{-7}$  einstein  $\text{s}^{-1}$ )

These experiments were carried out in the temperature range 278 - 303 K. The results are shown in table 3.7 and plotted in figure 3.12 as  $10^2 \times$  propanone concentration/ $\text{mol} \cdot \text{dm}^{-3}$  against time/min. and in figure 3.11 as  $\log(10^6 \times \text{rate of reaction}/\text{mol} \cdot \text{dm}^{-3} \cdot \text{s}^{-1})$  against  $10^3 T^{-1} \text{K}$ . The Arrhenius plot possessing a good linearity between 278 - 298 K gives an activation energy of  $20 \pm 1 \text{ kJ mol}^{-1}$  for propanone formation which is the same as that obtained using full light intensity. However, above 298 K the activation energy tends to zero.

TABLE 3.7

time/min.	$10^2 \times$ propanone concentration/mol.dm. <sup>-3</sup>					
	T/K					
	278	283	288	293	298	303
0	0	0	0	0	0	0
10	-	-	-	-	-	0.122
20	0.134	0.161	0.191	0.219	0.244	-
30	-	-	-	-	-	0.371
40	-	0.328	0.390	0.441	0.503	-
50	0.342	-	-	-	-	0.659
60	-	0.502	0.572	0.659	0.741	-
70	0.494	-	-	-	-	0.911
80	-	0.652	0.766	0.850	0.976	-
90	0.638	-	-	-	-	1.129
100	-	0.830	0.964	1.099	-	-
120	0.839	-	-	-	-	-
$10^6 \times$ rate/ mol.dm. <sup>-3</sup> s. <sup>-1</sup>	1.17	1.36	1.59	1.82	2.03	2.16

Figure 3.12



Photocatalytic oxidation of propan-2-ol on anatase at different temperatures with a light intensity of  $0.65 \times 10^{-7}$  einstein s<sup>-1</sup>

c) 4.4% relative light intensity ( $0.14 \times 10^{-7}$  einstein  $\text{s}^{-1}$ )

These experiments were carried out in the temperature range 278 - 303 K. The results are shown in table 3.8 and plotted in figure 3.13 as  $10^2 \times$  propanone concentration/mol.dm $^{-3}$  against time/min. and in figure 3.11 as  $\log (10^6 \times \text{rate of reaction/mol.dm}^{-3}\text{s}^{-1})$  against  $10^3 T^{-1}$  K. The Arrhenius plot is linear between 278 - 303 K and gives an activation energy of  $20 \pm 1$  kJ mol $^{-1}$  for propanone formation which is the same as that obtained using different light intensity. However above 293 K the activation energy tends to zero.

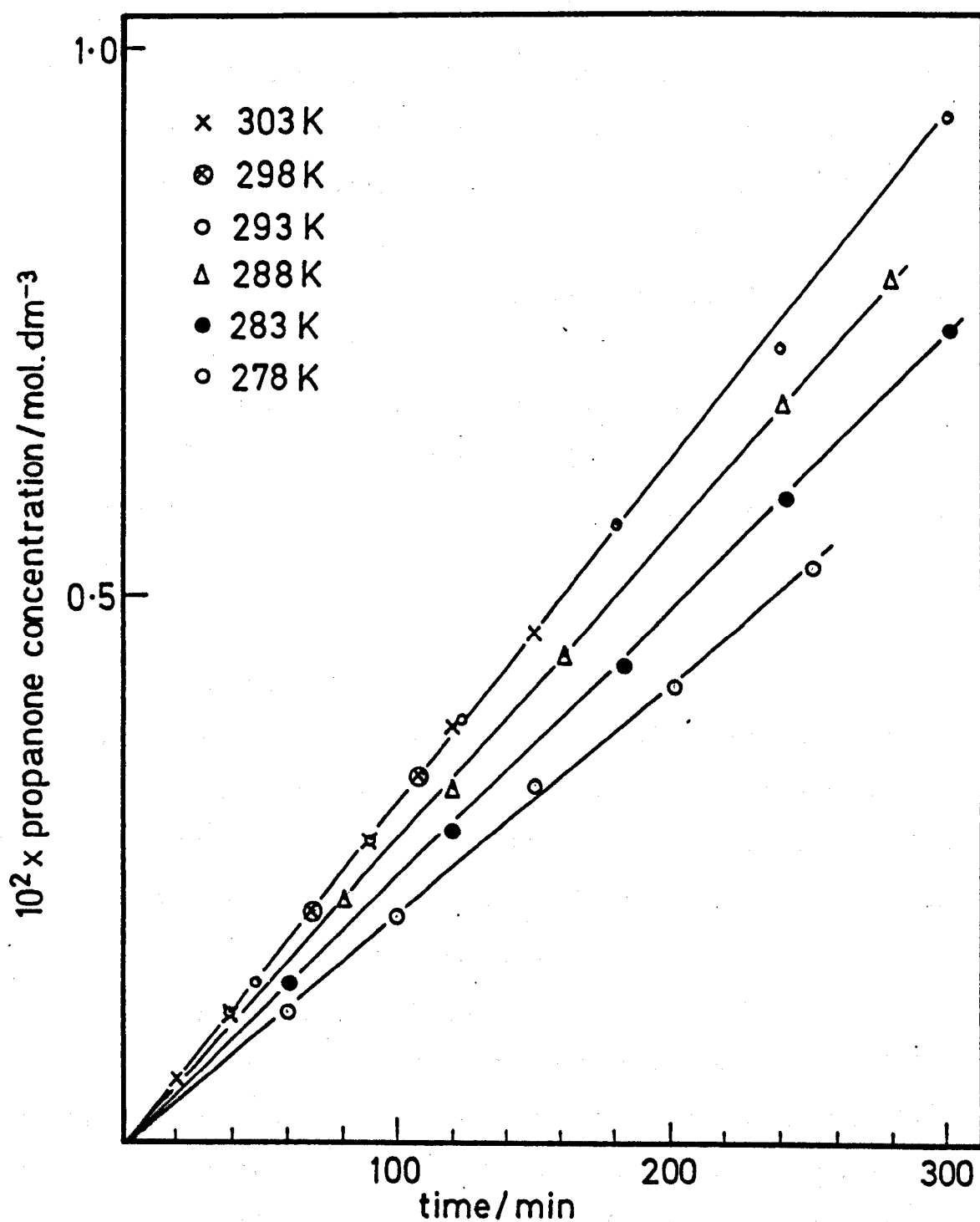
TABLE 3.8

time/min.	$10^2 \times$ propanone concentration/mol.dm $^{-3}$					
	T/K					
	278	283	288	293	298	303
0	0	0	0	0	0	0
20	-	-	-	-	0.058	-
40	-	-	-	-	0.118	0.121
50	-	-	-	0.150	-	-
60	0.124	0.149	-	-	-	-
70	-	-	-	-	0.215	-
80	-	-	0.221	-	-	-
90	-	-	-	-	0.275	0.278
100	0.212	-	-	-	-	-
110	-	-	-	-	0.336	-
120	-	0.290	0.328	-	-	0.372
122	-	-	-	0.390	-	-

Contd. over

150	0.330	-	-	-	-	0.459
180	-	-	0.452	0.568	-	-
182	-	0.442	-	-	-	-
200	0.425	-	-	-	-	-
240	-	0.589	0.681	0.730	-	-
250	0.531	-	-	-	-	-
280	-	-	0.791	-	-	-
300	-	0.742	-	0.941	-	-
$10^6 \times \text{rate}/$ $\text{mol} \cdot \text{dm}^{-3} \cdot \text{s}^{-1}$	0.35	0.41	0.47	0.53	0.52	0.53

Figure 3.13



Photocatalytic oxidation of propan-2-ol on anatase at different temperatures with a light intensity of  $0.14 \times 10^{-7} \text{ einstein s}^{-1}$

### 3.2 Dehydrogenation of alcohols on platinized anatase (Pt(0.5)/TiO<sub>2</sub>) prepared by hydrogen reduction (Method A)

These experiments were carried out under a nitrogen pressure of one atmosphere using 150 mg of catalyst which is the same mass used for anatase (see section 3.1.1). It is relevant that Pichat et al.,<sup>13</sup> achieved maximum activity with 50 mg of Pt(4.85)/TiO<sub>2</sub> prepared by an identical method for the photocatalytic oxidation of 20 cm<sup>3</sup> of an equi-volume mixture of methanol and water. However, in view of the maximum activity for platinized anatase Pt(0.5)/TiO<sub>2</sub> prepared by method C observed with a mass  $> 100$  mg (see section 3.4.1), a catalyst mass of 150 mg was used in the present experiments to ensure that maximum activity was achieved.

#### 3.2.1 The dark reaction

Pt(0.5)/TiO<sub>2</sub> prepared by method A exhibited a pronounced dark reaction in the presence of nitrogen resulting in curved reaction progress plots if it were not allowed to achieve completion before irradiation started. This dark reaction was studied at different temperatures for propan-2-ol and at 293 K for other alcohols.

##### a) The dark reaction of propan-2-ol

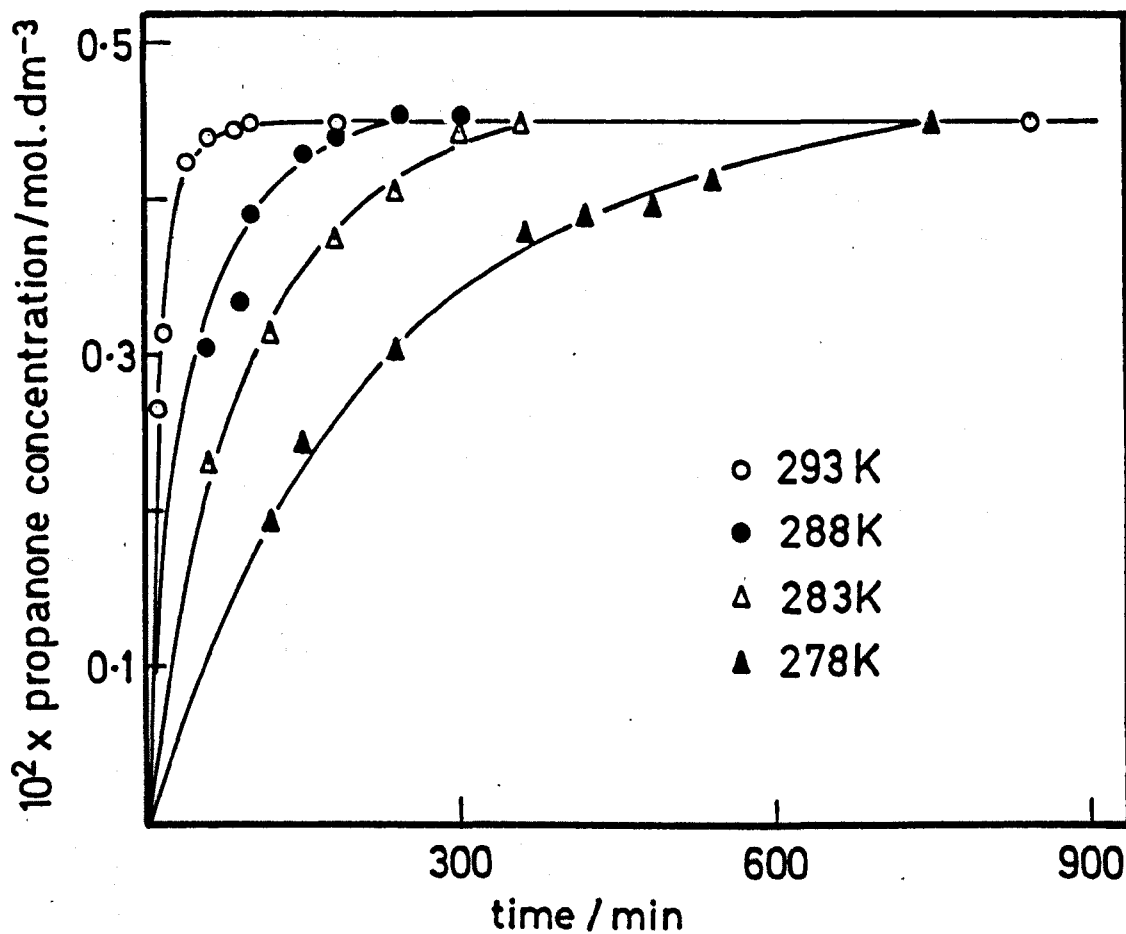
These experiments were made over the temperature range 278-293 K. The results are given in table 3.9 and plotted in figure 3.14 as  $10^2 \times$  propanone concentration/mol.dm.<sup>-3</sup> against time/min. The dark reaction obeyed first-order kinetics with respect to departure from a temperature independent propanone concentration at equilibrium of  $0.45 \times 10^{-2}$  mol.dm.<sup>-3</sup>. Plots of  $\log (C_{\infty} - C_t)/C_{\infty}$  against time/min., where  $C_t$  and  $C_{\infty}$  are the respective propanone concentrations in mol.dm.<sup>-3</sup> at time  $t$  and  $\infty$ , are shown in figure 3.15, and first-order rate constants are calculated from their slopes.

TABLE 3.9

time/min.	$10^2 \times \text{propanone concentration/}$ $\text{mol.dm}^{-3}$			
	T/K			
	278	283	288	293
0	0	0	0	0
15	-	-	-	0.267
20	-	-	-	0.314
40	-	-	-	0.424
60	-	0.232	0.305	0.440
80	-	-	-	0.445
90	-	-	0.335	-
100	-	-	-	0.448
120	0.194	0.314	0.393	-
150	0.244	-	0.432	-
180	-	0.377	0.440	0.451
240	0.306	0.406	0.455	-
300	-	0.446	0.451	-
360	0.378	0.451	-	-
420	0.388	-	-	-
480	0.395	-	-	-
540	0.414	-	-	-
750	0.449	-	-	-
840	-	-	-	0.450

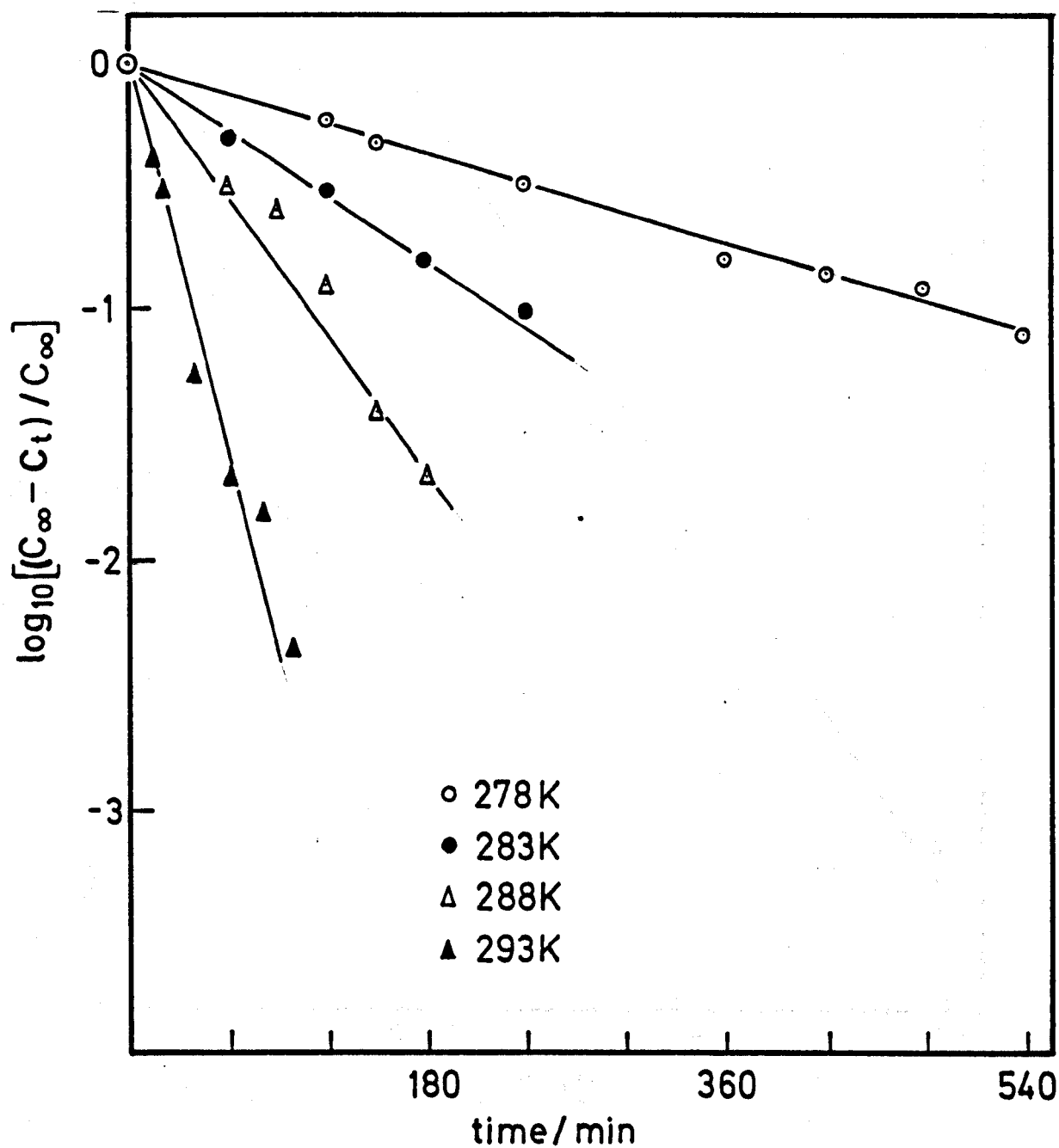
The Arrhenius plot of the first order rate constants,  $\log (10^3 k_1/\text{h}^{-1})$  against  $10^3 T^{-1} \text{K}$ , shown in figure 3.16 gives an activation energy of

Figure 3.14



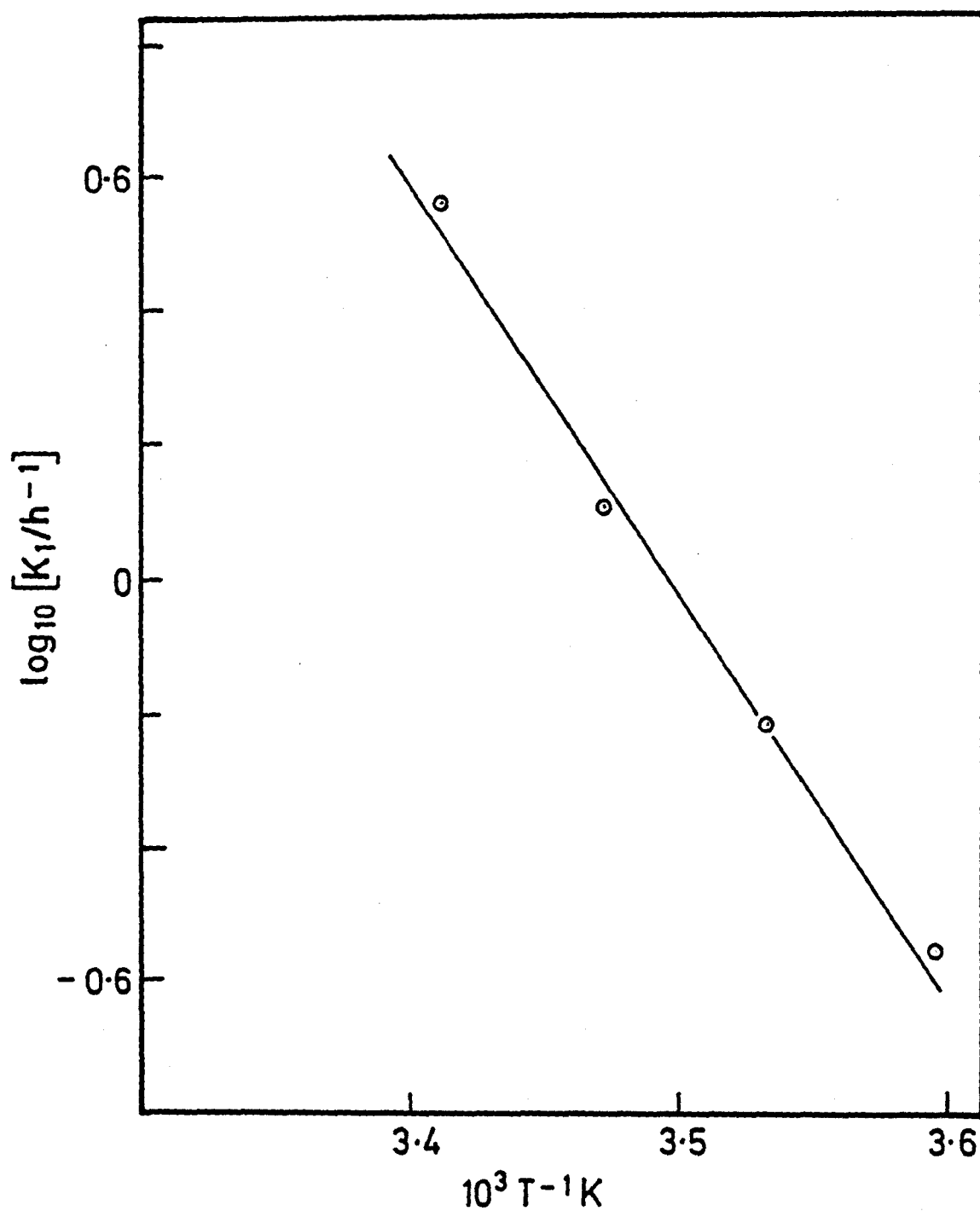
The dark reaction of propan-2-ol on Pt(0.5)/TiO<sub>2</sub>  
(method A) at different temperatures.

Figure 3.15



First order plots for the dark reaction of propan-2-ol on Pt(0.5)/TiO<sub>2</sub> (method A) at different temperatures

Figure 3.16



Temperature dependence for the dark reaction of propan-2-ol on Pt(0.5)/TiO<sub>2</sub> (method A)

$120 \pm 5 \text{ kJ mol}^{-1}$  for propanone formation.

b) The dark reaction with other alcohols at 293 K

These experiments were made at 293 K under a nitrogen pressure of one atmosphere. The results are given in table 3.10 and plotted in figure 3.17 as  $10^2 \times$  reaction product concentration/mol.dm.<sup>-3</sup> against time/min. and in figure 3.18 as  $\log (C_{\infty} - C_t)/C_{\infty}$  against time/min. where  $C_t$  and  $C_{\infty}$  are the methanal, ethanal, propanal or propanone concentration in mol.dm.<sup>-3</sup> at time  $t$  and  $\infty$  respectively, where  $0.45 \times 10^2$  mol.dm.<sup>-3</sup> was used for  $C_{\infty}$ . This value for  $C_{\infty}$  was not experimentally achieved for methanal, presumably due to its further oxidation. Nevertheless, the  $C$  value of  $0.45 \times 10^{-2}$  mol.dm.<sup>-3</sup> should yield an acceptable value for  $k_1$  with the lower methanal concentrations. Values of  $k_1$  determined from figure 3.18 are:

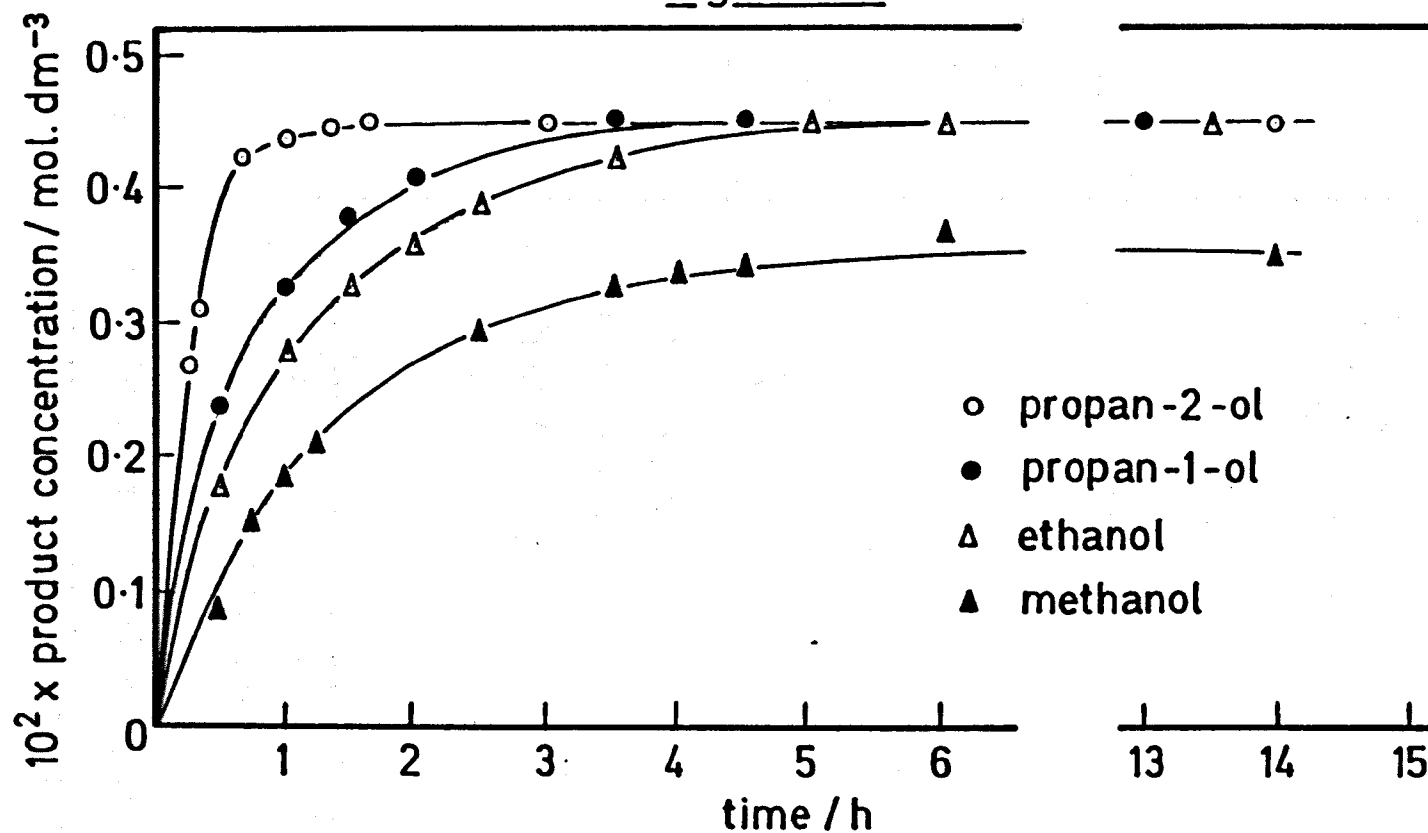
methanal	$0.507 \text{ h}^{-1}$ ,
ethanal	$0.875 \text{ h}^{-1}$ ,
propanal	$1.244 \text{ h}^{-1}$ ,
propanone	$3.639 \text{ h}^{-1}$ .

TABLE 3.10

time/min.	$10^2 \times$ product concentration/mol.dm. <sup>-3</sup>			
	methanal	ethanal	propanal	propanone
0	0	0	0	0
15	-	-	-	0.267
20	-	-	-	0.314
30	0.090	0.180	0.240	-
40	-	-	-	0.424
45	0.150	-	-	-

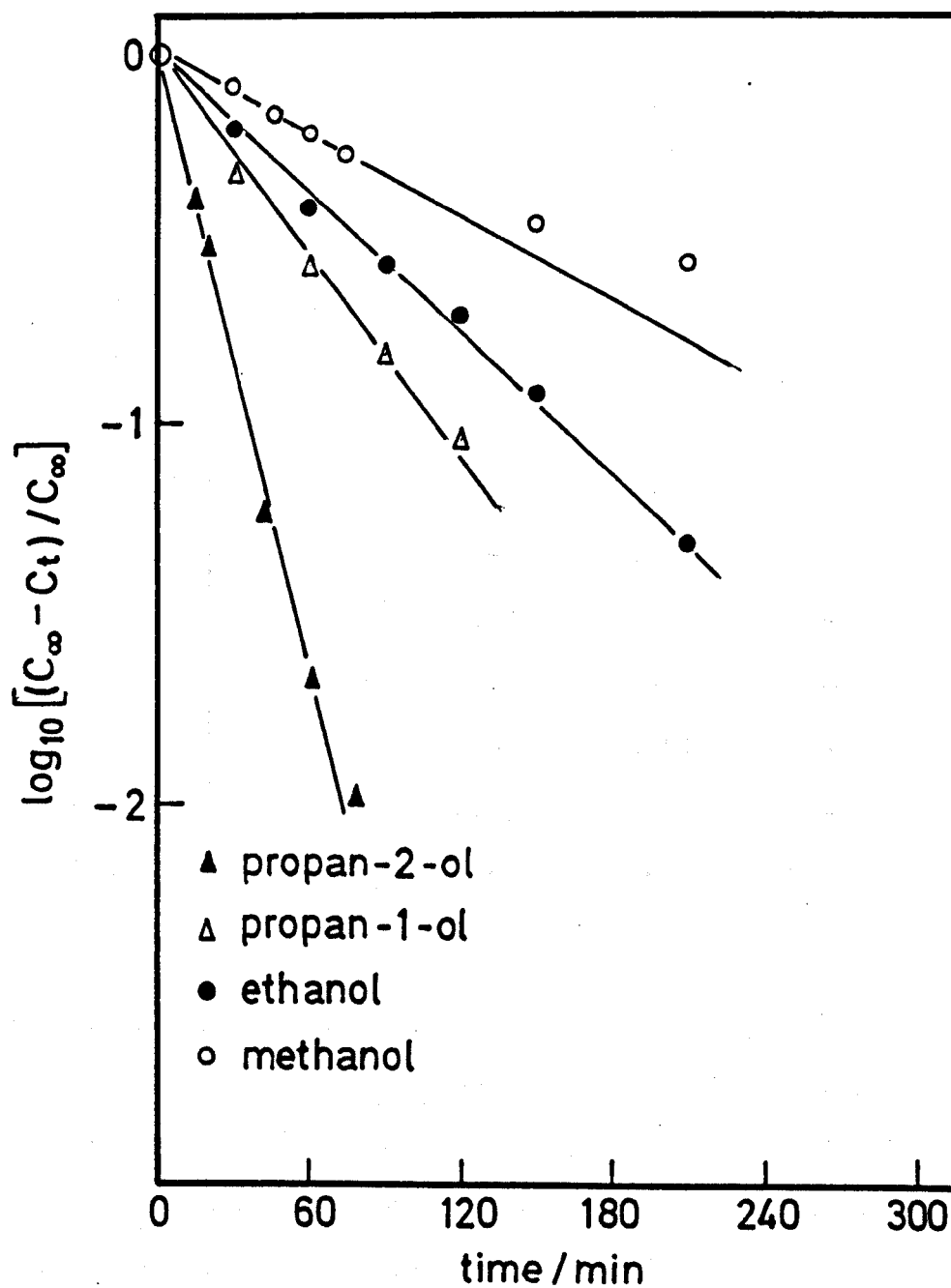
Contd. over

Figure 3-17



The dark reaction of different alcohols at 293K on  
Pt(0.5)/TiO<sub>2</sub> (method A)

Figure 3-18



First-order plots for the dark reaction of different alcohols at 293K on Pt(0.5)/TiO<sub>2</sub> (method A)

60	0.185	0.282	0.329	0.440
75	0.212	-	-	-
80	-	-	-	0.445
90	-	0.330	0.381	-
100	-	-	-	0.448
120	-	0.360	0.408	-
150	0.295	0.392	-	-
180	-	-	-	0.451
210	0.325	0.427	0.450	-
240	0.341	-	-	-
270	0.342	-	0.450	-
300	0.368	0.451	-	-
360	-	0.450	-	-
780	-	-	0.450	-
810	-	0.450	-	-
840	0.351	-	-	0.450

### 3.2.2 The photocatalytic reactions

The photocatalytic reactions of methanol, ethanol, propan-1-ol and propan-2-ol were studied under a nitrogen pressure of one atmosphere, using 150 mg of catalyst and 366 nm. radiation, having allowed sufficient time for the dark reaction to reach completion. The time for the dark reaction to be completed, ranged between 1 and 13 hours over the temperature range studied.

#### a) Temperature dependence for photocatalytic dehydrogenation of propan-2-ol

These reactions were studied over the temperature range 278-303 K using 366 nm radiation from lamp 3. The results are given in table 3.11,

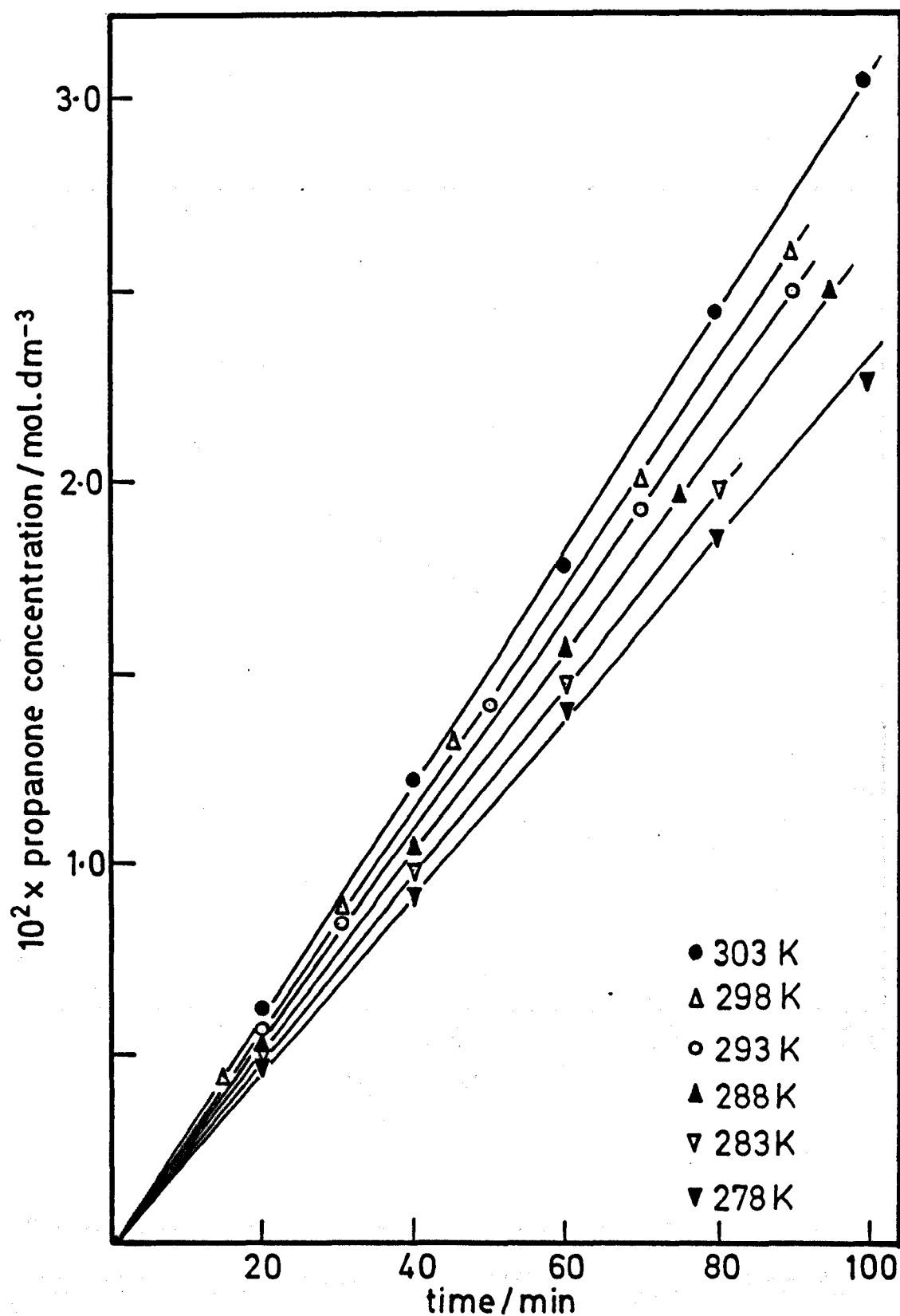
and plotted in figure 3.19 as  $10^2 \times \text{propanone concentration/mol.dm}^{-3}$  against time/min., and in figure 3.20 as  $\log (10^6 \times \text{rate of reaction/mol.dm}^{-3}\text{s}^{-1})$  against  $10^3 T^{-1} \text{K}$ .

TABLE 3.11

time/min.	$10^2 \times \text{propanone concentration/mol.dm}^{-3}$					
	T/K					
	278	283	288	293	298	303
0	0	0	0	0	0	0
15	-	-	-	-	0.440	-
20	0.470	0.490	0.530	0.560	-	0.624
30	-	-	-	0.843	0.890	-
40	0.913	0.980	1.037	-	-	1.219
45	-	-	-	-	1.327	-
50	-	-	-	1.420	-	-
60	1.415	1.478	1.571	-	-	1.780
70	-	-	-	1.926	2.000	-
75	-	-	1.964	-	-	-
80	1.855	1.981	-	-	-	2.444
90	-	-	-	2.500	2.600	-
95	-	-	2.497	-	-	-
100	2.263	-	-	-	-	3.056
$10^6 \times \text{rate/}$ $\text{mol.dm}^{-3}\text{s}^{-1}$	3.86	4.10	4.37	4.62	4.85	5.10

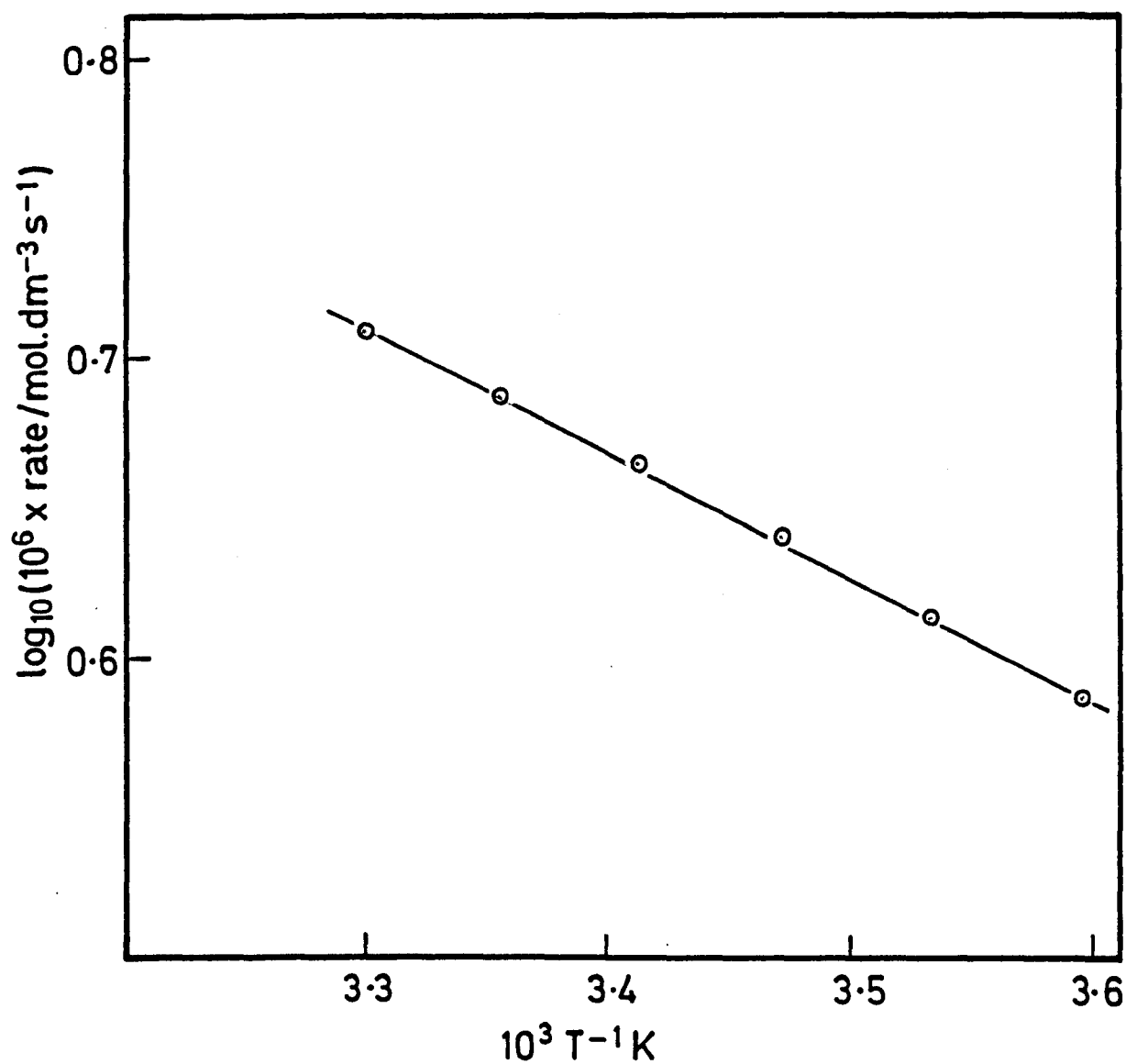
From these results an activation energy of  $8 \pm 1 \text{ kJ mol}^{-1}$  for propanone formation was obtained.

Figure 3-19



Photocatalytic dehydrogenation of propan-2-ol on  
Pt(0.5)/TiO<sub>2</sub> (method A) at different temperatures

Figure 3.20



Temperature dependence for the photocatalytic dehydrogenation of propan-2-ol on Pt(0.5)/TiO<sub>2</sub>(method A)

b) Photocatalytic dehydrogenation of propan-2-ol and other alcohols at 293 K

These experiments were conducted in order to determine whether the activity was independent of the reactant alcohol for photodehydrogenation on  $\text{Pt}(0.5)/\text{TiO}_2$  prepared by method A. The only detectable dehydrogenation product of methanol was methanal, of ethanol was ethanal and of propan-2-ol was propanone. All reactions were carried out using 366 nm radiation from lamp 5 at 293 K. The results are shown in table 3.12 and plotted in figure 3.21 as  $10^2 \times$  product concentration (methanal, ethanal or propanone)/ $\text{mol.dm}^{-3}$  against time/min.

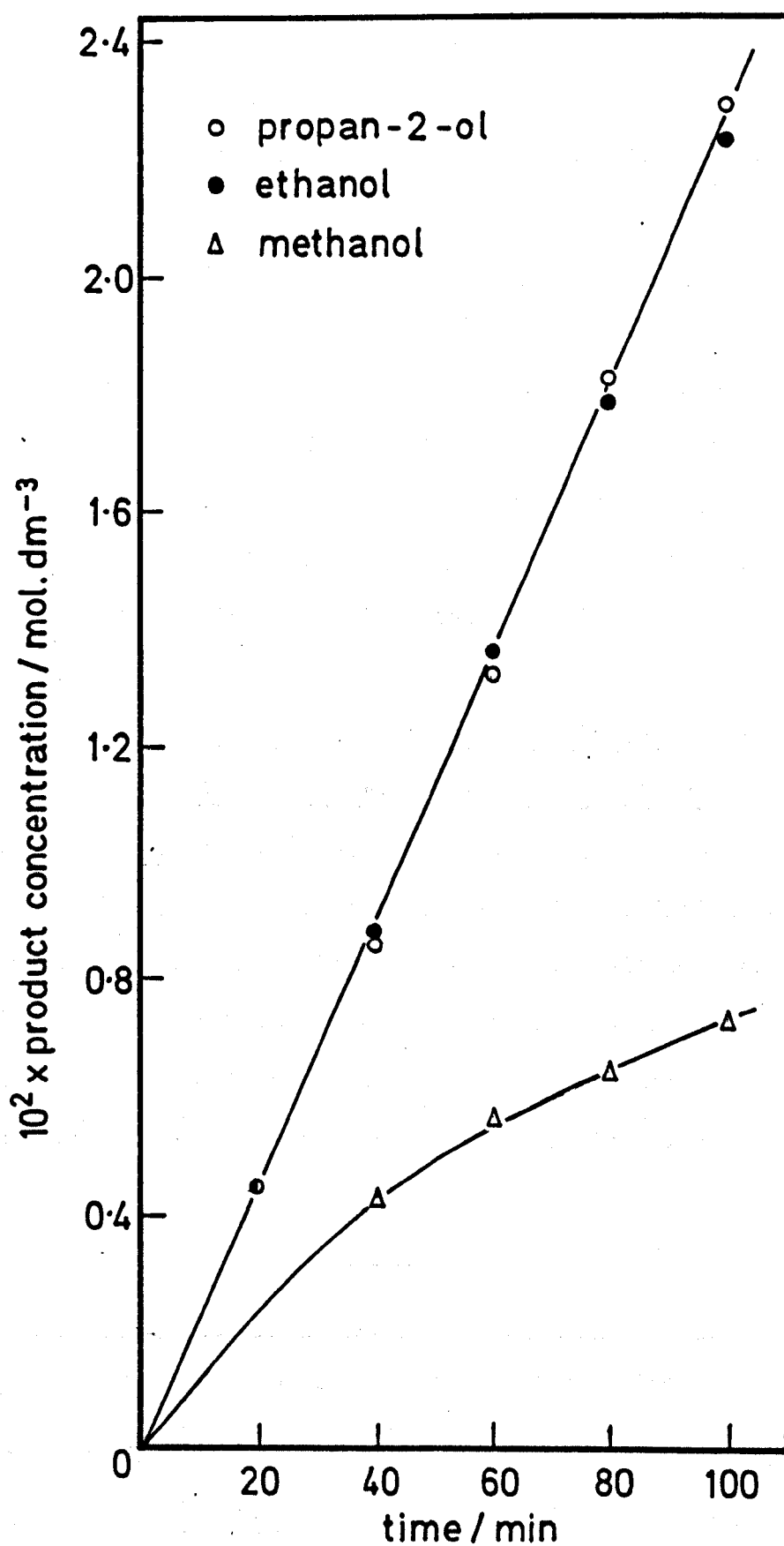
TABLE 3.12

time/min.	$10^2 \times$ product concentration/ $\text{mol.dm}^{-3}$		
	methanal	ethanal	propanone
0	0	0	0
20	0.210	0.441	0.442
40	0.429	0.882	0.869
60	0.563	1.351	1.322
80	0.651	1.780	1.821
100	0.732	2.225	2.285
$10^2 \times$ rate/ $\text{mol.dm}^{-3}\text{s}^{-1}$	1.08*	3.71	3.81

\* The rate determined from the first two points.

These results show that ethanol and propan-2-ol have similar

Figure 3·21



Photocatalytic dehydrogenation of different alcohols  
at 293K on Pt(0·5)/TiO<sub>2</sub> (method A)

activities for reaction on  $\text{Pt}(0.5)/\text{TiO}_2$  prepared by method A, while methanol failed to give a linear reaction progress plot. This was presumably due to further oxidation of methanal as mentioned above.

### 3.2.3 Photocatalytic dehydrogenation of alcohols on oxygen treated catalysts

$\text{Pt}(0.5)/\text{TiO}_2$  prepared by method A was treated with oxygen by two methods (see section 2.3,a). The temperature independent equilibrium yield of propanone from propan-2-ol was reduced from  $0.45 \times 10^{-2} \text{ mol.dm}^{-3}$  to  $0.20 \times 10^{-2} \text{ mol.dm}^{-3}$  following oxygen treatment at 573 K for 3 h. while the dark reaction was eliminated entirely following oxygen treatment at 753 K for 16 h.

#### a) Temperature dependence for photocatalytic dehydrogenation of propan-2-ol on the catalyst treated at 573 K for 3 h.

These experiments were carried out over the temperature range 278-298 K using 366 nm radiation from lamp 3. Sufficient time for the dark reaction to reach completion (1-6 h.) was allowed before commencing irradiation. The results are given in table 3.13 and plotted in figure 3.22 on  $10^2 \times \text{propanone concentration/mol.dm}^{-3}$  against time/min., and in figure 3.23 as  $\log(10^6 \times \text{rate of reaction/mol.dm}^{-3}\text{s}^{-1})$  against  $10^3 T^{-1} \text{K}$ .

TABLE 3.13

time/min.	$10^2 \times \text{propanone concentration/}$ $\text{mol.dm}^{-3}$				
	T/K				
	278	283	288	293	298
0	0	0	0	0	0
15	0.122	-	-	-	-

Contd. over

20	-	-	0.240	0.300	0.339
25	-	0.279	-	-	-
30	0.301	-	-	-	-
40	-	-	0.501	0.582	0.645
45	0.438	-	-	-	-
50	-	0.561	-	-	-
60	0.598	-	0.749	0.842	1.001
75	0.737	0.851	-	-	-
80	-	-	0.983	1.092	1.302
90	0.880	-	-	-	-
100	-	1.120	1.258	1.431	1.610
$10^6 \times \text{rate}/$ $\text{mol.dm}^{-3}\text{s}^{-1}$	1.62	1.87	2.10	2.38	2.70

These results show that the oxygen treatment halved the photocatalytic activity, whilst the activation energy was effectively doubled from  $8 \pm 1 \text{ kJ mol}^{-1}$  to  $17 \pm 1 \text{ kJ mol}^{-1}$ .

b) Photocatalytic dehydrogenation of alcohols on the catalyst treated at 753 K for 16 h.

There was no dark reaction detected on this catalyst. The photocatalytic dehydrogenation of methanol, ethanol, propan-1-ol and propan-2-ol were studied on this catalyst.

i) Temperature dependence for photocatalytic dehydrogenation of propan-2-ol

These experiments were carried out at temperatures in the range 283-303 K using 366 nm radiation from lamp 3, 150 mg of catalyst and a nitrogen pressure of one atmosphere. The results are given in table 3.14 and plotted in figure 3.24 as  $10^2 \times \text{propanone concentration/mol.dm}^{-3}$

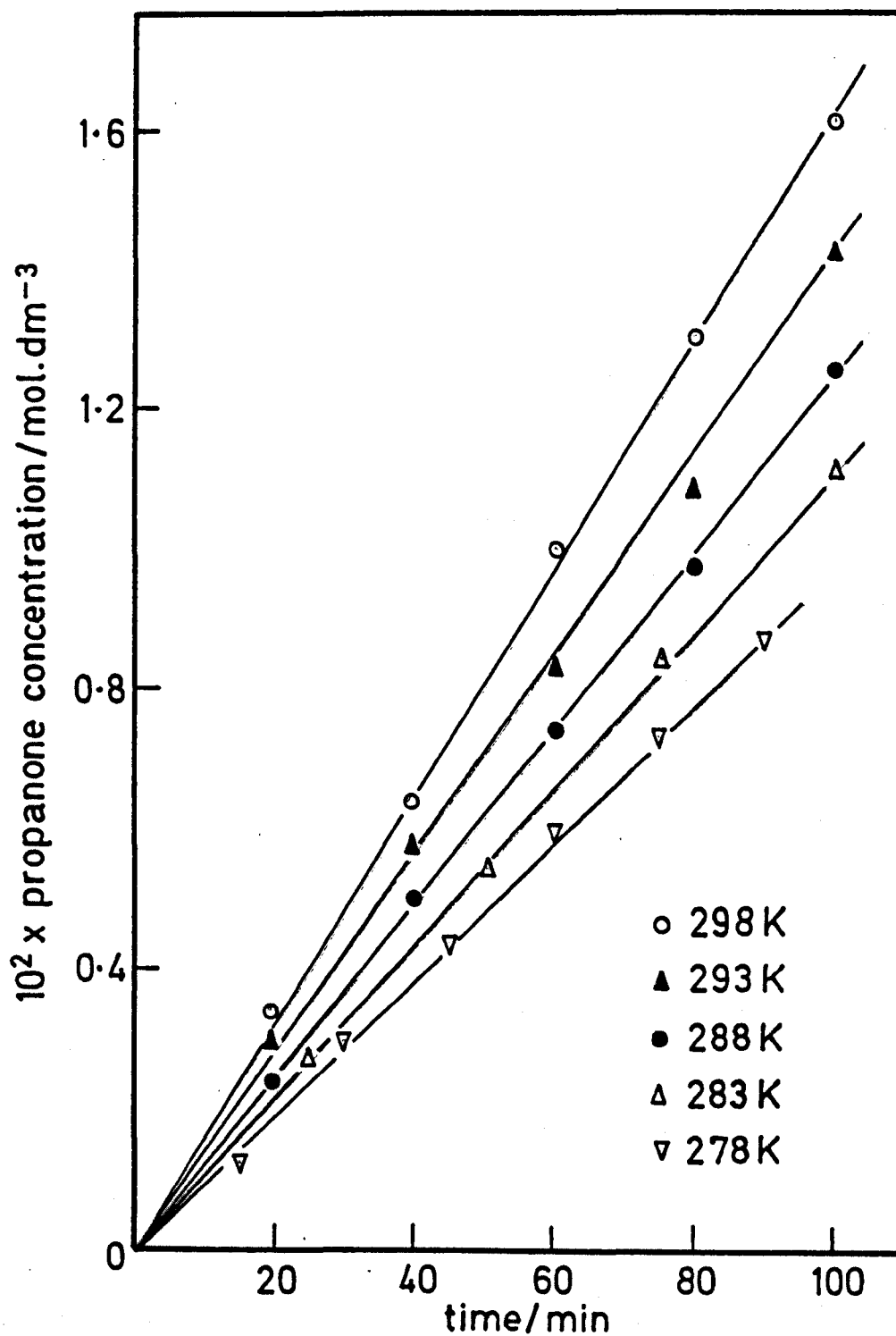
against time/min., and in figure 3.25 as  $\log(10^6 \times \text{rate of reaction/ mol.dm}^{-3}\text{s}^{-1})$  against  $10^3 T^{-1} \text{K}$ .

TABLE 3.14

time/min.	$10^2 \times \text{propanone concentration/ mol.dm}^{-3}$				
	T/K				
	283	288	293	298	303
0	0	0	0	0	0
20	0.092	-	0.119	-	0.158
25	-	-	-	0.182	-
30	-	0.151	-	-	-
40	0.190	-	-	0.286	0.300
41	-	-	0.254	-	-
50	-	0.262	-	-	-
60	0.292	-	0.360	0.420	0.460
75	-	0.406	-	-	-
80	0.357	-	0.458	0.550	0.618
100	0.462	0.505	0.600	0.682	0.792
120	-	0.620	-	-	-
$10^6 \times \text{rate/ mol.dm}^{-3}\text{s}^{-1}$	0.77	0.86	1.00	1.13	1.29

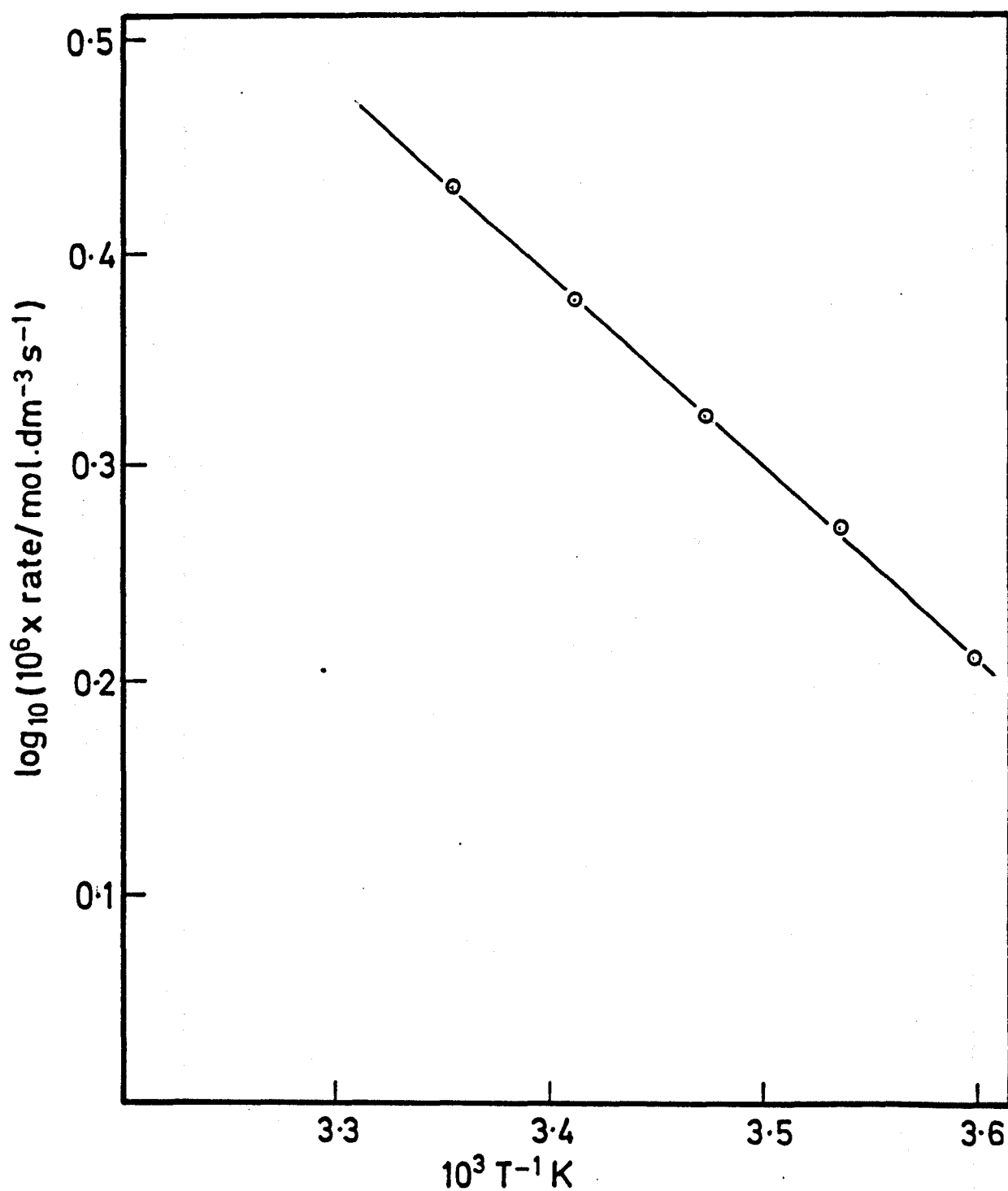
The activity of the catalyst was appreciably lower than those prior to oxygen treatment. However, the activation energy of  $19 \pm 1 \text{ kJ mol}^{-1}$  clearly exceeds the value obtained before oxygen treatment.

Figure 3.22



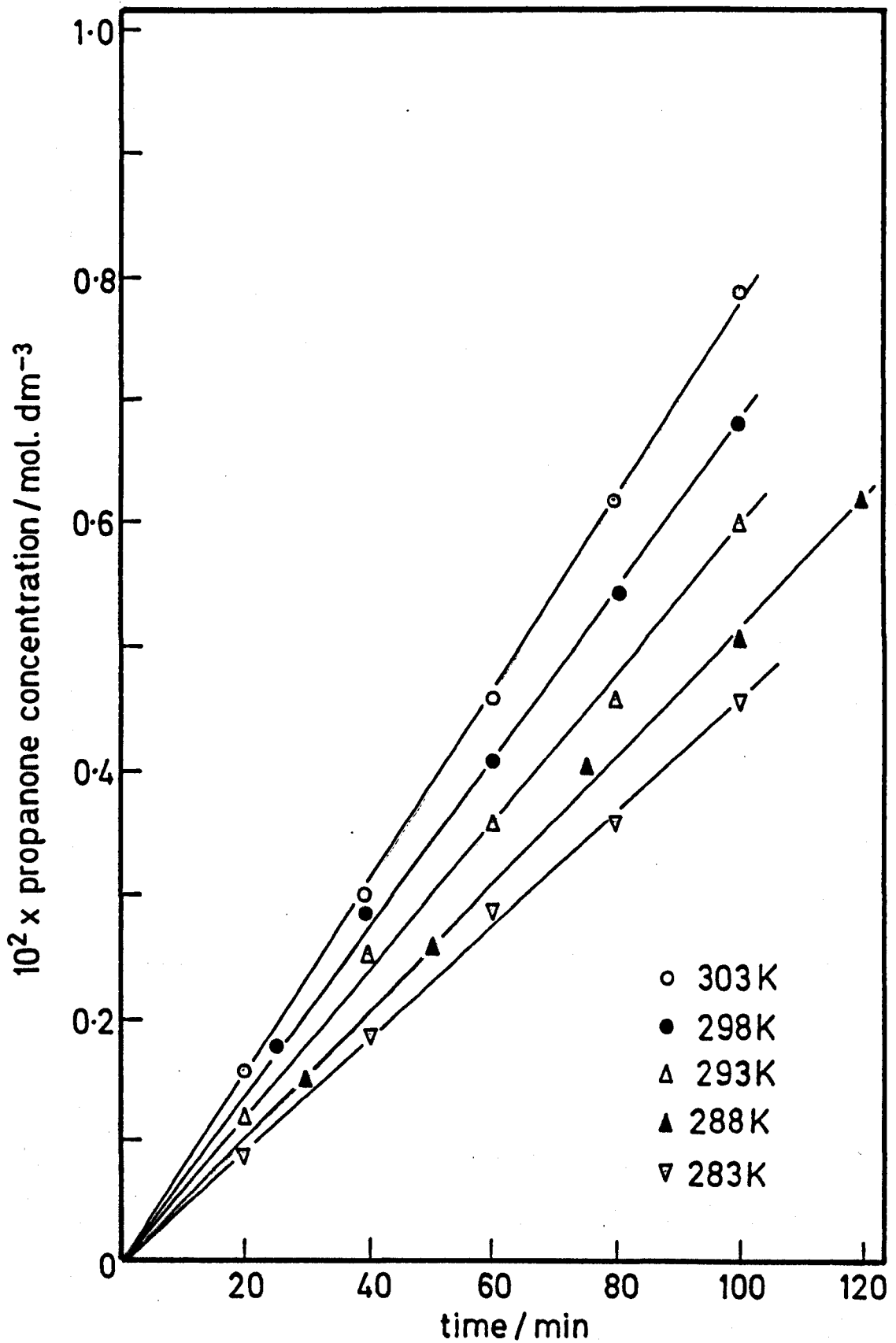
Photocatalytic dehydrogenation of propan-2-ol on oxygen treated (573 K) Pt(0.5)/TiO<sub>2</sub> (method A) at different temperatures.

Figure 3-23



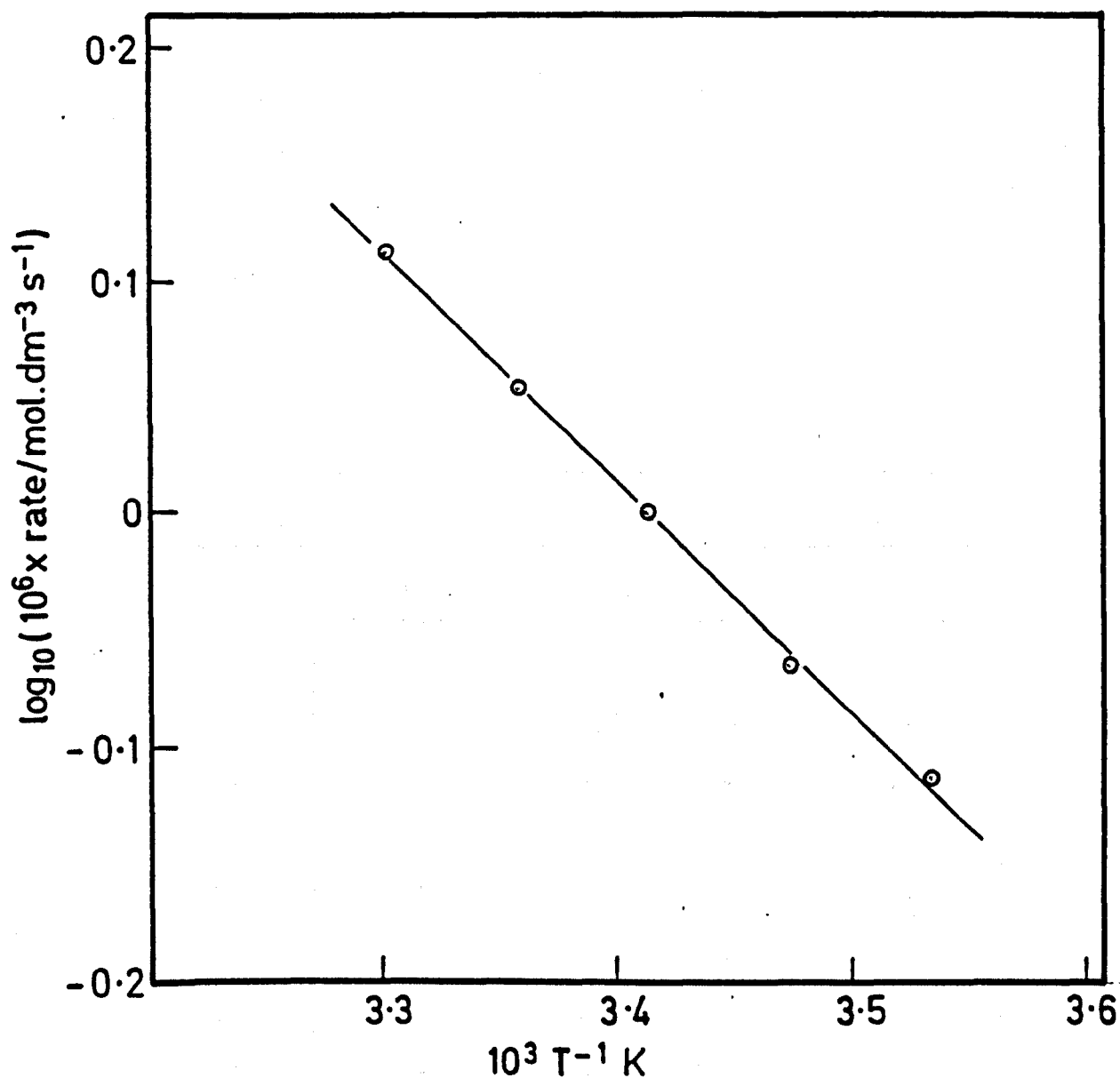
Temperature dependence for the photocatalytic dehydrogenation of propan-2-ol on oxygen treated (573K) Pt(0.5) / TiO<sub>2</sub> (method A)

Figure 3-24



Photocatalytic dehydrogenation of propan-2-ol on oxygen treated (753K) Pt(0.5)/TiO<sub>2</sub> (method A) at different temperatures

Figure 3.25



Temperature dependence for the photocatalytic dehydrogenation of propan-2-ol on oxygen treated (753K) Pt(0.5)/TiO<sub>2</sub> (method A)

ii) Photocatalytic dehydrogenation of other alcohols at 293 K

Photocatalytic dehydrogenation of methanol, ethanol and propan-1-ol was studied at 293 K using 366 nm radiation from lamp 3. The results are given in table 3.15 and for purposes of comparison the final column contains data for propan-2-ol. The data was plotted in figure 3.26 as  $10^2 \times$  product (methanal, ethanal, propanal, propanone) concentration/mol.dm.<sup>-3</sup> against time/min.

TABLE 3.15

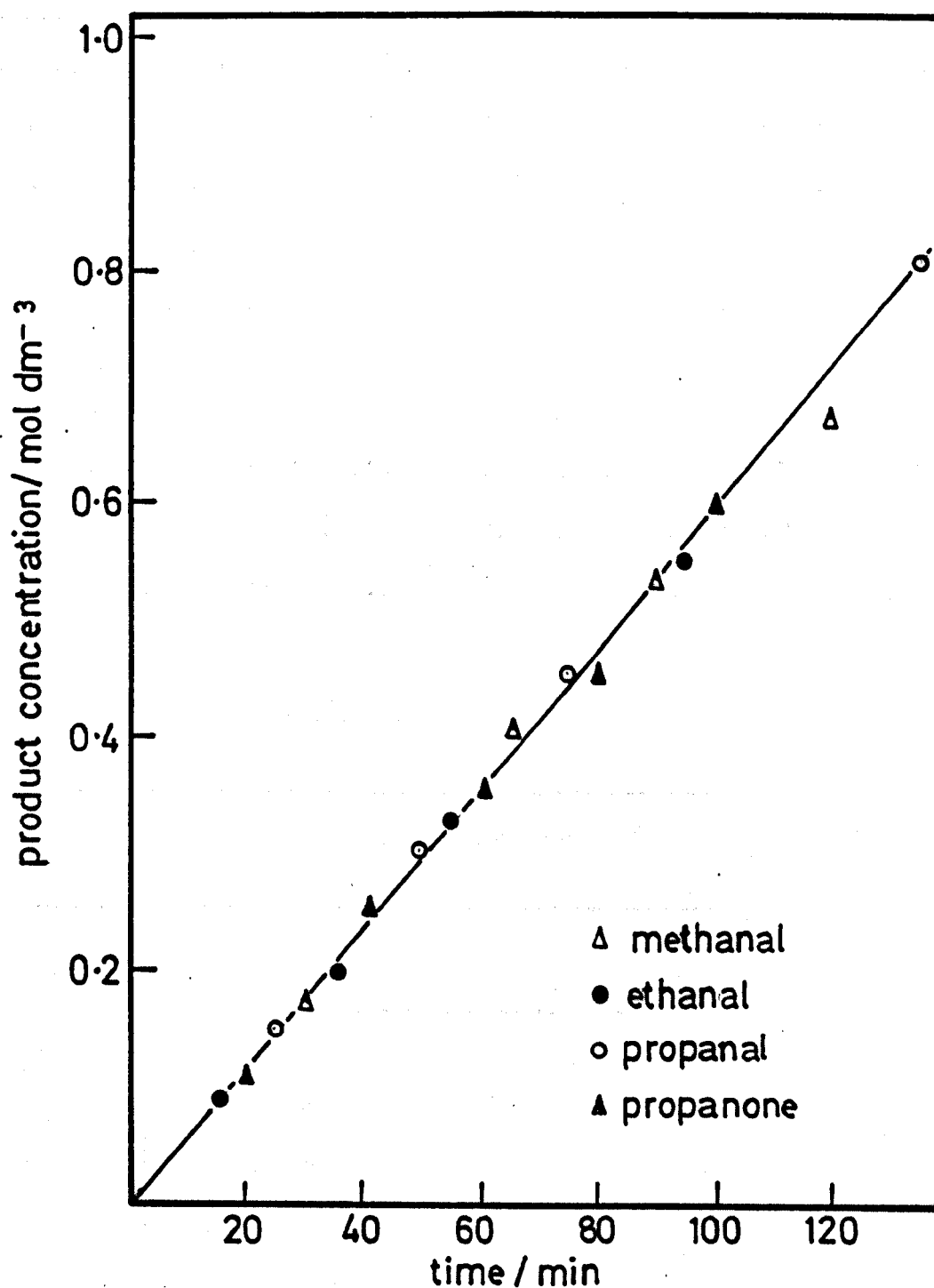
time/min.	$10^2 \times$ propanone concentration/mol.dm. <sup>-3</sup>			
	methanal	ethanal	propanal	propanone
0	0	0	0	0
15	-	0.093	-	-
20	-	-	-	0.119
25	-	-	0.150	-
30	0.176	-	-	-
35	-	0.200	-	-
41	-	-	-	0.254
50	-	-	0.304	-
55	-	0.330	-	-
60	-	-	-	0.360
65	0.410	-	-	-
75	-	-	0.454	-
80	-	-	-	0.458
90	0.536	-	-	-

Contd. over

95	-	0.550	-	-
100	-	-	-	0.600
120	0.669	-	-	-
135	-	-	0.803	-
$10^6 \times \text{rate}/$ $\text{mol.dm}^{-3}\text{s}^{-1}$	0.99	0.97	1.01	1.00

These results show that the photocatalytic activity was the same for all four alcohols.

Figure 3-26



Photocatalytic dehydrogenation of different alcohols  
on oxygen treated (753K)  $\text{Pt}(0.5)/\text{TiO}_2$  (method A)  
at 293K

### 3.3 Photocatalytic dehydrogenation of propan-2-ol on platinized anatase (Pt(0.5)/TiO<sub>2</sub>) prepared by photodeposition (method B)

These experiments were carried out using 366 nm radiation from lamp 1, 150 mg of Pt(0.5)/TiO<sub>2</sub> as catalyst and a nitrogen pressure of one atmosphere. There was no dark reaction detected with this catalyst.

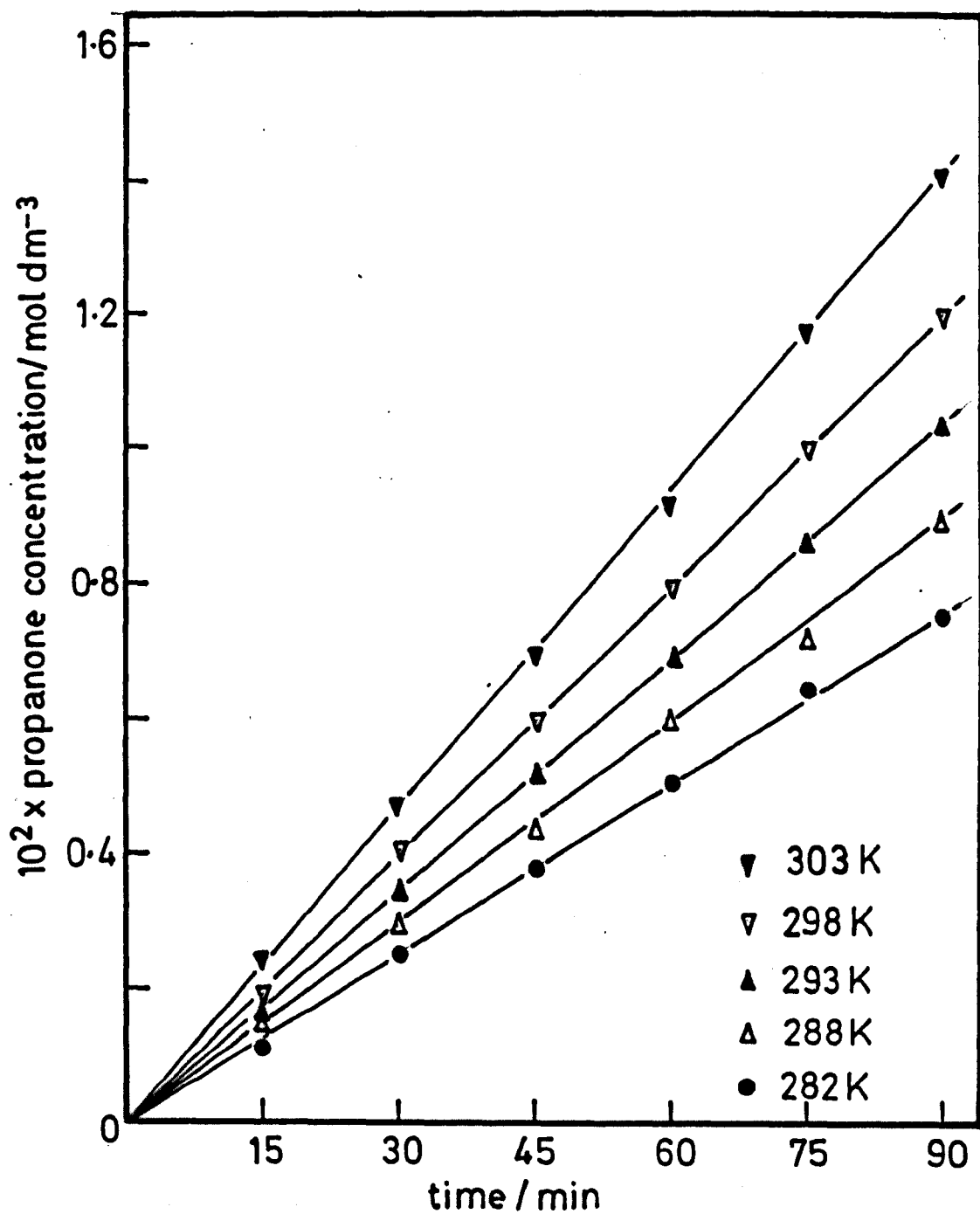
#### 3.3.1 Temperature dependence for the photocatalytic dehydrogenation of propan-2-ol

These reactions were studied in the temperature range 282-303 K. The results are given in table 3.16 and plotted in figure 3.27 as  $10^2 \times$  propanone concentration/mol.dm.<sup>-3</sup> against time/min., and in figure 3.28 as  $\log(10^6 \times \text{rate of reaction/mol.dm.}^{-3}\text{s.}^{-1})$  against  $10^3 T^{-1}$  K.

TABLE 3.16

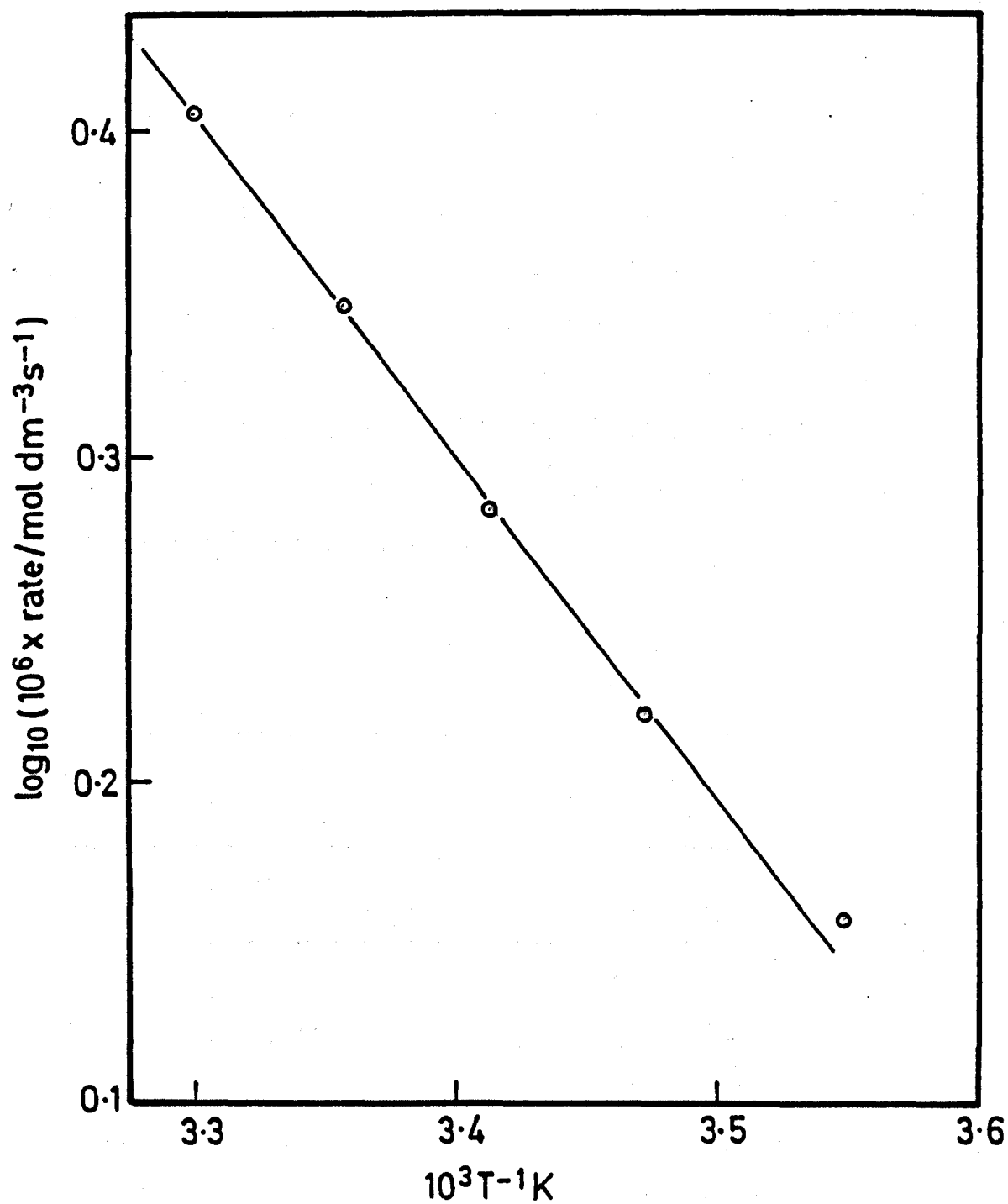
time/min.	$10^2 \times \text{propanone concentration/}$ mol.dm. <sup>-3</sup>				
	T/K				
	282	288	293	298	303
0	0	0	0	0	0
15	0.112	0.151	0.175	0.195	0.247
30	0.255	0.300	0.335	0.407	0.475
45	0.380	0.440	0.523	0.603	0.700
60	0.512	0.602	0.700	0.800	0.925
75	0.650	0.726	0.870	1.011	1.178
90	0.760	0.900	1.040	1.200	1.410
$10^6 \times \text{rate/}$ mol.dm. <sup>-3</sup> s. <sup>-1</sup>	1.44	1.67	1.93	2.22	2.62

Figure 3-27



Photocatalytic dehydrogenation of propan-2-ol on  
Pt(0.5)/TiO<sub>2</sub> (method B) at different temperatures

Figure 3-28



Temperature dependence for the photocatalytic dehydrogenation of propan-2-ol on Pt(0.5)/TiO<sub>2</sub> (method B)

From these results an activation energy of  $20 \pm 1 \text{ kJ mol}^{-1}$  for propanone production was obtained which is in good agreement with that obtained on anatase (see section 3.1.2), thus showing the two catalysts have the same energetics for the photodehydrogenation of propan-2-ol.

### 3.3.2 Light intensity dependence for the photocatalytic dehydrogenation of propan-2-ol

Rates of propanone formation at 293 K were measured using 366 nm radiation from lamp 1, where neutral density filters were used to obtain different light intensities. The results are given in table 3.17 and plotted in figure 3.29 as  $10^2 \times \text{propanone concentration/mol.dm}^{-3}$  against time/min. The rate of reaction  $\times 10^{-6}/\text{mol.dm}^{-3}\text{s}^{-1}$  is plotted either against  $10^7 \times \text{light intensity/einstein s}^{-1}$  or against  $10^4 \times \text{square root of light intensity}/(\text{einstein s}^{-1})^{\frac{1}{2}}$  in figure 3.30.

TABLE 3.17

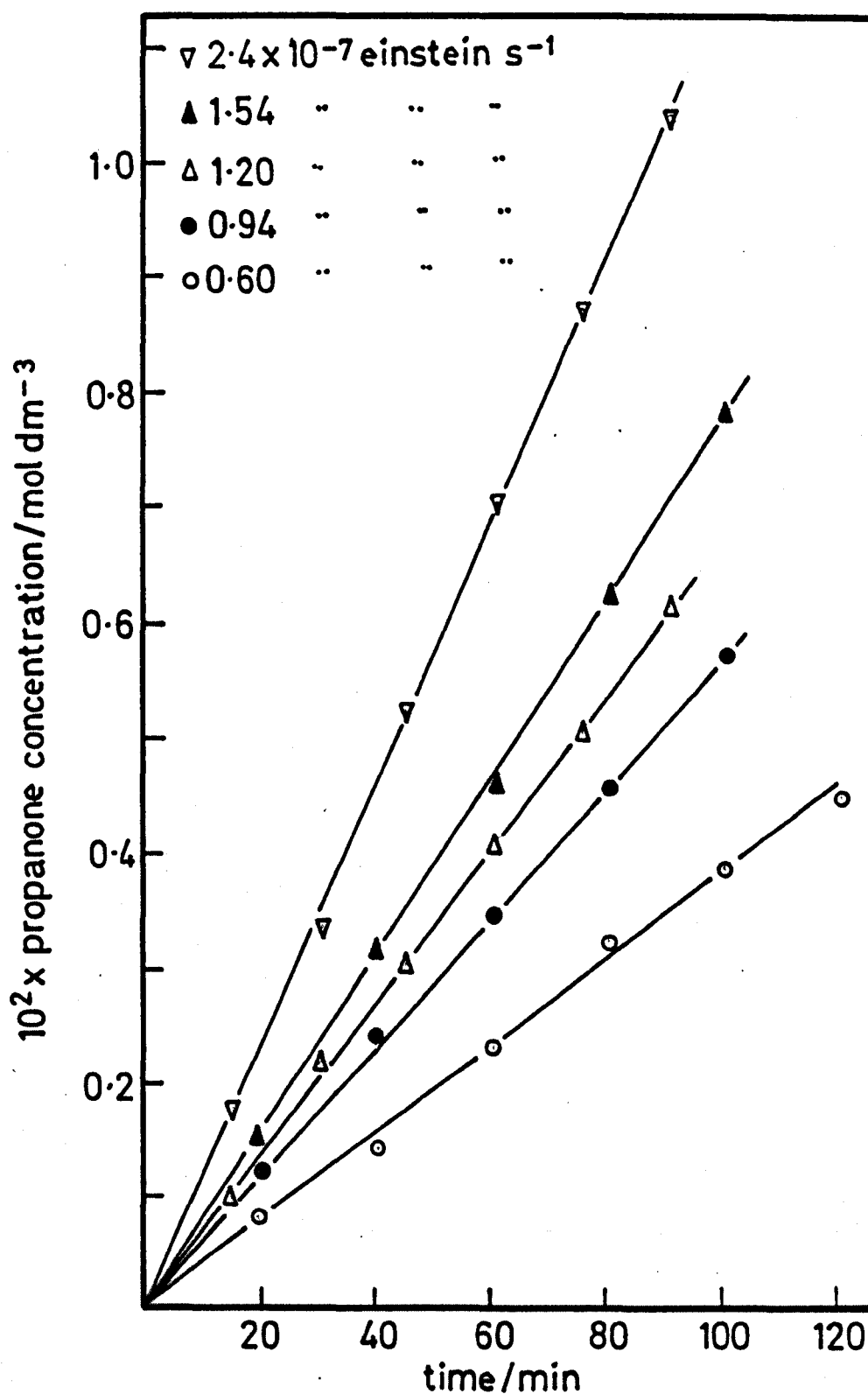
time/min.	$10^2 \times \text{propanone concentration/mol.dm}^{-3}$				
	I/einstein $\text{s}^{-1}$				
	2.4	1.54	1.20	0.94	0.60
0	-	0	0	0	0
15	0.175	-	0.095	-	-
20	-	0.160	-	0.118	0.078
30	0.335	-	0.216	-	-
40	-	0.315	-	0.241	0.141
45	0.523	-	0.298	-	-

Contd. over

60	0.700	0.460	0.407	0.345	0.229
75	0.870	-	0.505	-	-
80	-	0.625	-	0.460	0.325
90	1.040	-	0.614	-	-
100	-	0.785	-	0.575	0.390
120	-	-	-	-	0.452
$10^6 \times \text{rate}/$ $\text{mol.dm}^{-3}\text{s}^{-1}$	1.93	1.31	1.12	0.96	0.65

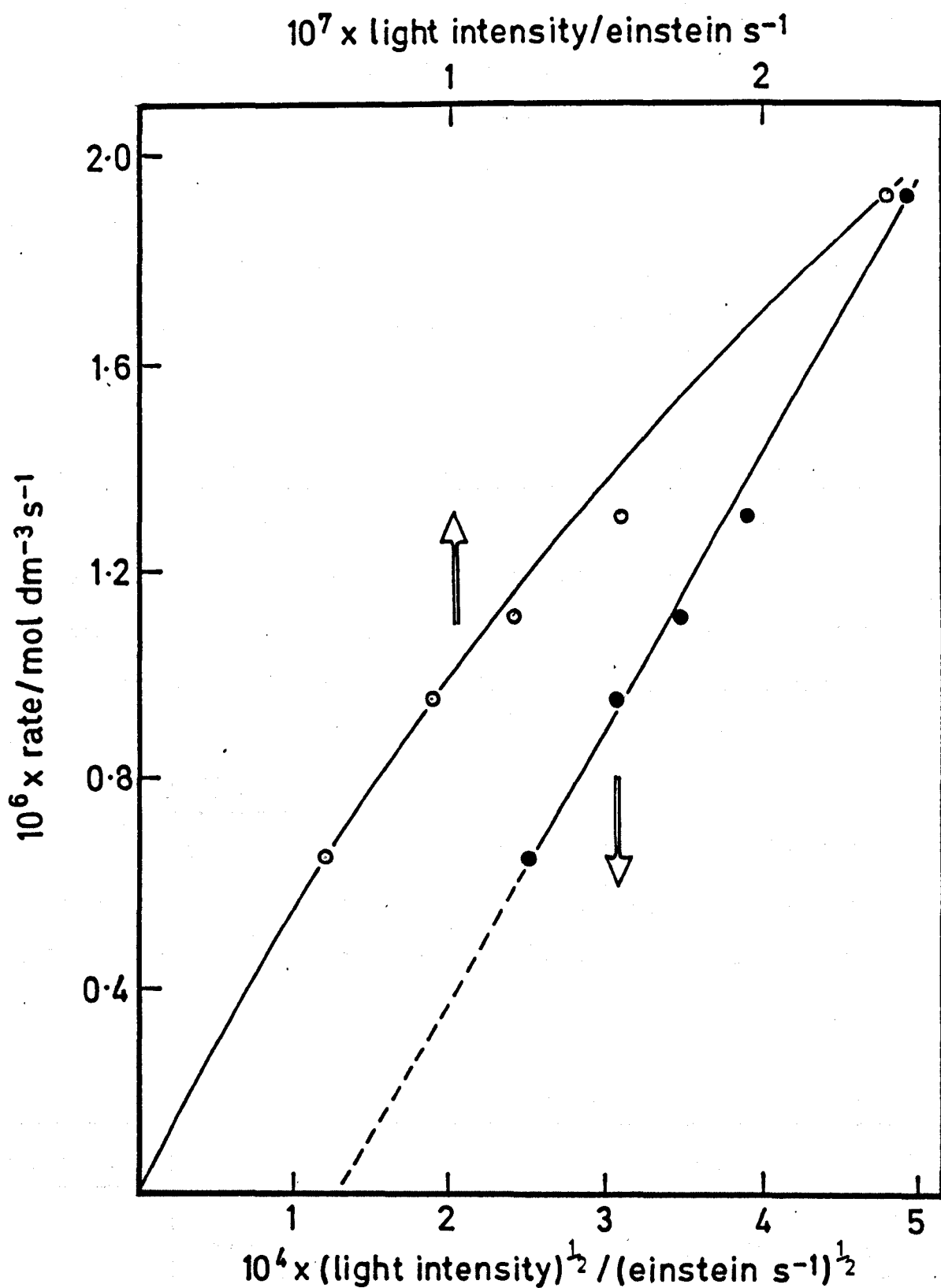
Clearly, neither treatment of the results gives an ideal plot. That for direct dependence on the light intensity is curved, whilst that for square root dependence has more points on the linear portion but fails to pass through the origin.

Figure 3.29



Photocatalytic dehydrogenation of propan-2-ol on  
Pt(0.5)/TiO<sub>2</sub> (method B) at different light intensities

Figure 3.30



Light intensity dependence for the photocatalytic dehydrogenation of propan-2-ol on Pt(0.5)/TiO (method B) at 293K

### 3.4 Photocatalytic dehydrogenation of alcohols on platinized anatase prepared by photodeposition (Method C)

All experiments in this section were made with 366 nm radiation and a nitrogen pressure of one atmosphere. With the exception of experiments where the effect of catalyst mass was being investigated, a catalyst mass of 150 mg was used. No dark reaction was detected with any of the catalysts prepared by method C, except following deliberate reduction with hydrogen.

#### 3.4.1 Photocatalytic dehydrogenation of propan-2-ol on different masses of catalysts

A series of reactions at 293 K, using different masses of Pt(0.5)/TiO<sub>2</sub> and Pt(2.0)/TiO<sub>2</sub> were made to determine the mass necessary for maximum activity. 366 nm radiation from lamp 1 was used throughout these experiments.

##### a) Pt(0.5)/TiO<sub>2</sub>

The results are given in table 3.18 and plotted in figure 3.31 as  $10^2 \times$  propanone concentration/mol.dm<sup>-3</sup> against time/min., and in figure 3.33 as  $10^6 \times$  rate of reaction/mol.dm<sup>-3</sup>s.<sup>-1</sup> against mass of catalyst/mg.

TABLE 3.18

time/min.	$10^2 \times$ propanone concentration/mol.dm <sup>-3</sup>						
	catalyst mass/mg						
	37.7	54.6	86.4	105.2	149.8	205.2	214.1
0	0	0	0	0	0	0	0
15	-	-	-	-	-	-	0.319
20	0.201	0.280	0.364	0.420	-	0.385	-
25	-	-	-	-	0.509	-	-

Contd. over

30	-	-	-	-	-	-	0.623
40	0.411	0.551	0.753	0.822	0.840	-	-
45	-	-	-	-	-	-	0.925
50	-	-	-	-	-	1.021	-
60	0.621	0.875	1.103	1.221	-	-	-
65	-	-	-	-	1.378	-	-
70	-	-	-	-	-	1.504	-
75	-	-	-	-	-	-	1.601
80	0.805	1.103	1.470	1.706	1.654	-	-
85	-	-	-	-	-	-	1.779
90	-	-	-	-	-	1.868	-
95	-	-	-	-	2.010	-	-
100	1.041	1.444	1.811	2.065	-	2.100	-
$10^6 \times \text{rate}/$ $\text{mol.dm}^{-3}\text{s}^{-1}$	1.73	2.40	3.10	3.48	3.50	3.51	3.50

b) Pt(2.0)/TiO<sub>2</sub>

The results are given in table 3.19 and plotted in figure 3.32 as  $10^2 \times \text{propanone concentration/mol.dm}^{-3}$  against time/min., and in figure 3.33 as  $10^6 \times \text{rate of reaction/mol.dm}^{-3}\text{s}^{-1}$  against catalysts mass/mg.

TABLE 3.19

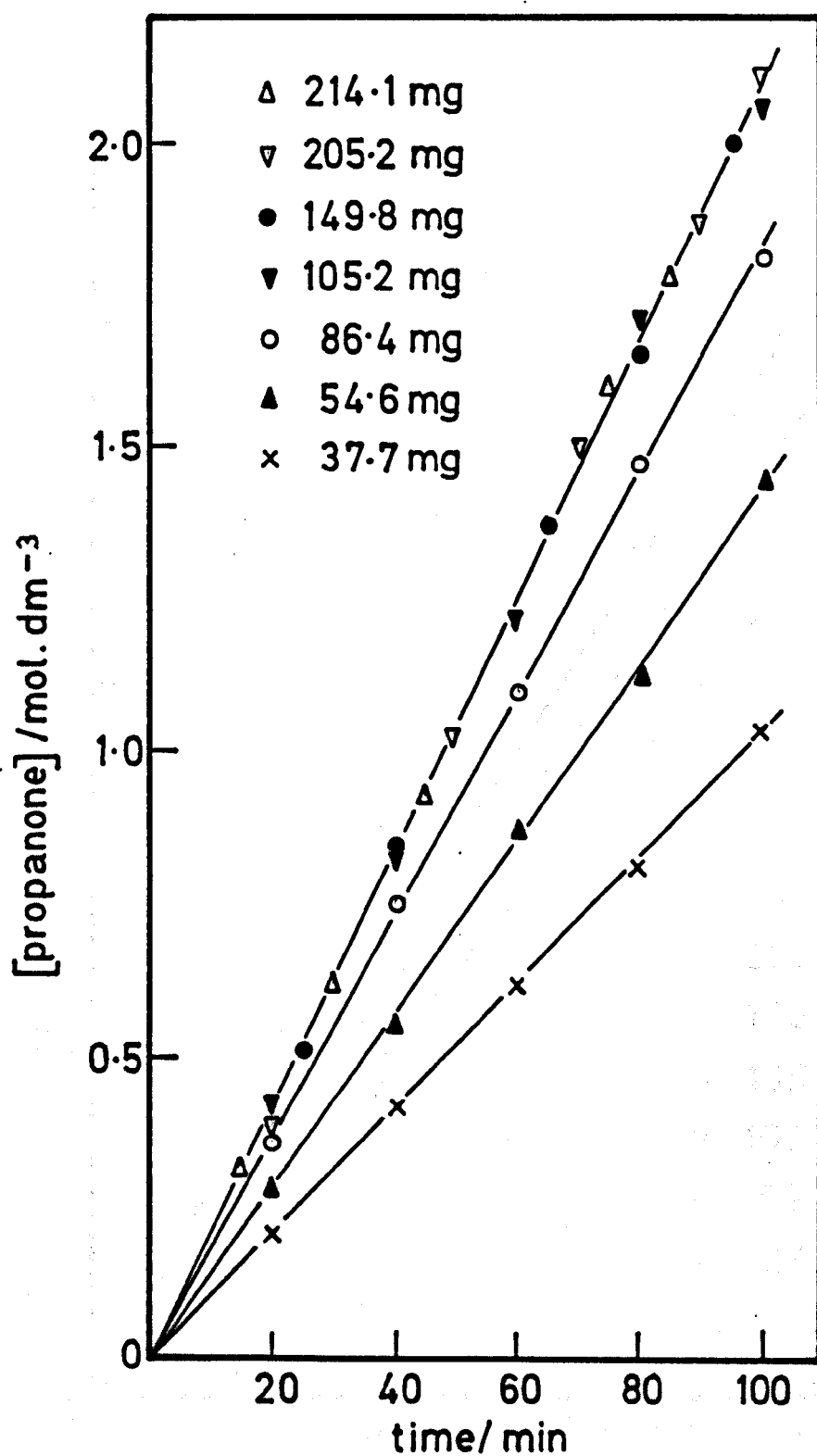
time/min.	$10^2 \times \text{propanone concentration/mol.dm}^{-3}$					
	catalyst mass/mg					
	35.6	69.1	107.6	135.1	160.2	220.0
0	0	0	0	0	0	0

Contd. over

10	-	-	-	-	-	0.161
15	-	-	-	0.260	-	-
20	0.243	0.311	0.328	-	-	-
25	-	-	-	-	0.403	-
30	-	-	-	0.482	-	-
40	0.442	0.571	0.639	-	-	-
45	-	-	-	0.712	-	-
50	-	-	-	-	0.802	-
60	0.741	0.840	0.941	-	-	-
65	-	-	-	1.021	-	-
75	-	-	-	1.165	1.181	-
80	0.963	1.130	1.223	-	-	-
85	-	-	-	-	-	1.331
90	-	-	-	1.432	-	-
95	-	-	-	-	1.498	-
100	1.201	1.400	1.560	-	-	-
105	-	-	-	-	-	1.668
110	-	-	-	-	1.719	-
120	-	-	-	-	-	1.880
$10^6 \times \text{rate}/$ $\text{mol.dm}^{-3}\text{s}^{-1}$	2.00	2.33	2.60	2.61	2.60	2.62

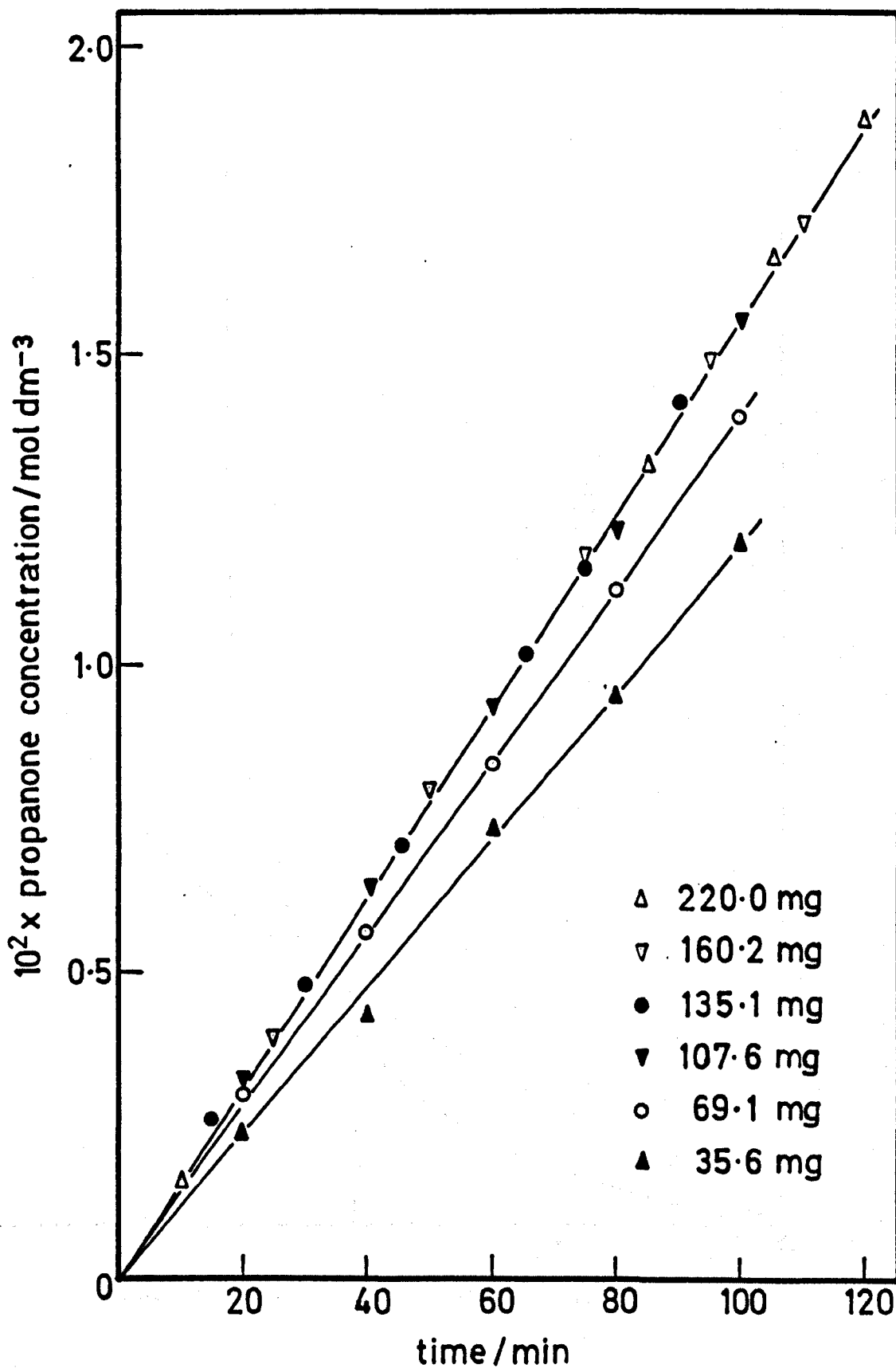
It is shown from these results that the maximum activity of both  $\text{Pt}(0.5)/\text{TiO}_2$  and  $\text{Pt}(2.0)/\text{TiO}_2$  is obtained using a catalyst mass of 150 mg, and this was used in all subsequent experiments.

Figure 3.31



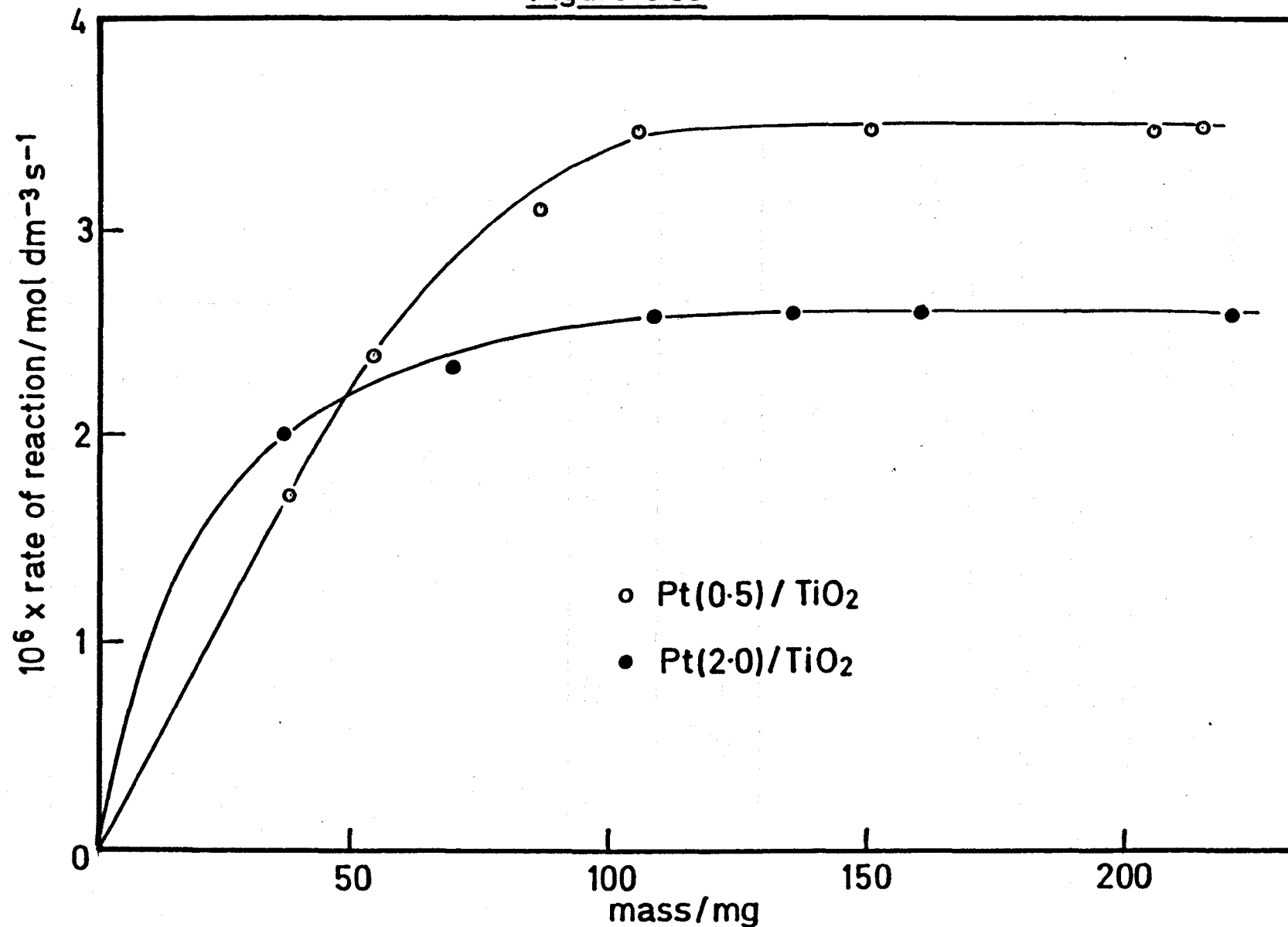
Photocatalytic dehydrogenation of propan-2-ol on different masses of Pt(0.5)/TiO<sub>2</sub> (method C) at 293 K.

Figure 3.32



Photocatalytic dehydrogenation of propan-2-ol on different masses of Pt(2.0)/TiO<sub>2</sub> (method C) at 293K

Figure 3.33



Photocatalytic dehydrogenation of propan-2-ol on different masses of Pt/TiO<sub>2</sub> (method C) at 293 K

### 3.4.2 Temperature dependence for the photocatalytic dehydrogenation of propan-2-ol on Pt(x)/TiO<sub>2</sub>

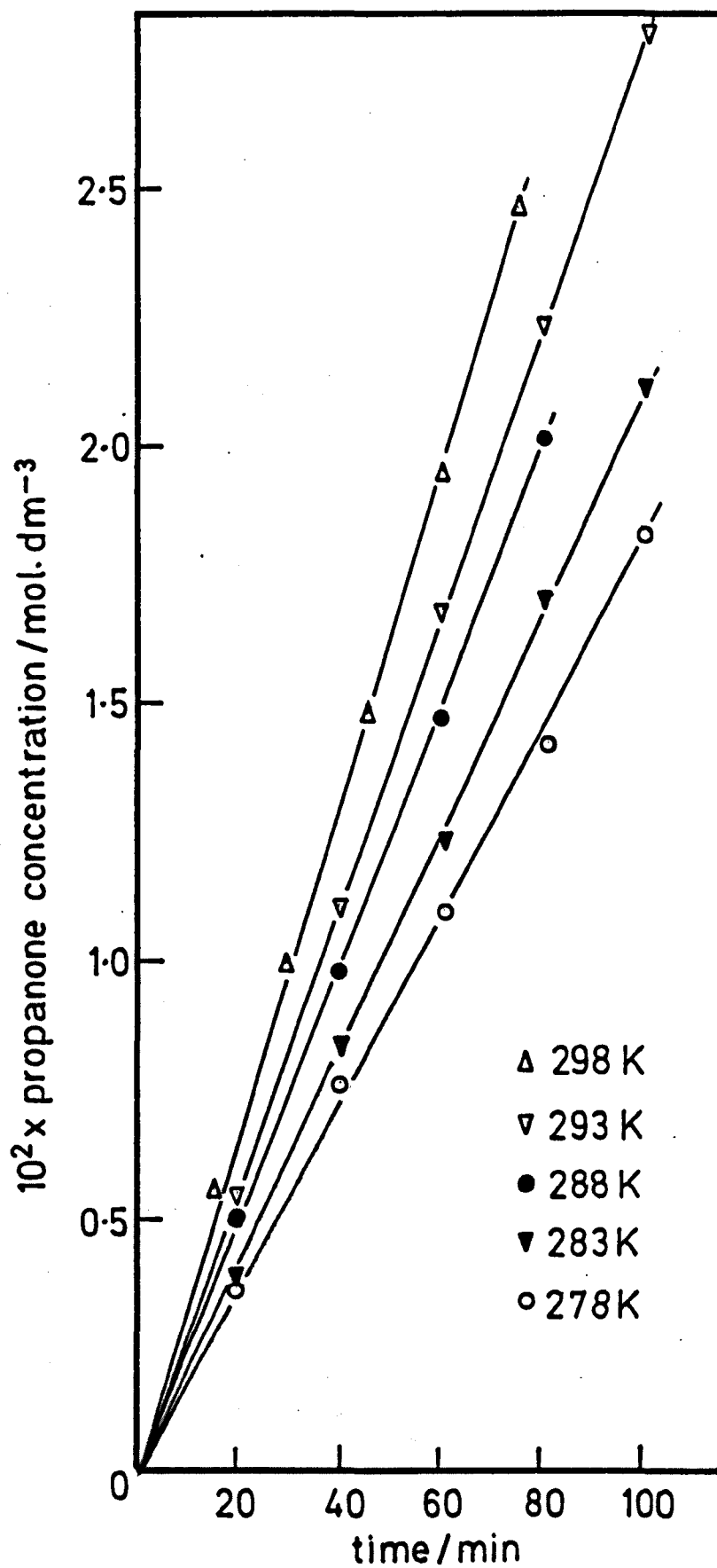
#### a) Pt(0.25)/TiO<sub>2</sub>

These reactions were carried out over the temperature range 278–298 K using 366 nm radiation from lamp 4. The results are shown in table 3.20 and plotted in figure 3.34 as  $10^2 \times$  propanone concentration/mol.dm.<sup>-3</sup> against time/min., and in figure 3.35 as  $\log(10^6 \times \text{rate of reaction/mol.dm.}^{-3}\text{s.}^{-1})$  against  $10^3 T^{-1}\text{K}$ .

TABLE 3.20

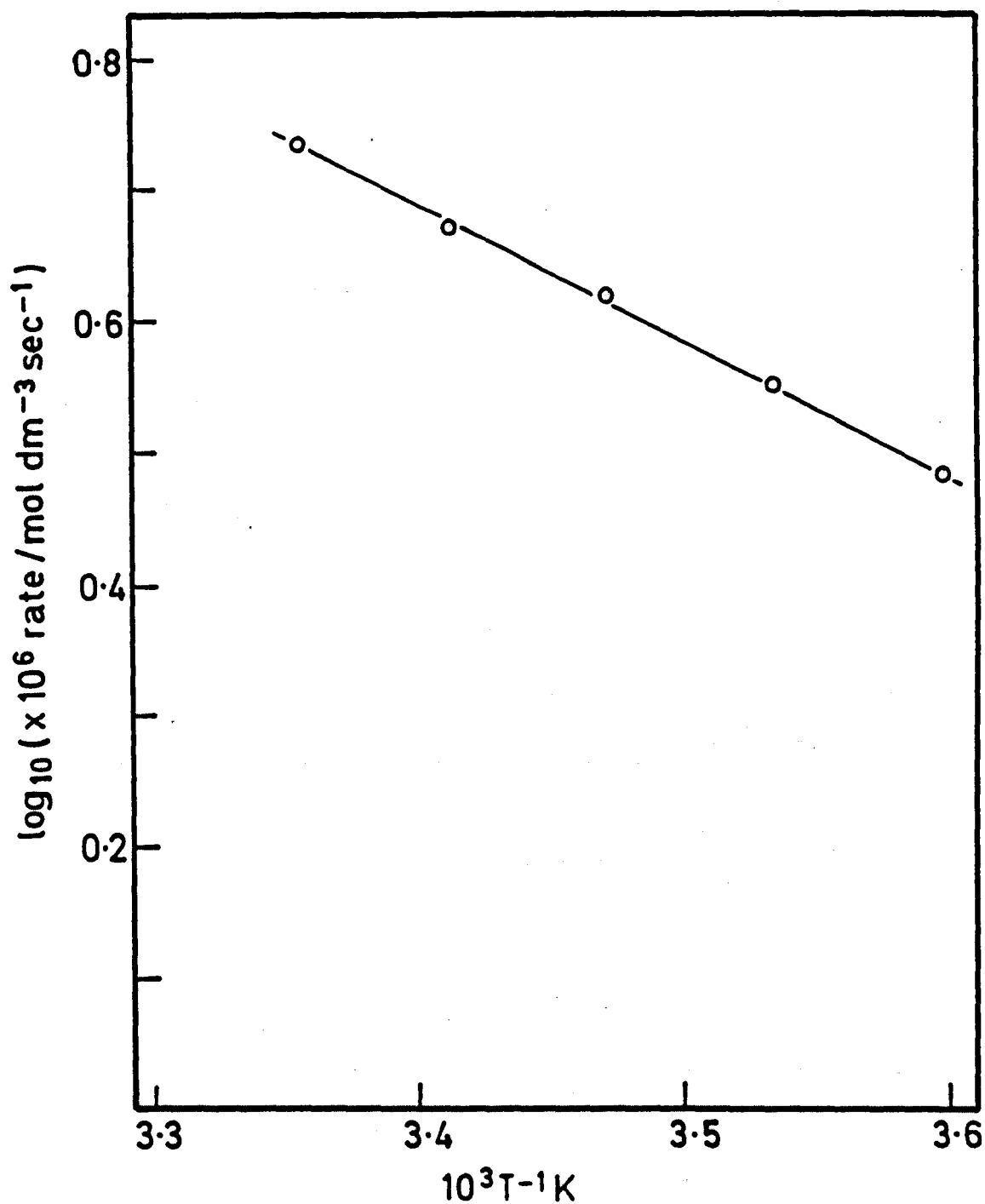
time/min.	$10^2 \times$ propanone concentration/ mol.dm. <sup>-3</sup>				
	T/K				
	278	283	288	293	298
0	0	0	0	0	0
15	-	-	-	-	0.560
20	0.37	0.385	0.501	0.552	-
30	-	-	-	-	0.998
40	0.760	0.829	0.980	1.110	-
45	-	-	-	-	1.480
60	1.110	1.240	1.482	1.678	1.950
75	-	-	-	-	2.460
80	1.430	1.701	2.024	2.240	-
100	1.824	2.120	-	2.900	-
$10^6 \times \text{rate}/$ mol.dm. <sup>-3</sup> s. <sup>-1</sup>	3.07	3.53	4.20	4.67	5.47

Figure 3.34



Photocatalytic dehydrogenation of propan-2-ol on  
Pt(0.25)/TiO<sub>2</sub> (method C) at different temperatures

Figure 3.35



Temperature dependence for the photocatalytic dehydrogenation of propan-2-ol on Pt(0.25)/TiO<sub>2</sub> (method C)

From these results an activation energy of  $20 \pm 1 \text{ kJ mol}^{-1}$  was calculated for propanone formation.

b) Pt(0.5)/TiO<sub>2</sub>

These experiments were carried out in the temperature range 278–303 K using 366 nm radiation from lamp 1 in the first series and from lamp 2 in the second series. Results for the first series are given in table 3.21 and plotted in figure 3.36 as  $10^2 \times \text{propanone concentration/mol.dm}^{-3}$  against time/min. Results for the second series are given in table 3.22 and plotted in figure 3.37 as  $10^2 \times \text{propanone concentration/mol.dm}^{-3}$  against time/min. The Arrhenius plots of  $\log(10^6 \times \text{rate of reaction/mol. dm}^{-3}\text{s}^{-1})$  against  $10^3 T^{-1} \text{ K}$  are shown in figure 3.38 and give an activation energy of  $20 \pm 1 \text{ kJ mol}^{-1}$  for propanone formation with lamp 1 and  $21 \pm \text{kJ mol}^{-1}$  with lamp 2.

TABLE 3.21

time/min.	$10^2 \times \text{propanone concentration/mol.dm}^{-3}$					
	T/K					
	278	283	288	293	298	303
0	0	0	0	0	0	0
15	-	-	-	-	-	0.401
20	0.281	0.339	0.354	0.419	0.458	-
30	-	-	-	-	-	0.799
40	0.522	0.621	0.711	0.835	0.939	-
45	-	-	-	-	-	1.202
60	0.803	0.922	1.080	1.260	1.380	1.598
75	-	-	-	-	-	2.000

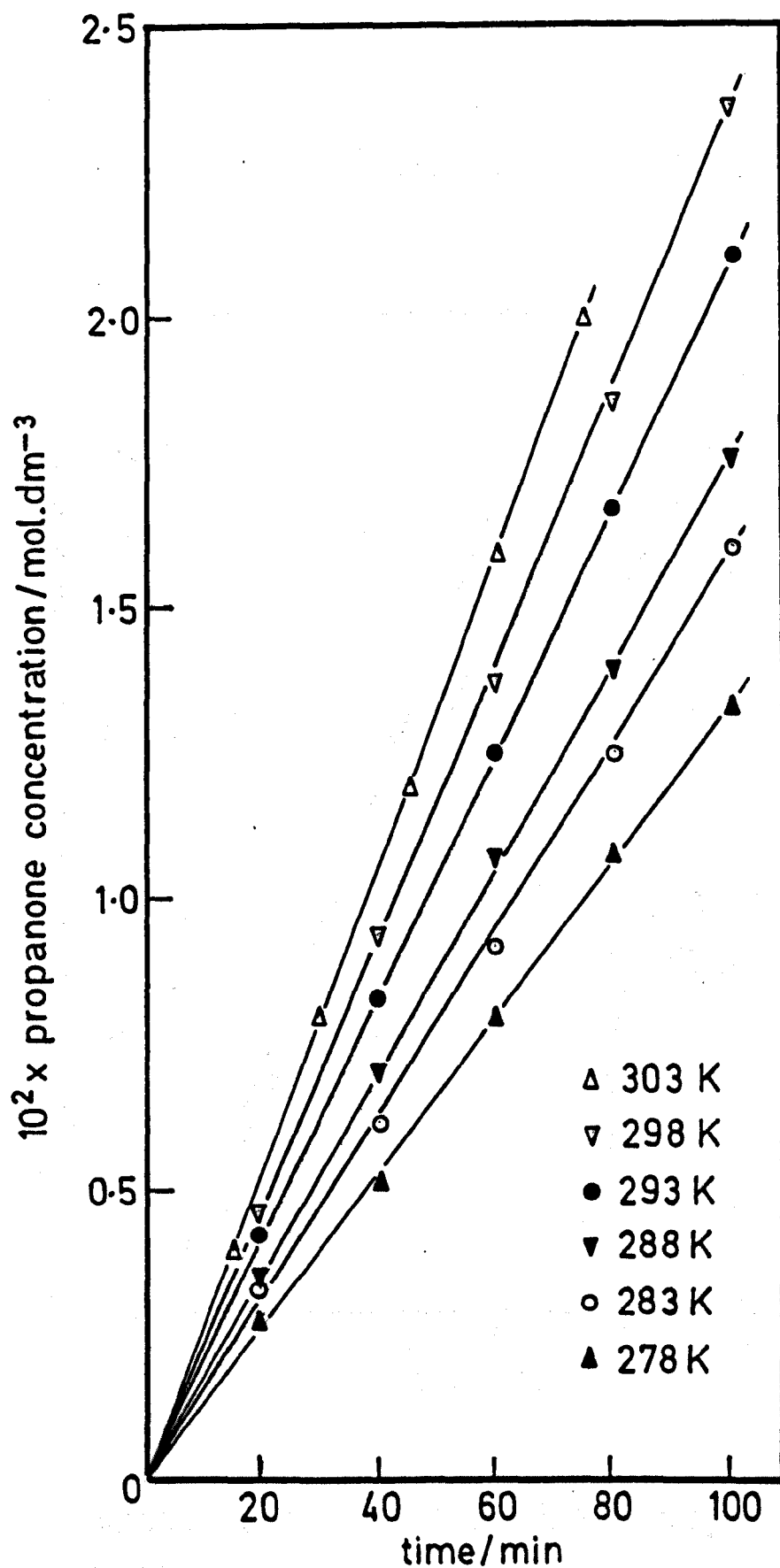
Contd. over.

80	1.081	1.259	1.411	1.681	1.857	-
90	-	-	-	-	-	-
100	1.340	1.614	1.771	2.110	2.359	-
$10^6 \times \text{rate}/$ $\text{mol.dm}^{-3}\text{s}^{-1}$	2.24	2.69	2.95	3.50	3.93	4.47

TABLE 3.22

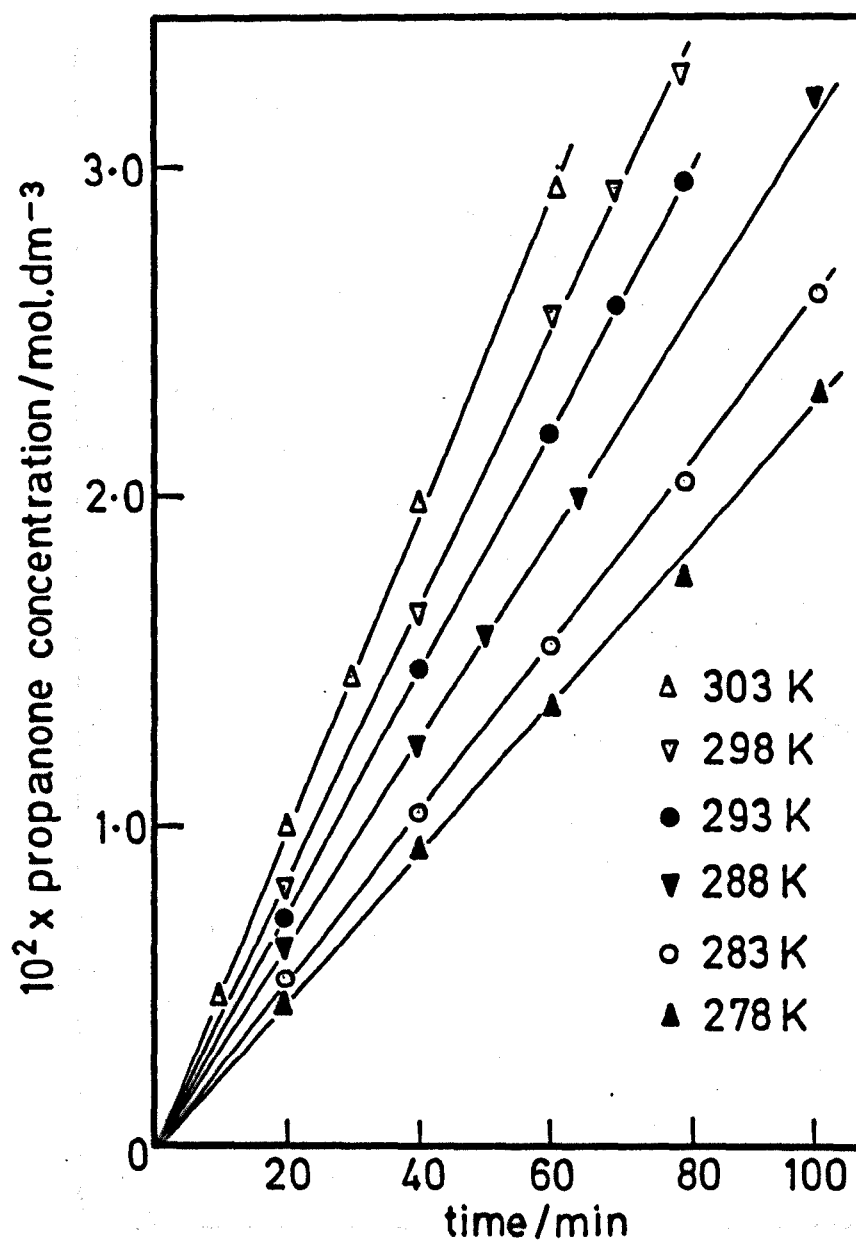
time/min.	$10^2 \times \text{propanone concentration/mol.dm}^{-3}$					
	T/K					
	278	283	288.4	293	298	303
0	0	0	0	0	0	0
10	-	-	-	-	-	0.487
20	0.463	0.534	0.644	0.730	0.816	1.000
30	-	-	-	-	-	1.450
40	0.942	1.036	1.256	1.480	1.664	1.974
50	-	-	1.601	-	-	-
60	1.382	1.570	-	2.198	2.560	2.955
64	-	-	2.010	-	-	-
70	-	-	-	2.581	2.942	-
80	1.774	2.057	-	2.967	3.297	-
100	2.339	2.638	3.219	-	-	-
$10^6 \times \text{rate}/$ $\text{mol.dm}^{-3}\text{s}^{-1}$	3.87	4.40	5.27	6.17	7.07	8.13

Figure 3.36



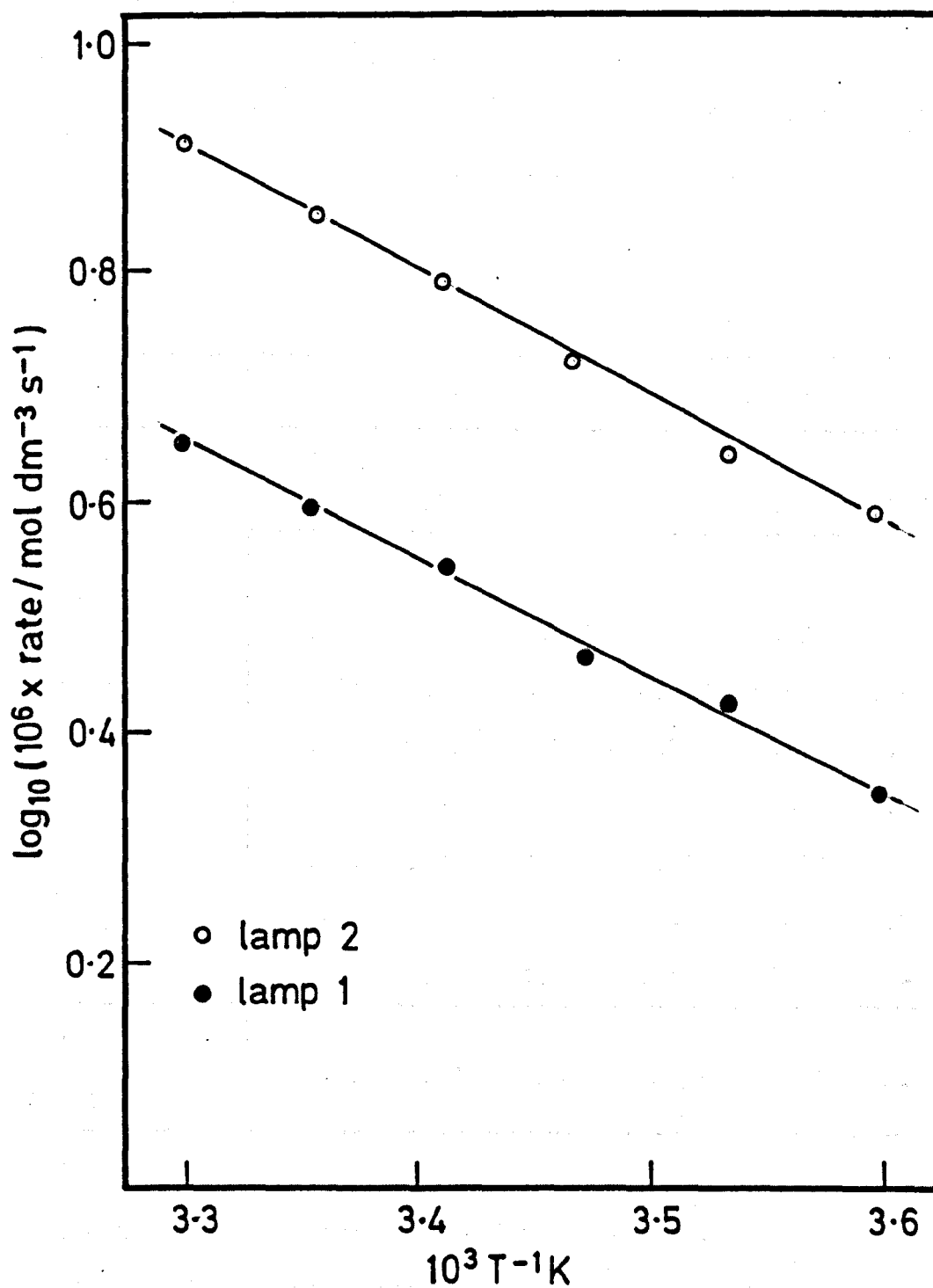
Photocatalytic dehydrogenation of propan-2-ol on  
Pt(0.5)/TiO<sub>2</sub> (method C) at different temperatures

Figure 3.37



Photocatalytic dehydrogenation of propan-2-ol on  
Pt(0.5)/TiO<sub>2</sub> (method C) at different temperatures

Figure 3.38



Temperature dependence for the photocatalytic dehydrogenation of propan-2-ol on Pt(0.5)/TiO<sub>2</sub> (method C)

c) Pt(2.0)/TiO<sub>2</sub>

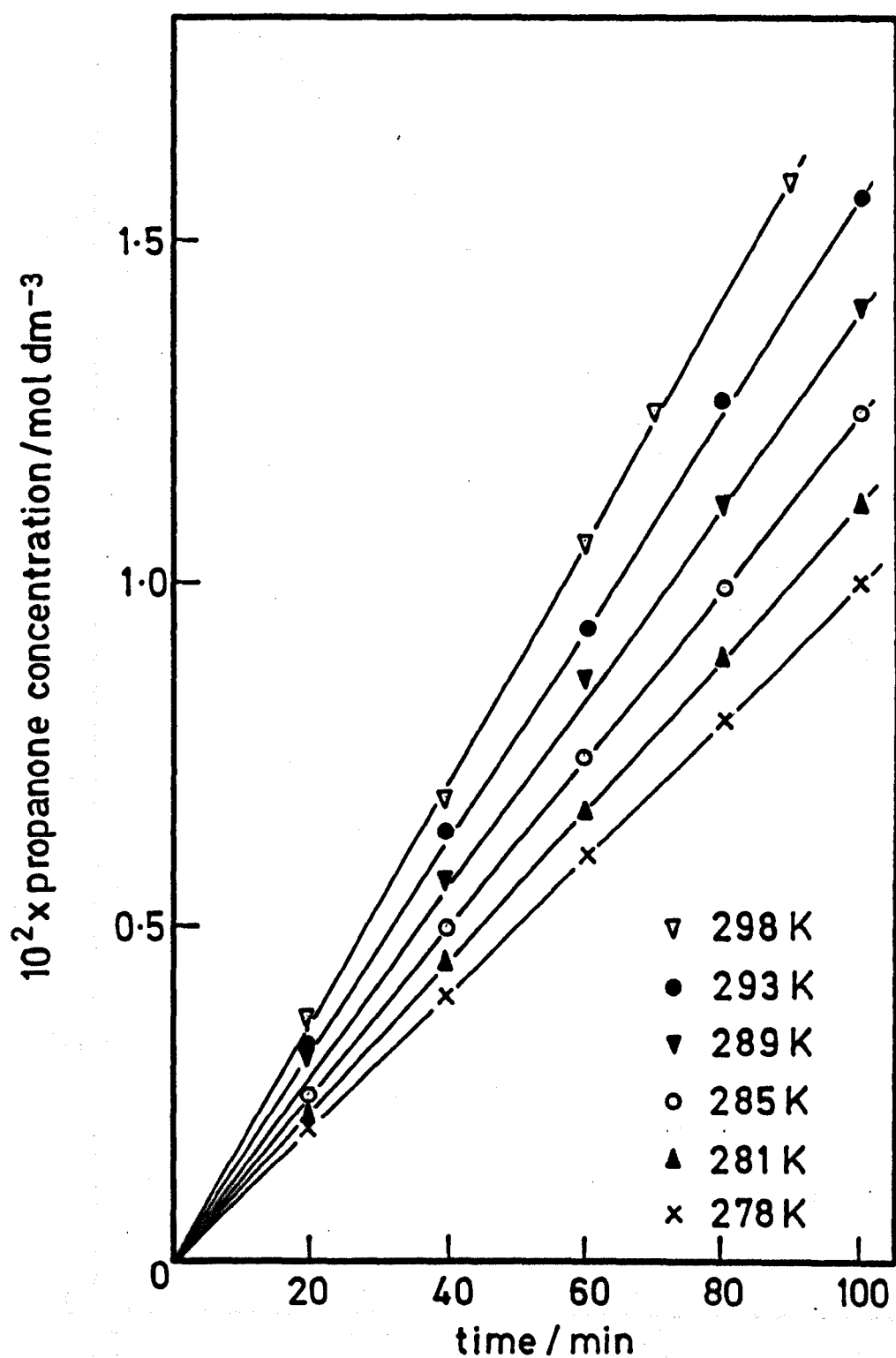
These experiments were carried out over the temperature range 278-298 K using 366 nm radiation from lamp 1. The results are given in table 3.23 and plotted in figure 3.39 as  $10^2 \times$  propanone concentration/mol.dm.<sup>-3</sup> against time/min., and in figure 3.40 as  $\log(10^6 \times$  rate of reaction /mol.dm.<sup>-3</sup>s.<sup>-1</sup>) against  $10^3 T^{-1}$  K. From these results an activation energy of  $20 \pm \text{kJ mol}^{-1}$  was obtained for propanone formation.

TABLE 3.23

time/min.	$10^2 \times$ propanone concentration/mol.dm. <sup>-3</sup>					
	T/K					
	278	281	285	289	293	298
0	0	0	0	0	0	0
20	0.2005	0.223	0.250	0.305	0.326	0.370
40	0.403	0.449	0.499	0.567	0.638	0.681
60	0.604	0.670	0.749	0.865	0.936	1.064
70	-	-	-	-	-	1.248
80	0.810	0.901	0.998	1.120	1.269	-
90	-	-	-	-	-	1.588
100	1.007	1.121	1.248	1.404	1.560	-
$10^6 \times$ rate/ mol.dm. <sup>-3</sup> s. <sup>-1</sup>	1.68	1.87	2.08	2.32	2.60	2.95

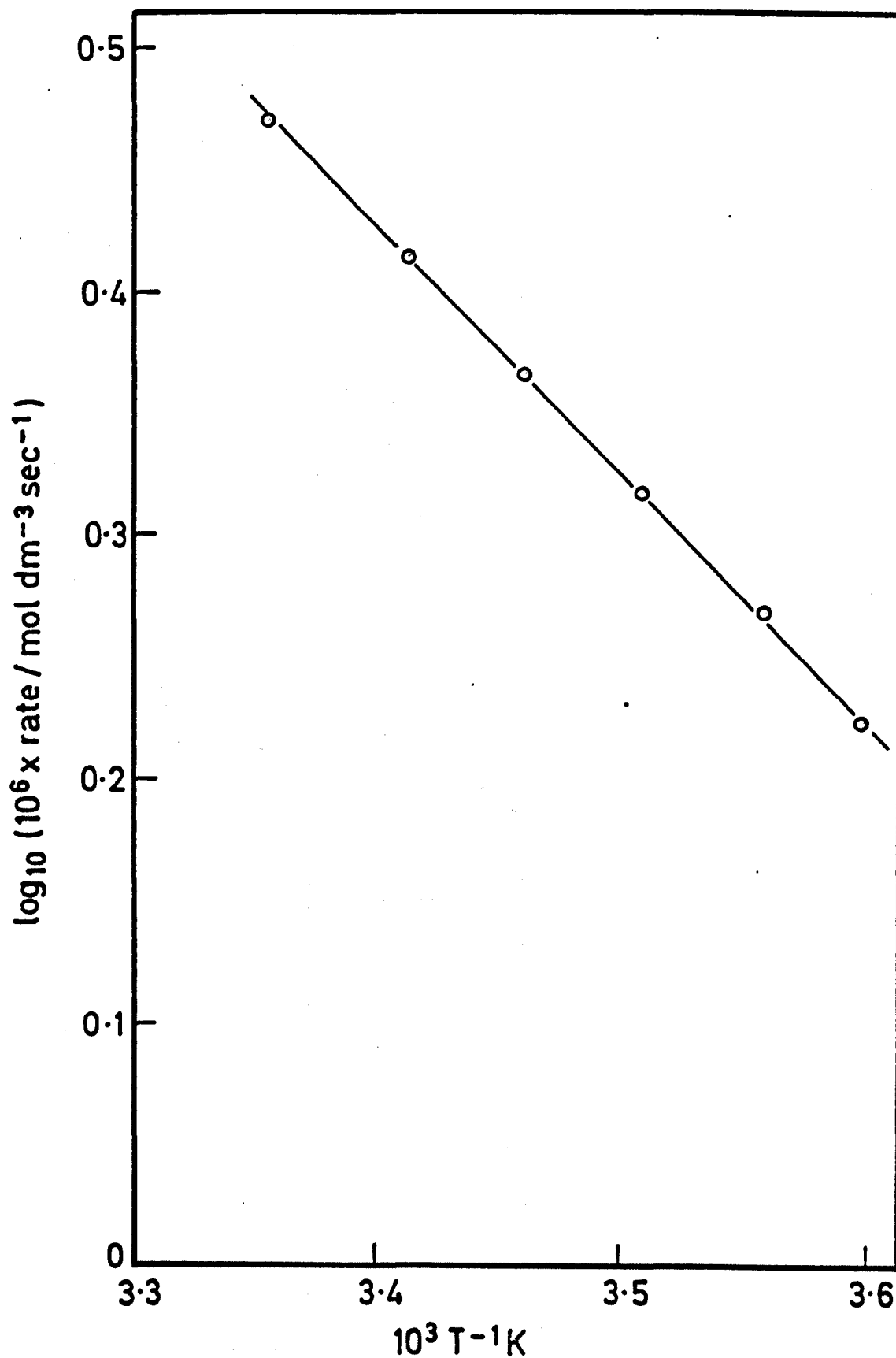
The activation energy of  $20 \pm 1 \text{ kJ mol}^{-1}$  obtained for propanone formation on platinized anatase with different platinum contents (0.25 wt%, 0.5 wt% and 2.0 wt%) indicates that the activation energy is independent of the amount of platinum on the anatase, and in a good agreement with the value obtained for anatase alone (see section 3.1.2).

Figure 3-39



Photocatalytic dehydrogenation of propan-2-ol on  
Pt(2.0)/TiO<sub>2</sub> (method C) at different temperatures

Figure 3.40



Temperature dependence for the photocatalytic dehydrogenation of propan-2-ol on Pt(2.0/TiO<sub>2</sub> (method C)

### 3.4.3 The effect of platinum content on reaction rate for the photocatalytic dehydrogenation of propan-2-ol

These experiments were carried out to determine the effect of platinum content on the photocatalytic dehydrogenation of propan-2-ol at 293 K using a single radiation intensity. Lamp 2 with 150 mg of the catalysts containing 0.25 wt%, 0.5 wt% or 2.0 wt% of platinum supported on anatase and a nitrogen atmosphere were used. The results are given in table 3.24 and plotted in figure 3.41 as  $10^2 \times$  propanone concentration/mol.dm.<sup>-3</sup> against time/min. The results show that the activity of the catalysts fell in the sequence:

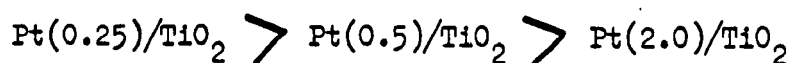
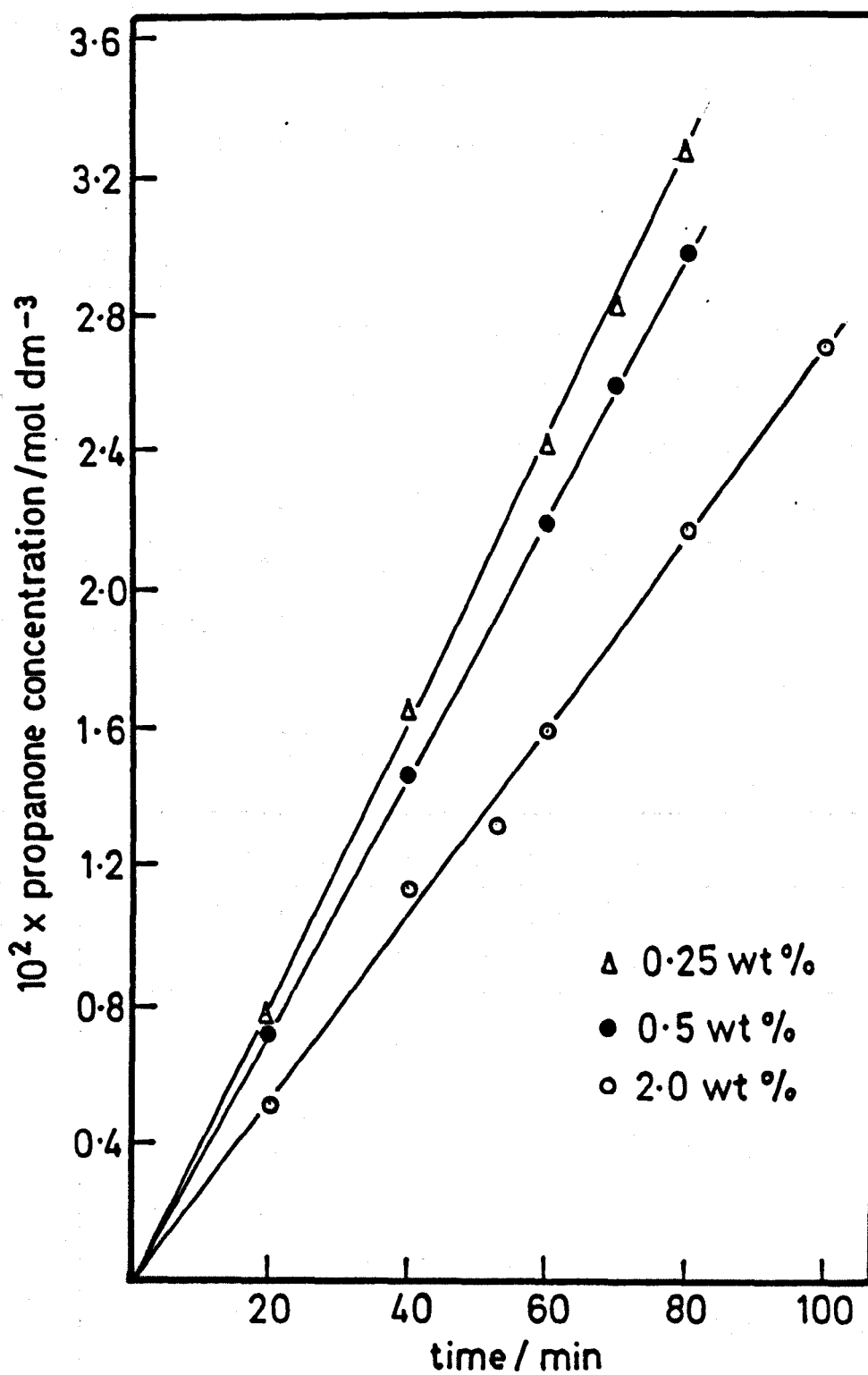


TABLE 3.24

time/min.	$10^2 \times$ propanone concentration/mol.dm. <sup>-3</sup>		
	Pt wt%		
	0.25	0.5	2.0
0	0	0	0
20	0.754	0.730	0.515
40	1.664	1.480	1.129
60	2.418	2.198	1.600
70	2.826	2.581	-
80	3.277	2.967	2.166
100	-	-	2.683
$10^6 \times$ rate/ mol.dm. <sup>-3</sup> s. <sup>-1</sup>	6.77	6.17	4.50

Figure 3.41



Photocatalytic dehydrogenation of propan-2-ol on different Pt content of Pt/TiO<sub>2</sub> (method C) at 293K

### 3.4.4 Light intensity dependence for the photocatalytic dehydrogenation of propan-2-ol

These experiments were carried out at 293 K using 366 nm radiation from lamp 4, 150 mg of catalyst ( $\text{Pt}(0.25)/\text{TiO}_2$  or  $\text{Pt}(0.5)/\text{TiO}_2$ ) and a nitrogen atmosphere. Neutral density filters were used to obtain reduced light intensities.

#### a) $\text{Pt}(0.25)/\text{TiO}_2$

These experiments were carried out with light intensities in the range  $0.14$ – $3.20$  einstein  $\text{s}^{-1}$ . The results are shown in table 3.25 and plotted in figure 3.42 as  $10^2 \times$  propanone concentration/ $\text{mol.dm}^{-3}$  against time/min., and in figure 3.44 as  $10^6 \times$  rate of reaction/ $\text{mol.dm}^{-3}\text{s}^{-1}$  against either  $10^7 \times$  light intensity/einstein  $\text{s}^{-1}$  or  $10^4 \times$  square root of light intensity/(einstein  $\text{s}^{-1}$ ) $^{1/2}$ .

TABLE 3.25

time/min.	$10^2 \times$ propanone concentration/ $\text{mol.dm}^{-3}$						
	$10^7 \times$ light intensity/einstein $\text{s}^{-1}$						
	3.20	2.74	1.67	1.16	0.82	0.65	0.14
0	0	0	0	0	0	0	0
20	0.552	0.481	0.315	0.253	-	0.166	-
25	-	-	-	-	0.269	-	-
30	-	0.726	-	-	-	-	-
40	1.110	-	0.628	0.520	-	-	-
45	-	-	-	-	-	0.354	-
50	-	-	-	-	0.489	-	-
60	1.678	1.425	1.028	0.765	-	-	0.105

Contd. over

70	-	-	-	-	-	0.565	-
75	-	-	-	-	0.739	-	-
80	2.240	1.908	1.360	1.036	-	-	-
90	-	-	-	-	-	0.722	-
100	2.800	2.418	1.680	1.300	0.984	-	-
120	-	-	-	-	-	-	0.230
125	-	-	-	-	1.248	-	-
140	-	-	-	-	-	1.120	-
180	-	-	-	-	-	-	0.330
240	-	-	-	-	-	-	0.470
330	-	-	-	-	-	-	0.606
$10^6 \times \text{rate}/$ $\text{mol.dm}^{-3}\text{s}^{-1}$	4.67	4.03	2.78	2.17	1.64	1.32	0.31

b) Pt(0.5)/TiO<sub>2</sub>

These experiments were carried out with light intensities in the range 0.14-3.20 einstein s<sup>-1</sup>. The results are given in table 3.26 and plotted in figure 3.43 as 10<sup>2</sup> x propanone concentration/mol.dm.<sup>-3</sup> against time/min., and in figure 3.44 as 10<sup>6</sup> x rate of reaction/mol.dm.<sup>-3</sup>s.<sup>-1</sup> against either 10<sup>7</sup> x light intensity/einstein s.<sup>-1</sup> or 10<sup>4</sup> x square root of light intensity/(einstein s.<sup>-1</sup>)<sup>1/2</sup>.

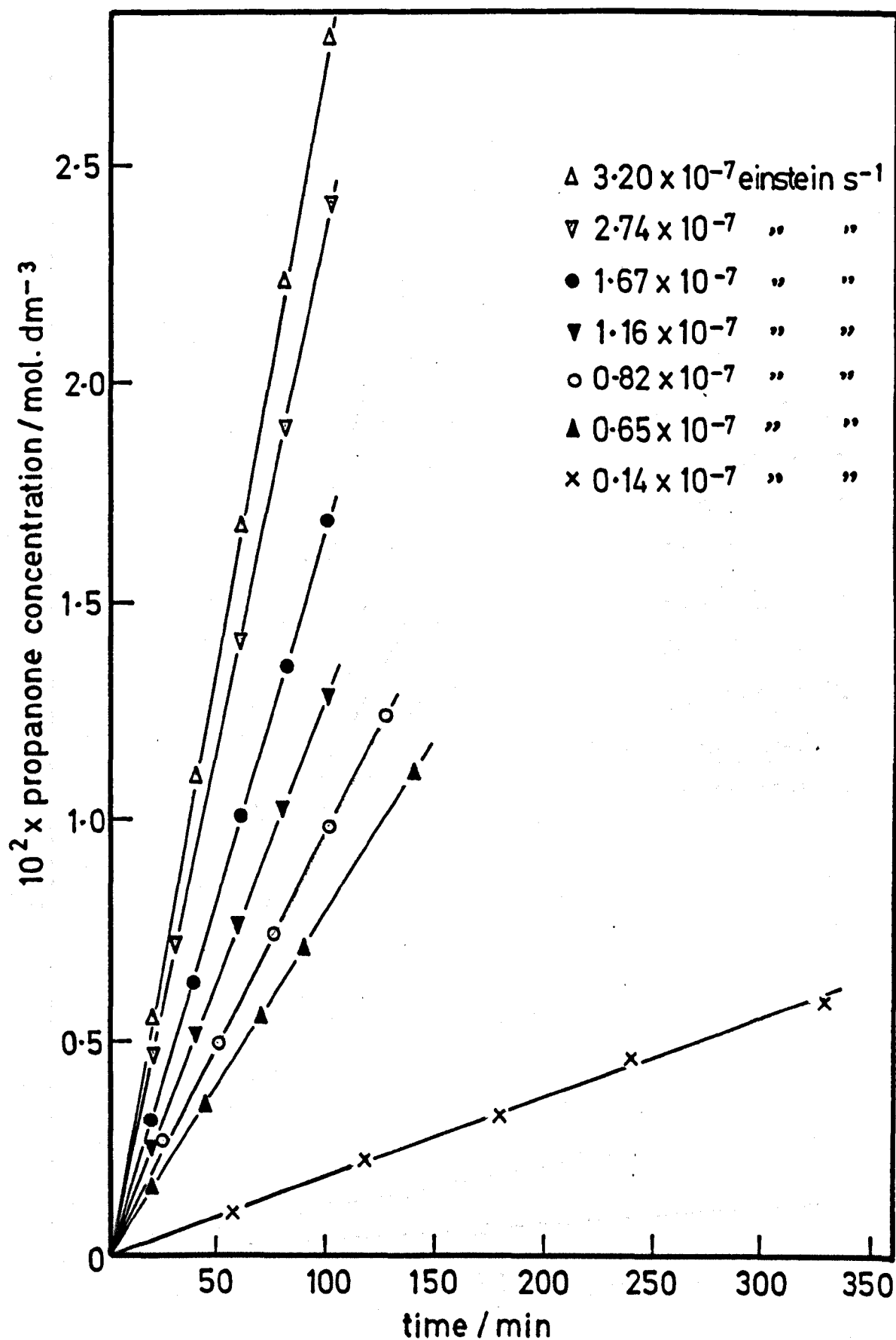
TABLE 3.26

time/min.	$10^2 \times \text{propanone concentration/mol.dm}^{-3}$									
	$10^7 \times \text{light intensity/einstein s}^{-1}$									
	3.20	2.74	2.08	1.67	1.44	1.16	0.82	0.65	0.14	0.06
0	0	0	0	0	0	0	0	0	0	0
20	0.549	-	0.410	0.353	-	0.310	0.215	0.181	-	-
25	-	0.597	-	-	-	-	-	-	-	-
30	-	-	-	-	-	-	-	-	0.060	-
40	1.131	-	0.819	0.716	-	0.597	0.423	0.343	-	-
50	-	1.256	-	-	0.820	-	-	-	-	-
60	1.611	-	1.270	1.062	-	0.885	0.604	0.503	0.119	-
70	-	-	-	-	1.162	-	-	-	-	-
75	-	1.921	-	-	-	-	-	-	-	-
80	2.201	-	1.650	1.431	-	1.217	0.860	0.681	0.156	-
90	-	-	-	-	1.476	-	-	-	-	-

Contd. over

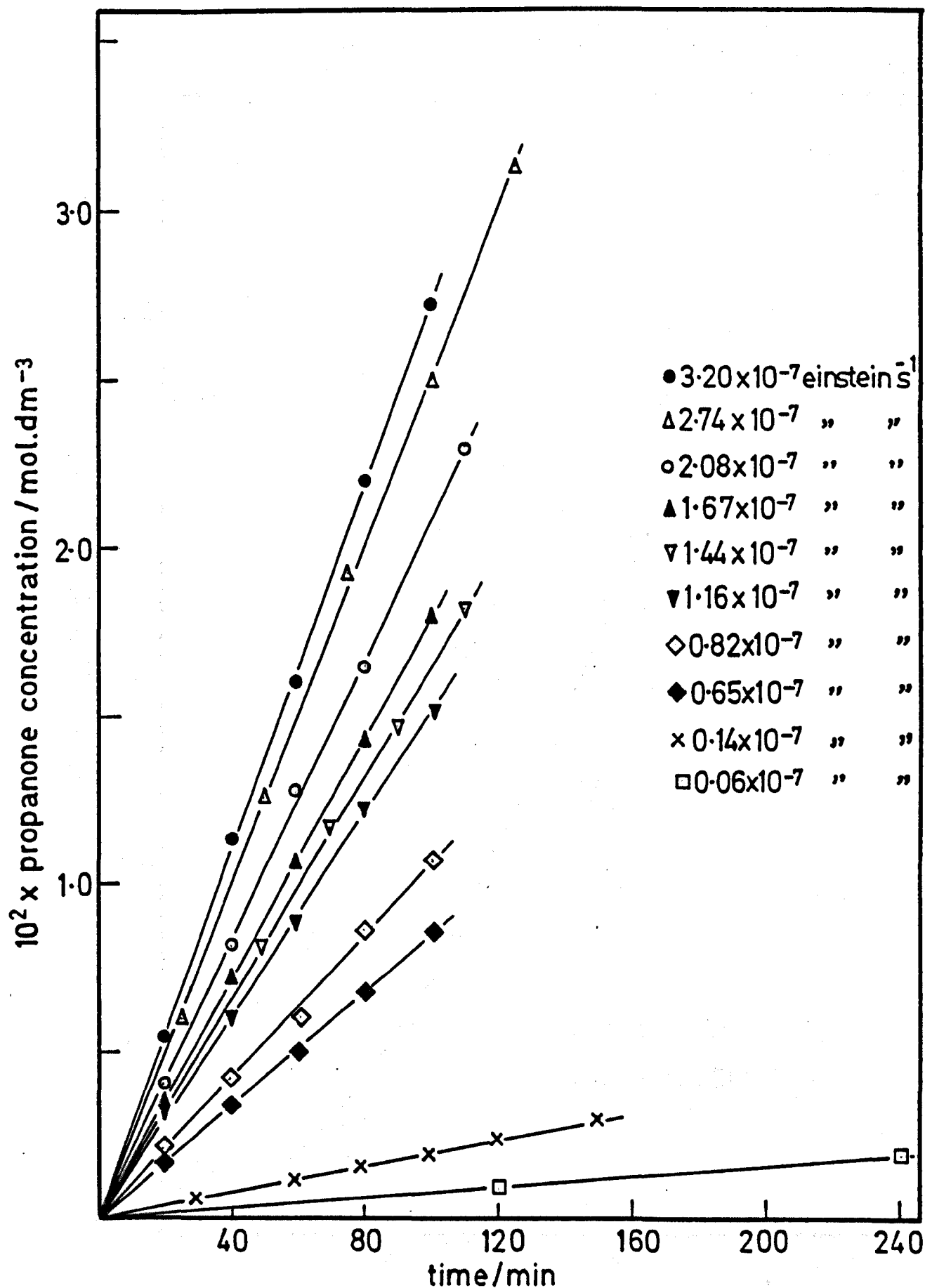
100	2.730	2.501	-	1.806	-	1.521	1.068	0.856	0.189	-
110	-	-	2.300	-	1.821	-	-	-	-	-
120	-	-	-	-	-	-	-	-	0.240	0.094
125	-	3.128	-	-	-	-	-	-	-	-
150	-	-	-	-	-	-	-	-	0.300	-
240	-	-	-	-	-	-	-	-	-	0.193
300	-	-	-	-	-	-	-	-	-	0.238
360	-	-	-	-	-	-	-	-	-	0.289
480	-	-	-	-	-	-	-	-	-	0.369
$10^6 \times \text{rate}/$ $\text{mol.dm}^{-3}\text{s}^{-1}$	4.53	4.17	3.48	3.00	2.75	2.52	1.78	1.42	0.32	0.134

Figure 3.42



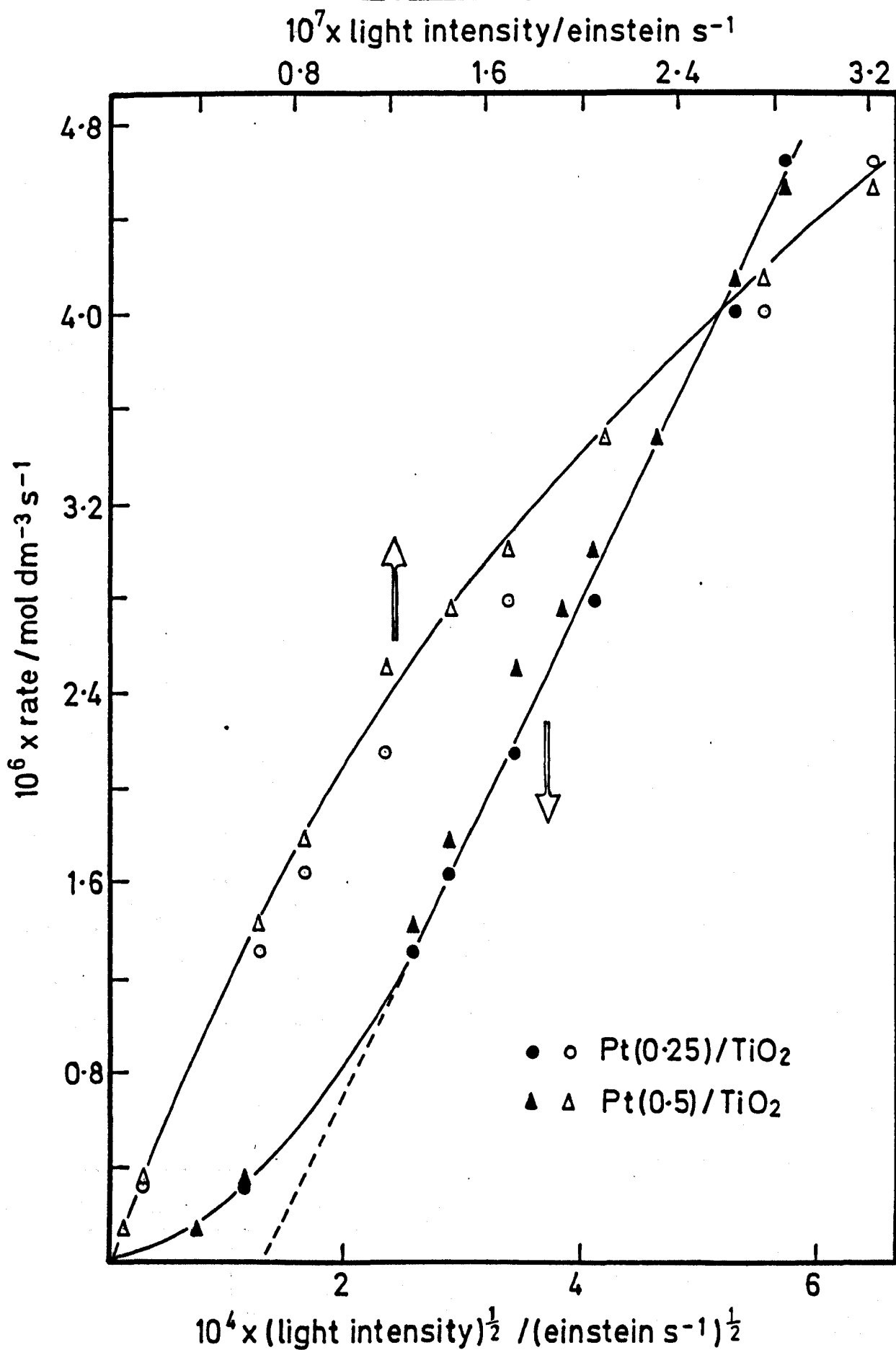
Photocatalytic dehydrogenation of propan-2-ol on Pt(0.25)/TiO<sub>2</sub> (method C) at different light intensities

Figure 3.43



Photocatalytic dehydrogenation of propan-2-ol on Pt(0.5)/TiO<sub>2</sub>  
(method C) at different light intensities

Figure 3.44



Light intensity dependence for the photocatalytic dehydrogenation of propan-2-ol on Pt/TiO<sub>2</sub> (method C) at 293K

The results show that a linear dependence holds for both catalysts up to a light intensity of  $\sim 1.0 \times 10^{-7}$  einstein  $s^{-1}$ , but above that a square root intensity dependence is obeyed. It is to be noted that the plot for the square root dependence does not pass through the origin.

3.4.5 Temperature dependence for the photocatalytic dehydrogenation of propan-2-ol at different light intensities on Pt(0.5)/TiO<sub>2</sub>

The light intensity effect on the reaction rate had been investigated before (section 3.4.4). Experiments were carried out using 366 nm radiation from lamp 4 to study possible effects of light intensity on the activation energy for the production of propanone on Pt(0.5)/TiO<sub>2</sub>. Neutral density filters were used to produce different light intensities.

a) Full light intensity ( $3.20 \times 10^{-7}$  einstein  $s^{-1}$ )

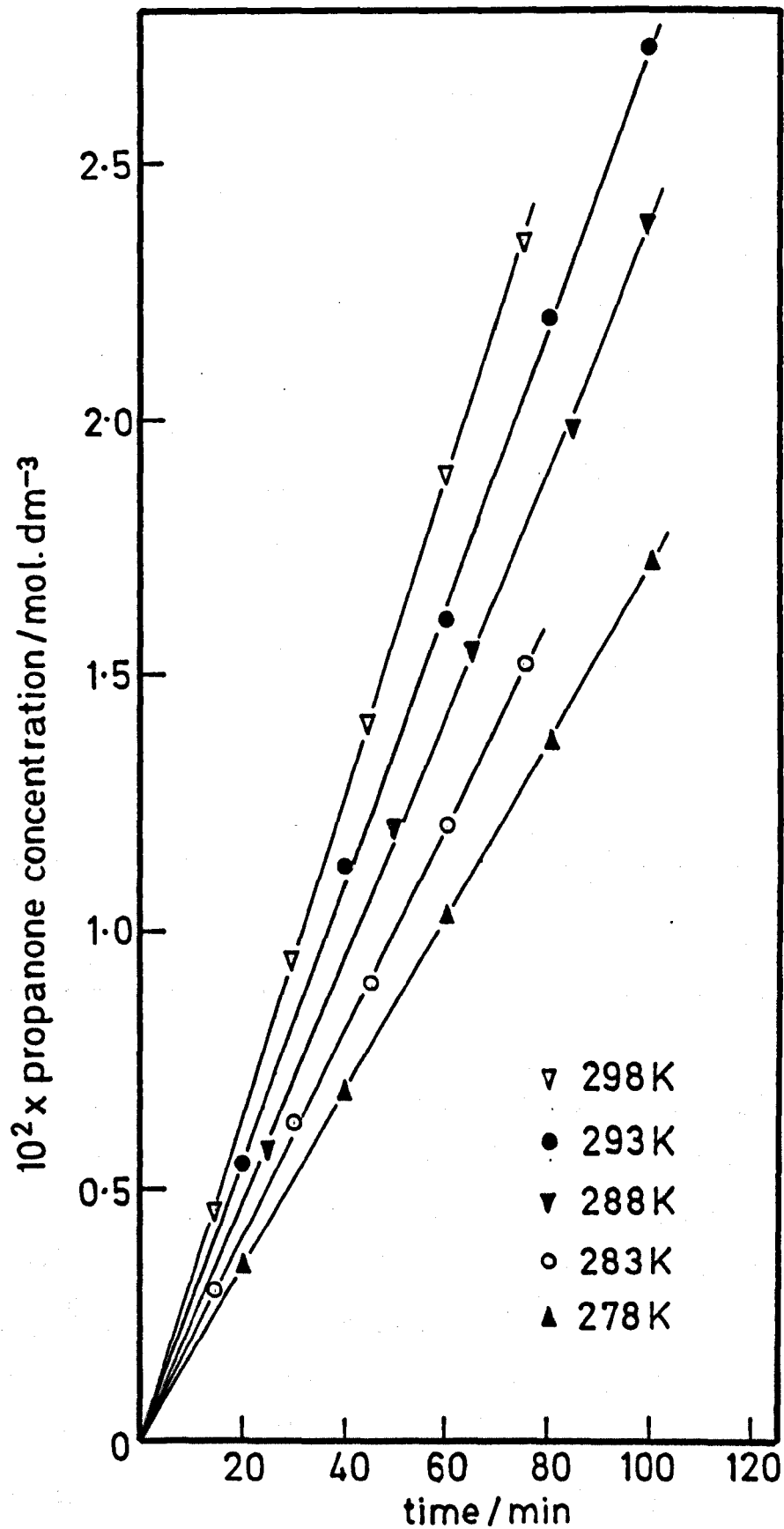
These experiments were carried out with unreduced light intensity over the temperature range 278-298 K. The results are shown in table 3.27 and plotted in figure 3.45 as  $10^2 \times$  propanone concentration/mol.dm.<sup>-3</sup> against time/min., and in figure 3.48 as  $\log(10^6 \times$  rate of reaction/mol.dm.<sup>-3</sup>s.<sup>-1</sup>) against  $10^3 T^{-1}$  K. These results give an activation energy of  $20 \pm 1$  kJ mol.<sup>-1</sup> for propanone formation which is identical to that obtained using full light intensity of lamp 1 (see section 3.4.2,b).

TABLE 3.27

time/min.	$10^2 \times$ propanone concentration/mol.dm. <sup>-3</sup>				
	T/K				
	278	283	288	293	298
0	0	0	0	0	0
15	-	0.298	-	-	0.458

Contd. over

Figure 3.45



Photocatalytic dehydrogenation of propan-2-ol on Pt(0.5)/TiO<sub>2</sub> (method C) at different temperatures with a light intensity of  $3.20 \times 10^{-7}$  einstein s<sup>-1</sup>

20	0.350	-	-	0.549	-
25	-	-	0.582	-	-
30	-	0.631	-	-	0.949
40	0.692	-	-	1.131	-
45	-	0.899	-	-	1.407
50	-	-	1.201	-	-
60	1.041	1.207	-	1.611	1.901
65	-	-	1.539	-	-
75	-	1.521	-	-	2.351
80	1.380	-	-	2.201	-
85	-	-	1.981	-	-
90	-	-	-	-	-
100	1.731	-	2.391	2.730	-
$10^6 \times \text{rate}/$ $\text{mol.dm}^{-3}\text{s}^{-1}$	2.88	3.39	3.98	4.53	5.23

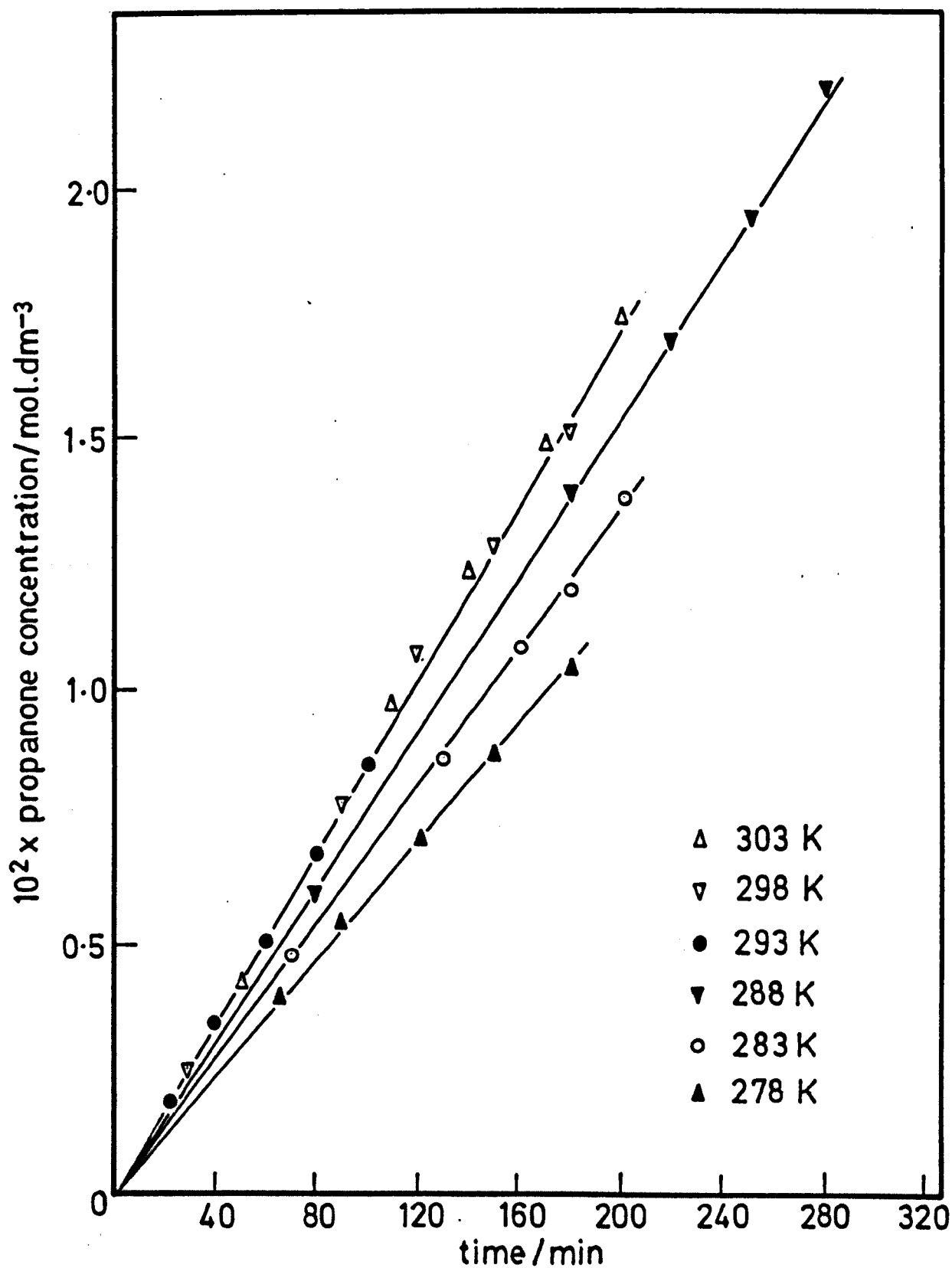
b) 20.2% relative light intensity ( $0.65 \times 10^{-7}$  einstein  $\text{s}^{-1}$ )

These experiments were carried out in the temperature range 278-303 K. The results are given in table 3.28 and plotted in figure 3.46 as  $10^2 \times$  propanone concentration/ $\text{mol.dm}^{-3}$  against time/min., and in figure 3.48 as  $\log(10^6 \times \text{rate of reaction}/\text{mol.dm}^{-3}\text{s}^{-1})$  against  $10^3 T^{-1} \text{K}$ . The Arrhenius plot possessing a good linearity between 278-293 K gives an activation energy of  $19 \pm 1 \text{ kJ mol}^{-1}$  for propanone formation which is not significantly different from that obtained using full light intensity. However, above 293 K the activation energy tends to zero.

TABLE 3.28

time/min.	$10^2 \times \text{propanone concentration/mol.dm}^{-3}$					
	T/K					
	278	283	288	293	298	303
0	0	0	0	0	0	0
20	-	-	-	0.181	-	-
30	-	-	-	-	0.253	-
40	-	-	-	0.343	-	-
50	-	-	-	-	-	0.434
60	-	-	-	0.503	-	-
65	0.401	-	-	-	-	-
70	-	0.478	-	-	-	-
80	-	-	0.597	0.681	-	-
90	0.547	-	-	-	0.770	-
100	-	-	-	0.856	-	-
110	-	-	-	-	-	0.981
120	0.719	-	-	-	1.083	-
130	-	0.871	-	-	-	-
140	-	-	-	-	-	1.256
150	0.880	-	-	-	1.301	-
160	-	1.099	-	-	-	-
170	-	-	-	-	-	1.502
180	1.080	1.210	1.400	-	1.523	-
200	-	1.388	-	-	-	1.751
220	-	-	1.710	-	-	-
250	-	-	1.953	-	-	-
280	-	-	2.201	-	-	-
$10^6 \times \text{rate/}$ $\text{mol.dm}^{-3}\text{s}^{-1}$	0.98	1.13	1.28	1.42	1.42	1.45

Figure 3.46



Photocatalytic dehydrogenation of propan-2-ol on Pt(0.5)/TiO<sub>2</sub>(method C) at different temperatures with a light intensity of  $0.65 \times 10^{-7}$  einstein s<sup>-1</sup>

c) 4.4% relative light intensity ( $0.14 \times 10^{-7}$  einstein  $s^{-1}$ )

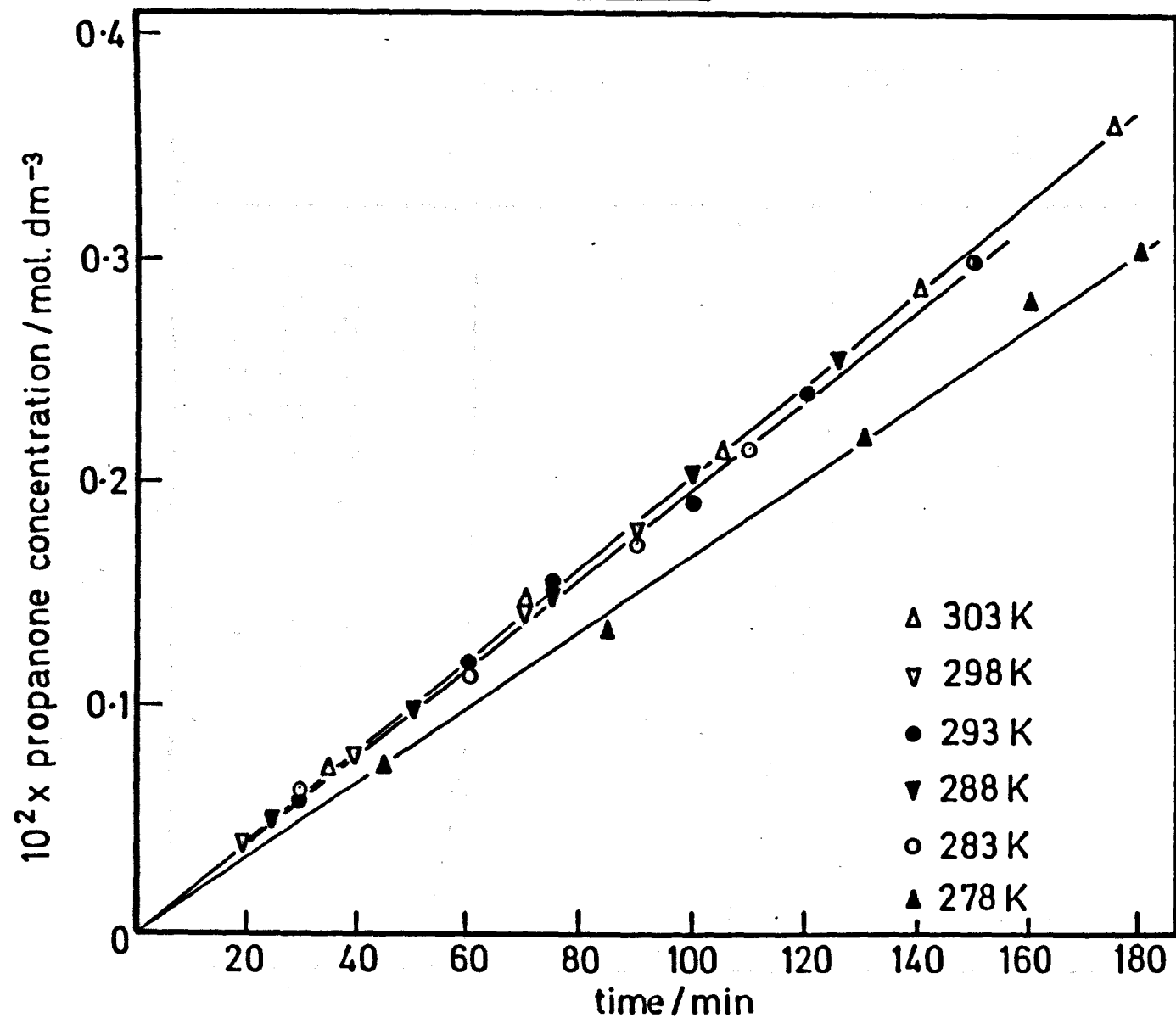
These experiments were carried out in the temperature range 278–303 K. The results are given in table 3.29 and plotted in figure 3.47 as  $10^2 \times$  propanone concentration/mol.dm.<sup>3</sup> against time/min., and in figure 3.48 as  $\log(10^6 \times \text{rate of reaction/mol.dm.}^3\text{s.}^{-1})$  against  $10^3 T^{-1}$  K. The rate of reaction reached a maximum above 283 K so the activation energy above 283 K tends to zero. However, at low temperatures an activation energy of  $20 \pm 1$  kJ mol.<sup>-1</sup> was obtained for propanone formation which is the same as that obtained using other light intensities.

TABLE 3.29

time/min.	$10^2 \times$ propanone concentration/mol.dm. <sup>3</sup>					
	T/K					
	278	283	288	293	298	303
0	0	0	0	0	0	0
20	-	-	-	-	0.040	-
25	-	-	0.052	-	-	-
30	-	0.065	-	0.060	-	-
35	-	-	-	-	-	0.074
40	-	-	-	-	0.080	-
45	0.075	-	-	-	-	-
50	-	-	0.100	-	-	-
60	-	0.115	-	0.119	-	-
70	-	-	-	-	0.141	0.150
75	-	-	0.149	-	-	-
80	-	-	-	0.156	-	-

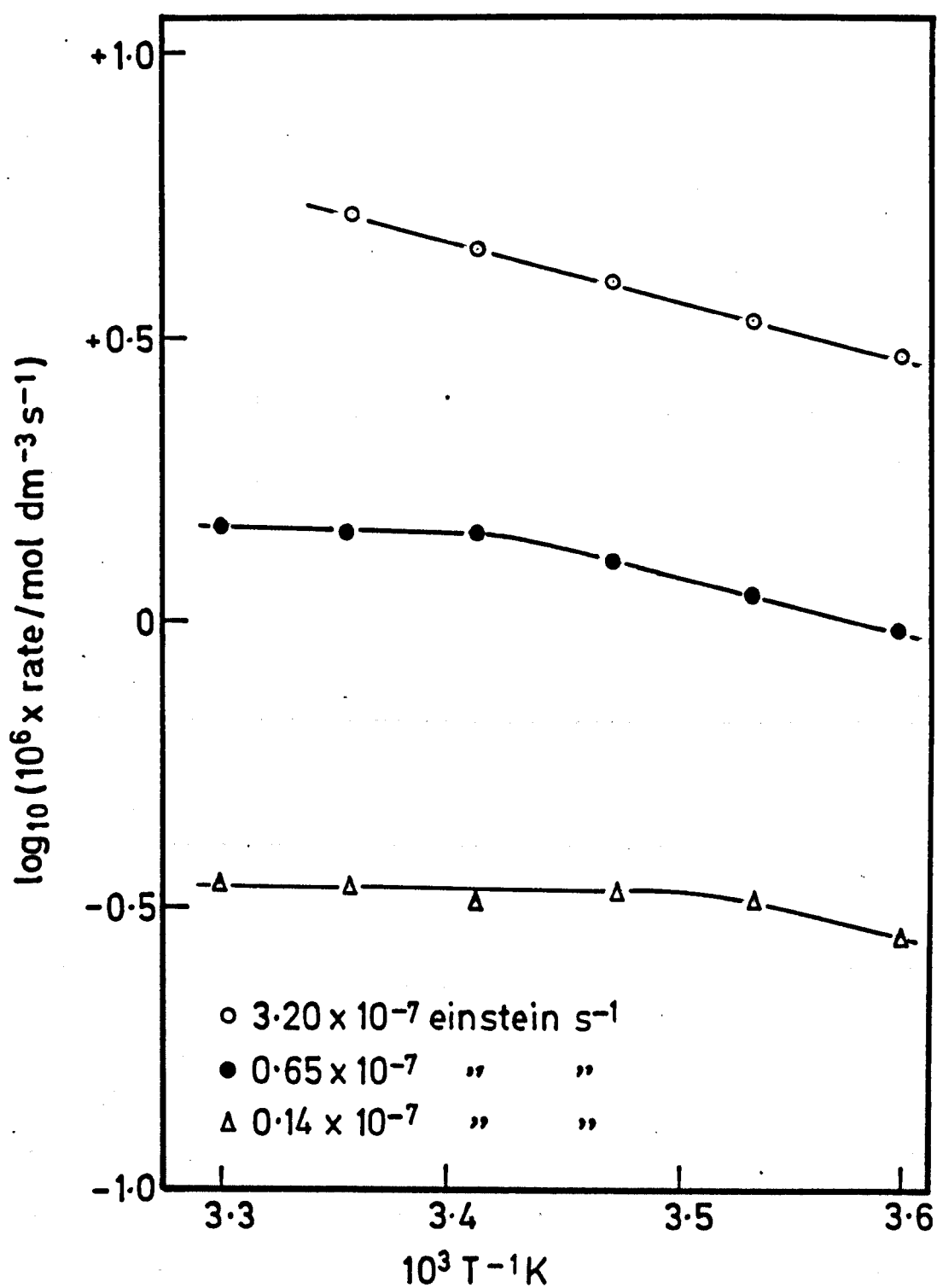
Contd. over

Figure 3.47



Photocatalytic dehydrogenation of propan-2-ol on Pt(0.5)/TiO<sub>2</sub> (method C)  
at different temperatures with a light intensity of  $0.14 \times 10^{-7}$  einstein s<sup>-1</sup>

Figure 3·48



Temperature dependence for the photocatalytic dehydrogenation of propan-2-ol using different light intensities

85	0.135	-	-	-	-	-
90	-	0.174	-	-	0.180	-
100	-	-	0.205	0.189	-	-
105	-	-	-	-	-	0.215
110	-	0.215	-	-	-	-
120	-	-	-	0.240	-	-
125	-	-	0.255	-	-	-
130	0.221	-	-	-	-	-
140	-	-	-	-	-	0.289
150	-	0.300	-	0.300	-	-
160	0.282	-	-	-	-	-
175	-	-	-	-	-	0.361
180	0.305	-	-	-	-	-
$10^6 \times \text{rate}/$ $\text{mol.dm}^{-3}\text{s}^{-1}$	0.28	0.33	0.34	0.32	0.34	0.35

#### 3.4.6 Photocatalytic dehydrogenation of other alcohols at 278 K and 293 K on Pt(0.5)/TiO<sub>2</sub>

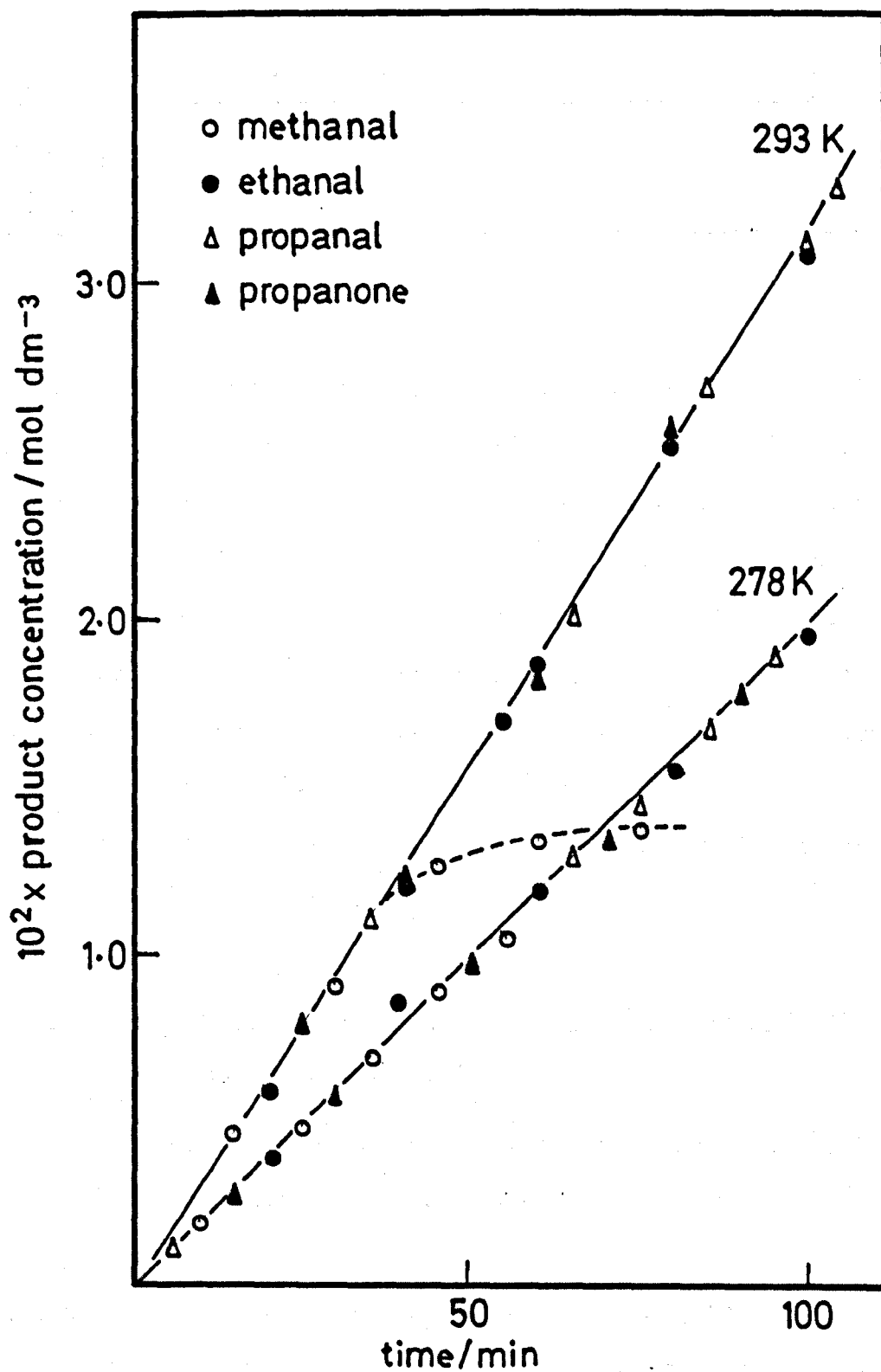
These experiments were conducted in order to determine whether the activity was independent on the reactant alcohol for photodehydrogenation on Pt(0.5)/TiO<sub>2</sub> prepared by method C. The only detectable dehydrogenation product of methanol was methanal, for ethanol was ethanal, for propan-1-ol was propanal and for propan-2-ol was propanone. All reactions were carried out using 366 nm radiation from lamp 3, 150 mg of the catalyst and nitrogen pressure of one atmosphere. The results are given in table 3.30 and plotted in figure 3.49 as  $10^2 \times$  product (methanal, ethanal, propanal or propanone) concentration/mol.dm<sup>-3</sup> against time/min.

TABLE 3.30

time/min.	$10^2 \times \text{product concentration/mol.dm}^{-3}$							
	alcohol							
	methanol		ethanol		propan-1-ol		propan-2-ol	
	T/K							
	278	293	278	293	278	293	278	293
0	0	0	0	0	0	0	0	0
5	-	-	-	-	0.120	-	-	-
10	0.218	-	-	-	-	-	-	-
15	-	0.472	-	-	-	-	0.282	-
20	-	-	0.400	0.604	-	-	-	-
25	0.500	-	-	-	-	-	-	0.799
30	-	0.910	-	-	-	-	0.579	-
35	0.720	-	-	-	-	1.110	-	-
40	-	-	0.860	1.205	-	-	-	1.241
45	0.897	1.310	-	-	-	-	-	-
50	-	-	-	-	-	-	0.973	-
55	1.060	-	-	-	-	-	-	-
60	-	1.350	1.200	1.856	-	-	-	1.828
65	-	-	-	-	1.300	2.225	-	-
70	-	-	-	-	-	-	1.376	-
75	-	1.425	-	-	1.460	-	-	-
80	-	-	1.561	2.531	-	-	-	2.580
85	-	-	-	-	1.700	2.695	-	-
90	-	-	-	-	-	-	1.810	-
95	-	-	-	-	1.901	-	-	-

Contd. over

Figure 3.49



Photocatalytic dehydrogenation of different alcohols  
on Pt(0.5)/TiO<sub>2</sub> (method C)

100	-	-	1.951	3.112	-	-	-	3.140
105	-	-	-	-	-	3.300	-	-
$10^6 \times \text{rate}/$ $\text{mol.dm}^{-3}\text{s}^{-1}$	3.33	5.21*	3.27	5.26	3.33	5.20	3.28	5.29

\* The initial rate of reaction.

The results show that the different alcohols have the same activity at 293 K, except methanol where methanal failed to increased linearly with time at a concentration  $> 1.0 \times 10^{-2} \text{ mol.dm}^{-3}$ . This could be due to further oxidation of the methanal to methanoic acid and carbon-dioxide. A further set of experiments were done at 278 K to minimize both the product concentration and the further oxidation of methanal. At this temperature all four alcohols gave the same reaction progress plot, with no deviation for methanal.

It is concluded from the results that the photocatalytic activity was independent of the alcohol used.

#### 3.4.7 Temperature dependence for the photocatalytic dehydrogenation of other alcohols on Pt(0.5)/TiO<sub>2</sub>

These experiments were carried out using 366 nm radiation, 150 mg of the catalyst and a nitrogen pressure of one atmosphere.

##### a) Methanol

These experiments were carried out over the temperature range 278-293 K using 366 nm radiation from lamp 3. The results are shown in table 3.31 and plotted in figure 3.50 as  $10^2 \times \text{methanal concentration}/\text{mol.dm}^{-3}$  against time/min., and in figure 3.51 as  $\log(10^6 \times \text{initial rate of reaction}/\text{mol.dm}^{-3}\text{s}^{-1})$  against  $10^3 T^{-1} \text{ K}$ . A curved reaction progress

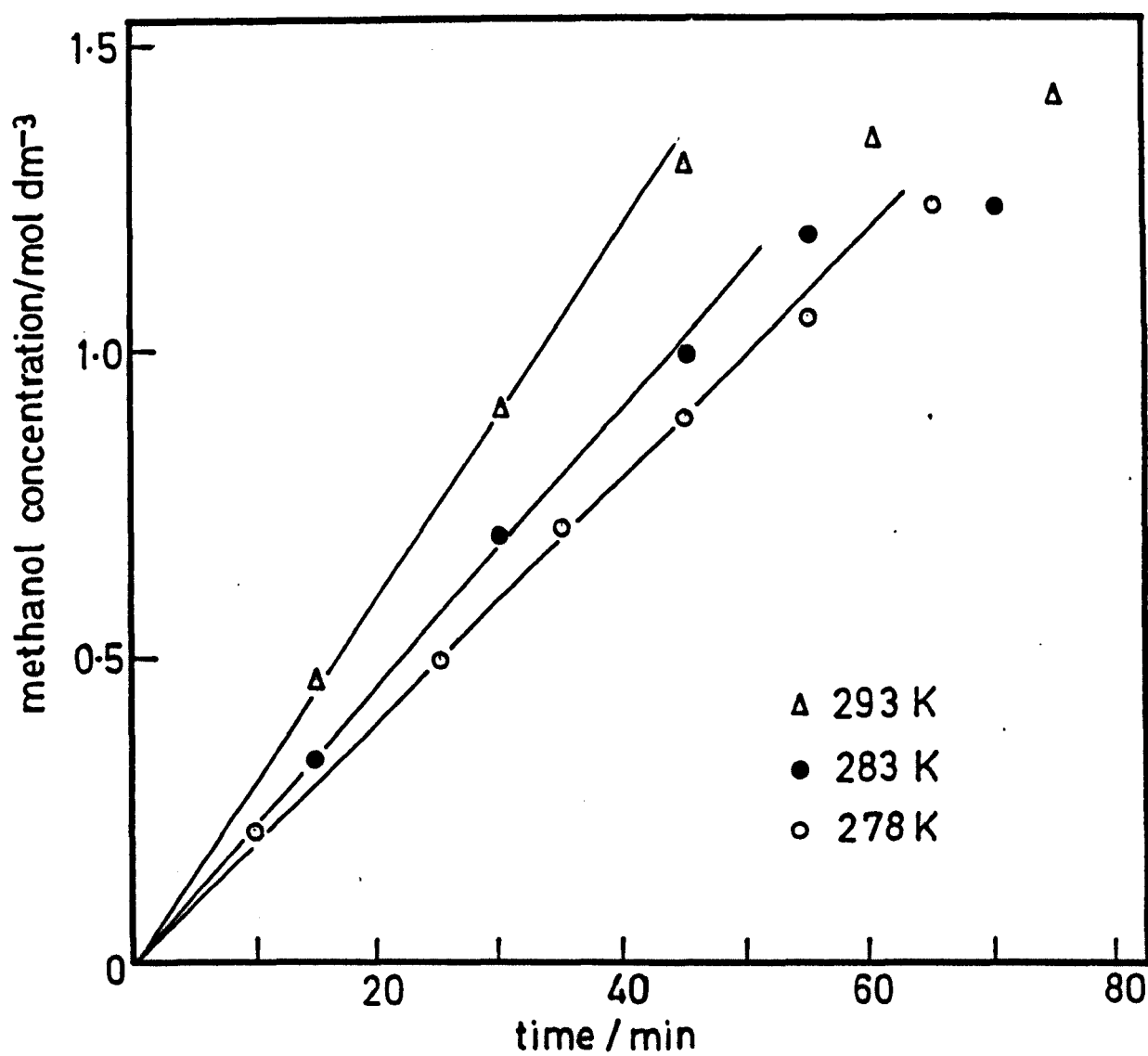
plot was obtained when the concentration of methanal exceeded  $1 \times 10^{-2} \text{ mol.dm}^{-3}$ , due to further oxidation of methanal.

TABLE 3.31

time/min.	methanal concentration/mol.dm. <sup>-3</sup>		
	T/K		
	278	283	293
0	0	0	0
10	0.218	-	-
15	-	0.339	0.472
25	0.500	-	-
30	-	0.698	0.910
35	0.720	-	-
45	0.897	1.003	1.310
55	1.060	1.200	-
60	-	-	1.350
65	1.239	-	-
70	-	1.238	-
75	-	-	1.425
10 <sup>6</sup> x intial rate mol.dm. <sup>-3</sup> s. <sup>-1</sup>	3.33	3.80	5.10

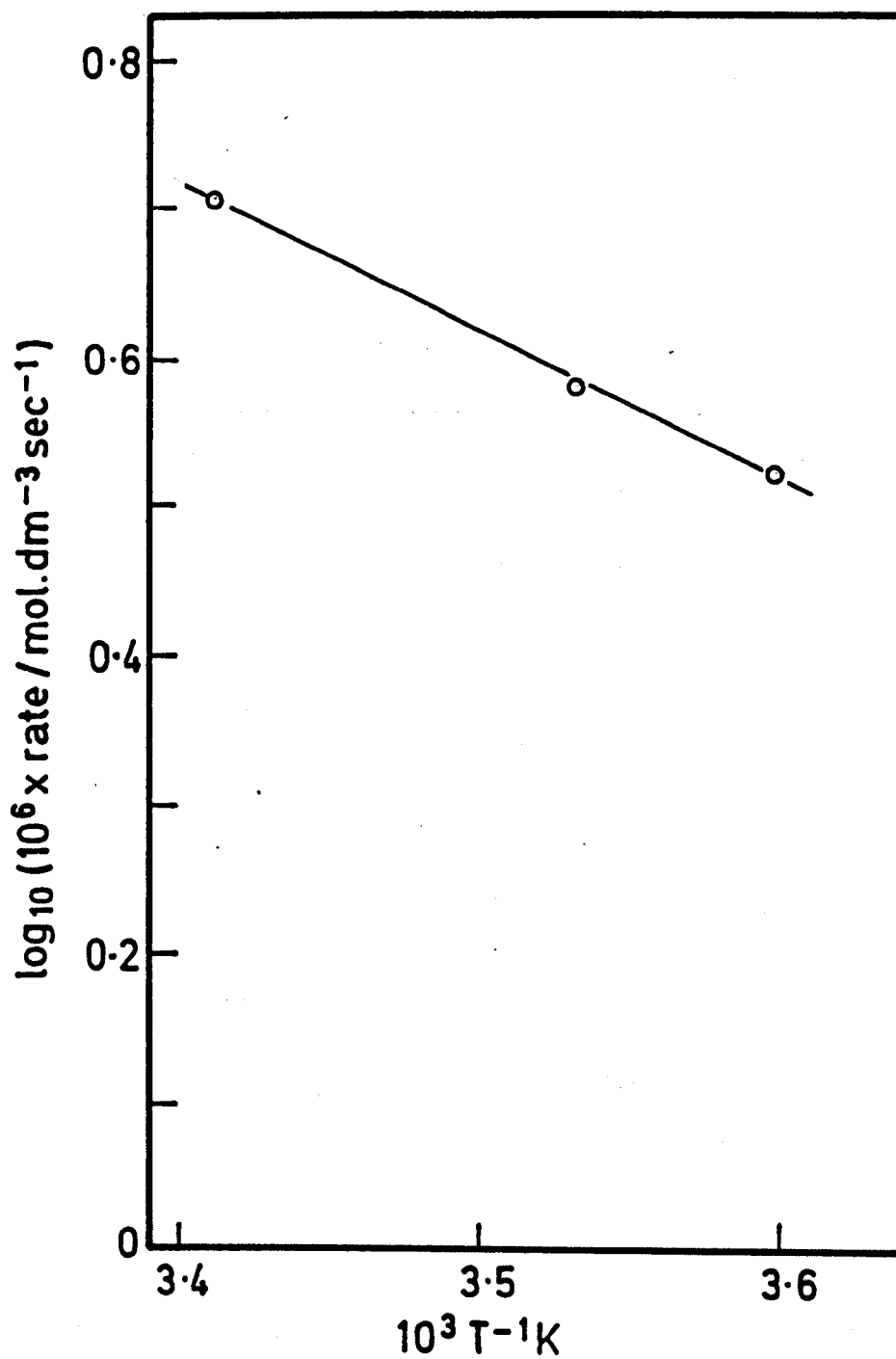
The results give an activation energy of  $19 \pm 1 \text{ kJ mol}^{-1}$  for methanal formation, which is not significantly different from that obtained for propanone formation ( $20 \pm 1 \text{ kJ mol}^{-1}$ ) on the same catalyst.

Figure 3.50



Photocatalytic dehydrogenation of methanol on Pt(0.5)/TiO<sub>2</sub>  
(method C) at different temperatures

Figure 3.51



Temperature dependence for the photocatalytic dehydrogenation of methanol on Pt(0.5)/TiO<sub>2</sub> (method C)

b) Ethanol

Two series of experiments were studied in the temperature range 278-293 K, using 366 nm radiation. Lamp 3 was used in the first series and the results are given in table 3.32 and plotted in figure 3.52 as  $10^2 \times$  ethanal concentration/mol.dm.<sup>-3</sup> against time/min. In the second series lamp 4 was used and the results are given in table 3.33 and plotted in figure 3.53 as  $10^2 \times$  ethanal concentration/mol.dm.<sup>-3</sup> against time/min.

TABLE 3.32

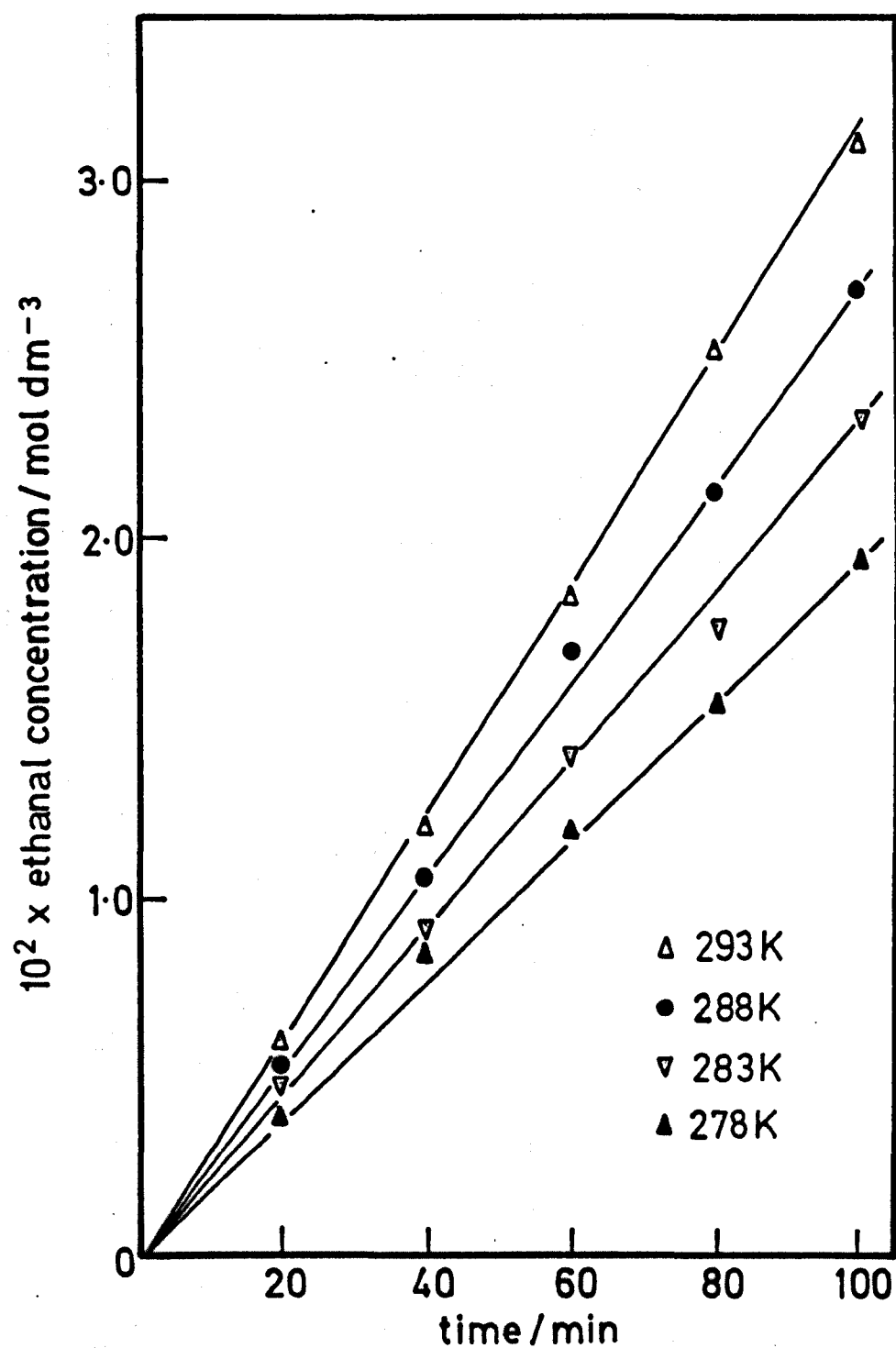
time/min.	ethanal concentration/mol.dm. <sup>-3</sup>			
	T/K			
	278	283	288	293
0	0	0	0	0
20	0.400	0.485	0.539	0.604
40	0.860	0.917	1.062	1.205
60	1.200	1.403	1.701	1.856
80	1.561	1.766	2.138	2.531
100	1.951	2.340	2.682	3.112
$10^6 \times$ rate/ mol.dm. <sup>-3</sup> s. <sup>-1</sup>	3.27	3.88	4.47	5.23

TABLE 3.33

time/min.	$10^2 \times$ ethanal concentration/mol.dm. <sup>-3</sup>				
	T/K				
	278	283	288	293	298
0	0	0	0	0	0

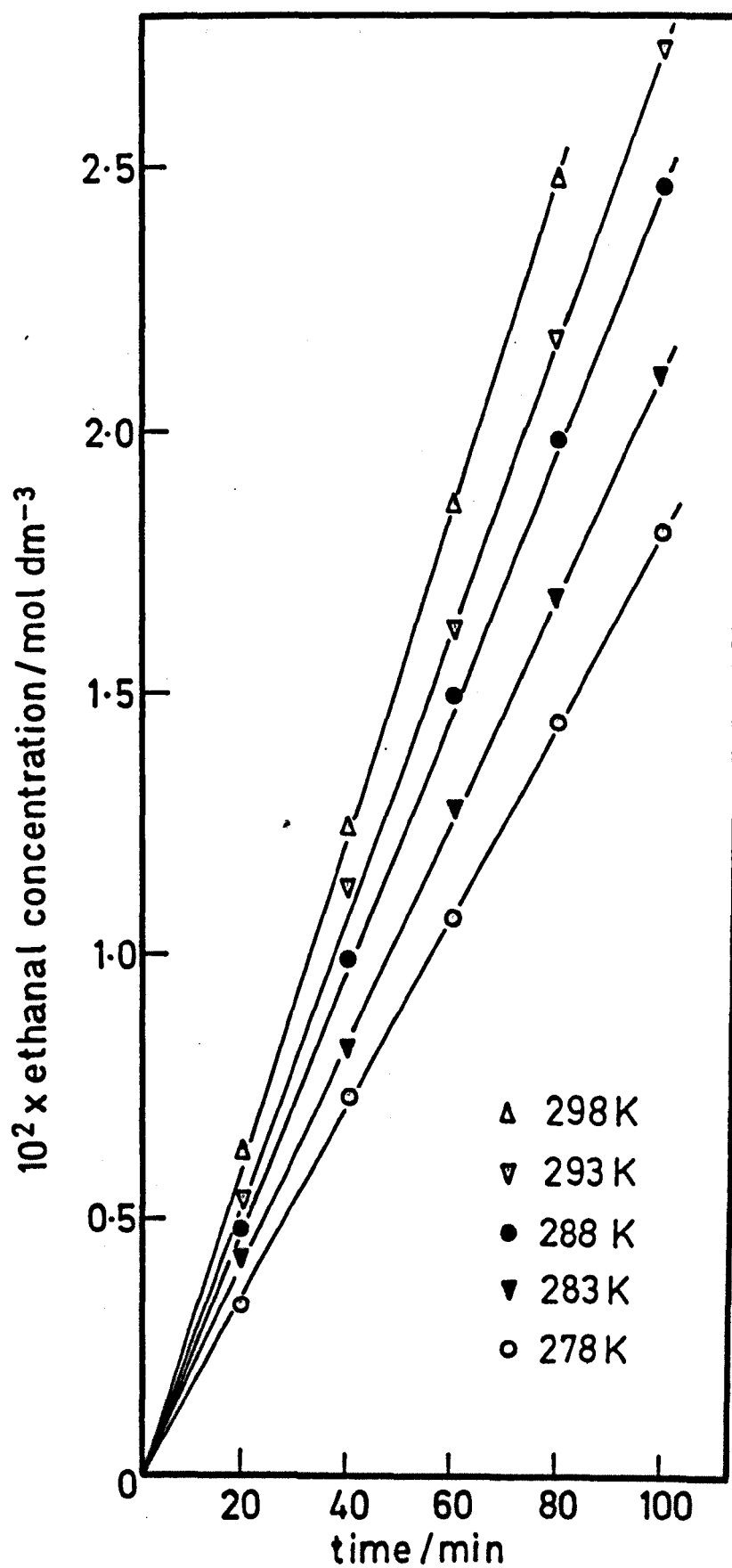
Contd. over

Figure 3.52



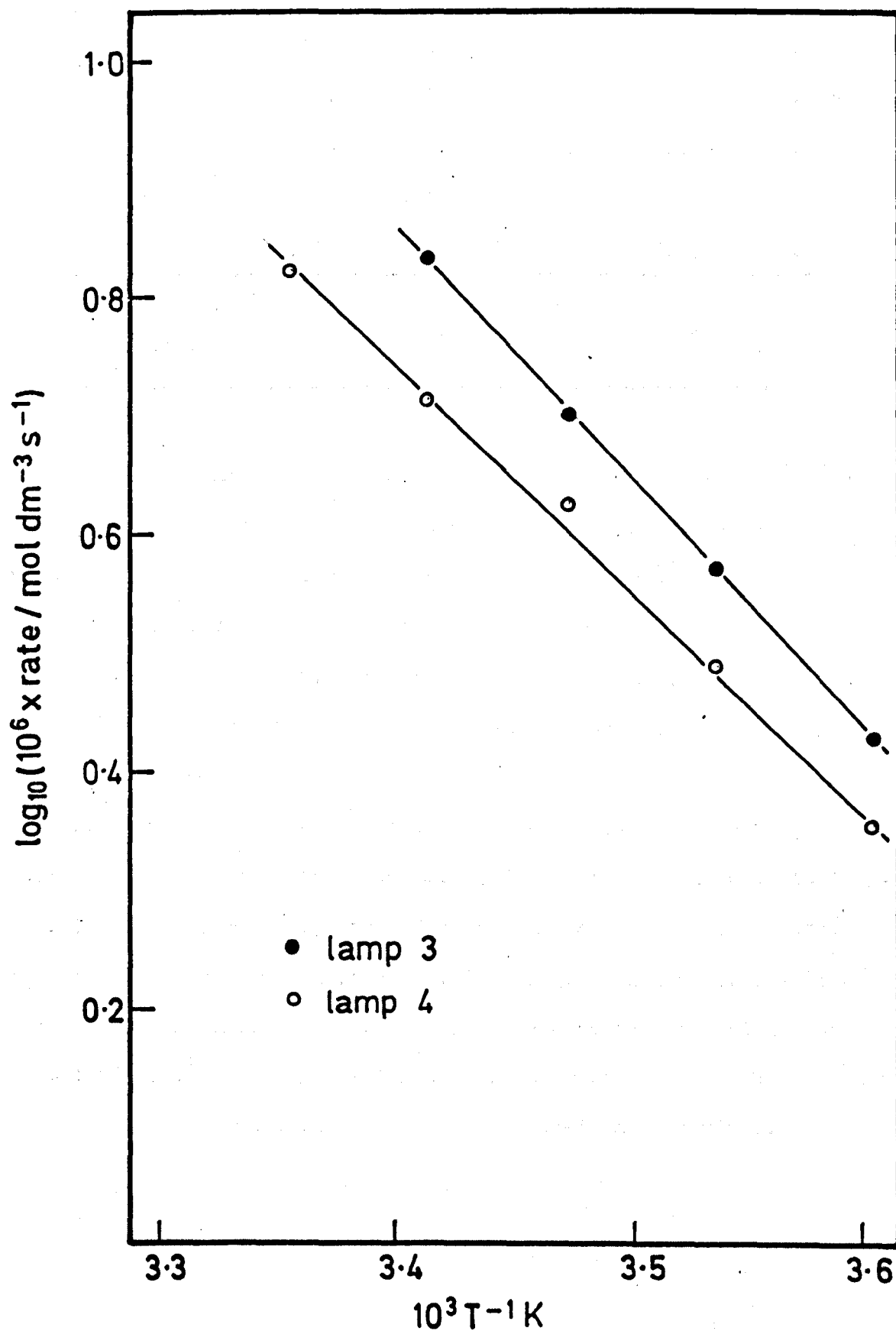
Photocatalytic dehydrogenation of ethanol on  
Pt(0.5)/TiO<sub>2</sub> (method C) at different temperatures

Figure 3.53



Photocatalytic dehydrogenation of ethanol on  
Pt(0.5)/TiO<sub>2</sub> (method C) at different  
temperatures

Figure 3.54



Temperature dependence for the photocatalytic dehydrogenation of ethanol on Pt(0.5)/TiO<sub>2</sub> (method C)

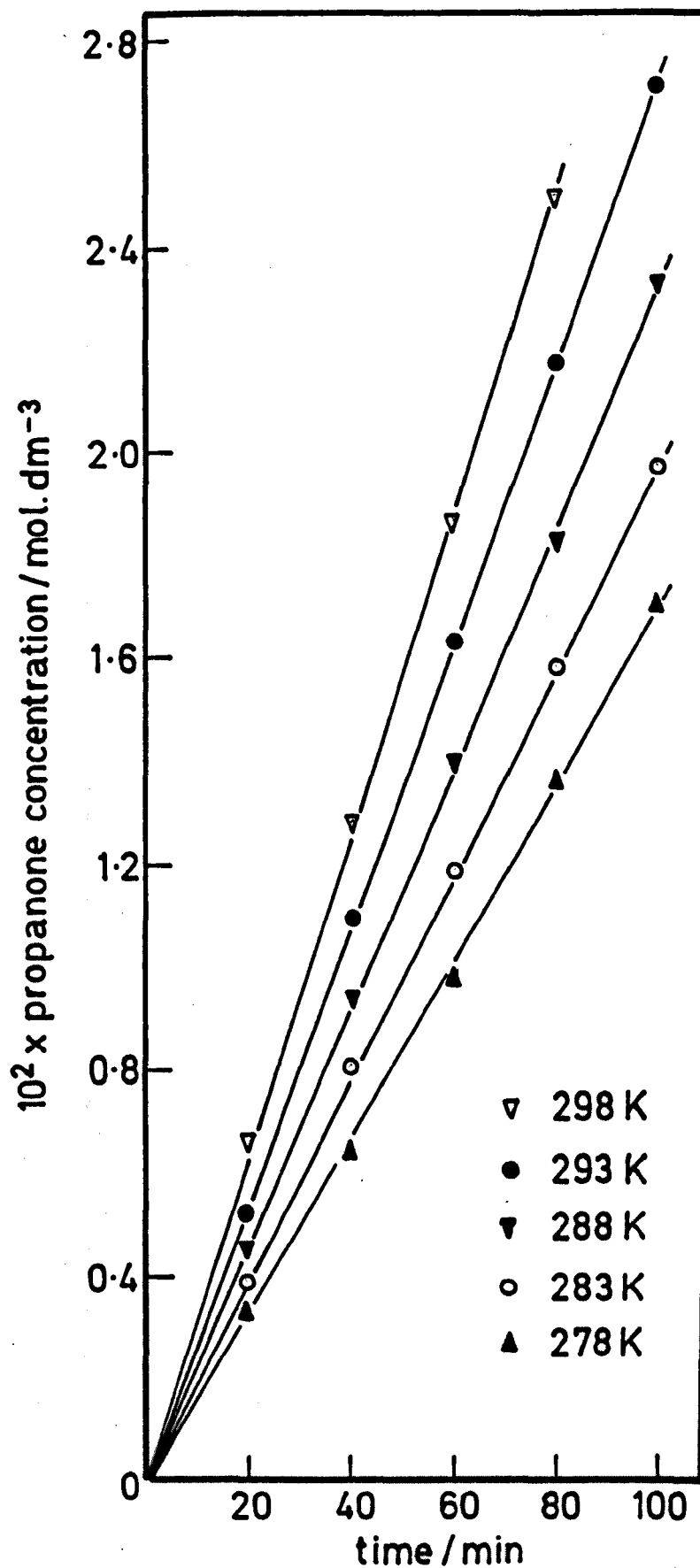
20	0.340	0.436	0.478	0.546	0.635
40	0.741	0.830	0.998	1.139	1.255
60	1.078	1.292	1.507	1.630	1.869
80	1.448	1.691	1.985	2.184	2.480
100	1.820	2.119	2.478	2.732	3.100
$10^6 \times \text{rate}/$ $\text{mol.dm}^{-3}\text{s}^{-1}$	2.99	3.53	4.12	4.55	5.17

The Arrhenius plots of  $\log(10^6 \times \text{rate of reaction/mol.dm}^{-3}\text{s}^{-1})$  against  $10^3 T^{-1} \text{K}$  for the two series are shown in figure 3.54. From these results an activation energy of  $20 \pm 1 \text{ kJ mol}^{-1}$  and  $19 \pm 1 \text{ kJ mol}^{-1}$  were obtained for ethanal formation in the first and second series respectively. These activation energies are in a good agreement with those obtained for methanal and propanone formation.

c) Propan-1-ol

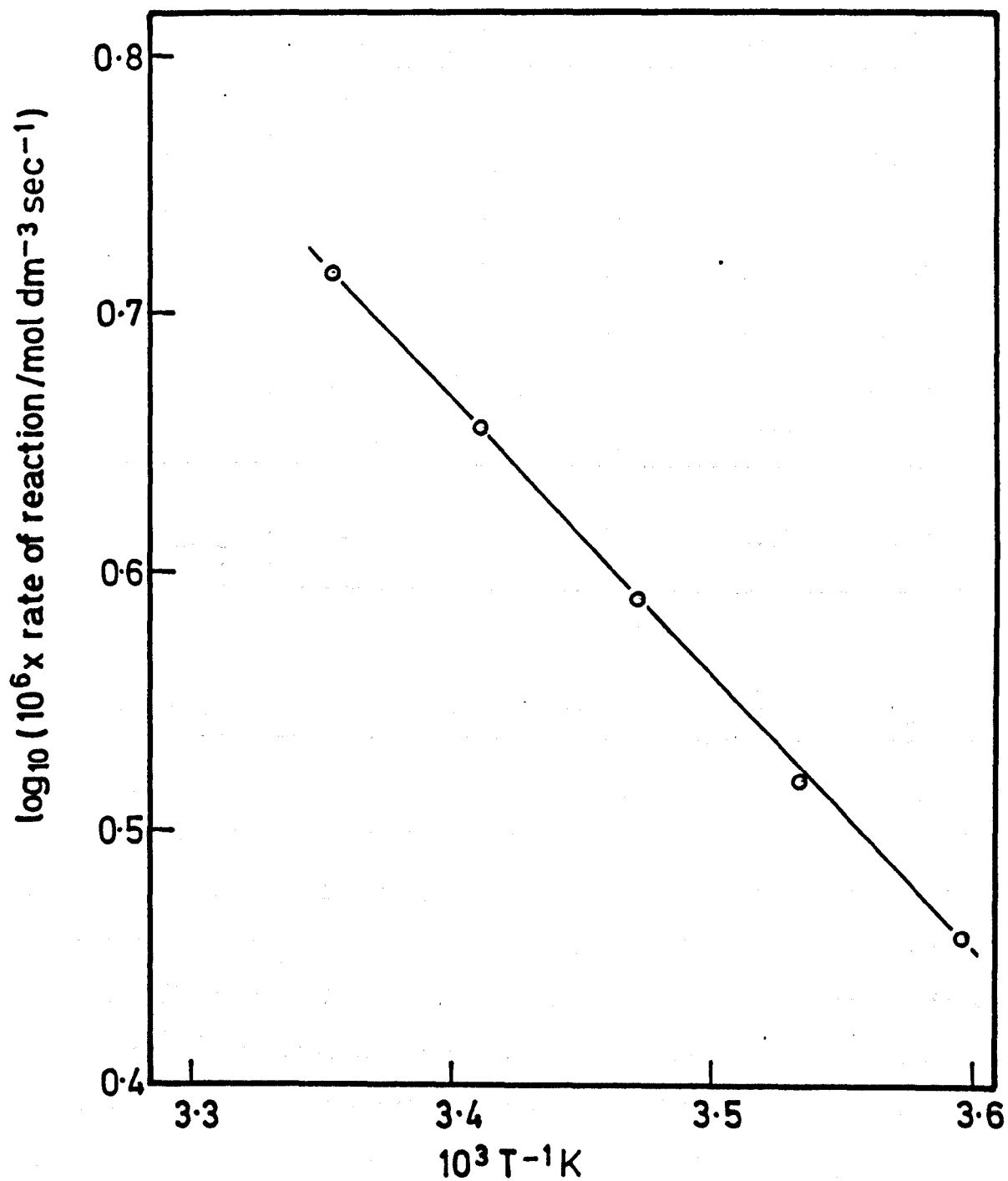
These experiments were carried out in the temperature range 278-298 K using 366 nm radiation from lamp 4. The results are shown in table 3.34 and plotted in figure 3.55 as  $10^2 \times \text{propanal concentration/mol.dm}^{-3}$  against time/min., and in figure 3.56 as  $\log(10^6 \times \text{rate of reaction/mol.dm}^{-3}\text{s}^{-1})$  against  $10^3 T^{-1} \text{K}$ . The results give an activation energy of  $20 \pm 1 \text{ kJ mol}^{-1}$  for propanal formation, in agreement with the activation energies obtained with the other alcohols used in this study.

Figure 3.55



Photocatalytic dehydrogenation of propan-2-ol  
on Pt(0.5)/TiO<sub>2</sub> (method C) at different  
temperatures

Figure 3.56



Temperature dependence for the photocatalytic dehydrogenation of propan-1-ol on Pt(0.5)/TiO<sub>2</sub> (method C)

TABLE 3.34

time/min.	propanal concentration/mol.dm. <sup>-3</sup>				
	T/K				
	278	283	288	293	298
0	0	0	0	0	0
20	0.340	0.399	0.461	0.529	-
21	-	-	-	-	0.666
40	0.658	0.816	0.949	1.104	1.291
60	0.994	1.200	1.406	1.640	1.872
80	1.380	1.591	1.842	2.183	2.500
100	1.720	1.979	2.341	2.718	3.136
10 <sup>6</sup> x rate/ mol.dm. <sup>-3</sup> s. <sup>-1</sup>	2.88	3.30	3.90	4.52	5.20

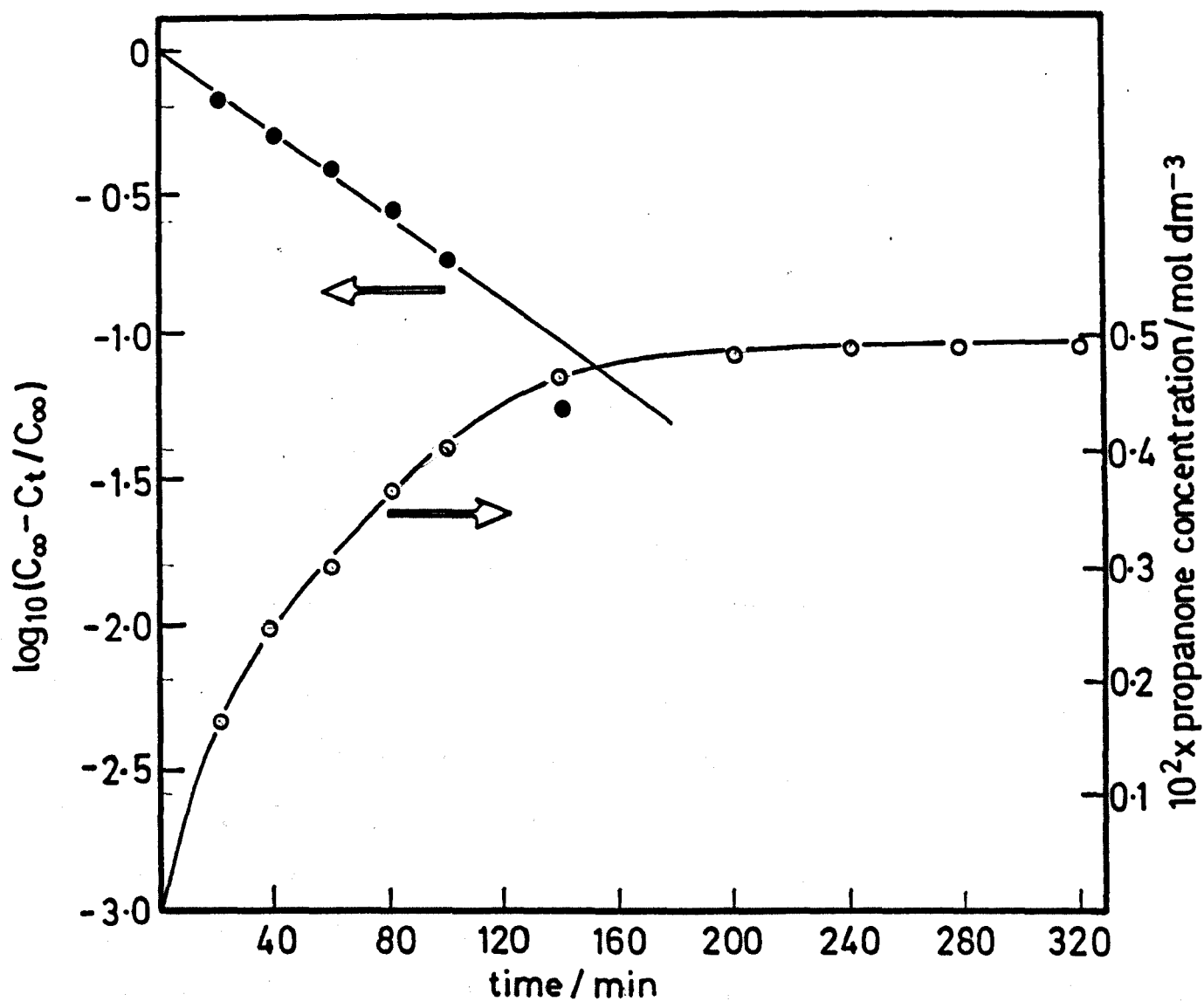
3.4.8 Dehydrogenation of propan-2-ol on Pt(0.5)/TiO<sub>2</sub> hydrogen reduced at 753 K

These experiments were conducted in order to determine whether the reduction of the catalyst prepared by method C affects its activity and activation energy. The catalyst was reduced with a hydrogen flow of 0.50 cm<sup>3</sup> s.<sup>-1</sup> at 753 K for 16 h., and then cooled under a nitrogen flow of 0.65 cm<sup>3</sup> s.<sup>-1</sup> to room temperature. The dark reaction and the photocatalytic reaction were studied using 150 mg of the catalyst and a nitrogen pressure of one atmosphere.

a) The dark reaction

These experiments were carried out at 293 K over the range time 0-320 min. The results are given in table 3.35 and plotted in figure 3.57 as  $\log (C_{\infty} - C_t)/C_{\infty}$  or 10<sup>2</sup> x propanone concentration/mol.dm.<sup>-3</sup> against time/min.

Figure 3.57



The dark reaction and first-order plots of propan-2-ol on hydrogen reduced (753K) Pt(0.5)/TiO<sub>2</sub> (method C) at 293K

TABLE 3.35

time/min.	propanone concentration/ mol.dm. <sup>-3</sup>
0	0
20	0.162
40	0.243
60	0.298
80	0.365
100	0.401
140	0.464
200	0.485
240	0.491
280	0.488
320	0.490

The results show that the dark reaction obeyed first-order kinetics with respect to departure from an equilibrium propanone concentration of  $0.49 \times 10^{-2}$  mol.dm.<sup>-3</sup>, which is not significantly different from that obtained on Pt(0.5)/TiO<sub>2</sub> prepared by method A ( $0.45 \times 10^{-2}$  mol.dm.<sup>-3</sup>). It is concluded that the existence of the dark reaction was due to hydrogen reduction at an elevated temperature which renders the anatase support non-stoichiometric.

b) The photocatalytic reaction

These reactions were carried out over the temperature range 278-298 K, having allowed sufficient time for the dark reaction to reach completion before irradiation commenced. Radiation of 366 nm from lamp 3 was used in these reactions. The results are given in table 3.36 and plotted in figure 3.58 as  $10^2 \times$  propanone concentration/mol.dm.<sup>-3</sup> against time/min.,

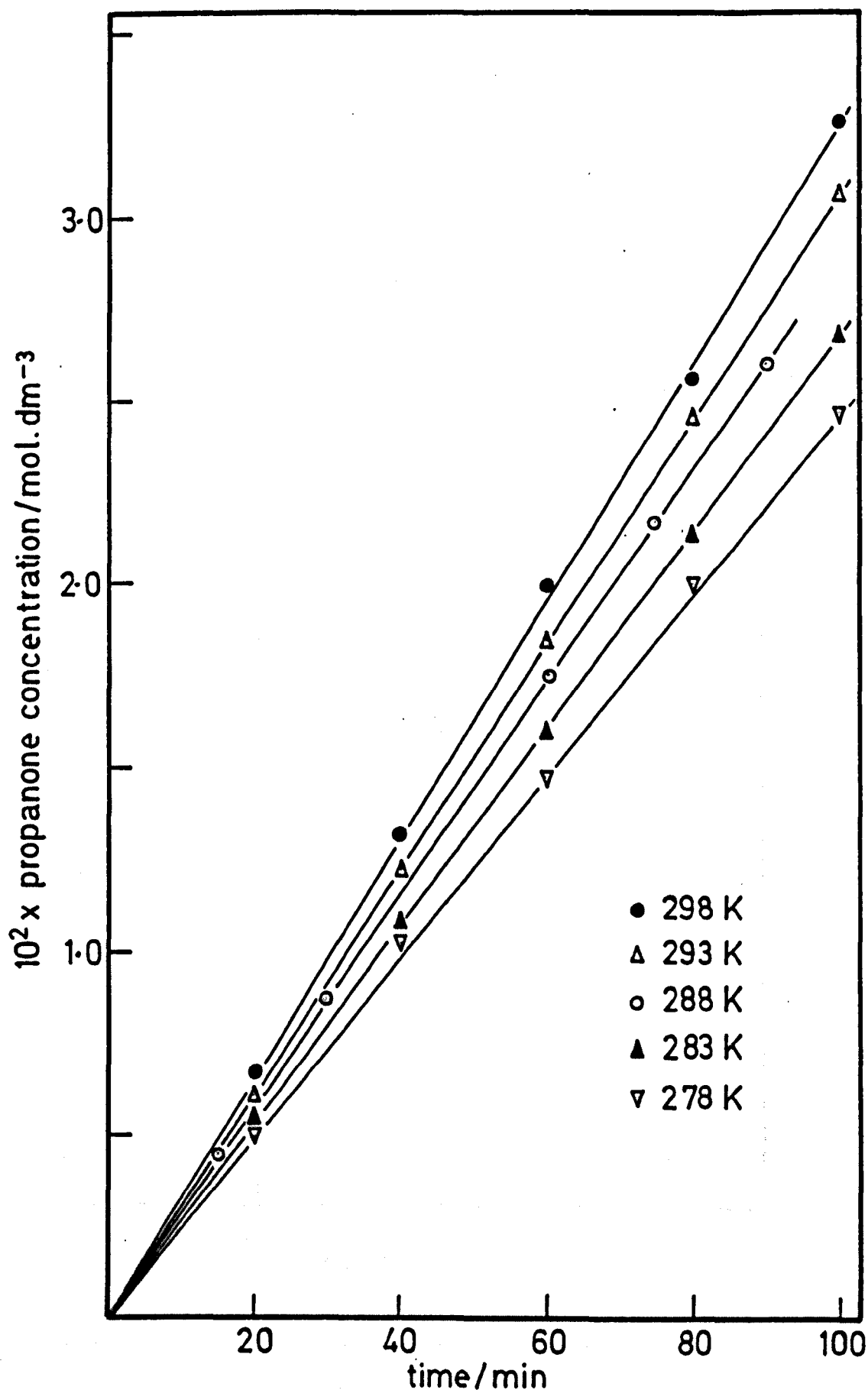
and in figure 3.59 as  $\log(10^6 \times \text{rate of reaction/mol.dm}^{-3}\text{s.}^{-1})$  against  $10^3 T^{-1} \text{K}$ .

TABLE 3.36

time/min.	$10^2 \times \text{propanone concentration/mol.dm}^{-3}$				
	T/K				
	278	283	288	293	298
0	0	0	0	0	0
15	-	-	0.450	-	-
20	0.503	0.558	-	0.613	0.682
30	-	-	0.870	-	-
40	1.017	1.078	-	1.224	1.321
60	1.467	1.604	1.759	1.841	2.000
75	-	-	2.168	-	-
80	2.000	2.141	-	2.458	2.568
90	-	-	2.615	-	-
100	2.470	2.680	-	3.062	3.267
$10^6 \times \text{rate/}$ $\text{mol.dm}^{-3}\text{s.}^{-1}$	4.11	4.46	4.82	5.10	5.45

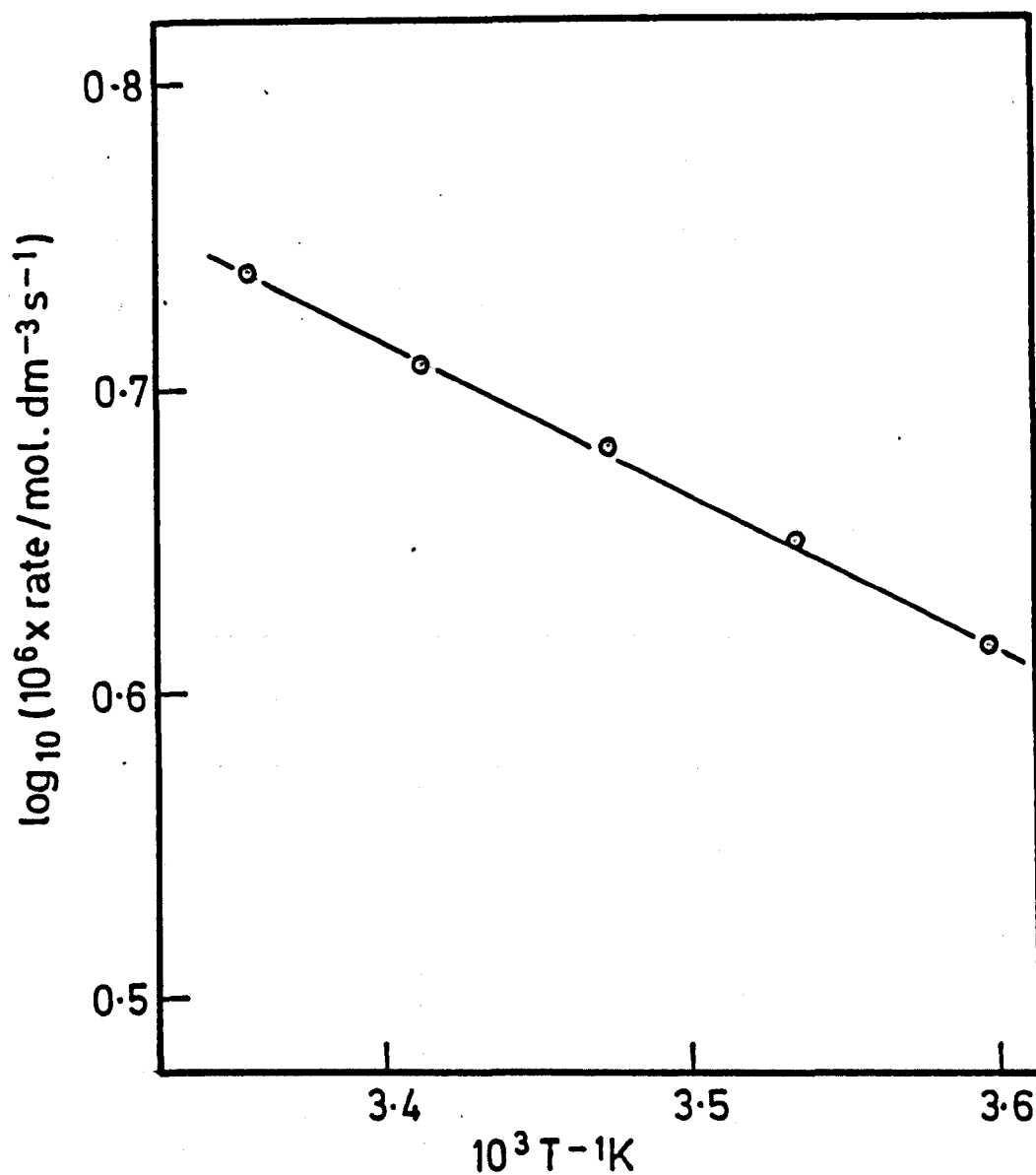
The results give an activation energy of  $9 \pm 1 \text{ kJ mol}^{-1}$  for propanone formation . The activation energy is not significantly different from that obtained for propanone production on  $\text{Pt}(0.5)/\text{TiO}_2$  prepared by method A. The drop in activation energy from  $20 \pm 1 \text{ kJ mol}^{-1}$  to  $9 \pm 1 \text{ kJ mol}^{-1}$  can be attributed to the non-stoichiometric nature of the anatase support.

Figure 3.58



Photocatalytic dehydrogenation of propan-2-ol on hydrogen reduced (753K) Pt(0.5)/TiO<sub>2</sub> (method C) at different temperatures

Figure 3.59



Temperature dependence for the photocatalytic dehydrogenation of propan-2-ol on hydrogen reduced (753 K) Pt(0.5)/TiO<sub>2</sub> (method C)

3.4.9 Photocatalytic dehydrogenation of propan-2-ol on Pt(0.5)/TiO<sub>2</sub>  
pretreated with propan-2-ol vapour at 373 K

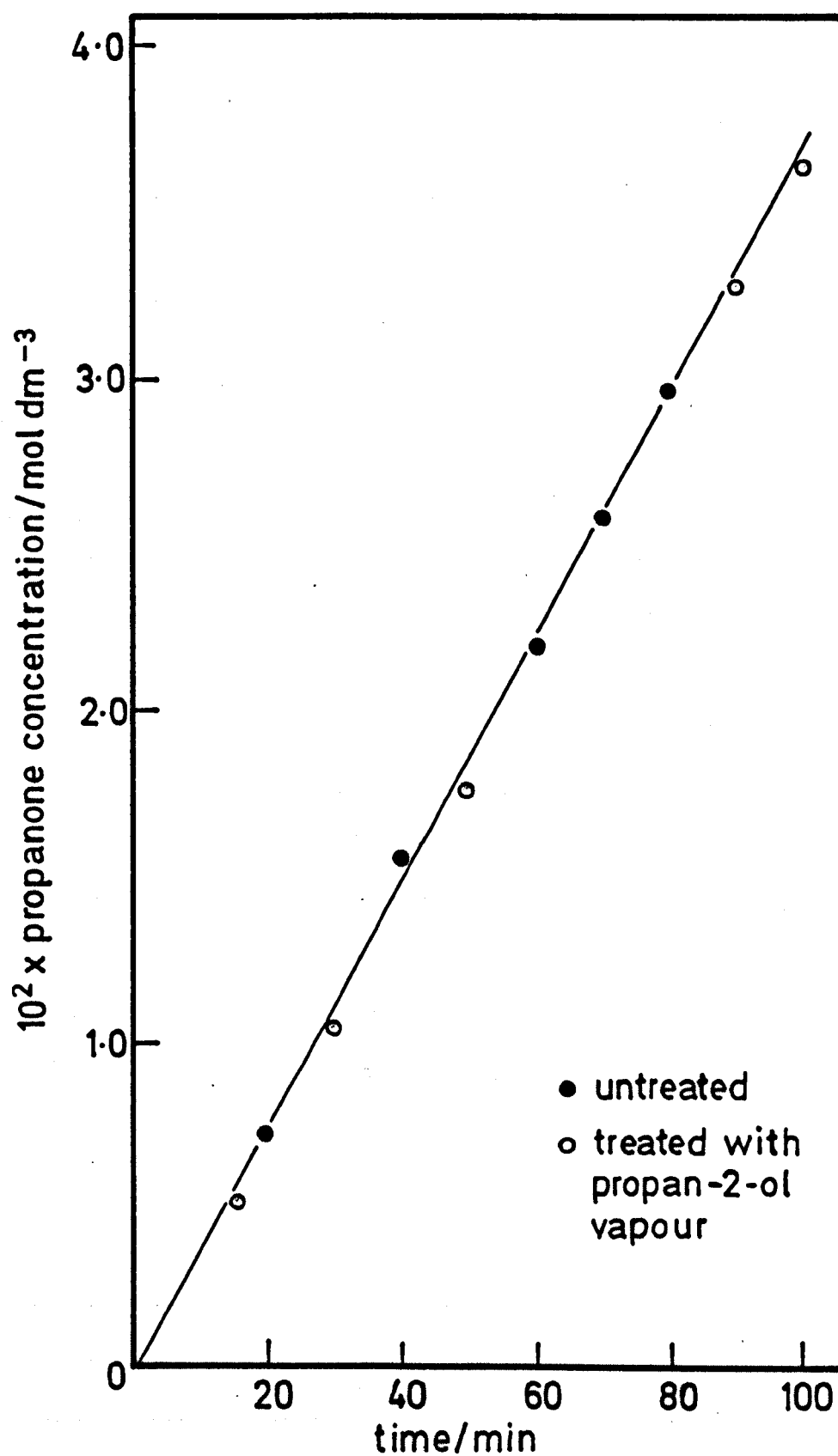
This experiment was made to determine whether the saturation of the catalyst surface with alkoxy groups affected the subsequent photocatalytic activity. Catalyst prepared by method C (150 mg) was introduced into a reaction vessel and contacted with a flow of propan-2-ol vapour for 5 h. at 373 K. After cooling to room temperature the standard charge of 20 cm<sup>3</sup> of propan-2-ol was added and the photocatalytic reaction followed at 293 K using 366 nm radiation from lamp 2. The results are compared with those obtained with untreated catalyst using the same lamp. The results, given in table 3.37 and plotted in figure 3.60 as 10<sup>2</sup> x propanone concentration/mol.dm.<sup>-3</sup> against time/min., show that pretreatment has negligible effect on photocatalytic activity.

TABLE 3.37

time/min.	10 <sup>2</sup> x propanone concentration/mol.dm. <sup>-3</sup>	
	The catalyst treated	non-treated
0	0	0
15	0.522	-
20	-	0.730
30	1.063	-
40	-	1.480
50	1.761	-
60	-	2.198

Contd. over

Figure 3.60



Photocatalytic dehydrogenation of propan-2-ol at 293 K  
on Pt(0.5)/TiO<sub>2</sub> (method C)

70	-	2.581
80	-	2.967
90	3.279	-
100	3.642	-
$10^6 \times \text{rate}/$ $\text{mol.dm}^{-3}\text{s}^{-1}$	6.07	6.17

#### 3.4.10 Photocatalytic dehydrogenation of propan-2-ol in a high purity helium atmosphere

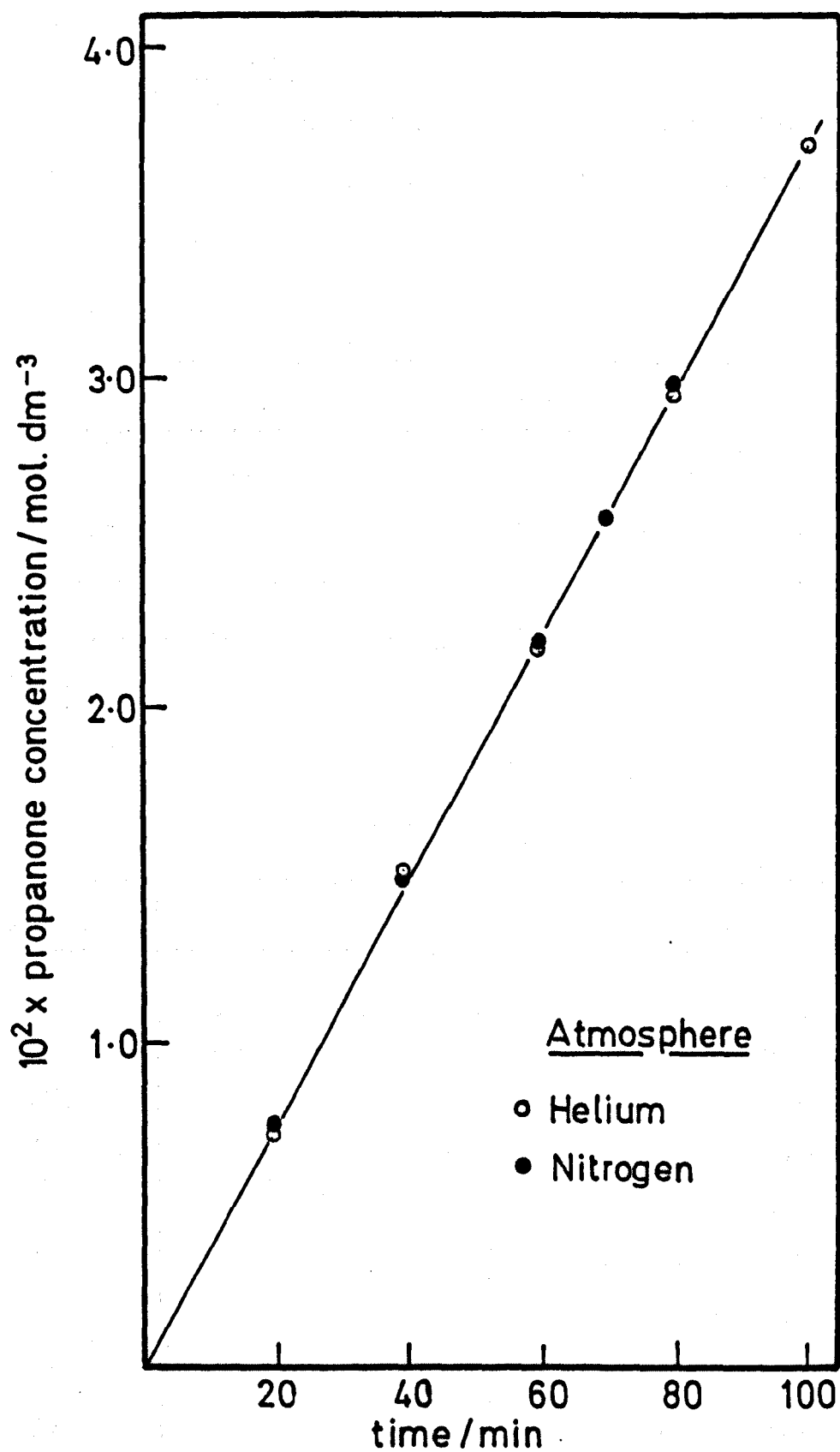
This experiment was made to determine whether different carrier gases affected the activity of the catalyst and so effectively checks the purity of the nitrogen gas. The experiment was carried out using 366 nm radiation from lamp 2, 150 mg of  $\text{Pt}(0.5)/\text{TiO}_2$  and a flow of helium at atmospheric pressure ( $0.34 \text{ cm}^3 \text{ s}^{-1}$ ). The results are given in table 3.38 together with the results obtained from the photo-dehydrogenation of propan-2-ol on  $\text{Pt}(0.5)/\text{TiO}_2$  under a nitrogen atmosphere using the same lamp. The results, plotted in figure 3.61 as  $10^2 \times \text{propanone concentration}/\text{mol.dm}^{-3}$  against time/min., clearly show the same activity for propanone formation. It follows that the nitrogen used throughout the present research is effectively pure.

TABLE 3.38

time/min.	$10^2 \times \text{propanone concentration}/$ $\text{mol.dm}^{-3}$	
	The atmosphere helium gas	nitrogen gas
0	0	0

20	0.728	0.730
40	1.502	1.480
60	2.192	2.198
70	-	2.581
80	2.954	2.967
100	3.698	-
$10^6 \times \text{rate}/$ $\text{mol.dm}^{-3}\text{s}^{-1}$	6.16	6.17

Figure 3.61



Photocatalytic dehydrogenation of propan-2-ol on Pt(0.5)/TiO<sub>2</sub> (method C) under different inert atmospheres.

### 3.5 Photocatalytic dehydrogenation of propan-2-ol on metallized anatase (other than Pt)

These experiments were made with 150 mg of catalyst (Pd(0.5)/TiO<sub>2</sub>, Rh(0.5)/TiO<sub>2</sub>, Au(0.5)/TiO<sub>2</sub>) prepared by method B or C using nitrogen as the inert atmosphere.

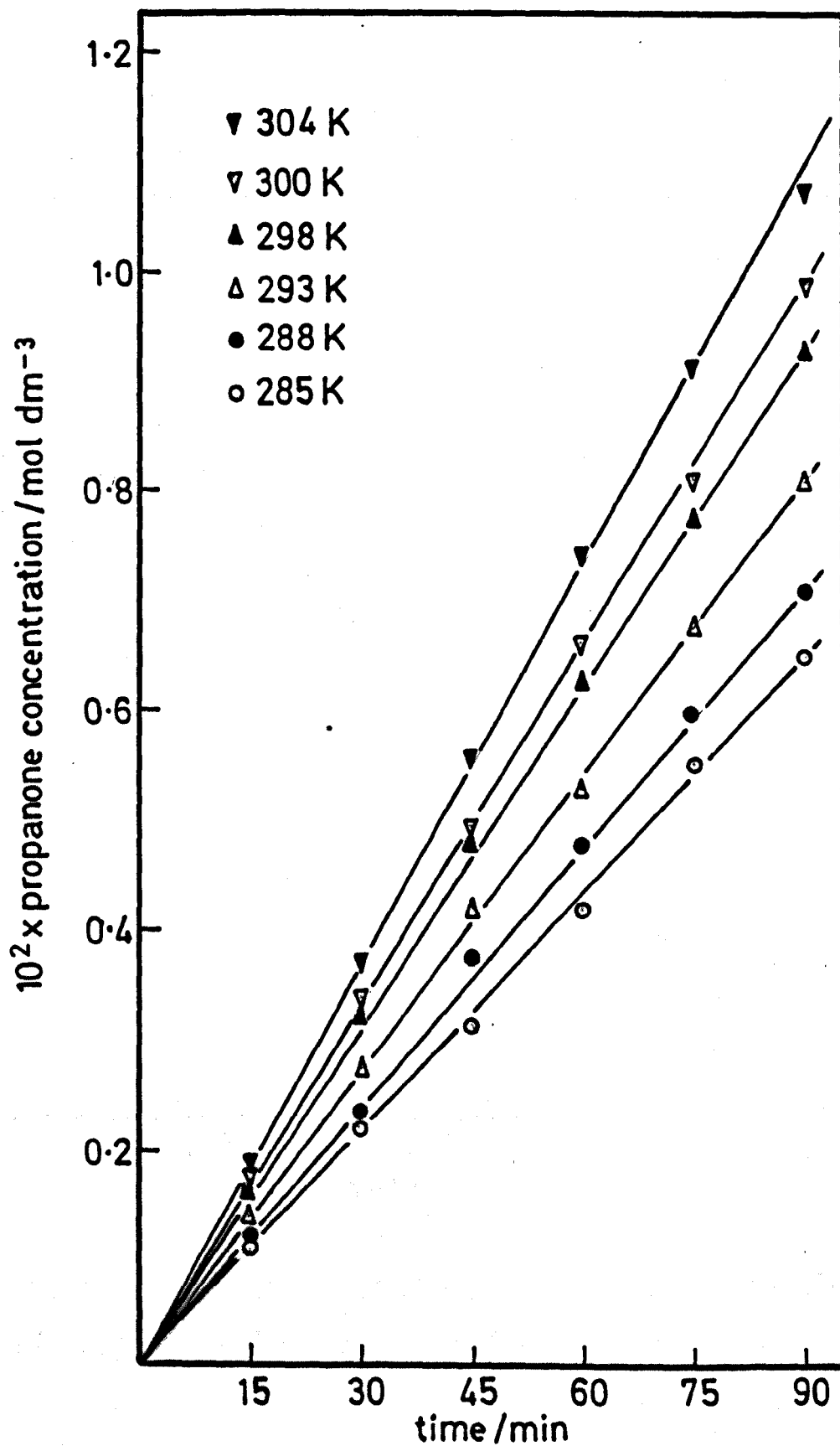
#### 3.5.1 Temperature dependence for the photocatalytic dehydrogenation of propan-2-ol on Pd(0.5)/TiO<sub>2</sub> prepared by method B

These experiments were carried out over the temperature range 285-304 K using 366 nm radiation from lamp 1. The results are given in table 3.39 and plotted in figure 3.62 as  $10^2 \times$  propanone concentration/mol.dm.<sup>-3</sup> against time/min. and in figure 3.63 as  $\log(10^6 \times \text{reaction rate/mol.dm.}^{-3}\text{s.}^{-1})$  against  $10^3 T^{-1} \text{K}$ .

TABLE 3.39

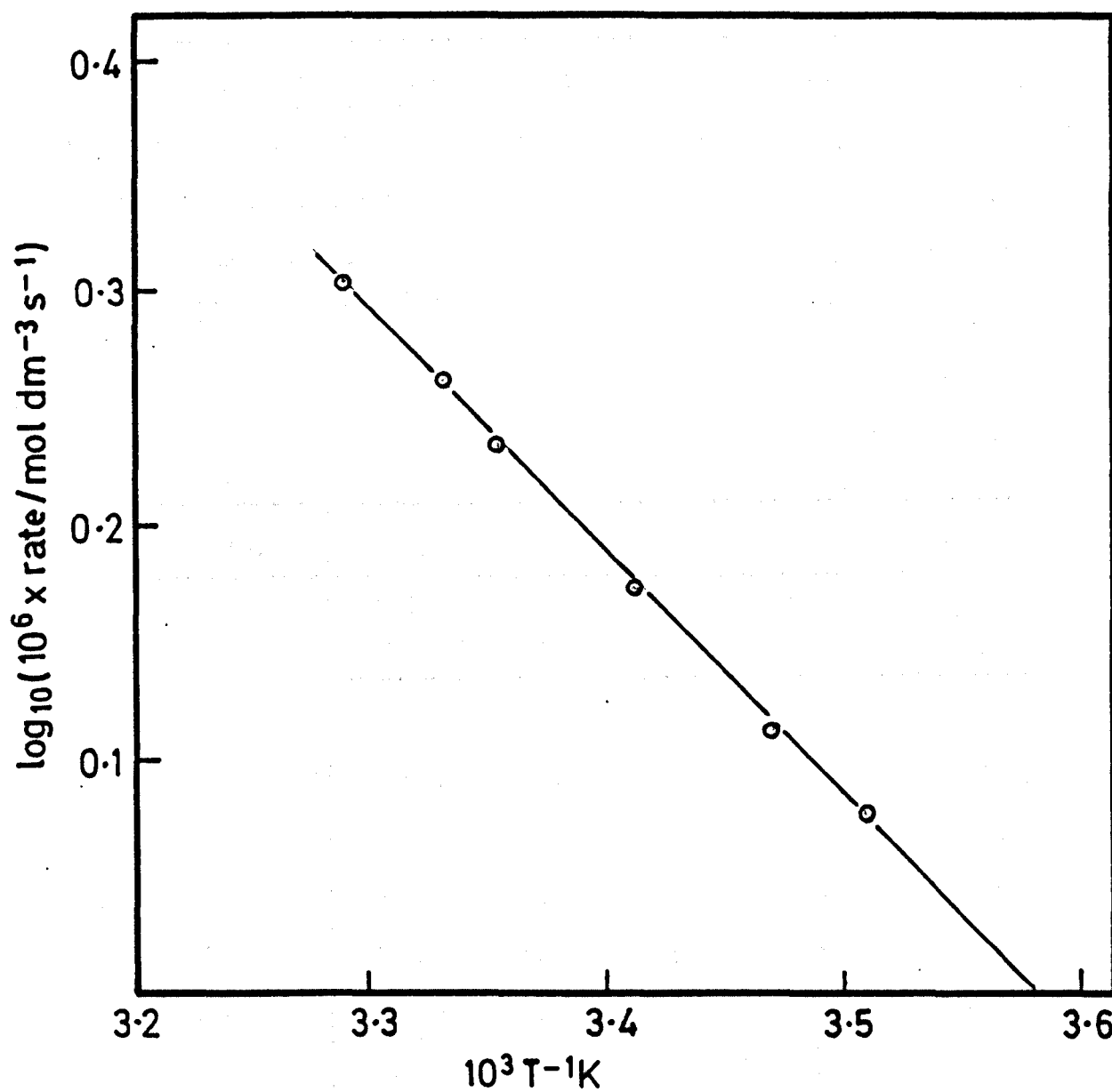
time/min.	$10^2 \times$ propanone concentration/mol.dm. <sup>-3</sup>					
	T/K					
	285	288	293	298	300	304
0	0	0	0	0	0	0
15	0.110	0.120	0.135	0.160	0.170	0.185
30	0.220	0.235	0.275	0.322	0.335	0.370
45	0.314	0.377	0.416	0.479	0.490	0.557
60	0.416	0.475	0.525	0.625	0.660	0.738
75	0.550	0.597	0.672	0.777	0.809	0.911
90	0.644	0.707	0.809	0.925	0.989	1.076
$10^6 \times \text{rate/mol.dm.}^{-3}\text{s.}^{-1}$	1.19	1.31	1.49	1.71	1.83	2.02

Figure 3-62



Photocatalytic dehydrogenation of propan-2-ol on  
Pd(0.5)/TiO<sub>2</sub> (method B) at different temperatures

Figure 3-63



Temperature dependence for the photocatalytic dehydrogenation of propan-2-ol on Pd(0.5)/TiO<sub>2</sub> (method B)

The results give an activation energy for propanone formation of  $20 \pm 1 \text{ kJ mol}^{-1}$ .

### 3.5.2 Temperature dependence for photocatalytic dehydrogenation of propan-2-ol on Pd(0.5)/TiO<sub>2</sub> prepared by method C

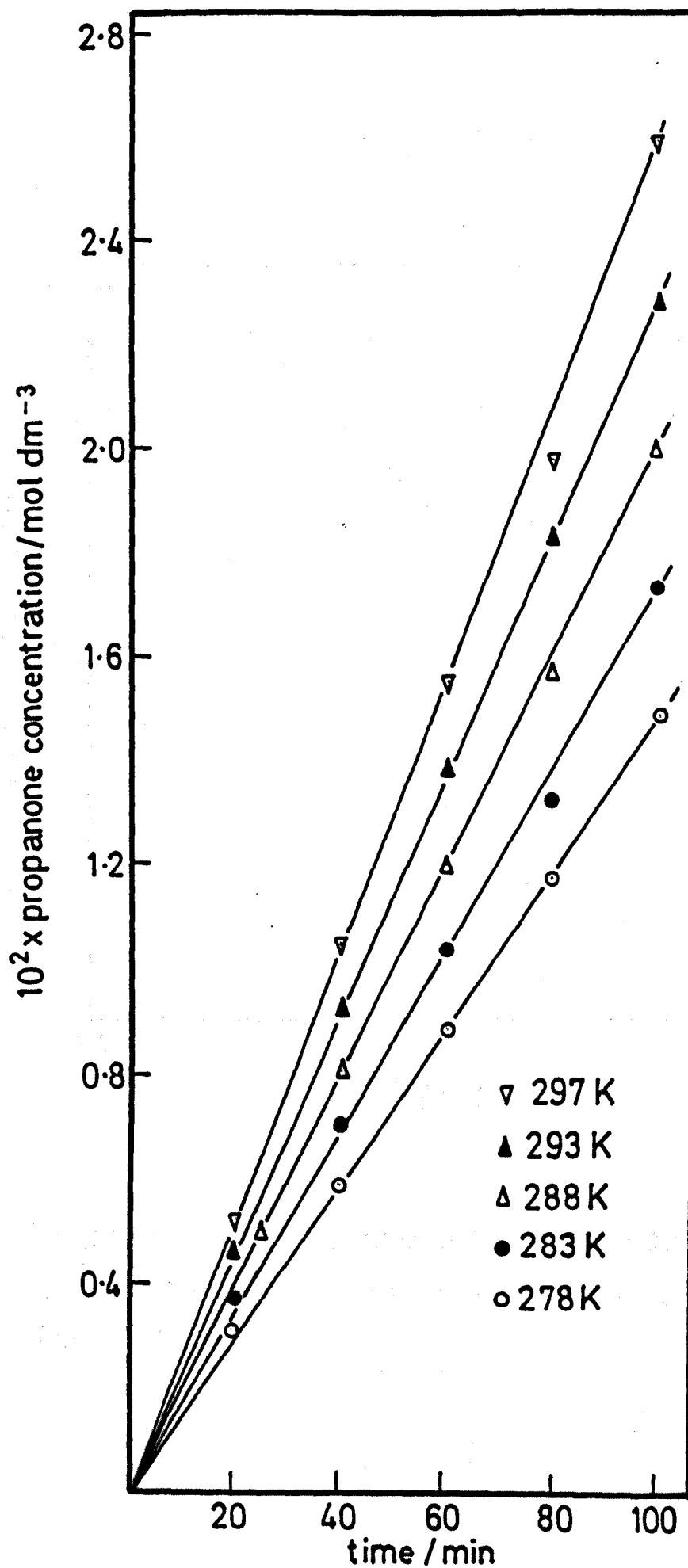
These experiments were studied over the temperature range 278-297 K using 366 nm radiation from lamp 2. The results are given in table 3.40 and plotted in figure 3.64 as  $10^2 \times \text{propanone concentration/mol.dm}^{-3}$  against time/min., and in figure 3.65 as  $\log(10^6 \times \text{rate of reaction/mol.dm}^{-3}\text{s}^{-1})$  against  $10^3 T^{-1} \text{ K}$ .

TABLE 3.40

time/min.	$10^2 \times \text{propanone concentration/mol.dm}^{-3}$				
	T/K				
	278	283	288	293	297
0	0	0	0	0	0
20	0.314	0.377	-	0.462	0.526
25	-	-	0.502	-	-
40	0.597	0.707	0.809	0.933	1.052
60	0.887	1.044	1.201	1.389	1.554
80	1.178	1.335	1.570	1.836	1.978
100	1.490	1.743	2.010	2.292	2.599
$10^6 \times \text{rate/mol.dm}^{-3}\text{s}^{-1}$	2.47	2.90	3.35	3.82	4.33

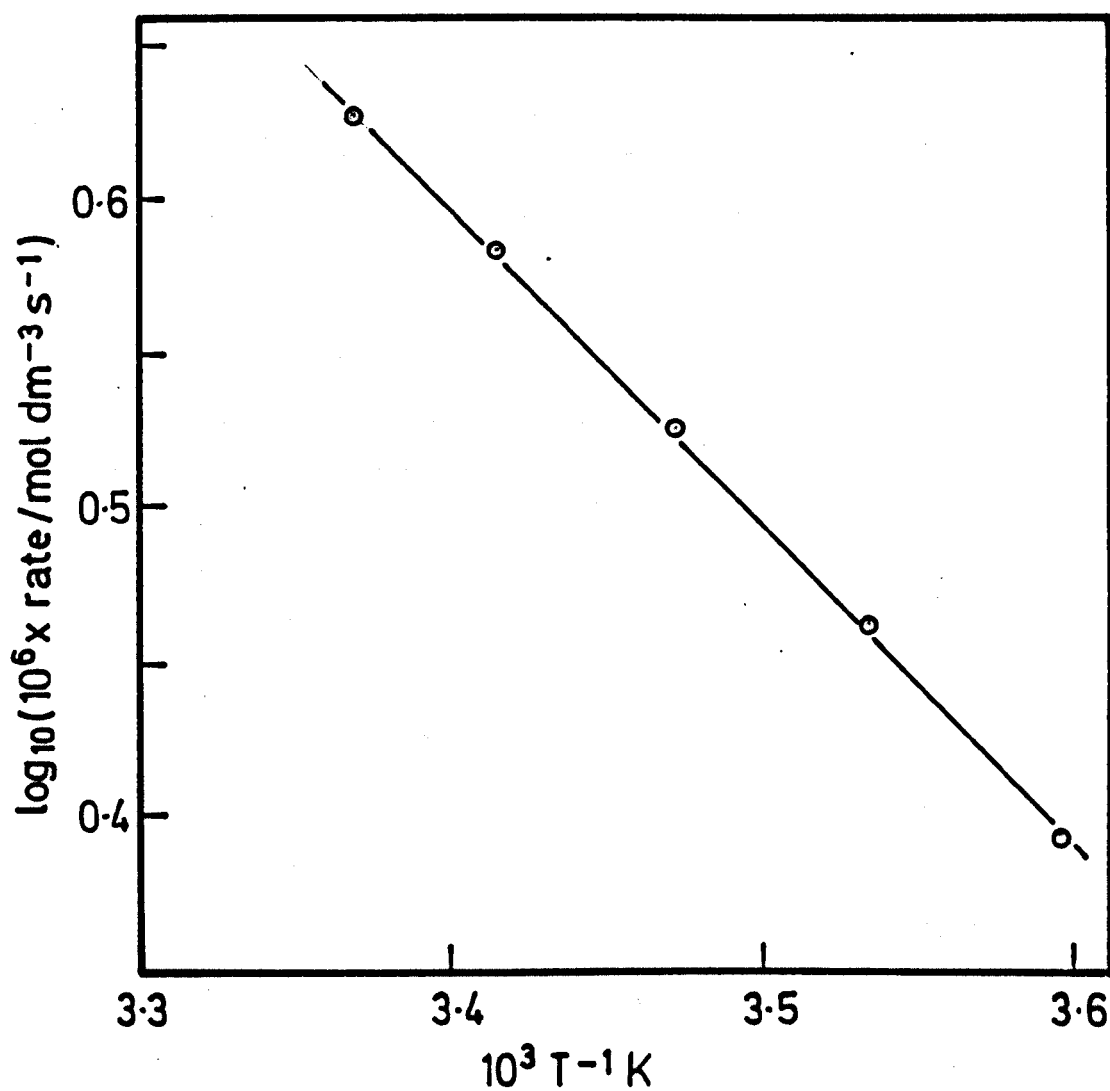
The results give an activation energy of  $20 \pm 1 \text{ kJ mol}^{-1}$  for propanone formation which is in excellent agreement with that obtained on Pd(0.5)/TiO<sub>2</sub> prepared by method B.

Figure 3.64



Photocatalytic dehydrogenation of propan-2-ol on  
 $\text{Pd}(0.5)/\text{TiO}_2$  (method C) at different temperatures

Figure 3.65



Temperature dependence for the photocatalytic  
dehydrogenation of propan-2-ol on Pd(0.5)/TiO<sub>2</sub>  
(method C)

### 3.5.3 Temperature dependence for the photocatalytic dehydrogenation of propan-2-ol on Rh(0.5)/TiO<sub>2</sub> prepared by method C

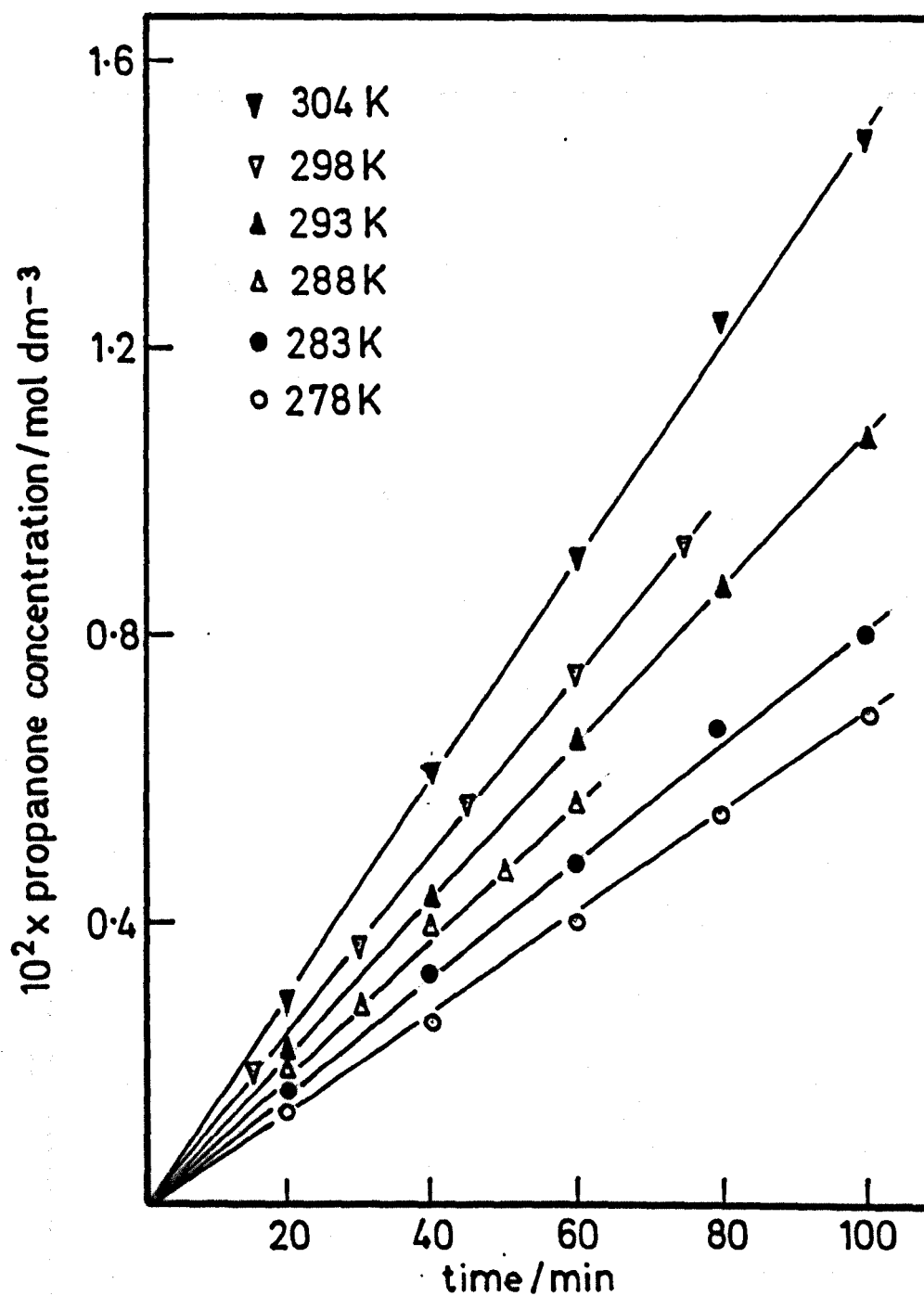
These experiments were carried out over the temperature range 278-304 K using 366 nm radiation from lamp 2. The results are given in table 3.41 and plotted in figure 3.66 as  $10^2 \times$  propanone concentration/mol.dm<sup>-3</sup> against time/min., and in figure 3.67 as  $\log(10^6 \times \text{rate of reaction/mol.dm}^{-3}\text{s}^{-1})$  against  $10^3 T^{-1}\text{K}$ .

TABLE 3.41

time/min.	$10^2 \times$ propanone concentration/mol.dm <sup>-3</sup>					
	T/K					
	278	283	288	293	298	304
0	0	0	0	0	0	0
15	-	-	-	-	0.188	-
20	0.141	0.169	0.196	0.220	-	0.291
30	-	-	0.283	-	0.369	-
40	0.259	0.330	0.393	0.432	-	0.612
45	-	-	-	-	0.565	-
50	-	-	0.471	-	-	-
60	0.400	0.479	0.565	0.660	0.754	0.911
75	-	-	-	-	0.926	-
80	0.550	0.667	-	0.864	-	1.240
100	0.691	0.801	-	1.083	-	1.500
$10^6 \times \text{rate}/$ mol.dm <sup>-3</sup> s <sup>-1</sup>	1.15	1.33	1.56	1.81	2.08	2.50

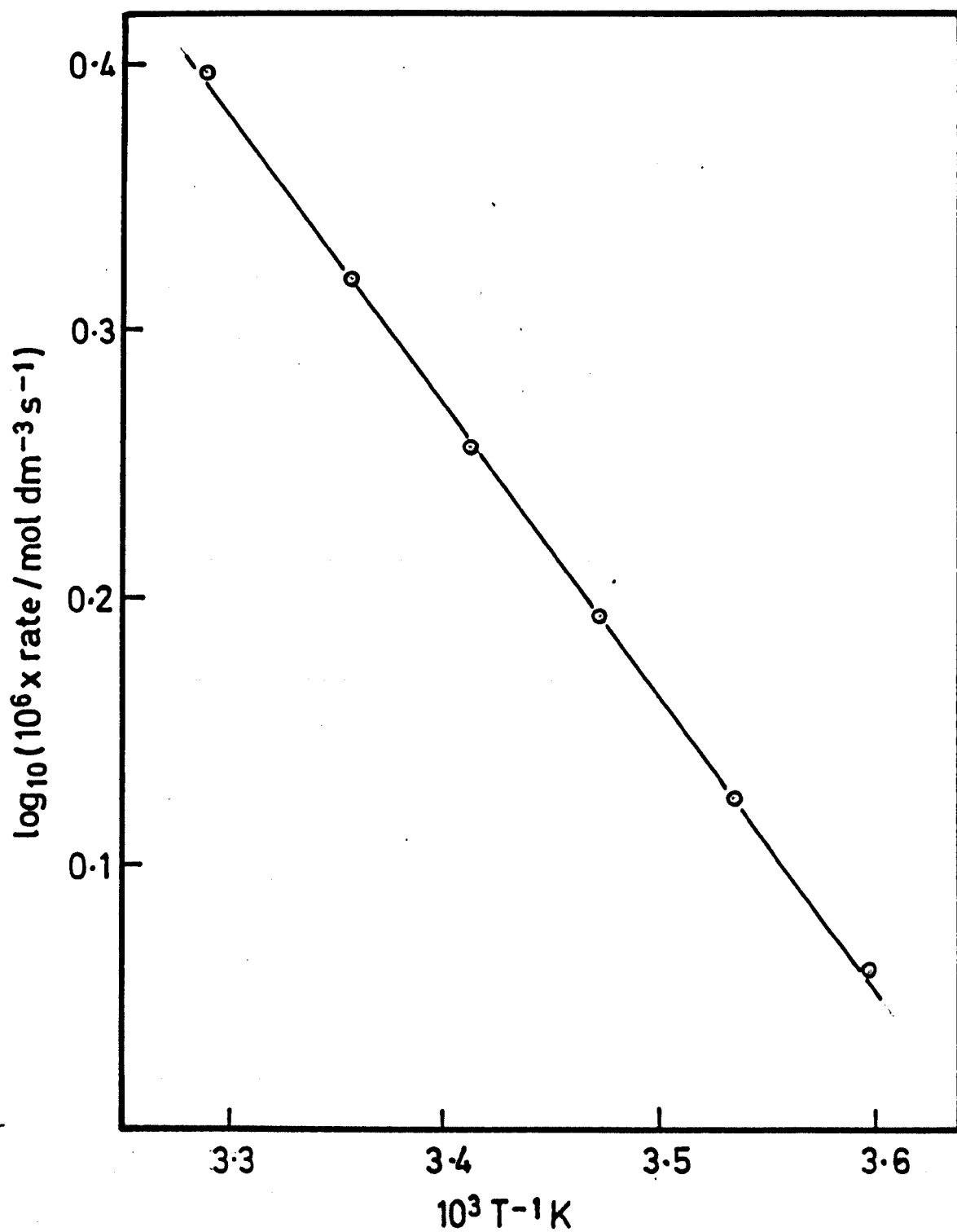
From these results an activation energy of  $20 \pm 1 \text{ kJ mol}^{-1}$  was

Figure 3.66



Photocatalytic dehydrogenation of propan-2-ol on  
Rh(0.5)/TiO<sub>2</sub> (method C) at different temperatures

Figure 3.67



Temperature dependence for the photocatalytic dehydrogenation of propan-2-ol on Rh(0.5)/TiO<sub>2</sub> (method C)

obtained for propanone formation, which is in good agreement with that obtained on Pd(0.5)/TiO<sub>2</sub> prepared by method B and C. It is concluded from these results that the activation energy for propanone formation is independent of the method of preparation and of the photodeposited metal on anatase.

#### 3.5.4 Photocatalytic dehydrogenation of propan-2-ol on Au(0.5)/TiO<sub>2</sub> prepared by method C

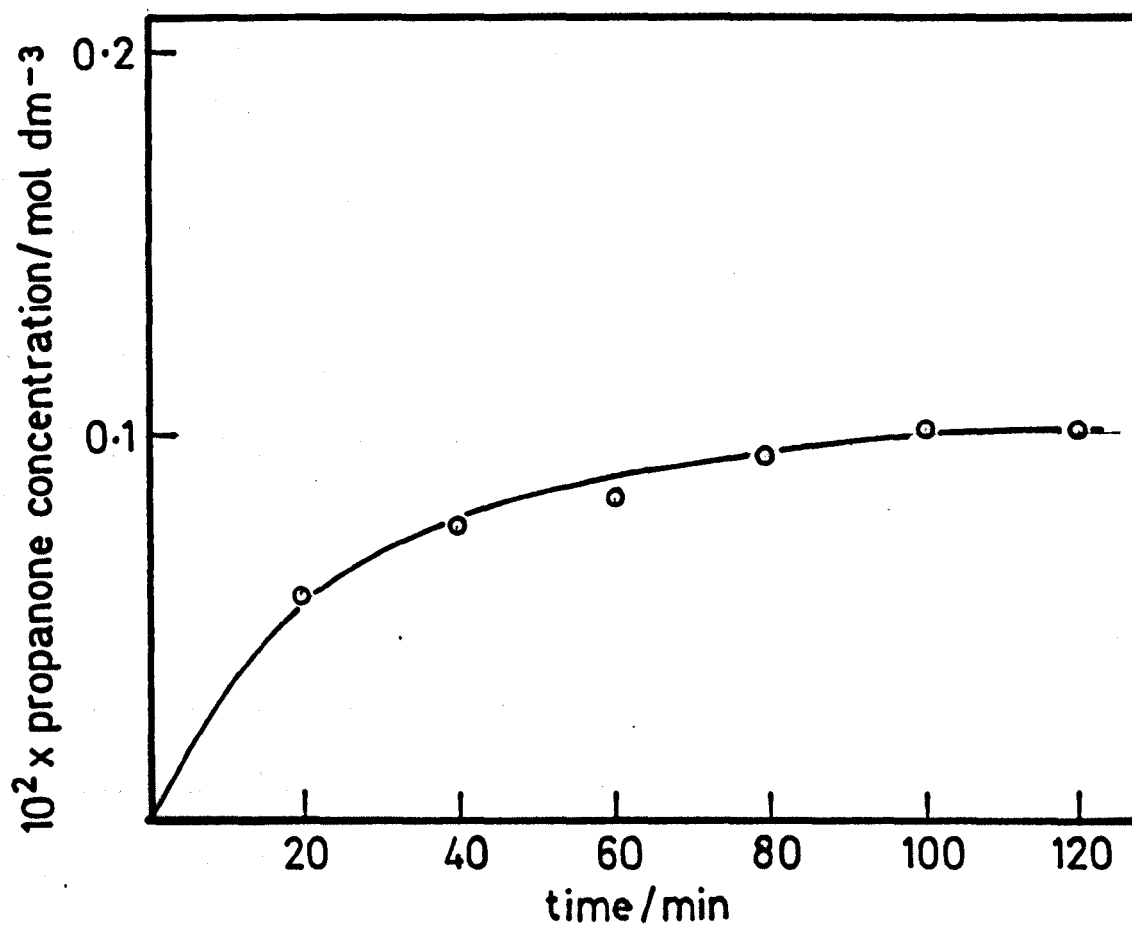
This experiment was carried out at 293 K using 366 nm radiation from lamp 2. The results are given in table 3.42 and plotted in figure 3.68 as  $10^2 \times$  propanone concentration/mol.dm.<sup>-3</sup> against time/min.

TABLE 3.42

time/min.	$10^2 \times$ propanone concentration/ mol.dm. <sup>-3</sup>
0	0
20	0.059
40	0.075
60	0.083
80	0.094
100	0.101
120	0.100

The propanone concentration failed to increase above the low value achieved after  $\sim$  80 min. irradiation.

Figure 3.68



Photocatalytic dehydrogenation of propan-2-ol on  
Au(0.5)/TiO<sub>2</sub> (method C) at 293K

3.5.5 Comparison between the activity of metallized anatase prepared by photodeposition (method B and C) for the photocatalytic dehydrogenation of propan-2-ol at 293 K

To facilitate comparisons between different metals supported on anatase it was necessary to determine reaction rates at 293 K using a single irradiation source. Activities at this temperature have been determined for Pt(0.5)/TiO<sub>2</sub> (method C), Pd(0.5)/TiO<sub>2</sub> (method C) and Rh(0.5)/TiO<sub>2</sub> (method C) using lamp 2. To complete the necessary data, reaction rates were determined for Pt(0.5)/TiO<sub>2</sub> (method B) and Pd(0.5)/TiO<sub>2</sub> (method B) using lamp 2. The results are given in table 3.43 and plotted in figure 3.69 as  $10^2 \times \text{reaction rate/mol.dm}^{-3}$  against time/min. The data obtained for the catalysts prepared by method C is also represented in table 3.43 and figure 3.69.

TABLE 3.43

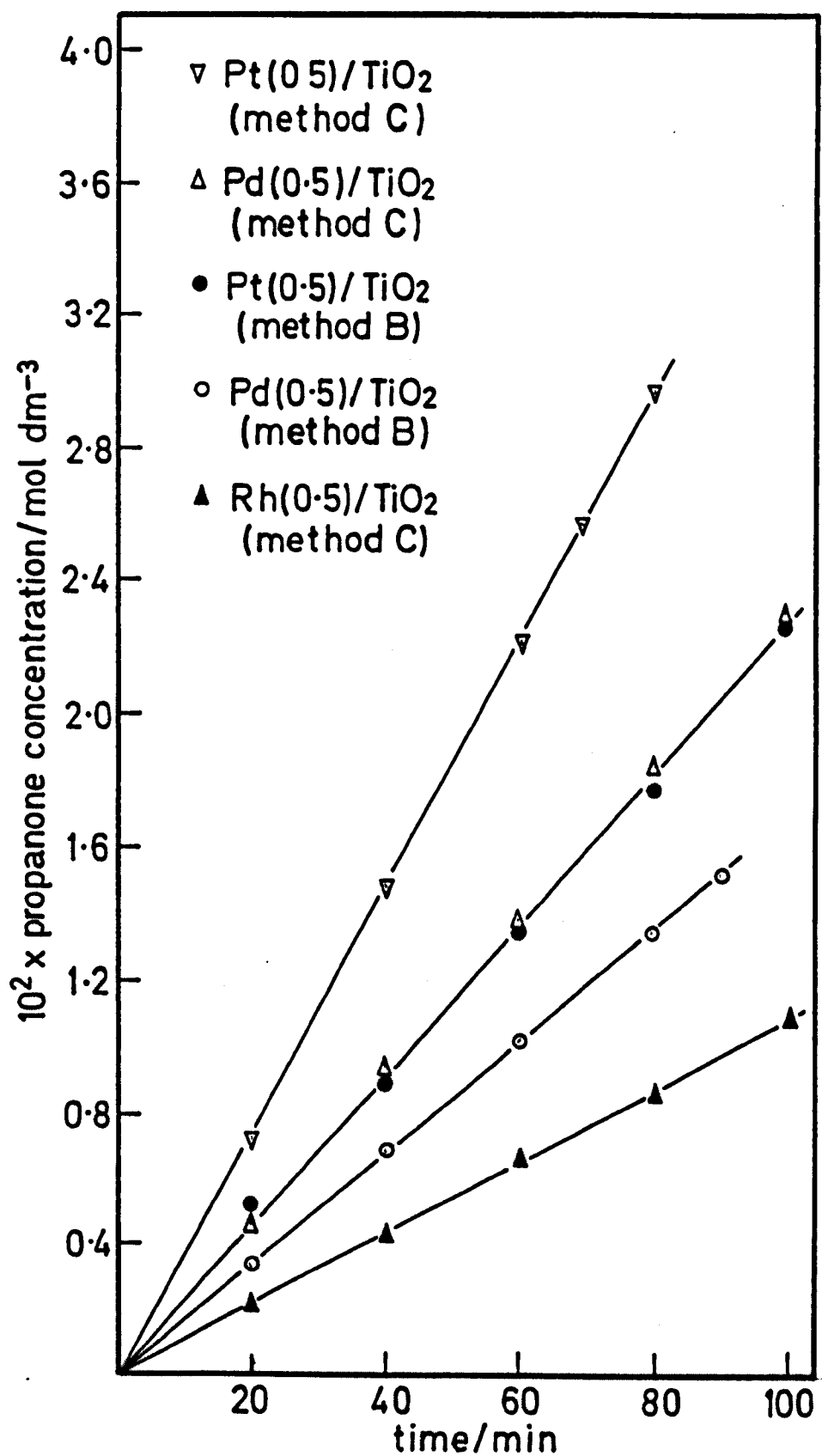
time/min.	$10^2 \times \text{propanone concentration/mol.dm}^{-3}$				
	catalyst				
	method B		method C		
	Pt(0.5)/ TiO <sub>2</sub>	Pd(0.5)/ TiO <sub>2</sub>	Pt(0.5)/ TiO <sub>2</sub>	Pd(0.5)/ TiO <sub>2</sub>	Rh(0.5)/ TiO <sub>2</sub>
0	0	0	0	0	0
20	0.518	0.330	0.730	0.462	0.220
40	0.887	0.675	1.480	0.933	0.432
60	1.336	1.021	2.198	1.389	0.660
70	-	-	2.581	-	-
80	1.758	1.335	2.967	1.836	0.864

Contd. over

90	-	1.499	-	-	-
100	2.261	-	-	2.292	1.083
$10^6 \times \text{rate}/$ $\text{mol.dm}^{-3}\text{s}^{-1}$	3.77	2.85	6.17	3.82	1.81

Clearly platinum consistently produces a more active catalyst than palladium, with those prepared by method C being more active than those prepared by method B.

Figure 3.69



Photocatalytic dehydrogenation of propan-2-ol at 293K on different catalysts

## CHAPTER FOUR

### DISCUSSION

#### 4.1 The photocatalytic oxidation of propan-2-ol on P-25 anatase

##### 4.1.1 Introductory discussion

The photocatalytic oxidation of liquid alcohols on both anatase and rutile has been the subject of several investigations in Nottingham University<sup>234-236</sup>. It has been established that:

1 - The simultaneous presence of  $\text{TiO}_2$ , oxygen and UV radiation was essential for sustained photocatalytic reaction.<sup>167,168,170,171</sup>

2 - The primary alcohols were photo-oxidised to the corresponding aldehydes whilst secondary alcohols were photo-oxidised to the corresponding ketones.<sup>171</sup>

3 - The activation energy for alcohol photo-oxidation on rutile over the temperature range of 278-308 K was independent of both the alcohol used and the reaction conditions.<sup>170,171</sup>

4 - When  $\text{H}_2\text{O}_2$  replaced gaseous oxygen as the oxidant the reaction rate increased, but the activation energy remained identical.<sup>170</sup> The constant activation energy was therefore associated with the solid state properties of the anatase or rutile rather than with the photocatalysed reaction.

5 - The rate of propanone formation was generally found to be proportional to the square root of the light intensity with both anatase and rutile.<sup>170</sup> However, Ward<sup>235</sup> suggested that the rate of propanone formation tended towards a direct dependence on light intensity when the incident intensity was low. A linear dependence on light intensity had been observed by Cundall et al.,<sup>168</sup> but this can be attributed to the lack of heat filters and precise temperature control.

#### 4.1.2 Preliminary experiments

The results in section 3.1.1 show that the photo-oxidation of propan-2-ol to propanone requires the simultaneous presence of anatase, oxygen and UV radiation, for the propanone concentration to increase linearly with irradiation time. However, when the reaction mixture was irradiated in the presence of a nitrogen atmosphere, propanone formation was extremely slow and ceased entirely after ca 2 h. irradiation, when the propanone yield was only  $1.26 \times 10^{-3} \text{ mol.dm}^{-3}$ . Since the anatase became pale grey in such experiments, it is believed that photo-oxidation involved lattice oxygen in addition to chemisorbed oxygen with the associated reduction of  $\text{Ti}^{4+}$  to  $\text{Ti}^{3+}$ . This is in agreement with the observation of Buss et al.,<sup>174</sup> who attributed the appearance of the blue-grey colour to the formation of  $\text{Ti}^{3+}$ .

Figure 3.3 shows that no dark reaction was observed with propan-2-ol/anatase in the presence of either oxygen or nitrogen. It follows that propanone formation from propan-2-ol on anatase is a photocatalytic reaction.

Previous experiments<sup>170</sup> with coated reaction vessels showed the total absorption of similar intensities of 366 nm radiation by 200 mg of rutile dispersed in 20 cm<sup>3</sup> of propan-2-ol. Furthermore calculations<sup>235</sup> based on the extrapolation of Hirds data<sup>243</sup>, for UV absorption by pigmented paint films, indicated that  $\sim 7.5 \text{ mg}$  of  $\text{TiO}_2$  was sufficient to absorb all incident 366 nm radiation. It follows that the mass effect shown in figure 3.2 must be caused by changes in the effective utilization of the absorbed radiation rather than by increased absorption. The anatase powder probably contains a range of particle sizes and there are two reasons for suggesting that small particles are more efficient than larger particles. Firstly, photoelectrons and photoholes generated in the bulk would have fewer traps and recombination centres to overcome

before reaching the surface. Secondly, a greater proportion of the material would be within the space-charge, arising from depletive oxygen chemisorption, which favours exciton dissociation and photohole migration to the surface. Hence increasing the catalyst mass increases the concentration of the efficient small particles within the illuminated region of the reaction vessel. The plateau is reached when this effect can no longer increase the overall efficiency of utilizing incident radiation. All values of the quantum yields quoted throughout the present work, using a catalyst mass of 150 mg, are thus calculated assuming complete absorption by the catalyst of all 366 nm radiation entering the reaction vessel.

#### 4.1.3 Temperature dependence for propanone formation

The activation energy for propanone production on P-25 anatase in an oxygen atmosphere was determined over the temperature range 278-308 K using the full intensity of 366 nm radiation from lamps 1 and 4 and also at reduced intensities from lamp 4.

At full intensity, both lamps, yielded linear Arrhenius plots (figure 3.5 and figure 3.11), which gave an activation energy of  $20 \pm 1 \text{ kJ mol}^{-1}$ . However, the Arrhenius plots for measurement at reduced intensity (figure 3.11) gave an activation energy of  $20 \pm 1 \text{ kJ mol}^{-1}$  at low temperatures, but the rate of reaction became temperature independent at high temperatures. The reason for temperature independence at higher temperatures will be discussed in a later section.

The activation energy of  $20 \pm 1 \text{ kJ mol}^{-1}$  observed at high intensity is to be compared with the value of  $31 \pm 1 \text{ kJ mol}^{-1}$  previously obtained for low area anatase<sup>170</sup> and the value of  $27 \pm 1 \text{ kJ mol}^{-1}$  obtained for low area rutile<sup>170</sup>. The manner in which the activation energy for propanone formation on rutile was independent of the reaction conditions led to the suggestion that it was the energy required to promote photo-electrons from traps into the conduction band where they would be free to migrate and become surface trapped by molecular oxygen as  $\text{O}_{2(\text{ads})}^-$ . It is most likely that the present activation energy of  $20 \pm \text{kJ mol}^{-1}$  is also associated with such a process.

The difference between the previous activation energy for propanone formation on anatase ( $31 \pm 1 \text{ kJ mol}^{-1}$ )<sup>170</sup> and the present value probably arises from differences in both surface area and purity of two catalysts. The catalyst used by Harvey *et al.*,<sup>170</sup> possessed a surface area of  $3.7 \text{ m}^2 \text{ g}^{-1}$  compared with  $\sim 50 \text{ m}^2 \text{ g}^{-1}$  for the present P-25 anatase. In addition to contributing to the difference in activation energy, the surface area may also account for the higher activity of the P-25 anatase. This

would arise from the fact that the space-charge energy from chemisorbed oxygen affects a much higher fraction of the bulk material in the smaller particles, thus aiding exciton dissociation and favouring fruitful surface trapping of photoholes. Harvey et al.,<sup>170</sup> showed that the activation energy for propanone formation was critically dependent on the purity of the catalyst, in that additions of 0.1 mole% of transition metal oxide invariably increased the activation energy. The low area anatase, which yielded an activation energy of  $31 \pm 1 \text{ kJ mol}^{-1}$  had been prepared by the calcination of hydrous titania at 1123 K, with the addition of  $\text{K}_2\text{SO}_4$  to prevent conversion of anatase to rutile. It is possible that aqueous Soxhlet extraction failed to remove all the  $\text{K}_2\text{SO}_4$ , thus yielding a sample that was effectively contaminated with both  $\text{K}^+$  and  $\text{SO}_4^{2-}$ . In addition to acting as bulk trapping centres, this impurity might also diminish the surface hydroxyl population, thus affecting both the activation energy and overall activity of the catalyst.

#### 4.1.4 Light intensity dependence for the photocatalytic oxidation of propan-2-ol

The variation of the rate of propanone formation on anatase with light intensity (366 nm) was determined and found to be proportional to the square root of light intensities  $> 0.65 \times 10^{-7}$  einstein  $\text{s}^{-1}$  (see figure 3.7 and figure 3.9). The results are summarized in table 4.1 for the different light intensities obtained from lamp 4 and lamp 6. The results are in a good agreement with the findings of Ward<sup>235</sup>, who observed a  $(\text{light intensity})^{\frac{1}{2}}$  dependence for propanone formation on rutile using 405 nm, 366 nm and  $> 340$  nm radiation for relative intensities  $> 20\%$ , and also in a good agreement with the observations of Harvey<sup>236</sup>, who studied the variation of reaction rate with light intensity (366 nm) on rutile at 293 K and on anatase at 308 K. Moreover, the results are also in good agreement with the results of Egerton and King<sup>169</sup>, who used 405 nm, 366 nm and 335 nm radiations and found a square root light intensity dependencies for all three wavelengths on pure rutile.

TABLE 4.1

lamp 4		lamp 6	
light intensity/ einstein $\text{s}^{-1}$	rate/mol.dm. <sup>3</sup> s. <sup>-1</sup>	light intensity/ einstein $\text{s}^{-1}$	rate/mol.dm. <sup>3</sup> s. <sup>-1</sup>
0.14	0.53	0.27	1.00
0.65	1.82	0.48	1.57
0.82	2.05	0.60	1.90
1.16	2.53	0.81	2.32

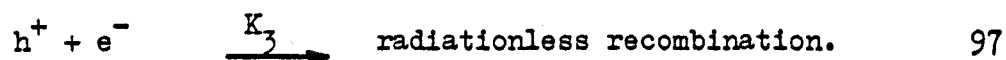
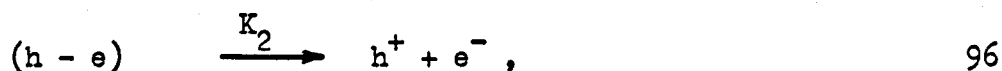
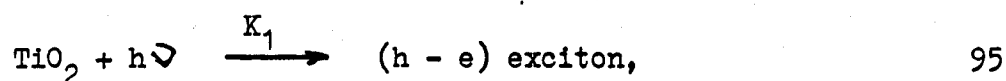
Contd. over

---

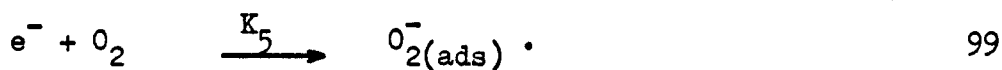
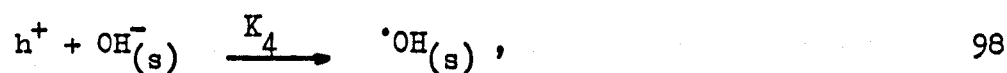
1.67	2.97	0.94	2.46
2.08	3.35	1.24	2.70
2.74	3.82	1.54	3.11
3.20	4.17	2.06	3.62
		2.50	3.82

---

The primary electronic processes which occur on the absorption of radiation of energy greater than the band gap of anatase are:



For photocatalysis to occur, it is necessary that the excitons dissociate and the photoelectrons and photoholes reach the surface, there to be trapped by surface species:



The concentration of excitons, photoholes and photoelectrons may be considered by applying a steady state treatment:

$$\frac{d[(h - e)]}{dt} = K_1 I_{(abs)} - K_2 [(h - e)] = 0 \quad 100$$

where I is the light intensity.

So that:

$$[(h - e)] = \frac{K_1}{K_2} I_{(abs)} . \quad 101$$

Similarly:

$$\frac{d[h]}{dt} = K_2 [(h - e)] - K_3 [h^+] [e^-] - K_4 [h^+] [OH_{(s)}^-] = 0 . \quad 102$$

Since  $[h^+] = [e^-]$  for electrical neutrality, and substituting for  $(h - e)$  gives:

$$\frac{d[h]}{dt} = K_1 I_{(abs)} - K_3 [h]^2 - K_4 [h^+] [OH_{(s)}^-] = 0 . \quad 103$$

So that:

$$K_1 I_{(abs)} = K_3 [h]^2 + K_4 [h] [OH_{(s)}^-] . \quad 104$$

For high light intensities, where the recombination of photoholes and photoelectrons would be expected to be high:

$$K_3 [h^+]^2 > K_4 [h^+] [OH_{(s)}^-] ,$$

so that equation 104 becomes:

$$K_1 I_{(abs)} = K_3 [h^+]^2 , \quad 105$$

thus,

$$[h^+] = \left(\frac{K_1}{K_3}\right)^{\frac{1}{2}} I_{(abs)}^{\frac{1}{2}} \quad . \quad 106$$

If the rate controlling step in the overall reaction involves the surface trapping of photoholes at surface  $OH^-$ , then the rate will be given by equation 98.

So that the reaction rate is given by:

$$\text{reaction rate} = K_4 \left(\frac{K_1}{K_3}\right)^{\frac{1}{2}} I_{(abs)}^{\frac{1}{2}} [OH_{(s)}^-], \quad 107$$

which incorporates the  $I^{\frac{1}{2}}$  dependence observed in the present work for high light intensities. If, on the other hand, the rate controlling step involves photoelectron trapping by oxygen, then the rate controlling step will be equation 99, so that the rate of reaction is given by:

$$\text{rate of reaction} = K_5 \left(\frac{K_1}{K_3}\right)^{\frac{1}{2}} I_{ab}^{\frac{1}{2}} [O_2 (ads)], \quad 108$$

which again gives the  $I^{\frac{1}{2}}$  dependence.

However, at low light intensities, it is expected that recombination of photoholes and photoelectrons will be low, then:

$$K_4 [h^+] [OH_{(s)}^-] > K_3 [h^+]^2 \quad .$$

So that equation 104 becomes:

$$K_1 I_{(abs)} = K_4 [h^+] [OH_{(s)}^-], \quad 109$$

and hence:

$$[h^+] = \frac{K_1 [I_{(abs)}]}{K_4 [OH^-_{(s)}]} . \quad 110$$

It follows that the rate of reaction is given by:

$$\text{rate of reaction} = K_1 [I_{(abs)}] . \quad 111$$

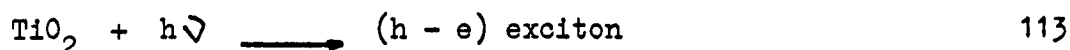
Alternatively, if photoelectron trapping is considered to be rate controlling, then:

$$\text{rate of reaction} = K_5 \frac{K_1}{K_4} [(I_{(abs)})] . \quad 112$$

Hence a linear dependence would be expected at low light intensities, and that was indicated in the present study for the light intensities  $< 0.65 \times 10^{-7}$  einstein  $s^{-1}$  .

#### 4.1.5 The mechanism for photocatalytic oxidation of propan-2-ol

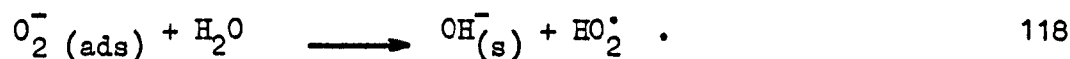
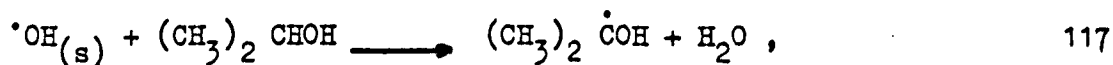
There is a general agreement that when  $\text{TiO}_2$  absorbs photons with energies greater than the band gap, the excitons dissociate and give rise to photoconduction by positive holes in the valence band and by electrons in the conduction band:



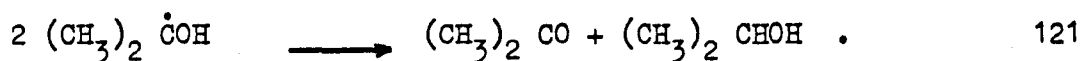
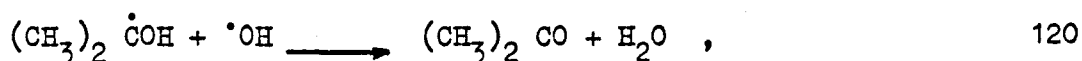
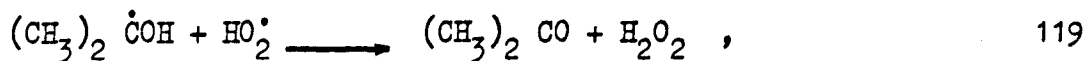
Following Bickley et al.,<sup>106,157</sup> it is believed that photoholes are trapped at surface hydroxyl groups ( $\text{OH}_{(s)}^-$ ) and photoelectrons are trapped by molecular oxygen, as follows:



There is nothing in the present work on anatase to contradict the suggestion made by Cundall, Rudham and Salim<sup>167</sup> for rutile that the  $\cdot\text{OH}_{(s)}$  radical is primarily responsible for reaction with the propan-2-ol molecule and that  $\text{O}_2^- (\text{ads})$  reacts with a water molecule:



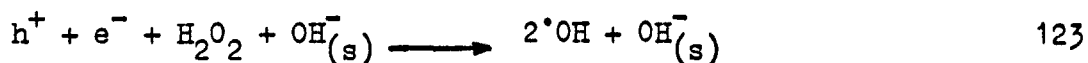
Volz et al.,<sup>244</sup> have shown the  $\cdot\text{OH}$  and  $\text{HO}_2\cdot$  radicals are the reactive species which are responsible for the photocatalytic degradation of  $\text{TiO}_2$  pigmented paint films. Formation of propanone from  $(\text{CH}_3)_2\dot{\text{C}}\text{OH}$  could then occur in the following ways:



In addition to step 119  $\text{H}_2\text{O}_2$  could also be formed by the interaction of  $\text{HO}_2\cdot$  radicals:



The  $\text{H}_2\text{O}_2$  formed in 122 or in 119 takes no further part in reaction unless decomposed by an electron from a further photon:



The  $\text{OH}^-_{(\text{s})}$  generated in 123 replaces that lost in 115, so that the catalyst surface returns to its initial state.

## 4.2 Photocatalytic dehydrogenation of alcohols on metallized anatase

### 4.2.1 Introductory discussion

Investigations of the photocatalysed dehydrogenation of aliphatic alcohols in both the gaseous and liquid phases established:

1 - Platinum or other transition metals supported on  $\text{TiO}_2$  are active photocatalysts for alcohol dehydrogenation in an inert atmosphere,<sup>13</sup> 14, 164, 172, 173, 178 whereas platinum supported on  $\text{SiO}_2$  or  $\text{AlO}_3$  is inactive.<sup>164</sup>

2 - There is no thermal dehydrogenation on the active photocatalysts at room temperature, so that U.V. radiation is essential.<sup>13</sup> In addition to releasing molecular hydrogen, the role of the metal is to trap photoelectrons thus minimising recombination with photoholes<sup>13, 14</sup>.

3 - Photocatalytic oxidation of the alcohols to the same carbonyl compounds and water occurs with the  $\text{TiO}_2$  support alone in the presence of oxygen. Here adsorbed oxygen acts as the photoelectron trap<sup>170, 171</sup>.

4 - A number of metals supported on  $\text{TiO}_2$  yield active photocatalysts, but platinum consistently yields the highest activity.<sup>164, 172, 178, 245</sup>

5 - The photocatalytic activity is a function of the platinum content, but no consistent pattern has emerged.<sup>14, 164, 173, 245</sup>

#### 4.2.2 Catalyst mass effects

The results in section 3.4.1 show the effect of catalyst mass on the photocatalytic dehydrogenation of propan-2-ol on platinized anatase ( $\text{Pt}(0.5)/\text{TiO}_2$  and  $\text{Pt}(2.0)/\text{TiO}_2$ ) prepared by method C. Throughout the experiments temperature, U.V. radiation intensity and an inert nitrogen atmosphere, were maintained constant. Figure 3.33 shows that the reaction rate increases with catalyst mass and becomes constant at masses above 100 mg. in  $20 \text{ cm}^3$  of propan-2-ol. It is to be noted that the activity plateau for  $\text{Pt}(0.5)/\text{TiO}_2$  is at a higher level than that for  $\text{Pt}(2.0)/\text{TiO}_2$ . The effect of variations in catalyst mass suspended in a constant volume of reactant upon the reaction rate has also been studied for the photocatalytic dehydrogenation of methanol by Pichat *et al.*,<sup>13</sup> and by Borgarallo and Pelizzetti<sup>173</sup>. Pichat *et al.*,<sup>13</sup> found that the activity plateau was achieved with a catalyst concentration of  $2.5 \text{ g.dm.}^{-3}$  of  $\text{Pt}(4.85)/\text{TiO}_2$  whereas Borgarallo and Pelizzetti<sup>173</sup> achieved a plateau at a concentration of  $1.0 \text{ g.dm.}^{-3}$  of  $\text{Pt}(2.0)/\text{TiO}_2$ . These values differ from that of  $5.0 \text{ g.dm.}^{-3}$  observed in the present work with  $\text{Pt}(0.5)/\text{TiO}_2$  and  $\text{Pt}(2.0)/\text{TiO}_2$ . In the published investigations<sup>13,14,173</sup> and in the present investigation of photocatalytic dehydrogenation of alcohols, all further rate measurements were made with a catalyst concentration in the plateau region. In the present research  $150 \text{ mg.}$  of catalyst in  $20 \text{ cm}^3$  of alcohol was constantly used, being sufficient to achieve maximum activity whilst conserving catalyst supplies.

Clearly from consideration of the catalyst concentrations at which the activity plateaux were achieved, the mass effect does not depend upon the platinum content of the individual catalysts. It is more likely to arise from variations in the intensity of radiation entering the reaction vessel and how the different catalysts utilize that radiation. In this connection the intensity of unfiltered U.V. radiation entering the

reaction vessel used by Pichat et al.,<sup>13,14</sup> was approximately 10% of the 366 nm. radiation entering the reaction vessel in the present work. It is therefore expected that less catalyst was required by Pichat et al.,<sup>13</sup> to achieve the most efficient utilisation of less radiation. Further comparisons are not possible since Borgarallo and Pelizzetti<sup>173</sup> do not report radiation intensities. It follows that the increase in activity with catalyst mass below the plateau region is associated with an increase in the efficiency of utilizing incident radiation, whilst the plateau itself represents the most efficient utilization of incident radiation that can be achieved within the system used.

#### 4.2.3 The effect of platinum content

Figure 3.33 shows that  $\text{Pt}(0.5)/\text{TiO}_2$  possesses a higher activity plateau than  $\text{Pt}(2.0)/\text{TiO}_2$  for photo-dehydrogenation of propan-2-ol. Furthermore, rates of propanone formation at 293 K reported in section 3.4.3 confirm that activity falls in the sequence:

$$\text{Pt}(0.25)/\text{TiO}_2 > \text{Pt}(0.5)/\text{TiO}_2 > \text{Pt}(2.0)/\text{TiO}_2 .$$

Pichat et al.,<sup>14</sup> showed that the rates of photodehydrogenation of methanol and propan-1-ol on hydrogen reduced  $\text{Pt}/\text{TiO}_2$  (method A) initially increased with platinum content, passed through a maximum at  $\sim 0.5$  wt% platinum before progressively falling with platinum content. The maximum in activity was attributed to an optimum attraction of photoelectrons in the  $\text{TiO}_2$  to the platinum crystallites. The authors rejected reflection of the U.V. radiation by platinum and the thermal rehydrogenation of the carbonyl product on the platinum as explanations for the fall in activity.

Teratani et al.,<sup>245</sup> found that the activity of photodeposited  $\text{Pt}/\text{TiO}_2$  catalysts prepared by method B for propan-2-ol photo-dehydrogenation initially increased with platinum content, but remained constant above  $\sim 0.4$  wt% platinum. With photodeposited  $\text{Pt}/\text{TiO}_2$  prepared by method C Borgarello and Pelizzetti<sup>173</sup> found that the activity for the photodehydrogenation of methanol progressively fell with platinum content over the range 1-10 wt%. Neither Teratani et al.,<sup>245</sup> nor Borgarello and Pelizzetti<sup>173</sup> offered a firm explanation for their results. However, Mills and Porter<sup>5</sup> used  $\text{Pt}/\text{TiO}_2$  prepared by method C to photocatalyse water decomposition; a fall in the rate of hydrogen evolution with platinum content between  $\sim 0.2$  and  $\sim 2.0$  wt% was attributed to screening of the  $\text{TiO}_2$  from the U.V. radiation by the supported metal. Clearly, no consistent behaviour or explanation emerges for the effect of platinum content on the photo-

catalytic dehydrogenation of liquid alcohols. There is, however, sufficient evidence to suggest that a platinum content  $> 0.5$  wt% can be detrimental in photocatalysis. It is for this reason that the majority of the present experiments were made with catalysts containing 0.5 wt% of supported metal.

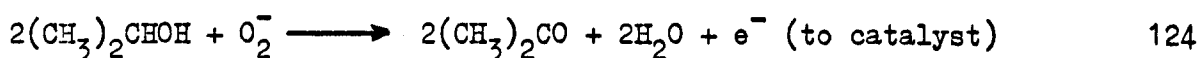
#### 4.2.4 The dark reaction on hydrogen reduced Pt(0.5)/TiO<sub>2</sub>

Unlike the anatase support, Pt(0.5)/TiO<sub>2</sub> prepared by method A exhibited a pronounced dark reaction in the presence of nitrogen, resulting in curved reaction-progress plots if it were not allowed to achieve completion before commencing irradiation. For propan-2-ol the dark reaction obeyed first-order kinetics with respect to departure from a temperature-independent propanone concentration at equilibrium of  $0.45 \times 10^{-2} \text{ mol.dm}^{-3}$  (see figure 3.14). Propan-1-ol, ethanol and methanol also showed first-order kinetics at 293 K with respect to an equilibrium concentration of carbonyl compound that was more slowly produced (see figure 3.17 and figure 3.18). There was excellent agreement between the yields of propanone, propanal and ethanal all being  $0.45 \times 10^{-2} \text{ mol.dm}^{-3}$ , whereas that of methanal fell short at  $0.35 \times 10^{-2} \text{ mol.dm}^{-3}$ . The lower equilibrium concentration of methanal was probably due to further oxidation of methanal to methanoic acid, and subsequently methanoic acid to carbon-dioxide.<sup>177</sup> Integral to such an explanation is a reaction step involving interaction of HCHO with H<sub>2</sub>O<sup>177</sup>. Although water was not deliberately added to the reaction mixture, residual water on the catalyst and reaction vessel surfaces and the fact that the methanol may not be entirely dry could provide sufficient water for this reaction step to be possible in the present reaction system.

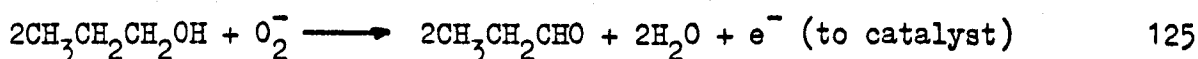
It is expected that in the preparation of Pt(0.5)/TiO<sub>2</sub> by method A, reduction in hydrogen at 753 K renders the anatase support non-stoichiometric, a process favoured by spillover of hydrogen atoms from the platinum particles.<sup>66</sup> However, cooling in nitrogen ensures maintenance of the non-stoichiometry, so that enhanced oxygen adsorption on the TiO<sub>2</sub>, most probably as O<sub>2</sub><sup>-</sup><sup>94,96</sup>, occurs on exposure to air at room temperature. Appreciable non-stoichiometry was still retained since the catalyst was a much darker grey than catalysts with the same platinum content prepared

by methods B and C. It is believed that interaction of adsorbed  $O_2^-$  with alcohols is responsible for the dark reaction observed with this catalyst. The first order kinetics reflect the limited amount of material within a chemisorbed layer, whilst the activation energy of  $120 \pm 5 \text{ kJ mol}^{-1}$  for propanone formation reflects the low reactivity of  $O_2^-$  relative to that of other chemisorbed oxygen species<sup>246</sup>. It is assumed that the reaction stoichiometry is as follows:

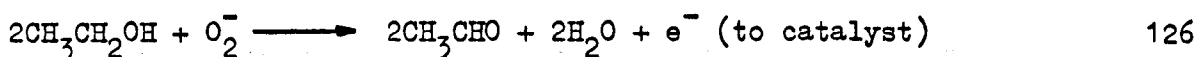
a) for propan-2-ol:



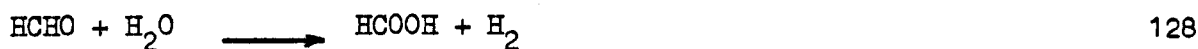
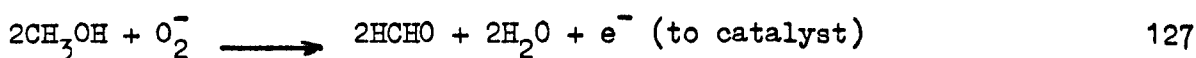
b) for propan-1-ol:



c) for ethanol:



d) for methanol:



The equilibrium yield of propanone, propanal or ethanal,  $9.0 \times 10^{-5}$  mol. with 150 mg of catalyst is thus equivalent to an  $O_2^-$  concentration of  $3.6 \times 10^{18}$  molecule  $\text{m}^{-2}$ . This is realistic in conditions where the concentration of electron donor  $\text{Ti}^{3+}$  is high, whereas association of the

oxygen solely with the platinum requires the unrealistic  $O_2$ :Pt ratio of 12:1. The present dark reaction would not have been observed by Pichat et al.,<sup>13,14</sup> in their studies of the photocatalytic dehydrogenation of alcohols on hydrogen reduced Pt/TiO<sub>2</sub> since they followed reaction progress by hydrogen evolution.

Oxygen treatment of hydrogen-reduced Pt(0.5)/TiO<sub>2</sub> at 573 K for 3 h. restores some stoichiometry in the anatase support so that a lower concentration of electrons is available for  $O_2^-$  adsorption. This effect is considered responsible for the temperature independent equilibrium yield of propanone from propan-2-ol being approximately halved. The high temperature oxygen treatment at 753 K for 16 h. entirely eliminated the dark reaction. Table 4.2 compares the temperature independent equilibrium yield of propanone on the catalyst prepared by method A and oxidised at different temperatures.

TABLE 4.2

oxidation temperature/ K	equilibrium yield of propanone/mol.dm. <sup>-3</sup>
-	$0.45 \times 10^{-2}$
573	$0.20 \times 10^{-2}$
753	0

The dark reaction observed with the catalyst prepared by method A was an undesirable complication, so that most studies were made with catalysts prepared by methods B and C; which are unlikely to generate non-stoichiometry within the anatase support. However, when the catalyst prepared by photodeposition (method C) was treated with hydrogen at 753 K

for 16 h. it also exhibited a dark reaction in the presence of nitrogen, resulting in curved photocatalytic reaction-progress plots unless allowed to achieve completion before commencing irradiation. Like the hydrogen reduced catalysts (method A) the dark reaction obeyed first-order kinetics (see figure 3.57) whilst the propanone concentration at equilibrium was  $0.49 \times 10^{-2} \text{ mol.dm}^{-3}$ . The propanone concentration of  $0.49 \times 10^{-2} \text{ mol.dm}^{-3}$  is not significantly different from that of  $0.45 \times 10^{-2} \text{ mol.dm}^{-3}$  obtained on the catalysts prepared by method A. The dark reaction on hydrogen reduced  $\text{Pt}(0.5)/\text{TiO}_2$ , prepared by photodeposition rather than by reduction, confirms that hydrogen spillover during the preparation of catalyst by method A is responsible for generation of dark reactivity. There is no reason to believe that the reaction stoichiometry is other than that given in equation 124.

#### 4.2.5 The temperature dependence of the photocatalytic dehydrogenation of propan-2-ol

Table 4.3 which summarises the results, includes the reaction rate and quantum yield at 293 K and the activation energy for propanone production from the photocatalytic dehydrogenation of propan-2-ol on anatase and metallized anatase prepared by different methods. The results show that the high temperatures oxygen treatment of Pt(0.5)/TiO<sub>2</sub> prepared by method A, not only reduced or eliminated the dark reaction but also decreased the photocatalytic activity below that of unoxidised material. The activity for photocatalytic dehydrogenation of propan-2-ol decreased with increasing temperature of oxidation. However, Teratani et al.,<sup>245</sup> reported that the air treatment of Pt(1.0)/TiO<sub>2</sub> (method B) at 653 K enhanced the catalytic activity for photodehydrogenation of propan-2-ol, but were uncertain as to the cause of the effect. In another study Teratani et al.,<sup>172</sup> observed that the catalytic activity of Pt(1.0)/TiO<sub>2</sub> (method B) for phenol production in photocatalytic benzene hydroxylation, decreased with the temperature of air-pretreatment above 673 K. XPS data obtained by the authors<sup>172</sup> showed that the air-pretreatment of Pt(1.0)/TiO<sub>2</sub> at temperatures lower than 673 K oxidised most of the platinum to the divalent state, whereas air-pretreatment at higher temperatures reduced the oxidised platinum to the metallic state. In the absence of XPS data it is not possible to say whether the reduction in activity presently observed after oxygen treatment of Pt(0.5)/TiO<sub>2</sub> (method A) is associated with changes in the oxidation state of the platinum. Furthermore, it is not possible to consider this in isolation from changes that occurred in the non-stoichiometric nature of the anatase support.

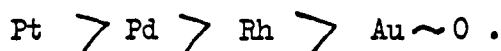
The activation energies for propanone formation from the photocatalytic dehydrogenation of propan-2-ol on oxidised Pt(0.5)/TiO<sub>2</sub> prepared by

TABLE 4.3

catalyst	method of preparation	reaction rate at 293 K/10 <sup>6</sup> mol.dm. <sup>-3</sup> s. <sup>-1</sup>	quantum yield at 293 K	activation energy/kJ mol. <sup>-1</sup>
TiO <sub>2</sub>	-	5.52 (2)	0.28	20 ± 1 (1)
Pt(0.5)/TiO <sub>2</sub>	A (unoxidised)	4.62 (3)	0.31	8 ± 1 (3)
Pt(0.5)/TiO <sub>2</sub>	A (oxidised at 573 K for 3 h.)	2.38 (3)	0.16	17 ± 1 (3)
Pt(0.5)/TiO <sub>2</sub>	A (oxidised at 753 K for 16 h.)	1.00 (3)	0.07	19 ± 1 (3)
Pt(0.5)/TiO <sub>2</sub>	B	3.77 (2)	0.19	20 ± 1 (1)
Pd(0.5)/TiO <sub>2</sub>	B	2.85 (2)	0.14	20 ± 1 (1)
Pt(0.25)/TiO <sub>2</sub>	C	6.77 (2)	0.34	20 ± 1 (3)
Pt(0.5)/TiO <sub>2</sub>	C	6.17 (2)	0.31	20 ± 1 (1)
Pt(2.0)/TiO <sub>2</sub>	C	4.50 (2)	0.23	20 ± 1 (1)
Pd(0.5)/TiO <sub>2</sub>	C	3.82 (2)	0.19	20 ± 1 (2)
Rh(0.5)/TiO <sub>2</sub>	C	1.18 (2)	0.09	20 ± 1 (2)
Au(0.5)/TiO <sub>2</sub>	C	0 (2)	0	-
Pt(0.5)/TiO <sub>2</sub>	C (Hydrogen reduced at 753 K)	5.10 (3)	0.34	9 ± 1 (3)

method A ( $17 \pm 1 \text{ kJ mol}^{-1}$  for the samples oxidised at 573 K for 3 h. and  $19 \pm 1 \text{ kJ mol}^{-1}$  for the samples oxidised at 753 K for 16 h.) are close to that found with support anatase and the photodeposited catalysts. However, the low activation energy for propanone production ( $8 \pm 1 \text{ kJ mol}^{-1}$ ) prior to oxygen treatment of  $\text{Pt}(0.5)/\text{TiO}_2$  is significantly different and may be associated with the non-stoichiometric nature of the anatase. Presumably this provides an energetically favourable mechanism for photoelectrons transport to the platinum particles and negates the photoelectron traps responsible for an activation energy of  $20 \pm 1 \text{ kJ mol}^{-1}$ . Furthermore, the activation energy of  $9 \pm 1 \text{ kJ mol}^{-1}$  observed with the hydrogen treated  $\text{Pt}(0.5)/\text{TiO}_2$  prepared by method C is very close to that obtained on  $\text{Pt}(0.5)/\text{TiO}_2$  prepared by method A. This lends weight to the view that a low activation energy is associated with a non-stoichiometric support.

Table 4.3 shows that catalysts prepared by method C were more active than those prepared by method B, although in all cases the activation energies for propanone production were identical to the value of  $20 \pm 1 \text{ kJ mol}^{-1}$  obtained with anatase in an oxygen atmosphere. This suggests that photoelectron transport within the anatase is consistently the process responsible for the activation energy, with metal particles or physically adsorbed oxygen acting as surface traps of different efficiency. Activities for catalysts with metal contents of 0.5 wt% prepared by method B suggest that the efficiency for photoelectron trapping by platinum is higher than that by palladium. Moreover, catalysts with metal contents of 0.5 wt% prepared by method C suggest that the efficiency for photoelectron trapping falls in the sequence:



In the absence of information on metal dispersion the sequence remains

qualitative. Nevertheless, the results show the need for a supported transition metal if sustained photocatalytic dehydrogenation is to occur in an inert atmosphere. The activity of  $\text{Au}(0.5)/\text{TiO}_2$  does not exceed that of the support anatase under identical reaction conditions and is thus effectively unreactive in photocatalytic dehydrogenation. The low concentration of propanone formed is associated with photocatalytic oxidation by chemisorbed and lattice oxygen from the support.

For a 150 mg of  $\text{Pt}(0.5)/\text{TiO}_2$  the total Pt content is  $3.8 \times 10^{-6}$  mole. Such a catalyst yields propanone with a rate of  $6.17 \times 10^{-6}$   $\text{mol.dm}^{-3}\text{s}^{-1}$ , so that the total amount of propanone produced in a typical run of 100 min. duration is  $7.4 \times 10^{-4}$  mole. Assuming that all the platinum atoms are accessible this yields a minimum value for the total turn-over number of  $7.4 \times 10^{-4} / 3.8 \times 10^{-6} = 195$ . Total turn-over numbers at 293 K calculated by this method range from 32 for  $\text{Rh}(0.5)/\text{TiO}_2$  to 427 for  $\text{Pt}(0.25)/\text{TiO}_2$ . Where total catalytic turn-over numbers considerably exceed unity there is no doubt concerning the photocatalytic nature of the reaction.<sup>48</sup>

Pichat et al.,<sup>13</sup> found that platinum was more well dispersed than rhodium on an anatase support and this was reflected in the higher activity of the platinum catalysts for the photocatalytic dehydrogenation of methanol at room temperature. It follows that information on the extent of metal dispersion on a series of catalysts prepared by the same method is required before such activity sequences have quantitative significance.

#### 4.2.6 Temperature dependence for the photocatalytic dehydrogenation of other alcohols

The aim of these experiments was to determine whether there were any differences in the activity and energetics for the photocatalytic dehydrogenation of methanol, ethanol, propan-1-ol and propan-2-ol on platinized anatase. Table 4.4 presents the rates of product formation/mol.dm.<sup>-3</sup>s.<sup>-1</sup> at 278 K and the activation energies obtained with Pt(0.5)/TiO<sub>2</sub> prepared by method C.

TABLE 4.4

reactant/product	10 <sup>6</sup> x rate of reaction at 278 K/mol.dm. <sup>-3</sup> s. <sup>-1</sup>	E <sub>a</sub> /kJ mol. <sup>-1</sup>
methanol/methanal	3.33 (3) <sup>a</sup>	19 ± 1 (3) <sup>b</sup>
ethanol/ethanal	3.27 (3)	20 ± 1 (3)
propan-1-ol/propanal	3.33 (3)	20 ± 1 (4)
propan-2-ol/propanone	3.28 (3)	20 ± 1 (4)

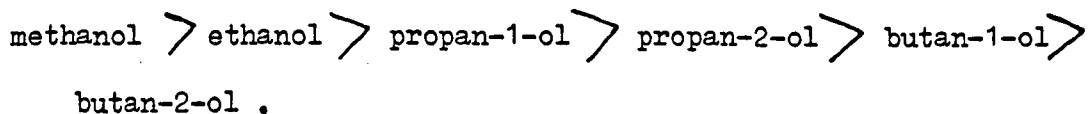
a - lamp number used to measure the reaction rate

b - lamp number used to measure the activation energy

Clearly, both the rates of product formation at 278 K and the associated activation energies are identical for the four alcohols. The present results thus differ from those of Pichat et al.,<sup>13</sup> and Borgarello and Pelizzetti<sup>173</sup>. Pichat et al.,<sup>13</sup> observed the following reactivity sequence for different alcohols on hydrogen reduced Pt(4.85)/TiO<sub>2</sub>:

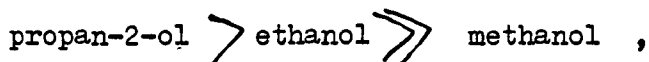
methanol > ethanol > propan-1-ol ≈ propan-2-ol ≈ butan-1-ol ,

whereas Borgarello and Pelizzetti observed the sequence:



on Pt(2.0)/TiO<sub>2</sub> prepared by photodeposition.

The discrepancy probably arises from the different techniques used to follow reaction progress. In the present research carbonyl compound formation was followed, whereas both Pichat *et al.*,<sup>13</sup> and Borgarello and Pelizzetti<sup>173</sup> followed hydrogen evolution. For reaction products which react beyond carbonyl compound formation the present technique would give an anomalously low reaction rate, whereas hydrogen evolution would give an anomalously high reaction rate. For methanol and ethanol there is published evidence for reaction beyond the aldehyde which produces further hydrogen<sup>165,177-179</sup>. Inspection of the authors',<sup>13,173</sup> data shows that it is methanol and ethanol which give high rates of hydrogen evolution. Complementary evidence for the further reaction of methanal and ethanal is given in the present research by the deviation from linearity of reaction progress plots for methanol and ethanol at 293 K on the catalyst prepared by method A and C (see section 3.2.2 and section 3.4.6), the activity sequence at 293 K on Pt(0.5)/TiO<sub>2</sub> (method A) which is:



and the lower equilibrium yield for methanal in the dark reaction (see section 3.2.1) on Pt(0.5)/TiO<sub>2</sub> prepared by method A.

The identical activities and activation energies for the photocatalytic dehydrogenation of the four alcohols on Pt(0.5)/TiO<sub>2</sub> prepared by method C is similar to the findings of Harvey, Rudham and Ward<sup>171</sup> for the photocatalytic oxidation of ethanol, propan-1-ol, propan-2-ol

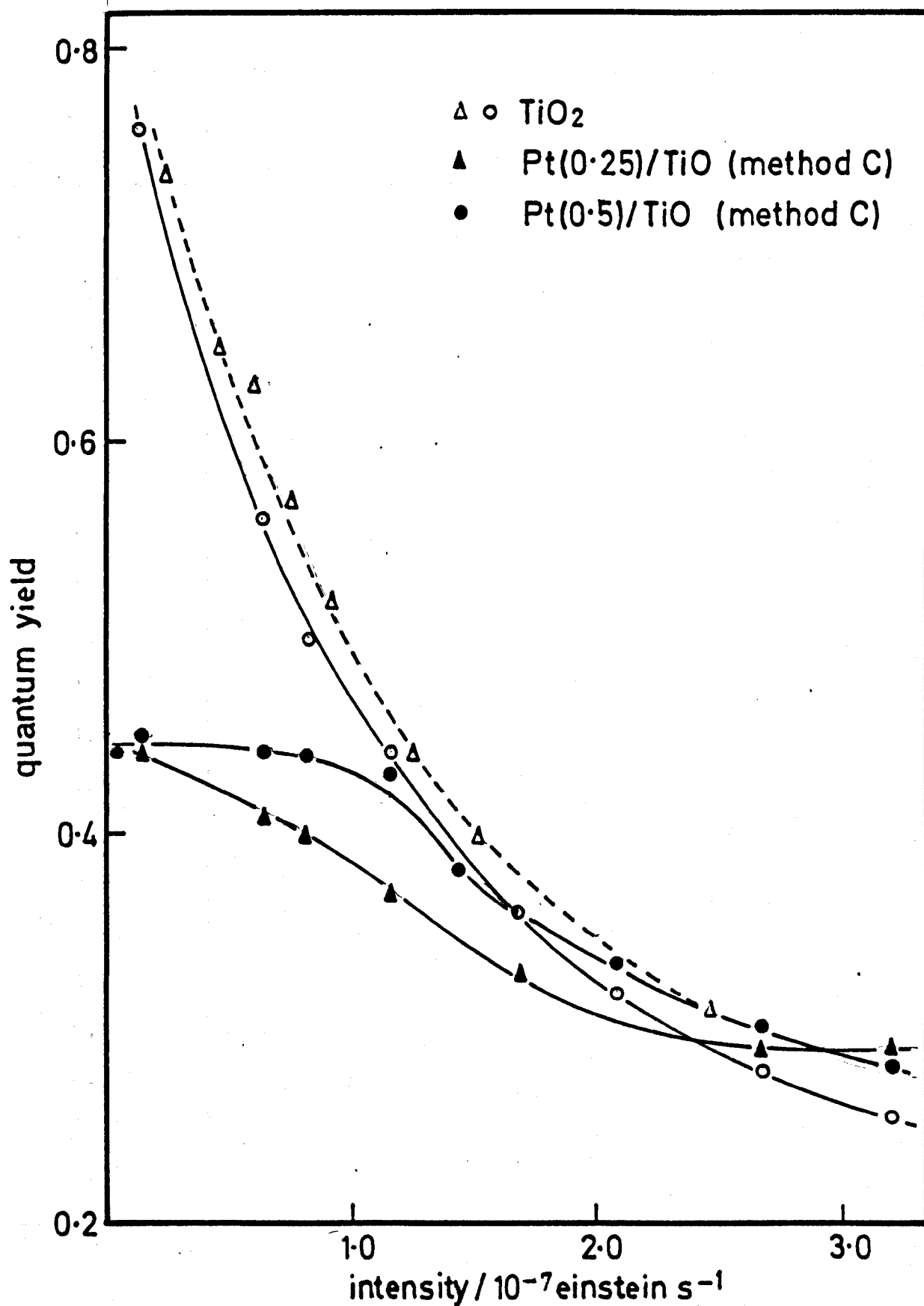
and butan-2-ol on pure rutile. They considered that the similarities arose from a common rate-controlling process, which was the transport of photoelectrons through the rutile to be surface trapped at adsorbed oxygen molecules. The experimental activation energy was associated with the energy required to promote photoelectrons from trapping centres into the rutile conduction band. A similar explanation may account for the present results, although the photoelectrons are trapped at supported metal particles since oxygen was excluded from the reaction mixture. Under conditions where there is no common rate controlling process associated with the bulk properties of the catalyst it is probable that differences in alcohol reactivity result in different reaction rates. The lower U.V. intensity and different catalyst preparation used by Pichat et al.,<sup>13</sup> may favour a condition in which the rate controlling process is associated with surface steps and thus give rise to different reaction rates with different alcohols.

#### 4.2.7 Light intensity dependence of the photocatalytic dehydrogenation of propan-2-ol

With the anatase support plots of reaction rate against the square root of the incident radiation intensity (see figure 3.7 and figure 3.9) were reasonably good straight lines, with deviations only at light intensities  $< 0.65 \times 10^{-7}$  einstein  $s^{-1}$ . However, with Pt(0.25)/TiO<sub>2</sub> (method C) and Pt(0.5)/TiO<sub>2</sub> (method B and C) the plots shown in figure 3.30 and figure 3.44 were considerably less linear and failed to pass through the origin. In this way the present research differs from earlier work on TiO<sub>2</sub><sup>170</sup>, where plots of reaction rate against the square root of the incident radiation intensity were linear for a number of samples of anatase and rutile. Consideration of the quantum yields in this earlier work shows that they were appreciably lower than the general level of quantum yields obtained throughout the present research. It follows that Harvey, Rudham and Ward<sup>170</sup> were working under conditions where the majority of photoelectrons and photoholes recombined, a necessary condition for the square root of intensity plot to be linear. Quantum yields have been calculated for the reactions rates used in figure 3.7, figure 3.9 and figure 3.44 and these are given in table 4.5. Inspection of the data shows that quantum yield ( $\Phi$ ) values range between 0.26 and 0.76 for anatase and between 0.28 and 0.46 for platinized anatase. Clearly, the present measurements are made under conditions where a considerable fraction of photoelectrons and photoholes are used in chemical reaction, so that formal plots of reaction rate against the square root of the incident radiation intensity, or directly against the incident radiation intensity, are not the best way of considering the experimental data.

Figure 4.1 presents plots of the quantum yield at 293 K against incident radiation intensity for the anatase support and for Pt(0.25)/TiO<sub>2</sub> and Pt(0.5)/TiO<sub>2</sub> (method C). For radiation intensities greater than

Figure 4.1



Variation of quantum yield for propanone formation with light intensity on different catalysts.

TABLE 4.5

light intensity /einstein s. <sup>-1</sup>	quantum yield ( $\phi$ )			
	TiO <sub>2</sub>		Pt(0.25)/TiO <sub>2</sub>	Pt(0.5)/TiO <sub>2</sub>
3.20	-	0.26	0.29	0.28
2.74	-	0.28	0.29	0.30
2.50	0.31	-	-	-
2.08	-	0.32	-	0.34
2.06	0.35	-	-	-
1.67	-	0.36	0.33	0.36
1.54	0.40	-	-	-
1.44	-	-	-	0.38
1.24	0.44	-	-	-
1.16	-	0.44	0.37	0.43
0.94	0.52	-	-	-
0.82	-	0.50	0.40	0.44
0.81	0.57	-	-	-
0.65	-	0.56	0.41	0.44
0.60	0.63	-	-	-
0.48	0.65	-	-	-
0.27	0.74	-	-	-
0.14	-	0.76	0.44	0.46
0.06	-	-	-	0.45

$1.5 \times 10^{-7}$  einstein  $s^{-1}$  there is a good agreement between the two types of catalysts, but the quantum yields diverge increasingly as the intensity falls below this value. Extrapolation to zero light intensity suggests a limiting quantum yield of 0.45 for photodehydrogenation on platinized anatase and a value higher than 0.80 for photo-oxidation on the anatase support. This difference in limiting quantum yield must be a consequence of differences in mechanism between the two types of catalytic system.

It is now necessary to consider the effect of light intensity on the energetics of propanone formation on anatase and Pt(0.5)/TiO<sub>2</sub> (method C). The results from section 3.1.4 and section 3.4.5 are summarised in table 4.6 and presented as Arrhenius plots in figure 4.2.

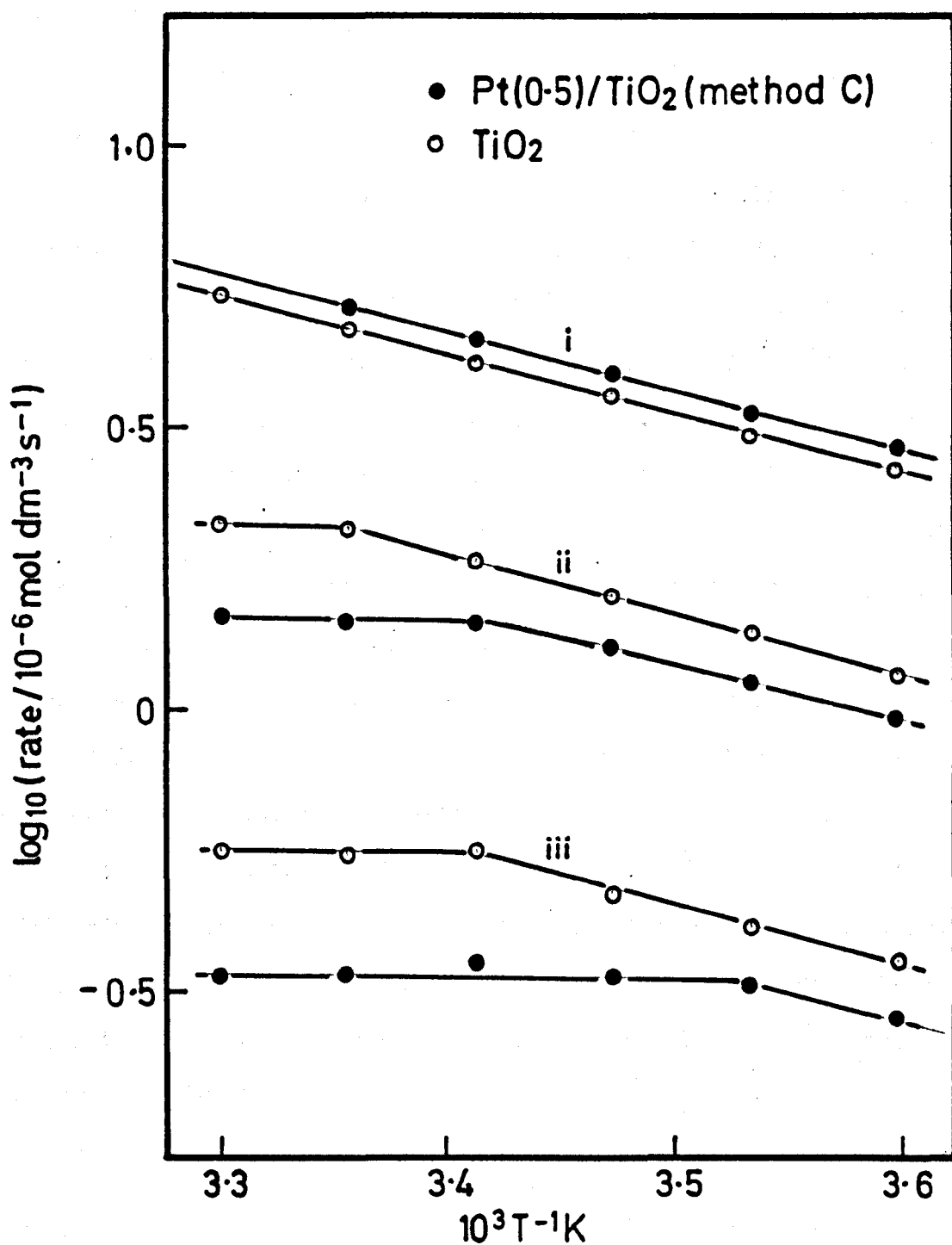
TABLE 4.6

T/K	TiO <sub>2</sub>			Pt(0.5)/TiO <sub>2</sub>		
	$10^7 \times I /$ einstein $s^{-1}$			$10^6 \times \text{rate} / \text{mol.dm}^{-3} s^{-1}$		
	3.2	0.65	0.14	3.2	0.65	0.14
278	2.67	1.17	0.35	2.88	0.98	0.28
283	3.08	1.36	0.41	3.39	1.13	0.33
288	3.63	1.59	0.47	3.98	1.28	0.34
293	4.17	1.82	0.53	4.53	1.42	0.32
298	4.82	2.03	0.52	5.23	1.42	0.34
3.03	5.46	2.16	0.53	-	1.45	0.35

At a full light intensity of  $3.20 \times 10^{-7}$  einstein  $s^{-1}$  both catalysts gave a linear plot yielding an activation energy of  $20 \pm 1$  kJ mol<sup>-1</sup>.

This activation energy is considered to be the energy necessary to promote

Figure 4.2



Temperature dependence for the photocatalytic dehydrogenation of propan-2-ol at different light intensities

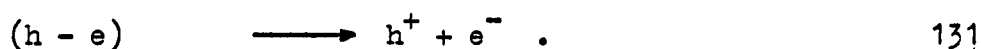
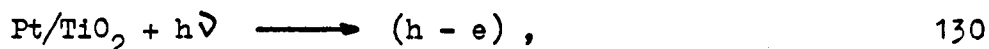
- i)  $3.20 \times 10^{-7}$  einstein s<sup>-1</sup>
- ii)  $0.65 \times 10^{-7}$  einstein s<sup>-1</sup>
- iii)  $0.14 \times 10^{-7}$  einstein s<sup>-1</sup>

photoelectrons from trapping centres into the conduction band of the support. At both reduced light intensities,  $0.65 \times 10^{-7}$  einstein  $\text{s}^{-1}$  and  $0.14 \times 10^{-7}$  einstein  $\text{s}^{-1}$ , the low temperature regions yield an activation energy of  $20 \pm 1$  kJ  $\text{mol}^{-1}$ , but this falls to zero as the temperature increased. Quantum yields corresponding to the horizontal portions of the Arrhenius plots for reactions at reduced light intensity approximate to the limiting quantum yields obtained from figure 4.1. With an irradiation intensity of  $0.65 \times 10^{-7}$  einstein  $\text{s}^{-1}$   $\phi$  is 0.67 for anatase and 0.45 for  $\text{Pt}(0.5)/\text{TiO}_2$ , whereas with  $0.14 \times 10^{-7}$  einstein  $\text{s}^{-1}$   $\phi$  is 0.76 for anatase and 0.49 for  $\text{Pt}(0.5)/\text{TiO}_2$ . It is believed that the horizontal portions of the Arrhenius plots are associated with a condition in which all photoelectrons are within the conduction band of the support and are thus surface trapped at either platinum or oxygen without loss through recombination processes.

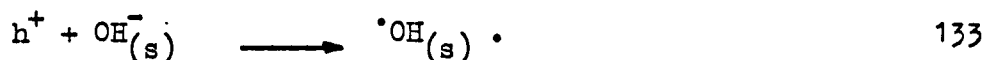
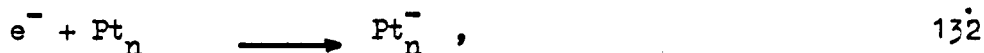
Pichat et al.,<sup>14</sup> report a curved Arrhenius plot for propan-1-ol dehydrogenation using a single sample of  $\text{Pt}(0.5)/\text{TiO}_2$  at progressively higher reaction temperatures. An approximately horizontal region was obtained between 293 K and 328 K, which the authors<sup>14</sup> associated with a rate determining interaction of photoholes with adsorbed alkoxide ions. Insufficient data is available to calculate a quantum yield from these results, but a value of approximately 0.50 can be calculated for room temperature from the data presented in a previous paper<sup>13</sup>.

#### 4.2.8 The mechanism for photocatalytic dehydrogenation of alcohols on metallized anatase

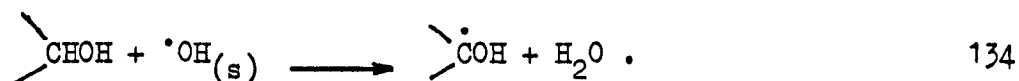
The reaction commences with the absorption of a photon by the anatase support giving an exciton, which subsequently dissociates to a photoelectron and a photohole:



To avoid recombination processes it is necessary that photoelectrons are trapped at platinum particles whilst photoholes are trapped at surface hydroxyl groups:



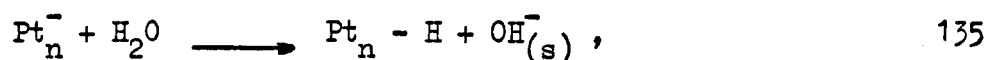
In keeping with mechanisms previously proposed for alcohol photo-oxidation<sup>167,170,171</sup>, and in the necessary absence of adsorbed oxygen ions ( $\text{O}_2^- (s)$ ), the hydroxyl radical abstracts a hydrogen atom from an alcohol molecule according to:



It is to be noted that hydrogen abstraction by  $\cdot\text{OH}$  radicals is frequently favoured as a step in photocatalytic reactions on metallized  $\text{TiO}_2$ <sup>15,178,211,221</sup>.

For continued photocatalysis the  $\text{OH}_{(s)}^-$  lost in equation 133 has to

be regenerated and this might occur through the interaction of  $\text{H}_2\text{O}$  from equation 134 with  $\text{Pt}_n^-$  according to:



but this requires  $\text{OH}_{(\text{s})}^-$  to be surface mobile. Alternatively, regeneration of  $\text{OH}_{(\text{s})}^-$  could proceed through the dissociative chemisorption of  $\text{H}_2\text{O}$ , which may be visualized as:

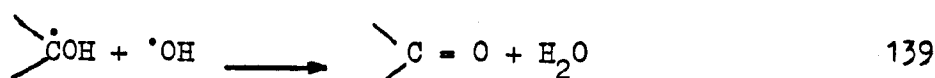
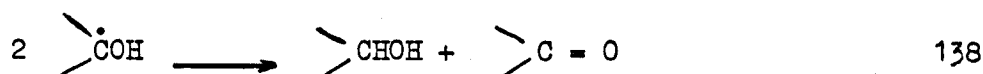


Since the  $\text{H}_{(\text{s})}^+$  is most likely attached to a surface anion it could be mobile through a proton-switch mechanism, which enables it to migrate to the  $\text{Pt}_n^-$ . So that:



would result in gaseous hydrogen formation by a mechanism that may be regarded as the reverse of hydrogen spillover.

The carbonyl compound is then formed according to the following equations:



The above mechanism gives a limiting quantum yield of 0.50 and is thus in good agreement with the limiting value obtained from the present results. A mechanism for alcohol photodehydrogenation on platinized

anatase has been proposed by Pichat et al.,<sup>13,14</sup>, in which an alcohol molecule is dissociatively chemisorbed on the anatase as an alkoxide ion and a proton. Photohole trapping by the alkoxide ion is considered to yield the carbonyl containing product and hydrogen atoms. The role of the platinum particles is to use photoelectrons to convert mobile protons to hydrogen atoms which are subsequently desorbed as molecular hydrogen. Although the mechanism has some attractive features, the carbonyl compound is produced with a limiting quantum yield of unity. It is for this reason that both the mechanism proposed by Pichat et al.,<sup>13,14</sup> and a less detailed mechanism proposed by Borgarello and Pelizzetti<sup>173</sup> are not considered to be applicable to the present results.

A dominant feature in the present research is the way in which the activation energy for photocatalytic dehydrogenation on photodeposited catalysis was independent of both the reactant alcohol and the supported metal at high radiation intensities. It follows that the activation energy is not associated with the processes represented in equations 137, 138 and 139. An identical activation energy of  $20 \text{ kJ mol}^{-1}$  for the photocatalytic oxidation of propan-2-ol on the unmetallized anatase indicates that the process responsible for the activation energy is associated with the support. As in previous studies with rutile,<sup>170,171</sup> the activation energy is equated with the energy required to promote photoelectrons from traps into the conduction band. Generation of non-stoichiometry in the anatase of platinized anatase by hydrogen spillover halves the activation energy for the photocatalytic dehydrogenation of propan-2-ol. Presumably non-stoichiometry provides an energetically more favourable mechanism for photoelectron transport to the platinum particles, thus negating the photoelectron traps responsible for the activation energy of  $20 \text{ kJ mol}^{-1}$ .

REFERENCES

1. C. Renz, *Helv. Chim. Acta.*, 4, 961, (1921).
2. S. Sato and J. M. White, *J. Am. Chem. Soc.*, 102, 7206, (1980).
3. S. Nishimoto, B. Ohtani, T. Yoshikawa and T. Kagiya, *J. Am. Chem. Soc.*, 105, 7180, (1983).
4. H. Courbon, J.-M. Herrmann and P. Pichat, *J. Catal.*, 72, 129, (1981).
5. A. Mills and G. Porter, *J. C. S. Farad. 1*, 78, 3659, (1982).
6. J. Kiwi and M. Gratzel, *J. Phys. Chem.*, 88, 1302, (1984).
7. B. Kraeutler and A. J. Bard, *J. Am. Chem. Soc.*, 100, 2239, (1978).
8. B. Kraeutler and A. J. Bard, *J. Am. Chem. Soc.*, 100, 5985, (1978).
9. H. Yoneyama, Y. Takao, H. Tamura and A. J. Bard, *J. Phys. Chem.* 87, 1417, (1983).
10. R. C. Gray and A. J. Bard, *Anal. Chem.*, 50, 1282, (1978).
11. B. Kraeutler, H. Reiche and A. J. Bard, *J. Polym. Sci. lett.*, 17, 535, (1979).
12. Y. Oosawa, *Chem. Soc. Japan Chem. Lett.*, 577, (1983).
13. P. Pichat, J.-M. Herrmann, J. Disdier, H. Courbon and M.-N. Mozzanega, *Nouv. J. De Chim.*, 5, 627, (1981).
14. P. Pichat, M.-N. Mozzanega, J. Disdier and J.-M. Herrmann, *Nouv. J. De Chim.*, 6, 559, (1982).
15. W. W. Dunn, Y. Aikawa and A. J. Bard, *J. Am. Chem. Soc.*, 103 6893, (1981).
16. M. Windholz, S. Budavari, R. F. Blumetti and E. S. Otterbein, *The Merck indx*, 10th edn. (Merck and Co., INC. Rathway, N. J., U.S.A.), (1983).
17. S. R. Yoganarasimhan and C. N. R. Rao, *Trans. Farad. Soc.*, 58, 1579, (1962).
18. A. W. Czanderna, C. N. R. Rao and J. M. Honig, *Trans. Farad. Soc.*, 54, 1069, (1958).

19. C. N. R. Rao and G. V. S. Rao, Transition Metal Oxides, (U.S. Government Printing Office, Washington), (1974).
20. R. W. G. Wyckoff, Crystal structures, 2nd edn. Vol. 1 (Interscience, New York), (1963).
21. W. L. Bragg, Atomic structure of Minerals, (Cornell University Press), (1937).
22. R. Kozlowski, R. F. Pettifer and J. M. Thomas, J. Phys. Chem. 87, 5172, (1983).
23. Yu. Ya. Bobyrenko, A. B. Zholnin and V. K. Konovalova, Russian J. Phys. Chem., 46, 749, (1972).
24. J. Trotter, Titanium Oxides, in (Structure Reports, W. B. Pearson), 26, 350, (1961).
25. M. E. Straumanis, T. Ejima and W. J. James, Acta. Cryst., 14, 493, (1961).
26. R. T. K. Baker, E. B. Prestridge and R. L. Garten, J. Catal., 56, 390, (1979).
27. R. T. K. Baker, E. B. Prestridge and R. L. Garten, J. Catal., 59, 293, (1979).
28. F. A. Grant, Rev. Mod. Phys., 31, 646, (1959).
29. G. D. Parfitt, Prog. Surf. and Mem. Sci., 11, 181, (1976).
30. N. B. Hannay, Semiconductors, (Reinhold Publishing Corporation, New York), (1959).
31. M. D. Earle, Phys. Rev., 61, 56, (1942).
32. A. L. Companion and R. E. Wyatt, J. Phys. Chem. Solids., 24, 1025, (1963).
33. R. H. Bube, Photoconductivity of Solids, (Joniu Wiley and Sons, INC.), (1960).
34. R. R. Addiss, A. K. Ghosh and F. G. Wakim, Appli. Phys. Letts., 12, 397, (1968).

35. T. J. Gray, J. Canad. Ceram. Soc., 38, 103, (1969).
36. K. Ghosh, F. G. Wakim and R. R. Addiss, Phys. Rev., 184, 979, (1969).
37. R. B. Lauer, R. R. Addiss and A. K. Ghosh, J. Appli, Phys., 42, 3508, (1971).
38. R. G. Breckenridge and W. R. Hosler, Phys. Rev., 91, 793, (1953).
39. Y. Tsuchiya, H. Segawa, H. Takagi and T. Kawakubo, J. Phys. Soc. Japan, 33, 859, (1972).
40. Y. Tsuchiya and H. Segawa, J. Phys. Soc. Japan, 36, 1566, (1974).
41. R. W. A. Hillhouse and J. Woods, Phys. Stat. Sol. (a), 46, 163, (1978).
42. R. W. A. Hillhouse and J. Woods, Phys. Stat. Sol. (a), 67, 119, (1981).
43. T. J. Gray and N. Lowery, Diss. Farad. Soc., 52, 132, (1971).
44. R. R. Addiss and F. G. Wakim, Photogr. Sci. and Eng., 13, 111, (1969).
45. S. K. Deb, Solid State Comm., 11, 713, (1972).
46. J.-M. Herrmann, J. Disdier and P. Pichat, Proc. 7th Intern. Vac. Congr. and 3rd Intern. Conf. Solid Surf., 951, (Vienna 1977).
47. F. G. Wakim, Phys. Stat. Sol. (a), 1, 479, (1970).
48. R. I. Bickley, S. P. R. Catalysis, 5, 308, (1982).
49. F. H. Hussein and R. R. Rudham, J. C. S. Farad. Trans. 1, 80 2817, (1984).
50. C. C. Kao, S. C. Tsai, M. K. Bahl, Y. W. Chung and W. J. Lo, Surf. Sci., 95, 1, (1980).
51. J. Disdier, J.-M. Herrmann and P. Pichat, J. C. S. Farad. Trans. 1, 79, 651, (1983).
52. G. A. Hope and A. J. Bard, J. Phys. Chem., 87, 1979, (1983).
53. B.-H. Chen and J. M. White, J. Phys. Chem., 86, 3534, (1982).

54. Y. W. Chung and W. B. Weissbard, *Phys. Rev. (B)*, 20, 3456, (1979).
55. B. Kraeutler and A. J. Bard, *J. Am. Chem. Soc.*, 100, 4317, (1978).
56. D. Duonghong, E. Borgarello and M. Gratzel, *J. Am. Chem. Soc.*, 103, 4685, (1981).
57. E. Borgarello, J. Kiwi, E. Pelizzetti, M. Visca and M. Gratzel, *J. Am. Chem. Soc.*, 103, 6324, (1981).
58. A. J. Bard, W. W. Dunn and B. Kraeutler, Patent, (U.S., 4264421), (1981).
59. W. W. Dunn and A. J. Bard, *Nouv. J. De Chim.*, 5, 651, (1981).
60. T. M. Apple, P. Gajardo and C. Dybowski, *J. Catal.*, 68, 103, (1981).
61. P. Gajardo and C. Dybowski, *Chem. Phys. Lett.*, 74, 306, (1980).
62. D. Resasco and G. L. Haller, *J. C. S. Chem. Comm.*, 1150, (1980).
63. P. Meriaudeau, H. Ellestad and C. Naccache, *Stud. Surf. Sci. Catal.*, 7B, 1464, (1981).
64. M. A. Vannice and R. L. Garten, *J. Catal.*, 56, 236, (1979).
65. P. Meriaudeau, O. H. Ellestad, M. Dufaux and C. Naccache, *J. Catal.*, 75, 243, (1982).
66. J. C. Conesa and J. Soria, *J. Phys. Chem.*, 86, 1392, (1982).
67. A. Takeuchi and J. R. Katzer, *J. Phys. Chem.*, 85, 937, (1981).
68. M. Koudelka, J. Sanchez and J. Auguslynski, *J. Phys. Chem.*, 86, 4277, (1982).
69. A. Mills, *J. C. S. Chem. Commun.*, 367, (1982).
70. T. Huizinga and R. Prins, *J. Phys. Chem.*, 85, 2156, (1981).
71. D. J. C. Yates, *J. Phys. Chem.*, 65, 746, (1961).
72. G. Munuera and F. S. Stone, *Disc. Farad. Soc.*, 52, 205, (1971).
73. P. Jones and J. A. Hockey, *J. C. S. Farad. Trans. 1*, 68, 907, (1972).
74. P. Jones and J. A. Hockey, *Tran. Farad. Soc.*, 67, 2669, (1971).
75. D. M. Griffith and C. H. Rochester, *J. C. S. Farad. Trans. 1*, 73, 1510, (1977).

76. J. Graham, C. H. Rochester and R. Rudham, J. C. S. Farad. Trans. 1, 77, 1973, (1981).
77. J. Graham, C. H. Rochester and R. Rudham, J. C. S. Farad. Trans. 1, 77, 2735, (1981).
78. A. D. Buckland, J. Graham, R. Rudham and C. H. Rochester, J. C. S. Farad. Trans. 1, 77, 2845, (1981).
79. J. Graham, Ph.D. Thesis, Nottingham University, (1982).
80. G. Munuera, V. Rives-Arnau and A. Saucedo, J. C. S. Farad. Trans. 1, 75, 736, (1979).
81. M. H. Herrmann and H. P. Boehm, Z. Anorg. Allg. Chem. 368, 73, (1969).
82. C. Morterra, G. Ghiotti and E. Garrone, J. C. S. Farad. Trans. 1, 76, 2102, (1980).
83. K. Tanaka and J. M. White, J. Phys. Chem., 86, 4708, (1982).
84. C. Morterra, A. Chiorino and A. Zecchina, Gaz. Chem. It., 109, 683, (1979).
85. C. Morterra, A. Chiorino and A. Zecchina, Gaz. Chem. It., 109, 691, (1979).
86. E. N. Figurovskaya, Kinet and Catal., 10, 374, (1969).
87. R. I. Bickley and R. K. M. Jayanty, Disc. Farad. Soc., 58, 194, (1974).
88. D. Iyengar, M. Codell, J. S. Karra and J. Turkevich, J. Am. Chem. Soc., 88, 5055, (1966).
89. P. C. Gravelle, F. Juillet, P. Meriaudeau and S. J. Teichner, Disc. Farad. Soc., 52, 140, (1971).
90. A. P. Griva, V. V. Nikisha, B. N. Shelimov, G. M. Zhidomirov and V. B. Kazanskii, Kinet. and Catal., 14, 1093, (1973).
91. I. D. Mikheikin, A. I. Mashchenko and V. B. Kazanskii, Kinet. and Catal., 8, 1153, (1967).

92. A. I. Mashchenko, V. B. Kazanskii, G. B. Pariiskii and V. M. Sharapov, *Kinet. and Catal.*, 8, 725, (1967).
93. A. A. Davvdov, M. P. Komarova, V. F. Anufrienko and N. G. Maksimov, *Kinet. and Catal.*, 14, 1342, (1973).
94. C. Naccache, P. Meriaudeau, M. Che and A. J. Tench, *Tran. Farad. Soc.*, 67, 506, (1971).
95. A. M. Volodin, A. E. Cherkashin and V. S. Zakharenko, *React. Kinet. Catal. Lett.*, 11, 107, (1979).
96. M. Iwamoto, Y. Yoda, N. Yamazoe and T. Selyama, *J. Phys. Chem.*, 82, 2564, (1978).
97. A. P. Griva, V. V. Nikisha, B. N. Shelimov and V. B. Kazanskii, *Kinet. and Catal.*, 15, 86, (1974).
98. D. R. Kennedy, M. Ritchie and J. Mackenzie, *Tran. Farad. Soc.*, 54, 119, (1958).
99. I. S. McLintock and M. Ritchie, *Tran. Farad. Soc.*, 61, 1007, (1965).
100. K. Tanaka, *J. Phys. Chem.*, 78, 555, (1974).
101. V. V. Nikisha, B. N. Shelimov and V. B. Kazanskii, *Kinet. and Catal.*, 15, 599, (1974).
102. J.-M. Herrmann, J. Disdier, M.-N. Mozzanega and P. Pichat, *J. Catal.*, 60, 369, (1979).
103. J.-M. Herrmann, J. Disdier and P. Pichat, *J. C. S. Farad. Trans. 1*, 77, 2815, (1981).
104. P. Meriaudeau and J. C. Vedrine, *J. C. S. Farad. Trans. 11*, 72, 472, (1976).
105. A. R. Gonzalez-Elipse, G. Munuera and J. Soria, *J. C. S. Farad. Trans. 1*, 75, 748, (1979).
106. R. I. Bickley and F. S. Stone, *J. Catal.*, 31, 389, (1973).
107. G. Munuera, A. R. Gonzalez-Elipse, J. Soria and J. Sanz, *J. C. S. Farad. 1*, 76, 1535, (1980).

108. G. Munuera and A. Navio, *Stud. Surf. Sci. Catal.*, 7B, 1185, (1981).
109. R. I. Bickley, *Chem. Phys. of Solids and their Surfaces*, S. P. R., 7, 118, (1978).
110. J. S. Smith, P. A. Thrower and M. A. Vannice, *J. Catal.*, 68, 270, (1981).
111. J.-M. Herrmann and P. Pichat, *J. Catal.*, 78, 425, (1982).
112. E. Yesodharan and M. Gratzel, *Helv. Chim. Acta.*, 66, 2145, (1983).
113. X-Z. Jiang, T. F. Hayden and J. A. Dumesic, *J. Catal.*, 83, 168, (1983).
114. S. J. Tauster, S. C. Fung and R. L. Garten, *J. Am. Chem. Soc.*, 100, 170, (1978).
115. P. Meriaudeau, B. Pommier and S. J. Teichner, *C. R. Acad. Sc. Paris*, 289, 395, (1979).
116. L. L. Murrell and D. J. C. Yates, *Stud. Surf. Sci. Catal.*, 7B, 1470, (1981).
117. B. A. Sexton, A. E. Hughes and K. Fogar, *J. Catal.*, 77, 85, (1982).
118. S. C. Fung, *J. Catal.*, 76, 225, (1982).
119. H. R. Sadeghi and V. E. Henrich, 87, 279, (1984).
120. D. N. Belton, Y-M. Sun and J. M. White, *J. Phys. Chem.*, 88, 1690, (1984).
121. S. J. Tauster, S. C. Fung, R. T. K. Baker, and J. A. Horsley, *Sci.*, 211, 1121, (1981).
122. G-M. Schwab, *Adv. Catal.*, 27, 1, (1978).
123. F. Solymosi, *Catal. Rev.*, 1, 233, (1967).
124. J. A. Horsley, *J. Am. Chem. Soc.*, 101, 2870, (1979).
125. J. R. Katzer, A. W. Sleight, P. Gajardo, J. B. Michel, E. F. Gleason and S. McMillan, *Farad. Disc. of the Chem. Soc.*, No. 72, 121, (1981).

126. B-H. Chen and J. M. White, *J. Phys. Chem.*, 87, 1327, (1983).
127. M. S. Spencer, *J. Phys. Chem.*, 88, 1046, (1984).
128. G. C. Bond and R. Burch, *S. P. R. Catalysis*, 6, 27, (1983).
129. S. Khoobiar, *J. Phys. Chem.*, 68, 411, (1964).
130. P. A. Sermon and G. C. Bond, *Catal. Rev.*, 8, 211, (1973).
131. P. A. Sermon and G. C. Bond, *J. C. S. Farad. Trans. 1*, 76, 889, (1980).
132. T. M. Apple and C. Dybowski, *J. Catal.*, 71, 316, (1981).
133. J-M. Herrmann and P. Pichat, *Stud. Surf. Sci. Catal.*, 17, 77, (1983).
134. D. D. Beck and J. M. White, *J. Phys. Chem.*, 88, 174, (1984).
135. G. C. Bond, *Stud. Surf. Sci. Catal.*, 17, 1, (1983).
136. K. Tanaka and J. M. White, *J. Catal.*, 79, 81, (1983).
137. F. Solymosi, I. Tombacz and M. Kocsis, *J. Catal.*, 75, 78, (1982).
138. S. J. Tauster and S. C. Fung, 55, 29, (1978).
139. M. A. Vannice and C. Sudhakar, *J. Phys. Chem.*, 88, 2429, (1984).
140. S. Sato and K. Kunimatsu, *J. Phys. Chem.*, 88, 175, (1984).
141. N. J. Arnold, Ph.D. Thesis, Nottingham University, (1984).
142. Yu. M. Shchekochikhin, V. N. Filimonov, N. P. Keier and A. N. Terenin, *Kinet. and Catal.*, 5, 94, (1964).
143. I. Carrizosa and G. Munuera, *J. Catal.*, 49, 174, (1977).
144. I. Carrizosa, G. Munuera and S. Castanar, *J. Catal.*, 49, 265, (1977).
145. I. Carrizosa and G. Munuera, *J. Catal.*, 49, 189, (1977).
146. V. N. Gerasimova, N. N. Sudakova and L. N. Kurina, *Russian J. Phys. Chem.*, 52, 1533, (1978).
147. M. Primet, P. Pichat and M-V. Mathieu, *J. Phys. Chem.*, 75, 1221, (1971).
148. C-Y. Hsiao, C-L. Lee and D. F. Ollis, *J. Catal.*, 82, 418, (1983).
149. R. Burch and A. R. Flambard, *J. C. S. Chem. Comm.*, 965, (1981).

150. Yu. P. Solonitsyn, G. N. Kuzmin, A. L. Shurygin and V. M. Yurkin, *Kinet. and Catal.*, 17, 1092, (1976).
151. F. Freund and W. P. Gomes, *Catal. Rev.* 3, 1, (1969).
152. M. Formenti and S. J. Teichner, *S. P. R., Catalysis*, 2, 87, (1978).
153. A. J. Bard, *J. Photo.* 10, 59, (1979).
154. V. N. Filimonov, *Doki-Akad. Nauk. S.S.S.R.*, 154, 922, (1964).
155. V. N. Filimonov, *Doki-Akad. Nauk. S.S.S.R.*, 158, 1408, (1964).
156. V. N. Filimonov, *Kinet. and Catal.*, 7, 451, (1966).
157. R. I. Bickley, G. Munuera and F. S. Stone, *J. Catal.*, 31, 398, (1973).
158. J. Cunningham, B. Doyle and E. M. Leahy, *J. C. S. Farad. Trans. 1*, 75, 2000, (1979).
159. J. Cunningham and B. K. Hodnett, *J. C. S. Farad. Trans. 1*, 77, 2777, (1981).
160. J. Cunningham, B. K. Hodnett, M. Ilyas, E. M. Leahy and J. P. Tobin, *J. C. S. Farad. Trans. 1*, 78, 3297, (1982).
161. A. Walker, M. Formenti, P. Meriaudeau and S. J. Teichner, *J. Catal.*, 50, 237, (1977).
162. L. P. Childs and D. F. Ollis, *J. Catal.*, 67, 35, (1981).
163. P. Pichat, J-M. Herrmann, H. Courbon, J. Disdier and M. N. Mozzanega, *Can. J. Chem. Eng.*, 60, 27, (1982).
164. A. Ichou, M. Formenti and S. J. Teichner, *Stud. Surf. Sci. Catal.*, 17, 63, (1983).
165. M. Kawai, S. Naito, K. Tamaru and T. Kawai, *Chem. Phys. Lett.*, 98, 377, (1983).
166. G. Irick, *J. Appl. Poly. Sci.*, 16, 2387, (1972).
167. R. B. Cundall, R. Rudham and M. Salim, *J. C. S. Farad. Trans. 1*, 72, 1642, (1976).
168. R. B. Cundall, B. Hulme, R. Rudham and M. S. Salim, *J. Oil Col. Chem. Assoc.*, 61, 351, (1978).

169. T. A. Egerton and C. J. King, J. Oil. Col. Chem. Assoc., 62, 45, (1979).
170. P. R. Harvey, R. Rudham and S. Ward, J. C. S. Farad. Trans. 1, 79, 1381, (1983).
171. P. R. Harvey, R. Rudham and S. Ward, J. C. S. Farad. Trans. 1, 79, 2975, (1983).
172. S. Teratani, C. Sungbom and K. Tanaka, Chin.-Jpn.-U.S. Symp. Heterog. Catal. Relat. Energy Probl., A22J, (1982).
173. E. Borgarello and E. Pelizzetti, Chim. Ind. (Milan), 65, 474, (1983).
174. A. D. Buss, M. A. Malati and R. Atkinson, J. Oil Chem. Assoc., 59, 369, (1976).
175. M. A. Malati and N. J. Seager, J. Oil Chem. Assoc., 64, 231, (1981).
176. F. H. Hussein, G. Pattenden, R. Rudham and J. J. Russell, Tetra. Lett., 25, 3363, (1984).
177. T. Kawai and T. Sakata, J. C. S. Chem. Comm., 694, (1980).
178. T. Sakata and T. Kawai, Chem. Phys. Lett., 80, 341, (1981).
179. J. F. Houlihan, R. J. Pollock and D. P. Madacs, Electrochim. Acta, 28, 585, (1983).
180. M. Gratzel, Farad. Diss. Chem. Soc., 70, 359, (1980).
181. H. Gerischer, Pure and Appl. Chem., 52, 2649, (1980).
182. J-M. Lehn, Photochemical Conversion and Storage of Solar Energy, (Academic Press, New York), (1981).
183. G. R. Peyton, D. W. DeBerry, Gov. Rep. Announce (U.S.), 82, 82, (1982).
184. A. Harriman, S. P. R., Photochemistry, 14, 513, (1983).
185. G. A. Korsunovskii, Russian J. Phys. Chem., 34, 241, (1960).
186. C. D. Jaeger and A. J. Bard, J. Phys. Chem., 83, 3146, (1979).
187. T. Kawai and T. Sakata, Stud. Surf. Sci. Catal., 7B, 1198, (1981).

188. A. Fujishima and K. Honda, *Natu.*, 238, 37, (1972).
189. A. J. Bard, *J. Phys. Chem.*, 86, 172, (1982).
190. V. V. Nikandrov, G. P. Brin and A. A. Krasnovsky, *Photobiochem-Photobiophys.*, 6, 101, (1983).
191. R. H. Baker, J. Lilie and M. Gratzel, *J. Am. Chem. Soc.*, 104, 422, (1982).
192. D. Duonghong, J. Ramsden and M. Gratzel, *J. Am. Chem. Soc.*, 104, 2977, (1982).
193. M. Gratzel and A. J. Frank, *J. Phys. Chem.*, 86, 2964, (1982).
194. V. H. Houlding and M. Gratzel, *J. Am. Chem. Soc.*, 105, 5695, (1983).
195. J. Cunningham and J. Tobin, *Rep. Eur.*, 6783, 34, (1980).
196. S.-M. Fang, B.-H. Chen and J. M. White, *J. Phys. Chem.*, 86, 3126, (1982).
197. S.-C. Tsai, C.-H. Kao and Y.-W. Chung, *J. Catal.*, 79, 451, (1983).
198. S.-C. Tsai and Y.-W. Chung, *J. Catal.*, 86, 231, (1984).
199. C. Yixuan, W. Zhaobin, C. Yanxin, L. Huaxin, H. Zupel, L. Huiqing, D. Yonglei, Y. Chunying and L. Wenzhao, *J. Molecu. Catal.*, 21 275, (1983).
200. S. Sato and J. M. White, *Chem. Phys. Lett.*, 70, 131, (1980).
201. S. Sato and J. M. White, *Stud. Surf. Sci. Catal.*, 7B, 1500, (1981).
202. S. Sato and J. M. White, *J. Phys. Chem.*, 85, 336, (1981).
203. H. Reiche and A. J. Bard, *J. Am. Chem. Soc.*, 101, 3127, (1979).
204. M. A. Fox and M.-J. Chen, *J. Am. Chem. Soc.*, 105, 4497, (1983).
205. W. R. McLean and M. Ritchie, *J. Appl. Chem.*, 15, 452, (1965).
206. H. Mozzanega, J.-M. Herrmann and P. Pichat, *J. Phys. Chem.*, 83, 2251, (1979).
207. R. I. Bickley and V. Vishwanathan, *Nature*, 280, 306, (1979).
208. F. Juillet, S. Teichner and M. Formenti, *Patent (Britain G.B. 1331084)*, (1973).

209. N. Djeghri, M. Formenti, F. Juillet and S. J. Teichner, Diss. Farad. Soc., 58, 185, (1974).
210. N. Djeghri and S. J. Teichner, J. Catal., 62, 99, (1980).
211. I. Izumi, W. W. Dunn, K. O. Wilbourn, F. R. F. Fan and A. J. Bard, J. Phys. Chem., 84, 3207, (1980).
212. C. Giannotti, S. Le Greneur and O. Watts, Tetra. Lett., 24, 5071, (1983).
213. H. Courbon, M. Formenti and P. Pichat, J. Phys. Chem., 81, 550, (1977).
214. M. Formenti, F. Juillet, P. Meriaudeau, and S. J. Teichner, Chem. Technol., 1, 680, (1971).
215. P. Pichat, J-M. Herrmann, J. Disdier and M-N. Mozzanega, J. Phys. Chem., 83, 3122, (1979).
216. M. R. St. John, A. J. Furgala and A. F. Sammells, J. Phys. Chem., 87, 801, (1983).
217. R. P. Viswanath, B. Viswanathan and V. Jeyanthi, Indian J. Chem., 21A, 447, (1982).
218. J-M. Herrmann, M-N. Mozzanega and P. Pichat, J. Photochem., 22 333, (1983).
219. A. J. Bard and B. Kraeutler, Patent, (U.S. 4303486), (1981).
220. B. Kraeutler, C. D. Jaeger and A. J. Bard, J. Am. Chem. Soc., 100, 4903, (1978).
221. I. Izumi, F-R. F. Fan and A. J. Bard, J. Phys. Chem., 85, 218, (1981).
222. R. W. Matthews, J. C. S. Farad. Trans. 1, 80, 457, (1984).
223. V. S. Zakharenko, A. E. Cherkashin, A. M. Volodin and N. P. Keier, React. Kinet. Catal. Lett., 10, 329, (1979).
224. A. M. Volodin, A. E. Cherkashin and V. S. Zakharenko, React. Kinet. Catal. Lett., 11, 235, (1979).

225. A. M. Volodin, A. E. Cherkashin and V. S. Zakharenko, *React. Kinet. Catal. Lett.*, 11, 277, (1979).
226. A. M. Volodin, A. E. Cherkashin and V. S. Zakharenko, *React. Kinet. Catal. Lett.*, 12, 1, (1979).
227. S. N. Frank and A. J. Bard, *J. Am. Chem. Soc.*, 99, 303, (1977).
228. K. Kogo, H. Yoneyama and H. Tamura, *J. Phys. Chem.*, 84, 1705, (1980).
229. S. N. Frank and A. J. Bard, *J. Phys. Chem.*, 81, 1484, (1977).
230. Y. Matsumoto, H. Nagai and E-I. Sato, *J. Phys. Chem.*, 86, 4664, (1982).
231. M. Miyake, H. Yoneyama and H. Tamura, *Bull. Chem. Soc. Japan*, 50, 1492, (1977).
232. J-M. Herrmann and P. Pichat, *J. C. S. Farad. Trans. 1*, 76, 1138, (1980).
233. B. Reichman and C. E. Byvik, *J. Phys. Chem.*, 85, 2255, (1981).
234. M. S. Salim, Ph.D. Thesis, Nottingham University, (1976).
235. S. Ward, Ph.D. Thesis, Nottingham University, (1979).
236. P. R. Harvey, Ph.D. Thesis, Nottingham University, (1981).
237. G. R. Lappin and L.C. Clark, *Anal. Chem.*, 23, 541, (1951).
238. P. E. Toren and B. J. Heinrich, *Anal. Chem.*, 27, 1986, (1955).
239. D. E. Jordan and F. C. Veatch, *Anal. Chem.*, 36, 120, (1964).
240. W. G. Leighton and G. S. Forbes, *J. Am. Chem. Soc.*, 52, 3139, (1930).
241. M. I. Christie and G. Porter, *Proc. Roy. Soc., (London)*, A212, 390, (1952).
242. J. G. Calvert and J. N. Pitts, *Photochemistry*, (J. Wiley and Son), (1966).
243. M. J. Hird, *J. Coatings Technol.*, 48, 75, (1976).
244. H. G. Volz, G. Kaempf, H. G. Fitzky and A. Klaeren, *Photodegradation and Photostabilization of coatings (A. C. S. Symposium series, no. 151) (Am. Chem. Soc. Washington D. C.,)*, (1981).

245. S. Teratani, J. Nakamichi, K. Taya and K. Tanaka, Bull. Chem. Soc. Japan, 55, 1688, (1982).
246. M. Iwamoto and J. H. Lunsford, J. Phys. Chem., 84, 3079, (1980).